UC Irvine

UC Irvine Electronic Theses and Dissertations

Title

Tuning the Protein Corona of Polymer Nanoparticle Hydrogels

Permalink

https://escholarship.org/uc/item/3t72p5fs

Author

O'Brien, Jeffrey Alan

Publication Date

2018

Peer reviewed|Thesis/dissertation

UNIVERSITY OF CALIFORNIA,
IRVINE

Tuning the Protein Corona of Polymer Nanoparticle Hydrogels

DISSERTATION

submitted in partial satisfaction of the requirements
for the degree of

DOCTOR OF PHILOSOPHY

in Chemistry

by

Jeffrey Alan O'Brien

Dissertation Committee:
Professor Kenneth Shea, Chair
Professor Zhibin Guan
Professor Rachel Martin

2018

DEDICATION

To

My parents Carol and Hank O'Brien, my brother Frank O'Brien and my friends
for all their love and support

"It was only a sunny smile, and little it cost in the giving, but like morning light it scattered the
night and made the day worth living"- F. Scott Fitzgerald

TABLE OF CONTENTS

LIST OF FIGURES

LIST OF TABLES

ACKNOWLEDGMENTS

I would like to thank my advisor Kenneth Shea for providing guidance and mentorship during my graduate studies at UC Irvine while also granting me significant creative freedom as a scientist. I also thank Professor Guan and Professor Martin for serving on my thesis committee.

Much of the work presented in this thesis resulted from collaborations with scientists at UC Irvine and abroad. In particular, I would like to specifically acknowledge Mr. Shunsuke Onogi, Dr. Shih-Hui Lee, Dr. Adam Weisman, Dr. Beverly Chou, Ms. Krista Fruehauf, Ms. Jacklynn Unangst, Mr. Zhicheng Yuan and Dr. José María Gutiérrez.

CURRICULUM VITAE

Jeffrey Alan O'Brien

WORK/RESEARCH EXPERIENCE

University of California, Irvine – Irvine, CA

Graduate Research in Shea Lab   **2013 – 2018**

- Determine importance of cross-linking in the nanoparticle-biomacromolecule interaction by synthesizing nanoparticles with various cross-linkers and cross-linking densities and assessing their ability to sequester a target peptide.
- Developed a high-throughput equilibrium dialysis assay for testing nanoparticles/polymers for their affinity to targeted biomacromolecules.
- Developed a nanoparticle composition capable of binding and inhibiting venomous lipophilic proteins/peptides with selectivity over serum proteins to develop a broad-spectrum antivenom. This nanoparticle is capable of inhibiting venom induced tissue necrosis *in vivo*.

University of San Diego – San Diego, CA

Undergraduate Research in Iovine Lab   **2011 – 2013**

- Developed an expertise in inert atmosphere techniques and organometallic synthesis. Also experienced in the use of NMR, automated column chromatography, UV-Vis spectroscopy, IR, fluorescence spectroscopy, differential scanning-calorimetry, thermogravimetric analysis, and gel-permeation chromatography.
  - o **Starch-Containing Protein Repellent Surfaces and Materials:**   **Nov 2011 – June 2013**
    Synthesis and Characterization of Starch Graft Copolymers
    - The goal of this research program was to synthesize hybrid copolymers that may find application as protein repellent surfaces and materials
    - This research resulted in the discovery of a hybrid starch containing polymer capable of encapsulating bioactive small molecules
  - o **Synthesis and Noncovalent Functionalization of a 7-azaindole-Containing**   **Feb – Nov 2011**
    Polymer
    - We were interested in probing the noncovalent functionalization of a 7-azadinole polymer or copolymer using small molecule Lewis acidic boroxine species.

Calcimedica, Inc., La Jolla, CA

Pharmaceutical Research – Drug Application Development   **2010 - 2012**

- Studied the physical and metabolic changes that resulted from structurally modifying small molecule drugs
- Promoted after two months of internship to part-time employee
- Extensive work on LC-MS/MS
- Developed expertise for analyzing and interpreting data from mass spectrometer

AWARDS

Winner of the UC Irvine Beall New Venture Business Competition (Life Science Track)	**2017**
UC Irvine Dissertation Fellowship	**2017**
NIH Chemical and Structural Biology Trainee Fellowship	**2015 – 2017**
Journal of General Physiology Best Poster Award	**2016**
Summer Program in Materials Chemistry Fellow	**2013**
University of San Diego Outstanding Achievement in Chemistry	**2013**
ACS Undergraduate Award in Organic Chemistry	**2013**
Jean Dreyfus Boissevain Undergraduate Fellow	**2012**
ACS Undergraduate Award in Analytical Chemistry	**2011**
ACS POLYED Undergraduate Award in Organic Chemistry	**2011**

PATENTS

- O'Brien, J. Shea, K. J. **"Compositions and Methods for Neutralizing Venomous Biomacromolecules"** 62/435,559, filed December 15, 2017, *Serial No. PCT/US17/66613*
- O'Brien, J. Shea, K. J. **"Bandages and Dispensers for Neutralizing Venomous Biomacromolecules"** 62/472,277, filed March 16, 2017, *PROVISIONAL*

PUBLICATIONS

- **"Rapid evaluation of polymer–biomacromolecule interactions. A discovery platform for nanoparticle – biomacromolecule affinity pairs"**
  O'Brien, J., Yuan, Z., Onogi, S., Fruehauf, K., Shea, K. J.
  Submitted to *J. Am. Chem. Soc.* December 2017

  RECENTLY SUBMITTED

- **"Inhibition of venom induced dermonecrosis via an engineered nanoparticle with affinity and selectivity for elapid snake venom"**
  O'Brien, J., Lee, S. H., Gutierrez, J. M., Shea, K. J.
  Submitted to *J. Am. Chem. Soc..* January 2018

- **"Engineering the protein corona of a synthetic polymer nanoparticle for broad-spectrum sequestration and neutralization of venomous biomacromolecules"**
  O'Brien, J., Lee, S. H., Shunsuke, O., Shea, K.J. *J. Am. Chem. Soc.,* **2016**, 138, 16604-16607.

  2016

  - * Featured in **Science Magazine**: Robert Service, "Antivenom made from nanoparticles could eventually treat bites from any snake" Dec. 20, 2016
  - ** Featured in **The Boston Globe**: Usha Lee McFarling, "Can Science Rob Snakes of Their Deadly Weapon?" March 22, 2017.
  - *** Altmetric score of 192 (14th highest score of all *J. Am. Chem. Soc.* articles)

- **"Tuning the Protein Corona of Hydrogel Nanoparticles; the Synthesis of Abiotic Protein/Peptide Affinity Reagents."**
  O'Brien, J., Shea, K. J., *Acc. Chem. Res*., **2016**, *49*, 1200-1210.

- **"Polymer antidotes for toxin sequestration**
  Weisman, A., Chou, B., O'Brien, J., Shea, K. J., *Adv. Drug Deliver. Rev*.,**2015**, 90, 81-100.

  2015

- **"Improved Metal-Adhesive polymers from Cu(I)-Catalyzed Azide-Alkyne Cycloaddition."**
  Accurso, A. A., Delaney, M., O'Brien, J., Kim, H., Iovine, P. M., Díaz, D. D., Finn, M. G. *Chem. Eur. J.*, **2014**, 20, 10710–10719.

  2014

- **"Amphiphilic Graft Copolymers from End-Functionalized Starches: Synthesis, Characterization, Thin Film Preparation, and Small Molecule Loading."**
  Ryno, L. M., Reese, C., Tolan, M., O'Brien, J., Short, G., Sorriano, G., Nettleton, J., Fulton, K., Iovine, P. M. *Biomacromolecules* **2014**, *15*, 2944-2951.

PRESENTATIONS

- **"Venom Aid: A Portable and Universal Snake Venom Antidote"**
  Translational Science Research Day
  University of California, Irvine, CA, June 13, 2017

  2017

- **"Engineering the Protein Corona for Broad-Spectrum Venom Sequestration"**
  Center for Advanced Design and Manufacturing of Integrated Microfluidics
  University of California, Irvine, CA, March 1st, 2017

  2017

PRESENTATIONS CONTINUED

- **"Engineering the Protein Corona for Broad-Spectrum Venom Sequestration"**   **2016**
  XII Pan American Section of the International Society on Toxinology,
  Miami Beach, FL, September 18th-22nd, 2016
      Won the Journal of General Physiology Best Poster Award
- **"Engineering the Protein Corona for Broad-Spectrum Venom Sequestration"**   **2016**
  252nd ACS National Meeting, PMSE, Philadelphia, PA, August 21st-25th, 2016
- **"Engineering the Protein Corona for Broad-Spectrum Venom Sequestration"**   **2016**
  San Diego POLYGRID, University of San Diego, CA, February 4, 2016
- **"Synthesis and Reactivity of End-Functionalized Starches"**
  244th ACS National Meeting, CELL, Philadelphia, PA, August 19-23, 2012   **2012**
  Iovine, Peter M.; O'Brien, Jeff; Apramian, Austin; Short, Gabriel
- **"Synthesis and Reactivity of End-Functionalized Starches"**
  244th ACS National Meeting, Sci-Mix, Philadelphia, PA, August 19-23, 2012   **2012**
  Iovine, Peter M.; O'Brien, Jeff; Apramian, Austin; Short, Gabriel
- **"Synthesis, Characterization, and Film-Forming Properties of Lignin core-Hyperbranched
  Polyglycerol Materials."**   **2012**
  243rd ACS National Meeting, CHED, San Diego, CA, March 25- 29, 2012
  Iovine, Peter M.; Korich, Andrew L.; Short, Gabriel; O'Brien, Jeff; Walker, Amanda R.;
  Morris, Raylina; Lehn, Kristiana

EDUCATION

University of California, Irvine-Irvine, CA   2013 – 2018
  PhD in Chemistry
  Advisor: Kenneth J. Shea

University of San Diego – San Diego, CA   2012
Bachelor of Arts in Biochemistry - Minor Psychology
  Dean's Honors List in 7 of 9 academic semesters
  GPA: 3.52; Majors GPA: 3.720
  Cum Laude

ABSTRACT OF THE DISSERTATION

Tuning the Protein Corona of Polymer Nanoparticle Hydrogels

By

Jeffrey Alan O'Brien

Doctor of Philosophy in Chemistry

University of California, Irvine, 2018

Professor Kenneth J. Shea, Chair

Subjecting a nanoparticle to a complex biological mixture results in a near instantaneous protein adsorption event. The type and quantity of protein adsorbed is termed the protein corona. The synthetic identity of a nanoparticle is perhaps the most important determining factor in the protein corona composition. However, the relationship between synthetic identity and the protein corona is complicated by multiple variables which makes rational nanoparticle optimization a challenge and favors high-throughput screens of nanoparticle compositions in order to optimize and tune the protein corona. In chapter one, a number of examples of tuning the protein corona by changing the synthetic composition of a nanoparticle are presented. Additionally, other factors influencing the protein corona of a nanoparticle are discussed including pH and temperature. In chapter two, a systematic study analyzing the effect of cross-linking in a nanoparticle is discussed. Information from this study played an important role in the protein corona optimization of a toxin-sequestering nanoparticle in chapter three. This nanoparticle, with a demonstrated ability to selectively sequester and neutralize diverse toxins found in snake venom, is shown to inhibit venom-induced dermonecrosis in chapter four. Using a quartz crystal microbalance in chapter five to analyze the relative affinity of toxin isoforms to the venom-binding nanoparticle, it is shown that the

nanoparticle interacts with toxins through diverse mechanisms. The complex stoichiometry between a nanoparticle and a protein complicates the analysis of binding event making comparisons between Langmuir derived disassociation constants inadequate. Finally, in chapter six, a high-throughput analytical technique using a modified version of equilibrium dialysis is presented. This solution-based method of studying capacity and affinity of a nanoparticle of a biomacromolecule is amenable to automation and has the potential to accelerate the largely empirical optimization process used to tune the protein corona.

Chapter 1

Tuning the Protein Corona of Hydrogel Nanoparticles: The Synthesis of Abiotic Protein/Peptide Affinity Reagents

A. Abstract

Nanomaterials, when introduced into a complex, protein rich environment, rapidly acquire a protein corona. The type of proteins and amount of proteins that constitute the corona depends significantly on the synthetic identity of the nanomaterial. For example, hydrogel nanoparticles (NPs) such as poly(*N*-isopropylacrylamide) (NIPAm) have little affinity for plasma proteins, in contrast, carboxylated poly(styrene) NPs acquire a dense protein corona. This range of protein adsorption suggests that the protein corona might be "tuned" by controlling the chemical composition of the NP. In this account we demonstrate that synthetic polymer NP libraries incorporating a diverse pool of functional monomers, can be screened for candidates with high affinity and selectivity to targeted biomacromolecules. Through directed synthetic evolution of NP formulations, one can tailor the protein corona to create synthetic organic hydrogel polymer NPs with high affinity and specificity to peptide toxins, enzymes and other functional proteins as well as to specific domains of large proteins. In addition, many NIPAm NPs undergo a change in morphology as a function of temperature. This transformation often correlates with a significant change in NP-biomacromolecule affinity, resulting in a *temperature-dependent* protein corona. This temperature dependence has been used to develop NP hydrogels with autonomous affinity switching for the protection of proteins from thermal stress and as a method of biomacromolecule-

purification through a selective thermally induced catch and release. In addition to temperature, changes in pH or buffer can also alter a NPs protein corona composition, a property that has been exploited for protein purification. Finally, synthetic polymer nanoparticles (NPs) with low nanomolar affinity for a peptide toxin were shown to capture and neutralize the toxin in the bloodstream of living mice. While the development of synthetic polymer alternatives to protein affinity reagents is in its early stages, these early successes using only small libraries of functional monomers is encouraging. It is likely that by expanding the chemical diversity of functional hydrogels, a much broader range of NP-biomacormolecule affinity pairs will result.

B. Background

When a nanomaterial is introduced into a biological environment, it takes on a new identity resulting from instantaneous biomacromolecule adsorption.[1,2] If the environment is rich in proteins, such as plasma, this new identity is termed the protein corona. The protein corona can be divided into two functional components, a hard and soft corona.[3] The hard corona describes proteins that have very slow exchange rates with the environment and thermodynamically favor association with the nanomaterial, while the soft corona describes proteins that exchange rapidly with the surrounding environment. A variety of factors dictate the composition of the hard corona including size, shape, and in particular, the synthetic identity of the nanomaterial.[4,5]

The relationship between the chemical composition and the protein corona of a nanomaterial is defined by multiple interdependent variables. Thus, it is often difficult to relate individual NP characteristics to biological responses. For example, the homology in the human plasma protein corona composition between a 50 nm carboxyl modified-polystyrene nanoparticle (NP) and a 100 nm carboxyl-modified polystyrene NP is roughly 50%.[5] This is particularly true for nanomaterials that inherently adsorb large quantities of proteins such as polystyrene or silica NPs.[6] The degree

to which a NP composition will interact with a protein rich environment depends largely on the chemical composition of the NP. Typically, hydrophilic nanomaterials such as hydrogel NPs, adsorb fewer biomacromolecules compared to more hydrophobic NPs. This is dramatically illustrated by the difference in protein hard coronas adsorbed on a negatively charged (carboxylated) polystyrene NP compared to a poly(N-isopropylacrylamide) (NIPAm) NP (Figure 1.1).
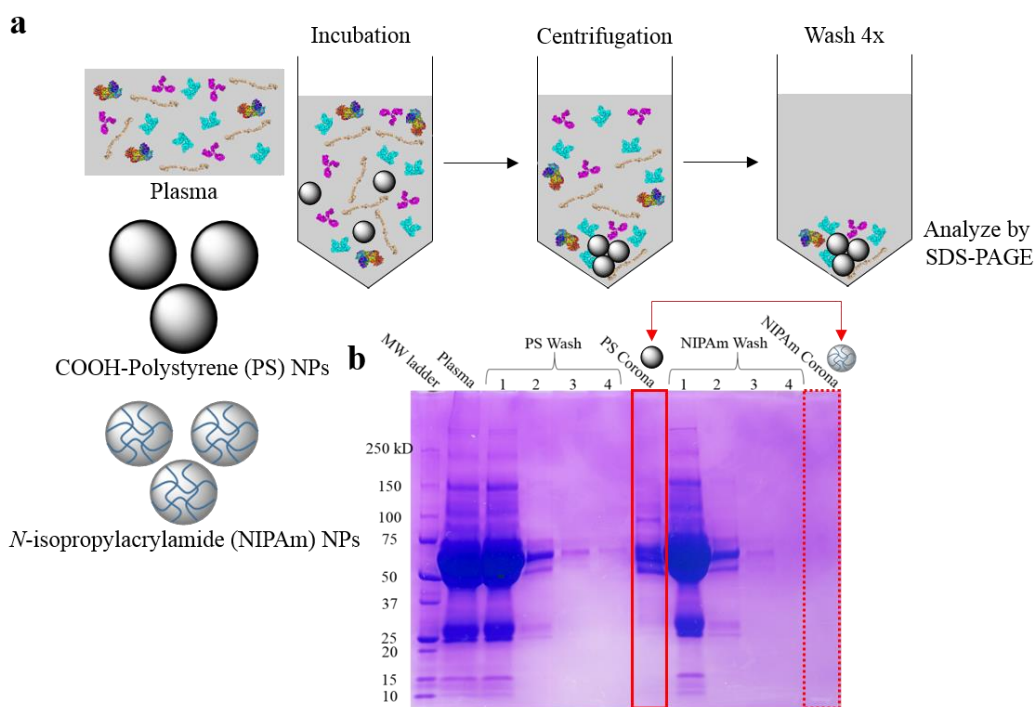
Figure 1.1. Composition of the *hard* NP-protein corona following exposure to 25% ovine (sheep) plasma for COOH-polystyrene (PS) NPs (solid red rectangle) and 5% *N-N'*-methylenebisacrylamide (Bis)-95%NIPAm NPs (dashed red rectangle). (a) Each NP (1 mg/mL) was incubated in 25% ovine plasma in phosphate buffer saline (PBS) for 30 min., pelleted by centrifugation (15,000 RPM, 10 min.), and washed with PBS four times. SDS-PAGE loading buffer was then added to the pellet to remove the hard corona, which was then analyzed by (b) SDS-PAGE.

This difference in corona composition calls attention to the potential for "tuning" the protein corona by adjusting the chemical composition of the NP. The focus of this chapter is to review previously reported methods used to engineer the hard corona by altering the chemical composition of the NP (Figure 1.2). This strategy has produced abiotic (synthetic polymer) biomacromolecule

affinity reagents for peptides, proteins and carbohydrates. We demonstrate in the following

sections that it is now possible to synthesize, in the chemistry laboratory, synthetic polymer NPs

with high affinity and selectivity to targeted biomacromolecules.
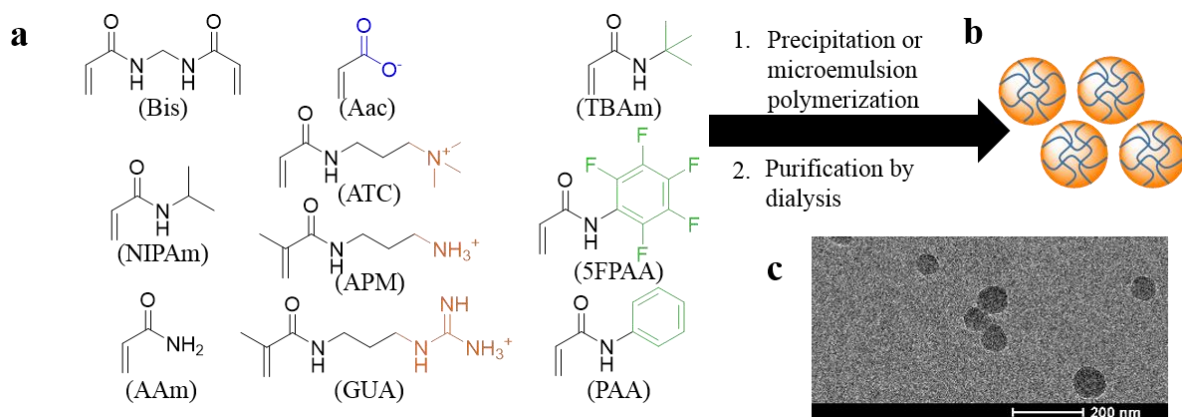
Figure 1.2. (a) Representative pool of monomers (*N,N'*-methylenebisacrylamide (Bis), *N*-isopropylacrylamide (NIPAm), acrylamide (AAm), acrylic acid (Aac), (3-acrylamidopropyl) trimethylammonium chloride (ATC), *N*-(3-aminopropyl)methacrylamido (APM), *N*-(3-methacrylamidopropyl) guanidinium chloride (GUA), *N*-(*tert*-butyl)acrylamide (TBAm), pentafluorophenyl acrylamide (5FPAA), *N*-phenylacrylamide (PAA)) used to generate (b) a library of NPs. (c) TEM image of a 1 mg/mL NP solution.

C. Designing libraries and general strategy for engineering the chemical composition of a NP for selective protein adsorption

NPs of uniform size are synthesized via precipitation[7] or emulsion polymerizations[8] in water and

are purified by dialyzing the resulting colloidal suspension against a large excess of water. The

chemical composition of these copolymer systems contain carbon backbones with randomly

distributed functional side chains. Most monomers are acrylamide based, and generally have

similar reactivity ratios, which usually results in their stoichiometric incorporation corresponding

to the feed ratio. Monomer incorporation for lightly cross-linked NPs can be quantified through

solution ^{1}H and ^{13}C NMR spectroscopy.[7,9]

An important factor in tuning the corona of synthetic polymer NPs is the use of NIPAm as the base monomer for NP synthesis. NIPAm has very little innate biomacromolecule affinity (Figure 1.1), which allows for direct correlations to be made between the addition of functional monomers and the protein corona composition. If polystyrene were used in place of NIPAm as the base material, the relationship would be significantly diminished due to greater non-specific affinity.[5] Thus, the use of NIPAm is strategic in that it reduces the number of interdependent variables contributing to the protein corona.

Libraries of NPs featuring different ratios and types of functional monomers can be used to identify NP formulations with high affinity to targeted biomacromolecules. Often lead NP compositions are those that complement the charge and hydrophobicity of the targeted biomacromolecule. However, the optimized ratio of privileged monomers is typically determined empirically through several analytical techniques for evaluating NP-biomacromolecule affinity. These include centrifugation filtration coupled with UV-Vis spectroscopy, quartz crystal microbalance, surface plasmon resonance spectroscopy and ELISA-mimic and protein/peptide activity assays.

NP specificity is situational; it depends on the application and what else is present. The specificity of a NP to a target biomacromolecule is often assessed after optimizing NP composition for affinity to the target. As with many affinity reagents, as a result of targeted optimization and biological diversity, the NP interacts strongest with the targeted biomacromolecule. It is important to note that the conditions used to analyze protein binding play a critical role in the observed NP-biomacromolecule interaction. These conditions include, but are not limited to, pH, ionic strength, and the temperature at which the NP-biomacromolecule interaction is studied. Selectivity and affinity therefore must be thought of as situational and parameter dependent phenomena.

D. Thermoresponsiveness

The solubility of a number of synthetic polymers including NIPAm and PEG is counterintuitive. The polymers are solvent swollen at low temperatures (below their lower critical solution temperature, LCST) and collapsed and less solvated above their LCST.[10,11] The behavior has been attributed to an entropically driven desolvation at elevated temperatures.[12] Below the LCST, NIPAm NPs are highly solvated, and therefore NP-biomacromolecule hydrophobic interactions are significantly diminished. This reduces the thermodynamic gain of fixing a biomacromolecule in the entropically unfavorable hard corona. However, by warming above the LCST, the collapsed NP groups functionality in closer proximity in a less hydrophilic environment allowing hydrophobic interactions to play a greater role. These two factors lower the energy of the hard corona often resulting in greater protein affinity (Figure 1.3).

Indeed, in many cases we have observed biomacromolecule affinity in NIPAm copolymers is strongest above the LCST, when the polymer is in the "collapsed," more hydrophobic state. It is also noteworthy that the LCST of a NP can be "tuned" or eliminated much like the protein corona of a NP. Depending on the degree of cross-linker, type of cross-linker, pKa of the NP, and hydrophobicity (chemical composition) of the NP, the temperature and magnitude of the transition can be adjusted. Considering NPs often have significantly reduced affinity to biomacromolecules in their solvent swollen state (below LCST), the LCST of NIPAm-NPs can be used to turn off or on the affinity of a NP to a targeted biomacromolecule. This thermally induced catch and release of a biomacromolecule has been exploited in several examples to design NPs for protein purification and protection (vide infra).
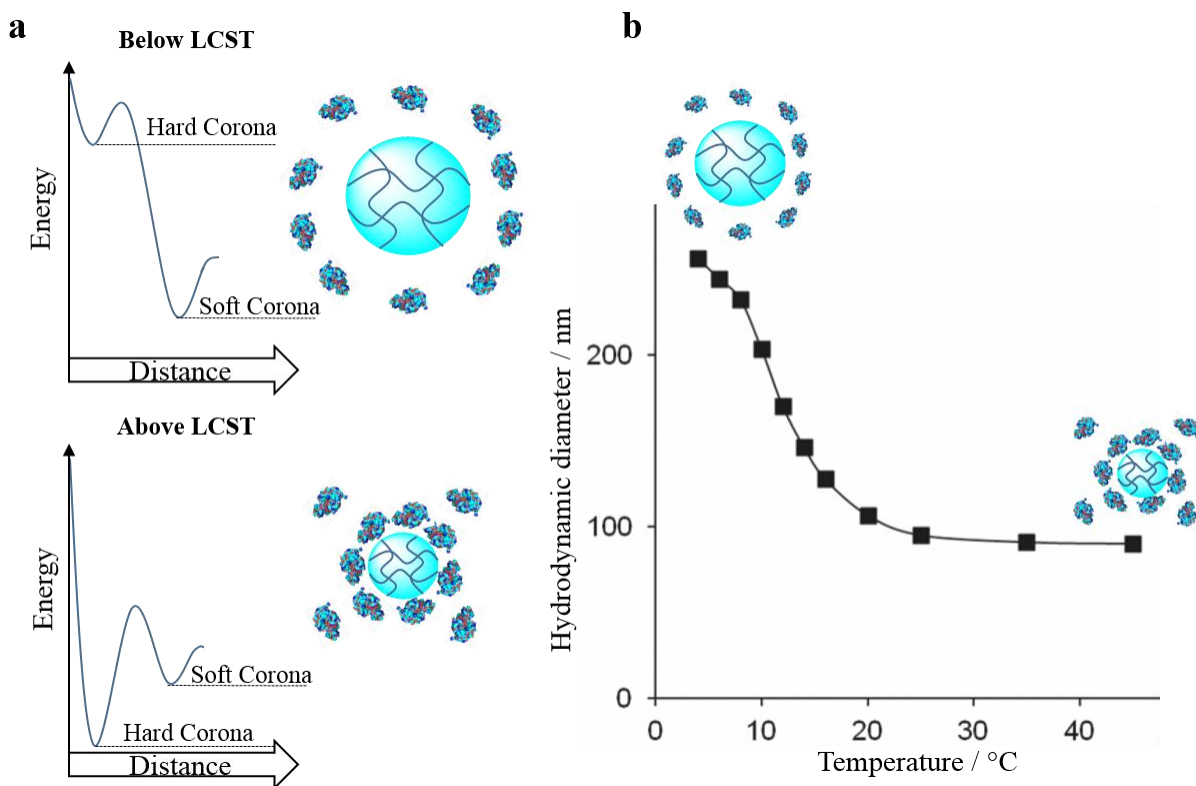
Figure 1.3. Correlation between the (a) energy of the hard and soft corona above and below the lower critical solution temperature (LCST) and (b) hydrodynamic diameter above and below the LCST.

E. Thermodynamics of interaction

The thermodynamics of the NP-biomacromolecule interaction arises from multiple physical and chemical parameters. These include both conditional parameters such as temperature, pH, and ionic strength, and physicochemical characteristics of the NP and biomacromolecule of interest. To elucidate how these parameters influence NP-biomacromolecule binding, a systematic study was conducted using acrylamide and NIPAm based copolymers and the biomacromolecule heparin.[13]

In this isothermal titration calorimetry (ITC) study, heparin was titrated against solutions of NIPAm-based NPs synthesized by precipitation polymerization, and acrylamide (AAm)-based NPs synthesized by emulsion polymerization (Figure 1.4). Heparin is a polysulfated linear

polysaccharide with repeating disaccharide units containing uronic acid and glucosamine moieties (Figure 1.4d).[14]   Both NPs incorporated similar loadings of (3-acrylamidopropyl) trimethylammonium chloride (ATC) a positively charged monomer to complement the negatively charged (polyanionic) heparin biomacromolecule. Both NPs bind to heparin, however the ITC data indicates that the interaction between the two types of NPs (AAm and NIPAm-based) are fundamentally different. The AAm NP-heparin interaction is enthalpically driven (Figure 1.4a) while the NIPAm NP-interaction is entropically driven (Figure 1.4b). Although electrostatics contribute to binding in both systems, the striking difference can be attributed to differences in the chemical properties of the core monomers, NIPAm and AAm. AAm-heparin affinity is due in large part to its hydrogen bonding capacity with the AAm polymer backbone. NIPAm NPs are not as strong of a hydrogen bond donor compared to AAm. Consequently, upon binding of a biomacromolecule such as heparin to a NIPAm NP, heparin displaces water molecules leading to an observed interaction that is overall entropically driven. Moreover, at 35 °C, above LCST, the association constant (Ka) for the NIPAm NP to heparin increases from 1.2×10^6 M to 2.5×10^6 M (Figure 1.4c). This observation highlights the potential utility of turning on and off the protein affinity with temperature, pH and ionic strength.
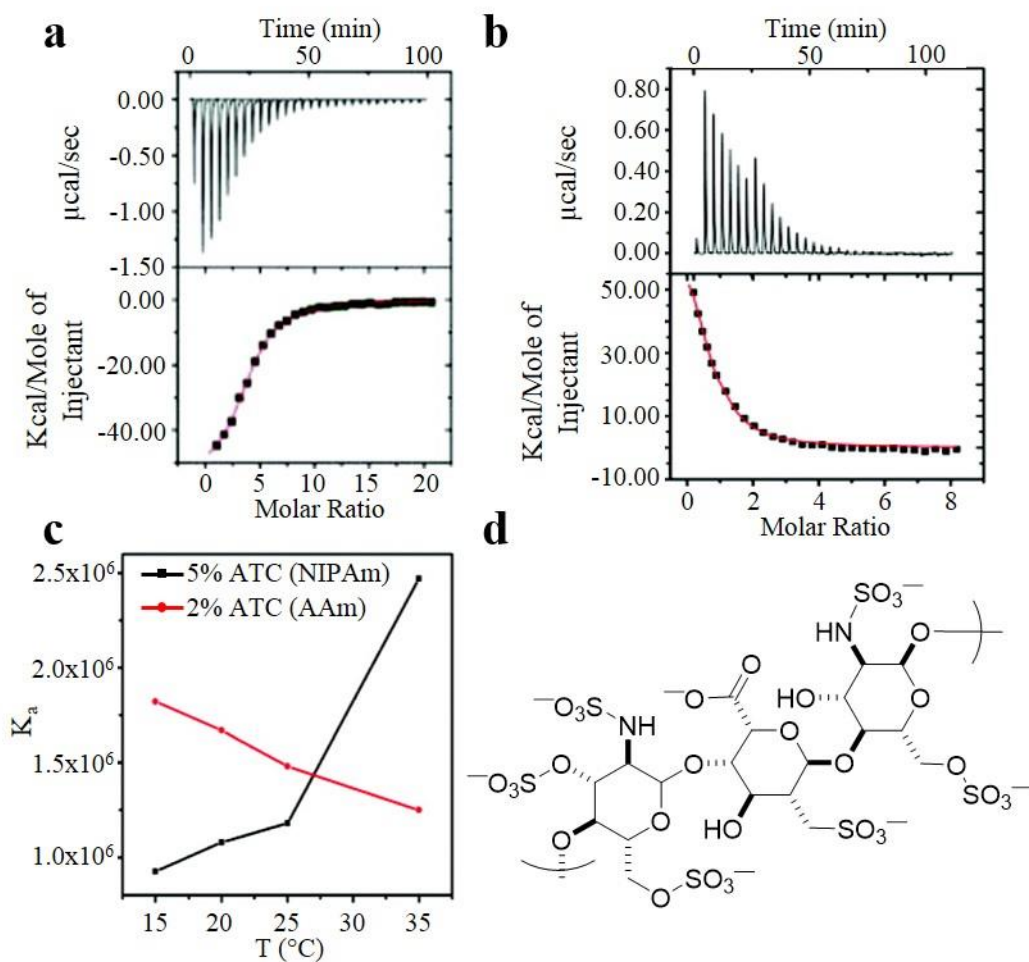
Figure 1.4. Isothermal titration calorimetry (ITC) study of the heparin-NP interaction using (a) 2% ATC AAm NPs and (b) 5% ATC NIPAm NPs. (c) Change in heparin affinity as a function of temperature for NIPAm (black) NPs and AAm (red) NPs. (d) Structure of heparin.

F. NP Heterogeneity

The free-radical polymerization used to synthesize NIPAm-based NPs is kinetically driven which produces a random distribution of functional monomers along the polymer chain. Without control of the monomer sequence, NPs are compositionally homogeneous on average but heterogeneous with respect to one another. The NPs can therefore be characterized as crude polyclonals. However, the backbone of a NIPAm based NP is aliphatic and sp3 hybridized, and has considerable conformational flexibility compared to more rigid, amide-linked proteins.

9

Therefore, a large number of multi-stranded three-dimensional conformations and sequences are presented simultaneously. Nevertheless, some progress has been made in tightening the affinity distribution of synthetic polymer NPs. This strategy takes advantage of the nano-sized NP, which permits "purification" by affinity chromatography. A NP sample with a broad distribution of affinity for the peptide toxin melittin, the principle toxic component of honey-bee venom, was enriched (purified) using an affinity purification strategy.[15] Low (μM) affinity NIPAm NPs incorporating *N*-tert-butyl acrylamide (TBAm) and acrylic acid (Aac) were shown to neutralize the cytotoxicity of melittin.[16] To enhance the average affinity of the ensemble of NPs, biotinylated melittin was loaded onto a streptavidin agarose column and the heterogeneous NP solution was eluted through the column. At room temperature (above LCST), where these NPs were collapsed, high-affinity NPs remained on the column while the lower affinity NPs eluted. Once the temperature was reduced below the LCST, the now solvent swollen NPs were released from the melittin containing affinity column and collected. This resulted in a purified NP solution that had nM affinity to melittin when analyzed by quartz crystal microbalance (QCM), and displayed a narrowed distribution of affinity with respect to the initial NP sample.[15]

G. Catch and release

The dynamic, temperature dependent affinity for NPs can also be used to purify targeted proteins from a complex mixture. To demonstrate, a library of NPs each with a unique composition was screened for high affinity and selectivity to lysozyme, a 14 kDa basic protein (isoelectric point (pI) = 9.3).[17] The NPs featured various feed ratios of TBAm and Aac and were analyzed for their temperature responsive lysozyme affinity. The lead NP, synthesized with a feed ratio of 40% TBAm, 5% Aac, 53% NIPAm, and 2% Bis, had an LCST of~13°C, and therefore high affinity for lysozyme at room temperature but below 10 °C, became solvent swollen and released lysozyme.
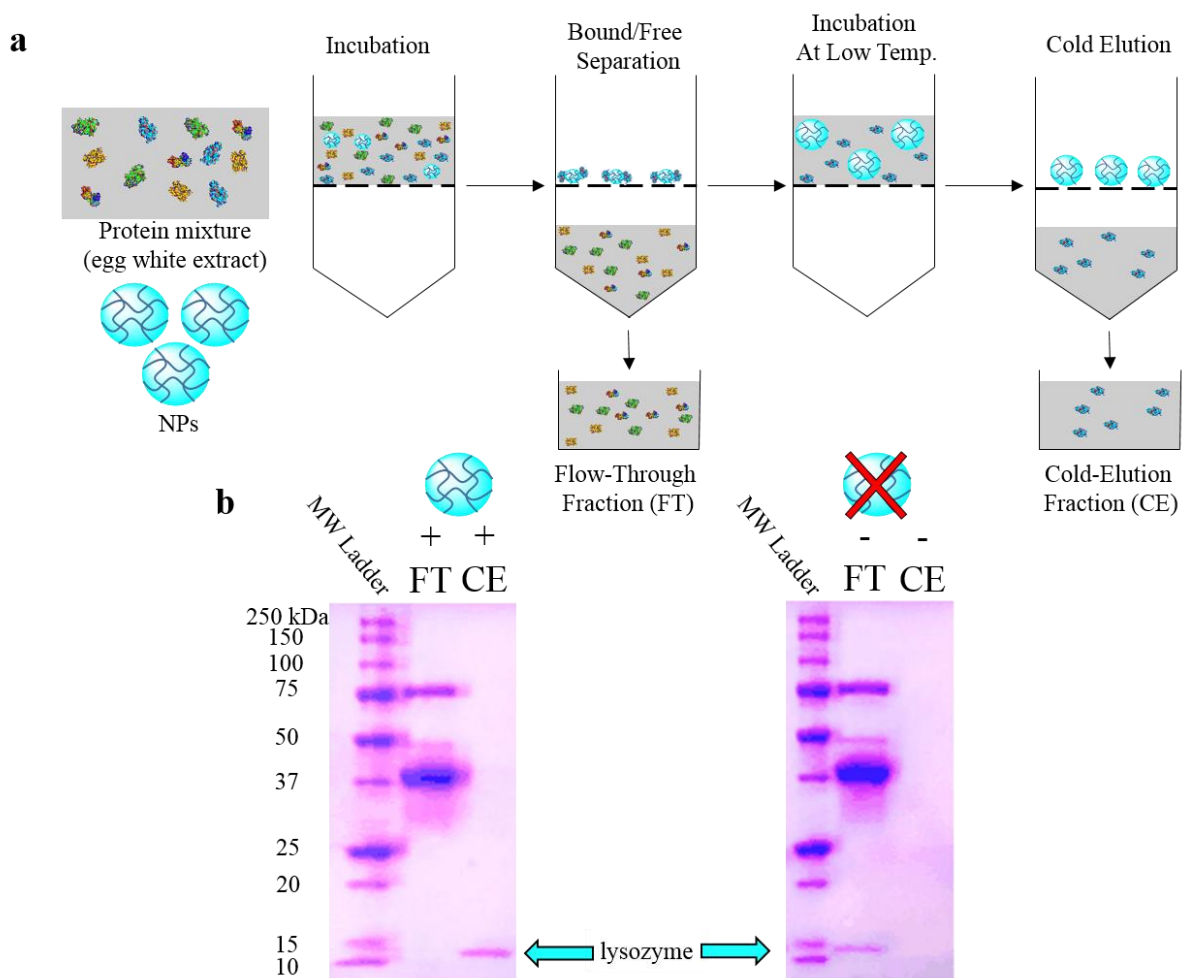
Figure 1.5. Purification of lysozyme from egg white via temperature dependent NP-lysozyme affinity. (a) NPs, above their LCST, are incubated and filtered via centrifugation (Flow-through, FT). The protein(s) bound to the NP are released by treating with cold buffer and filtered via centrifugation (cold elution, CE) releasing protein (lysozyme) from the NP. (b) SDS-PAGE analysis with NPs (+) and without NPs (-).

This NP had considerable selectivity for lysozyme (4% w/w-total protein in egg white) over the more than 40 proteins found in chicken-egg white as shown through centrifugation filtration and SDS-PAGE analysis (Figure 1.5). Other egg white proteins including ovalbumin (pI = 4.7) and ovotransferrin (pI = 6.1) showed negligible affinity to the NP when incubated at pH 7.4, and two basic proteins, RNase A (pI = 8.6) and avidin (pI = 10.0) had substantially less affinity compared to lysozyme. This establishes that the observed affinity for lysozyme is a result of both

hydrophobic and electrostatic complementarity. The NP bound lysozyme was eluted during cold (<10 °C) filtration and retained enzymatic function. After two purification cycles, 79% of purified lysozyme was recovered (Figure 1.5).[17] These results demonstrate that a NIPAm-based NP can be engineered with high affinity and selectivity for a target protein and function in a complex biological milieu.

H. NPs mimicking heat shock proteins
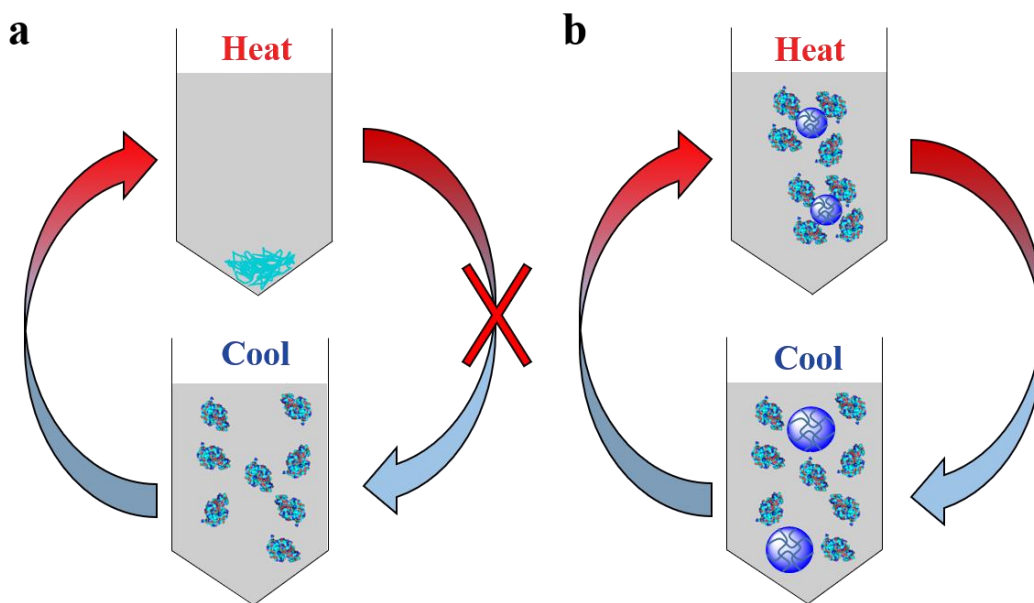
Figure 1.6. Effect of heat on the stability of a protein (a) without NPs and (b) in the presence of NPs.

The degree of hydrophobicity in a NP often dictates the LCST. In many cases, increasing the hydrophobicity is inversely correlated with the LCST. This is useful for engineering synthetic polymer NPs that function as heat shock proteins. Exposing proteins to heat can result in denaturation, aggregation and loss of function. One method of circumventing this undesirable consequence is to utilize the dynamic, temperature dependent, affinity observed for NIPAm-based NPs to prevent protein denaturation at elevated temperatures (Figure 1.6). For NPs to function as

viable heat-protectants, it is necessary that they bind noncovalently with high affinity at elevated temperatures, but release the targeted protein at low temperature so that they can be easily separated from the protein. For practical applications, it is advantageous to engineer the NP such that it is only weakly associated to the target protein at room temperature in order to not interfere with the protein function at room temperature or to avoid additional cooling protocols to remove protein from the NPs.

With these parameters in mind, the NP formulation optimized for purifying lysozyme from chicken-egg white was further modified to release lysozyme at room temperature.[18] This more hydrophilic NP was synthesized with a molar feed ratio of 10% TBAm, 5% Aac, 83% NIPAm, and 2% Bis and had an LCST of 42 °C. Through a lysozyme activity assay, it was shown that lysozyme subjected to temperatures 10-15 °C (85 °C) above the proteins T_m for 20 min retained 80% of its activity upon cooling back to room temperature. This strategy can be applied to stabilize therapeutic biomacromolecules such as antibodies or other thermally sensitive proteins.

I. Peptide tags for protein purification

The industrial purification of recombinant proteins often involves biosynthetic incorporation of a cleavable peptide tag to the C/N-terminus of the protein. These tags are typically removed after purification by incorporating a proteolytic cleavage site directly adjacent to the peptide tag. If high purity is required, then a tandem two-step affinity purification method is used.[19] This is often the case when using the immobilized metal ion chromatography (IMAC) system featuring His6-tagged

proteins and a Ni^{2+}-NTA column, because histidine rich proteins will often elute with the His6-tagged protein causing contamination.[20]

Based on our previous experience with NPs optimized to sequester the 26-amino acid peptide toxin melittin, we began developing a truncated non-cytotoxic version of melittin that retained its affinity for the optimized NP. It was discovered that the toxin melittin could be reduced to 15 key amino acids and still retain nearly all of its NP affinity. Moreover, this truncated peptide sequence did not display any hemolytic toxicity making it a suitable candidate as a protein fusion tag.[21]
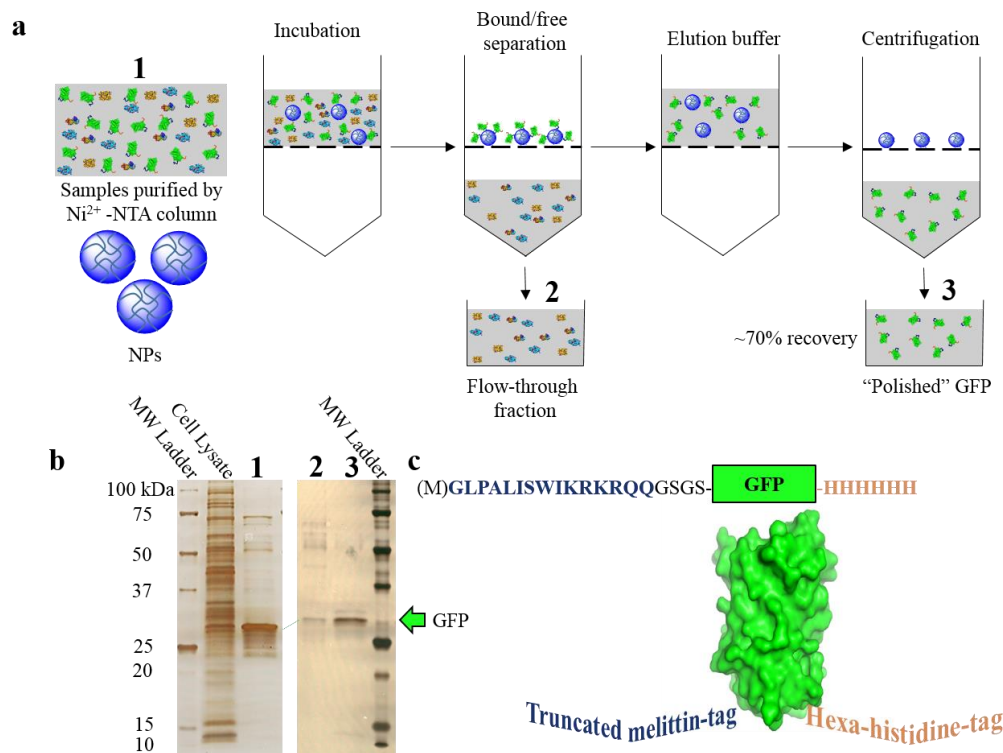
Figure 1.7. (a) Protein purification procedure using centrifugation filtration to "polish" Ni^{2+}-NTA purified GFP. (b) SDS-PAGE analysis of the initial cell lysate, (1) Ni^{2+}-NTA purified sample, (2) flow-through sample from polishing procedure, (3) polished GFP. (c) Illustration of truncated melittin tag (blue) and hexa-histidine tag (brown).

Demonstrating the utility of a synthetic polymer as a peptide-affinity reagent, green fluorescent protein (GFP) incorporating an N-terminal truncated melittin tag and thrombin cleavage site and a C-terminal His6-tag was expressed in E. coli (Figure 1.7c). Samples purified by a Ni^{2+}-NTA column were then incubated with NPs (5% Aac, 40% TBAm, 2% Bis, 53% NIPAm). Using centrifugation filtration, the NP-GFP complex was purified from the contaminating proteins. Next, the GFP was eluted from the NP using an optimized buffer system resulting in an overall 70%

recovery of active GFP determined by fluorescence intensity (Figure 1.7a). Analysis of the final elution fraction by SDS-PAGE suggests that the epitope tagged GFP band intensity was >95% (Figure 1.7b).

J. NPs that target larger proteins

Many biomacromolecules used in research and therapeutic settings are substantially larger than lysozyme and possesses complex quaternary structures. Of particular interest is the antibody protein known as immunoglobulin G (IgG), a 150 kDa protein composed of two identical 50 kDa heavy chains, and two identical 25 kDa light chains resulting in a distinctive Y-shaped tetrameric fold. Recombinant IgG has been developed with many functions including use as protein affinity reagents for separations, diagnostics and for therapeutic applications.

IgG is produced by recombinant technology and requires extensive purification prior to in vitro or in vivo use. A key step in the process involves purification with protein A or protein G affinity chromatography. These proteins bind to the conserved Fc domain of IgG, and are used to purify all recombinant IgG regardless of the composition of the variable region. However, these biogenic affinity reagents agents also require extensive purification as they themselves are biosynthetically produced. Hence, developing a relatively inexpensive synthetic polymer alternative IgG protein affinity reagent could reduce costs and broaden the availability of IgG-based reagents.

For an effective abiotic IgG purification strategy, it is necessary for the affinity reagent to bind to the conserved (Fc) region of IgG, much like protein A/G. Second, the affinity should be reversible under mild conditions in order to separate the purified functional IgG. To satisfy these requirements, NPs were optimized to bind the Fc-domain of IgG. NPs synthesized with a feed ratio of 20% Aac, 40% TBAm, 2% Bis, and 38% NIPAm interacted strongly with the Fc fragment

and Fc-oriented IgG.[22] Moreover, the NP exhibited little affinity for common proteins including bovine serum albumin, TNFα, and hemoglobin.

The optimized NP had high affinity to Fc-oriented IgG at pH 5.5, and outcompeted protein A at this pH. However, at pH 7.4, NP affinity dropped significantly and protein A had greater affinity. X-ray structural analysis of the protein A-IgG interaction suggests that there are a number of histidine residues (pKa = 6).   involved with binding.[23] NPs that bind to targeted biomacromolecules through electrostatic complementarity often exhibit pH dependent interactions. At low pH (5.5), negatively charged carboxylate containing NPs bind to the protonated histidines of the Fc domain of IgG. At pH 7.4, the histidines on IgG are neutral. The electrostatic NP-IgG attraction is reduced but the hydrophobic interaction between protein A and IgG now dominates. The pH control is useful for NP-protein interactions that are dependent on the charged state of histidine. The competition binding studies with protein A establish that a synthetic polymer NP can be engineered with affinity to a specific domain of a large protein.

These findings suggest that optimized synthetic NPs have the potential to serve as an alternative to current IgG purification methods. The work presented has since been used as a platform to develop NP formulations capable of purifying IgG from cell lysate. This promising application of pH dependent NP affinity reagents will be reported on soon.

K. Evaluating positively charged groups on NP-Protein affinity.

Engineering the chemical composition of a NP to optimize affinity for a specific protein can present a number of choices of functional groups. For example, if a positively charged monomer is needed there are many to choose from. To evaluate the effectiveness of positively charged NPs to interact with biomacromolecules, three positively charged monomers bearing guanidinium,

primary amine, or quaternary ammonium functional side chains were incorporated into NPs and

their interaction with several biomacromolecules was compared.
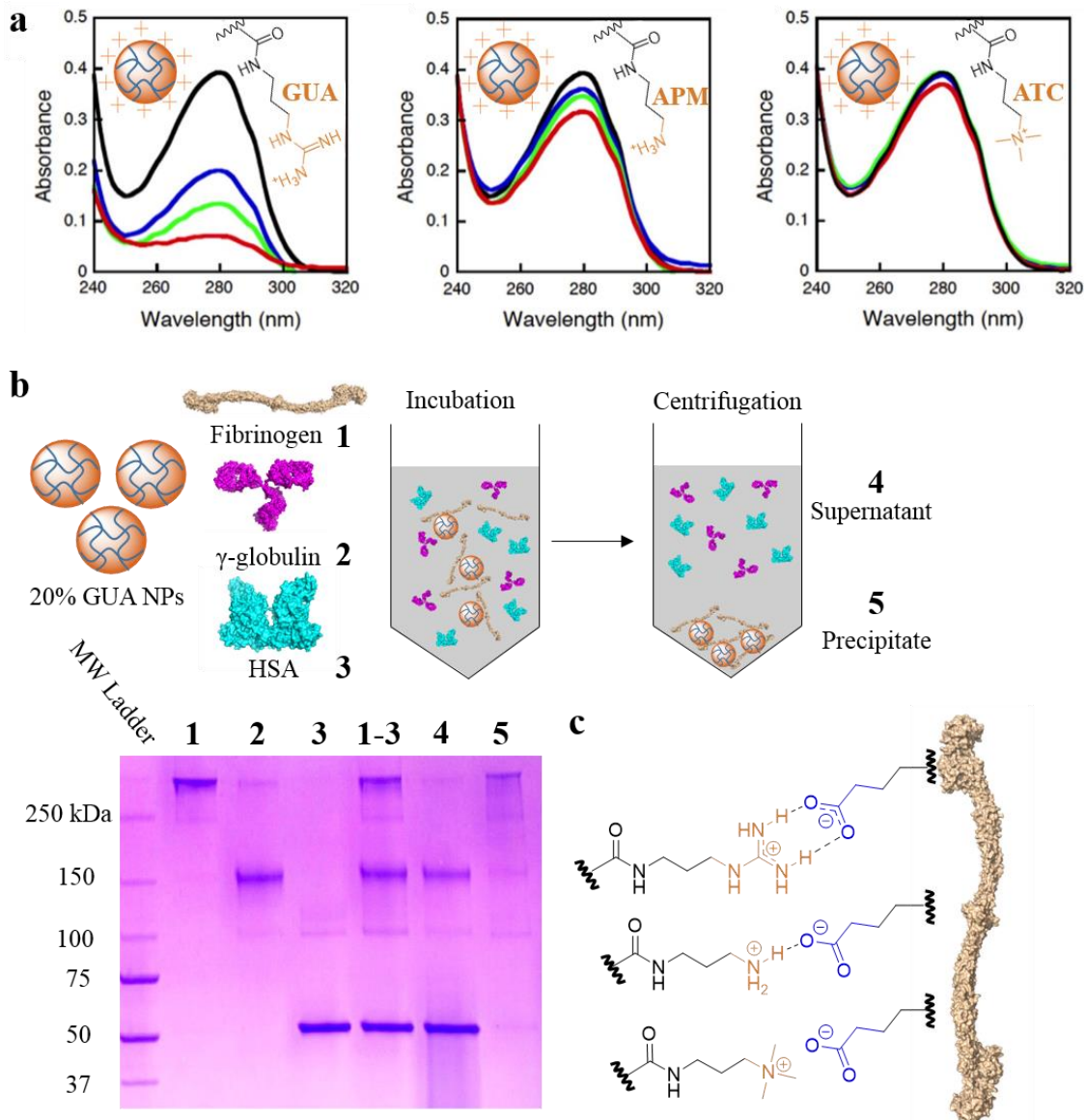
Figure 1.8. (a) Analysis of the interaction of positively charged NPs and fibrinogen by centrifugation filtration. Fibrinogen without NPs (black) 5%, 10%, and 20% charged monomer are represented by blue, green and red respectively. (b) Selective precipitation of fibrinogen by 20% GUA containing NPs in the presence of γ-globulin and HSA analyzed by SDS-PAGE. (1) fibrinogen, (2) γ-globulin, (3) HSA, (4) Supernatant after centrifugation, and (5) Precipitate after centrifugation. (c) Difference in hydrogen-bonding capabilities of GUA, APM, and ATC monomers.

A library of NPs consisting of 40% TBAm, 2% Bis, and varying amounts of either N-(3-methacrlamidopropyl)guanidinium chloride (GUA), N-(3-aminopropyl)methacrylamide (APM), or (3-acrylamidopropyl)triethylammonium chloride (ATC) (at the expense of NIPAm) were evaluated for their ability to bind to various proteins (Figure 1.8).[9] None of the positively charged NPs interacted strongly with any of the basic proteins (avidin, ribonuclease A, and myoglobin). However, the guanidinium containing NP appeared to interact with considerable selectively for fibrinogen (pI = 5.5) over γ-globulin (pI = 6.9) and human serum albumin (pI = 4.6). The total binding across all three NPs correlated to the number of H-bond donors found on each of the positively charged monomers (Figure 1.8a). NPs synthesized with the GUA monomer have two hydrogen bond donors for each GUA monomer as compared to APM and ATC which have one and zero hydrogen bond donors respectively (Figure 1.8c).

Fibrinogen is a relatively hydrophobic acidic protein that has an elongated structure (45 nm). Considering the GUA-NP had a hydrodynamic diameter of 27 nm, incubating the NP with fibrinogen resulted in precipitation likely due to cross-linking by the multivalent NP. This precipitation event was not observed for the other NP-protein interactions. The precipitation permitted isolation of fibrinogen from a mixture of fibrinogen, γ-globulin, and human serum albumin (Figure 1.8b). The precipitated fibrinogen could be reconstituted by incubating the NP-fibrinogen mixture in acidic buffer (citric acid buffer, pH = 4.0), which resulted in a 50% recovery of native-fibrinogen by centrifugation filtration as determined by circular dichroism. Although the selectivity observed for fibrinogen may be driven by affinity precipitation, these results establish the importance of hydrogen bonding in NP-protein interactions. Long range charge-charge interactions are important for initial interactions and likely influence the composition of the early protein corona. However, the likely proton transfer event from a positively charged NP

to a negatively charged carboxylic acid on a protein is necessary to provide a thermodynamic bias for a particular protein in the entropically unfavorable hard corona. A similar case was observed for NPs optimized for the polycationic protein histone. NPs synthesized with 40% TBAm, 2% Bis, and 5 or 20% Aac or vinyl sulfonate (SAc) at the expense of NIPAm, were analyzed for their ability to bind and sequester histone. The 20% Aac containing NPs were able to bind and sequester nearly 100% of the histone, whereas the 20% SAc NPs were only successful at sequestering ~17% as determined by centrifugation filtration and UV-Vis spectroscopy (A_{280}).[24] This is consistent with the hypothesis that strong hydrogen bond acceptor/donor pairs in addition to electrostatic complementarity are necessary for strong NP-protein binding.
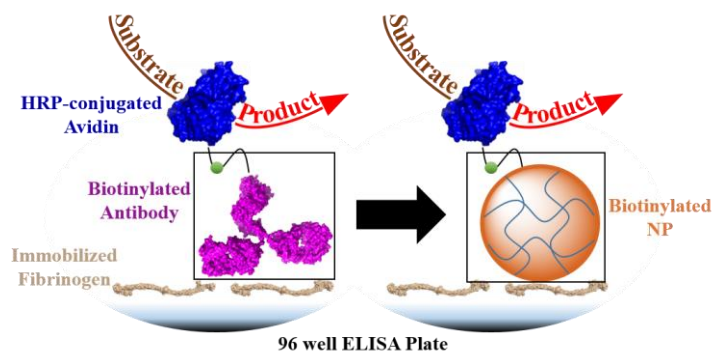
Figure 1.9. ELISA-mimic NP screen for discovering high affinity NP formulations (right) inspired by the standard ELISA (left).

These results, gathered from QCM and centrifugation filtration, were replicated in a modified enzyme-linked immunosorbent assay (ELISA).[24] In ELISA, a sample is first immobilized onto the surface of the well and a target specific antibody featuring a biotinylated Fc-domain (non-antigen binding domain) is incubated and washed extensively. Next, horseradish peroxidase (HRP) conjugated with avidin is added and again washed extensively to remove excess HRP-avidin. Finally, the HRP substrate mixture is added to each well producing a colorimetric change that can be quantified by monitoring the change in absorbance at 492 nm (Figure 1.9). In this modified ELISA, solutions of histone or fibrinogen were immobilized onto a multi-well plate. Instead of

histone or fibrinogen-specific antibodies, biotinylated (1 mol%) NPs of varying compositions are used. Considering the specific antigen is known (histone and fibrinogen), the independent variable for this modified ELISA is the NP composition. Therefore, the colorimetric change observed upon adding the HRP-avidin and the HRP substrate mixture is directly correlated to the NPs intrinsic affinity for the immobilized biomacromolecule (histone or fibrinogen).

Since libraries of NPs are easily synthesized, a variety of compositions are available for screening against targeted biomacromolecules. However, in many cases, the analytical method used to detect the interaction is time consuming and is low-throughput. Therefore, by using an analytical method capable of functioning in a multi-well plate, such as the ELISA-mimic assay, high affinity NP formulations can be evolved rapidly, which is necessary for developing a catalog of synthetic polymer NP formulations with targeted protein affinity.

L. NPs for toxin sequestration

NPs optimized to bind and sequester cytotoxic biomacromolecules have the potential to function as an alternative therapeutic antidote. For a NP to function efficaciously in vivo, it must bind with considerable selectivity and sequester the biomacromolecule in the slowly exchanging hard corona. Furthermore, following sequestration, the NP complex must remain non-toxic until cleared from the bloodstream and eliminated.

NPs with engineered affinity for the peptide toxin melittin are candidates for use as an abiotic antidote. Melittin, the principle component of honey bee venom, is a pore forming toxin that lyses red blood cells (Figure 1.10b).[25] Thus, the activity of the peptide can be monitored through a hemolytic assay (Figure 1.10a). Using this strategy, it was discovered that NPs synthesized with the hydrophobic TBAm and negatively charged Aac monomers were effective for the neutralization of the peptide toxin. Efficiency was optimized by a systematic variation of the feed

ratio of both of these monomers. This resulted in an increased neutralization constant and binding constant of the NP to melittin. The NPs themselves were shown to be non-toxic toward HT-1080 cells using a cell viability assay.

Following in vitro testing, two lead NP formulations synthesized with a feed ratio of 40% TBAm, and 5% or 40% Aac were subjected to in vivo biocompatibility studies. NPs (10 mg/kg) were injected into mice, and the change in body mass of the mice was monitored over 14 days. Compared to the control (isotonic glucose solution), no significant weight change was observed for either NP. Furthermore, the NPs exhibited no signs of immunogenic response. Next, these NPs
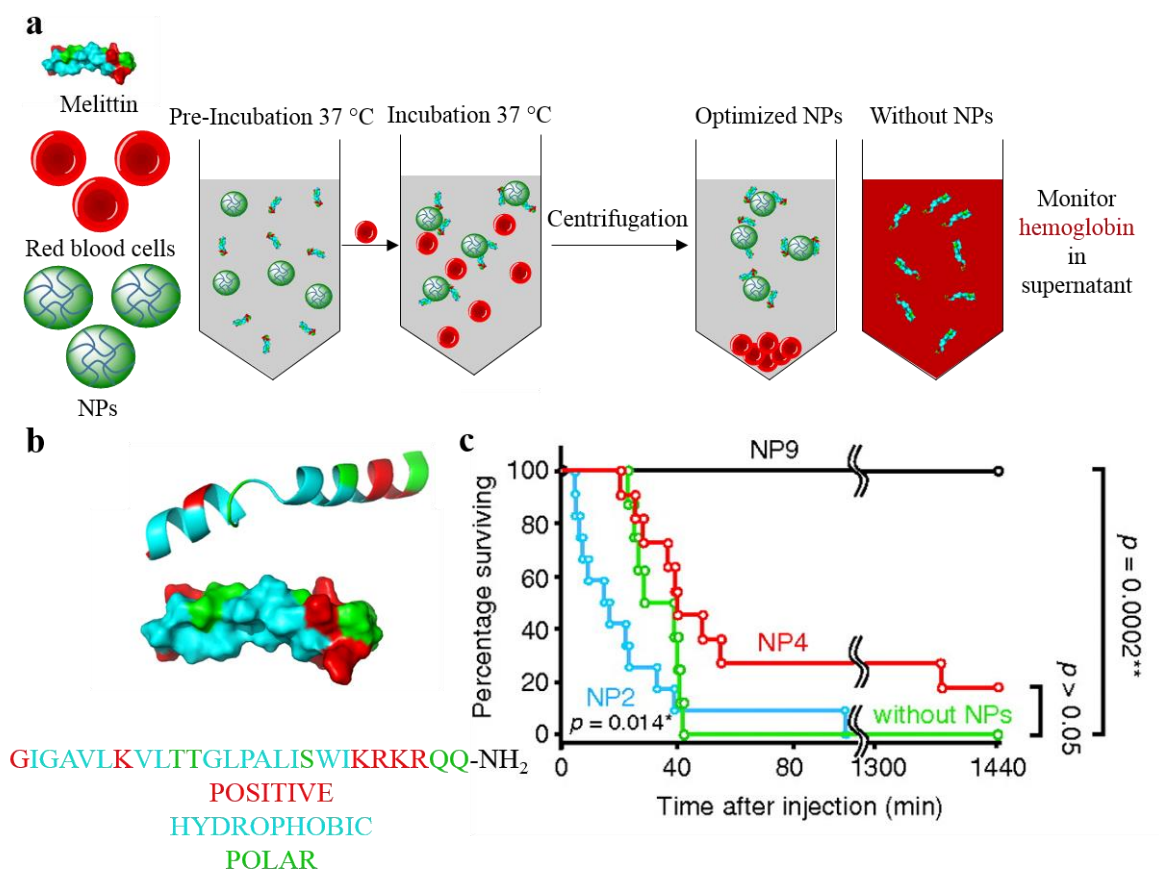
Figure 1.10. (a) Red blood cell assay used to identify NPs capable of neutralizing the hemolytic toxin melittin. (b) Crystal structure and sequence of the amphiphilic peptide melittin. (c) Survival rates of mice intravenously administered with 4.5 mg/kg melittin (green) and 30 mg/kg of NP2 (blue, 40% TBAm, 2% Bis, 58% NIPAm), NP 4 (red, 40% TBAm, 5% Aac, 2% Bis, 53% NIPAm), or NP9 (black, 40% TBAm, 40% Aac, 2% Bis, 18% NIPAm).

were assessed for their ability to detoxify melittin in vivo. A lethal dose of melittin (4.5 mg/kg) was administered intravenously followed by NPs (30 mg/kg) and the inhibition of melittin was monitored as a function of survival rate over 24 h. Mice injected with the optimized NP formulation with a feed ratio of 40% TBAm, 40% Aac, 18% NIPAm, and 2% Bis (NP 9) had a 100% survival rate, which was significantly higher than any other NP formulation tested (Figure 1.10c). Ex-vivo analysis of mice administered fluorescently labelled analogs of NP 9 and melittin indicates that the NP-melittin complex accumulated in the liver and kidney. Moreover, the melittin and NPs appear to accumulate in the same macrophages within the liver. Although the exact mechanism by which these NPs are cleared from the liver remains unclear, these preliminary results suggest that optimized NPs have the potential to function in vivo as an inexpensive therapeutic sequestrant.

M. Phenol-soluble modulin 3 (PSMα3)

Methicillin resistant Staphylococcus aureus (MRSA) is a pathogenic bacterium capable of releasing peptide and protein toxins that dismantle the host immune system. Of the various toxins secreted by different MRSA strains, the peptide phenol-soluble modulin α3 (PSMα3) is known to be released by the most lethal strains. PSMα3 aids in dismantling the host immune system by lysing human polymorphonuclear neutrophils (PMNs), which play a fundamental role in the innate immune system. Thus, developing a high-affinity NP capable of recognizing and neutralizing PSMα3 could reduce the pathogenesis of highly virulent MRSA strains and increase the survival of important PMNs.

The lytic activity of PSMα3, was used as an initial screen to identify lead NP formulations capable of inhibiting PSMα3 from lysing red blood cells. The primary sequence of PSMα3 contains a large number of aromatic amino acids, and therefore a variety of aromatic monomers

were included in the pool of monomers used to generate the NP library. NPs synthesized with a feed ratio of 20% Aac and 20-40% aromatic monomers (N-phenylacrylamide (PAA) or pentafluorophenyl acrylamide (5FPAA)) neutralized PSMα3 significantly better than NPs featuring only TBAm as the hydrophobic monomer. Moreover, upon subjecting PSMα3 and the lead NPs to a cell viability assay using human promyelocytic leukemia cells (HL60), which are closely related to PMNs, the NPs synthesized with aromatic monomers produced results indistinguishable from the control (no PSMα3).[26] This indicates that the NPs featuring aromatic monomers are not themselves cytotoxic, and that they are effective at inhibiting PSMα3 regardless of the cell type. To this extent, the apparent interaction between a NP formulation synthesized with 20% Aac, 20% 5FPAA and 20% TBAm versus a NP synthesized with 20% Aac and 40% PAA with PSMα3 was minimal. However, when the hemolytic red blood cell assay was performed in the presence of human serum albumin (HSA), the two NPs performed differently. The 40% PAA NP showed a slight decrease in %neutralization in the presence of HSA while the 5FPAA containing NP was not affected by the presence of HSA. Thus, substituting PAA for 5FPAA may allow for greater selectivity for PSMα3 in the hard corona over other biomacromolecules.

N. NP lipophilicity

An important aspect of hydrophobic NIPAm-based NPs is that they interact favorably with lipophilic molecules. Dawson and co-workers have previously shown that 50:50 NIPAm: TBAm NPs will bind, with considerable selectivity, to apolipoprotein A-1 when incubated in human serum.[5] This striking selectivity lead to subsequent studies showing that this NP composition will bind to high density lipoprotein particles.[27] The similarities between the optimized NPs capable of neutralizing melittin and PSMα and the 50:50 NIPAm: TBAm NP suggests that these NPs are also lipophilic. Considering both of these toxins function through lipid association, hydrophobic

NIPAm based NPs are therefore ideal for lipid-bound toxin sequestration. It is therefore likely that other lipid-mediated toxins can also be sequestered by similar NPs and function as therapeutic sequestrants. We are currently pursuing this line of research.

O. Outlook

The aqueous precipitation polymerization used to synthesize NIPAm-based NPs offers a facile and inexpensive platform for developing large, chemically diverse libraries of NPs. This highly compatible system allows for protein corona tuning through directed synthetic evolution. Thus far, significant progress has been made in understanding both fundamental and application-based aspects of NP-biomacromolecule interactions. The initial successes were made with an almost embarrassing small selection of functional monomers. However, as the pool of monomers grows to include other multifunctional monomers and other types of functional monomers, new NP-biomacromolecule affinity pairs will undoubtedly result. Ultimately, incorporating a high-throughput synthesis and analysis technique will likely lead to rapid generation of inexpensive and uniquely selective NPs suitable for biomarker detection, protein purification/stabilization, and antibody-replacing medication.

P. References

(1)   Walkey, C. D.; Chan, W. C. W.: Understanding and controlling the interaction of nanomaterials with proteins in a physiological environment. *Chem. Soc. Rev.* **2012**, *41*, 2780-2799.

(2)   Monopoli, M. P.; Aberg, C.; Salvati, A.; Dawson, K. A.: Biomolecular coronas provide the biological identity of nanosized materials. *Nat. Nanotechnol.* **2012**, *7*, 779-786.

(3)   Fleischer, C. C.; Payne, C. K.: Nanoparticle-Cell Interactions: Molecular Structure of the Protein Corona and Cellular Outcomes. *Acc. Chem. Res.* **2014**, *47*, 2651-2659.

(4)   Nel, A. E.; Madler, L.; Velegol, D.; Xia, T.; Hoek, E. M. V.; Somasundaran, P.; Klaessig, F.; Castranova, V.; Thompson, M.: Understanding biophysicochemical interactions at the nano-bio interface. *Nat. Mater.* **2009**, *8*, 543-557.

(5)   Lundqvist, M.; Stigler, J.; Elia, G.; Lynch, I.; Cedervall, T.; Dawson, K. A.: Nanoparticle size and surface properties determine the protein corona with possible implications for biological impacts. *P. Natl. Acad. Sci. U.S.A.* **2008**, *105*, 14265-14270.

(6)   Monopoli, M. P.; Walczyk, D.; Campbell, A.; Elia, G.; Lynch, I.; Bombelli, F. B.; Dawson, K. A.: Physical-Chemical Aspects of Protein Corona: Relevance to in Vitro and in Vivo Biological Impacts of Nanoparticles. *J. Am. Chem. Soc.* **2011**, *133*, 2525-2534.

(7)   Yoshimatsu, K.; Koide, H.; Hoshino, Y.; Shea, K. J.: Preparation of abiotic polymer nanoparticles for sequestration and neutralization of a target peptide toxin. *Nat. Protoc.* **2015**, *10*, 595-604.

(8)   Candau, F.; Leong, Y. S.; Pouyet, G.; Candau, S.: Inverse Microemulsion Polymerization of Acrylamide - Characterization of the Water-in-Oil Microemulsions and the Final Microlatexes. *J. Colloid Interface Sci.* **1984**, *101*, 167-183.

(9)   Yonamine, Y.; Yoshimatsu, K.; Lee, S. H.; Hoshino, Y.; Okahata, Y.; Shea, K. J.: Polymer Nanoparticle-Protein Interface. Evaluation of the Contribution of Positively Charged Functional Groups to Protein Affinity. *ACS Appl. Mater. Interfaces* **2013**, *5*, 374-379.

(10)   Klouda, L.: Thermoresponsive hydrogels in biomedical applications A seven-year update. *Eur. J. Pharm. Biopharm.* **2015**, *97*, 338-349.

(11)   Klouda, L.; Mikos, A. G.: Thermoresponsive hydrogels in biomedical applications. *Eur. J. Pharm. Biopharm.* **2008**, *68*, 34-45.

(12)   Schild, H. G.: Poly (N-Isopropylacrylamide) - Experiment, Theory and Application. *Prog. Polym. Sci.* **1992**, *17*, 163-249.

(13)   Zeng, Z.; Patel, J.; Lee, S. H.; McCallum, M.; Tyagi, A.; Yan, M.; Shea, K. J.: Synthetic polymer nanoparticle-polysaccharide interactions: a systematic study. *J. Am. Chem. Soc.* **2012**, *134*, 2681-90.

(14)   Jones, C. J.; Beni, S.; Limtiaco, J. F. K.; Langeslay, D. J.; Larive, C. K.: Heparin Characterization: Challenges and Solutions. *Annu. Rev. Anal. Chem.* **2011**, *4*, 439-465.

(15)   Hoshino, Y.; Haberaecker, W. W.; Kodama, T.; Zeng, Z. Y.; Okahata, Y.; Shea, K. J.: Affinity Purification of Multifunctional Polymer Nanoparticles. *J. Am. Chem. Soc.* **2010**, *132*, 13648-13650.

(16)   Hoshino, Y.; Urakami, T.; Kodama, T.; Koide, H.; Oku, N.; Okahata, Y.; Shea, K. J.: Design of Synthetic Polymer Nanoparticles that Capture and Neutralize a Toxic Peptide. *Small* **2009**, *5*, 1562-1568.

(17)   Yoshimatsu, K.; Lesel, B. K.; Yonamine, Y.; Beierle, J. M.; Hoshino, Y.; Shea, K. J.: Temperature-Responsive "Catch and Release" of Proteins by using Multifunctional Polymer-Based Nanoparticles. *Angew. Chem. Int. Edit.* **2012**, *51*, 2405-2408.

(18)   Beierle, J. M.; Yoshimatsu, K.; Chou, B.; Mathews, M. A. A.; Lesel, B. K.; Shea, K. J.: Polymer Nanoparticle Hydrogels with Autonomous Affinity Switching for the Protection of Proteins from Thermal Stress. *Angew. Chem. Int. Edit.* **2014**, *53*, 9275-9279.

(19)   Li, Y. F.: Commonly used tag combinations for tandem affinity purification. *Biotechnol. Appl. Biochem.* **2010**, *55*, 73-83.

(20)   Howell, J. M.; Winstone, T. L.; Coorssen, J. R.; Turner, R. J.: An evaluation of in vitro protein-protein interaction techniques: Assessing contaminating background proteins. *J. Proteomics* **2006**, *6*, 2050-2069.

(21)   Yoshimatsu, K.; Yamazaki, T.; Hoshino, Y.; Rose, P. E.; Epstein, L. F.; Miranda, L. P.; Tagari, P.; Beierle, J. M.; Yonamine, Y.; Shea, K. J.: Epitope Discovery for a Synthetic Polymer Nanoparticle: A New Strategy for Developing a Peptide Tag. *J. Am. Chem. Soc.* **2014**, *136*, 1194-1197.

(22)   Lee, S. H.; Hoshino, Y.; Randall, A.; Zeng, Z. Y.; Baldi, P.; Doong, R. A.; Shea, K. J.: Engineered Synthetic Polymer Nanoparticles as IgG Affinity Ligands. *J. Am. Chem. Soc.* **2012**, *134*, 15765-15772.

(23)   Martin, W. L.; West, A. P.; Gan, L.; Bjorkman, P. J.: Crystal structure at 2.8 angstrom of an FcRn/heterodimeric Fc complex: Mechanism of pH-dependent binding. *Mol. Cell* **2001**, *7*, 867-877.

(24)   Yonamine, Y.; Hoshino, Y.; Shea, K. J.: ELISA-Mimic Screen for Synthetic Polymer Nanoparticles with High Affinity to Target Proteins. *Biomacromolecules* **2012**, *13*, 2952-2957.

(25)   Raghuraman, H.; Chattopadhyay, A.: Melittin: A membrane-active peptide with diverse functions. *Bioscience Rep.* **2007**, *27*, 189-223.

(26)   Weisman, A.; Chen, Y. A.; Hoshino, Y.; Zhang, H. T.; Shea, K.: Engineering Nanoparticle Antitoxins Utilizing Aromatic Interactions. *Biomacromolecules* **2014**, *15*, 3290-3295.

(27)   Hellstrand, E.; Lynch, I.; Andersson, A.; Drakenberg, T.; Dahlback, B.; Dawson, K. A.; Linse, S.; Cedervall, T.: Complete high-density lipoproteins in nanoparticle corona. *Febs J.* **2009**, *276*, 3372-3381.

Chapter 2

Chemical cross-linking in hydrogel nanoparticles: A systematic study

A. Abstract

Stimuli-responsive poly(*N*-isopropylacrylamide) (p(NIPAm)) nanoparticle (NP) hydrogels are useful in application driven biomedical research. The Shea lab has shown that lightly cross-linked p(NIPAm) NPs functionalized with hydrophobic and negatively charged monomers can be engineered with intrinsic affinity to melittin, the active component in bee venom, and are capable of sequestering the hemolytic toxin *in vivo*. In an effort to understand how chemical crosslinking of the NP influences melittin affinity, a library of NPs was synthesized with different quantities and types of cross-linkers. Their ability to neutralize melittin was compared using an *in vitro* assay. In general, NPs synthesized with cross-linkers containing aliphatic bridges neutralized melittin more efficiently at higher cross-linking ratios. However, NPs cross-linked with 2% *N,N'*-(1,4-phenylene)bisacrylamide, a monomer capable of π-π stacking interactions, were the most efficient at neutralizing melittin. This discovery will be directly implemented in application driven research on abiotic affinity hydrogels.

B. Introduction

Poly(*N*-isopropylacrylamide) (p(NIPAm)) hydrogels have gained traction as a useful stimuli-responsive macromolecular system.[1] Soon after Pelton and Chibante reported the monodisperse synthesis of p(NIPAm) NPs,[2] they discovered that p(NIPAm) NPs are thermally responsive, that is they are solvent swollen below their lower critical solution temperature (LCST) and desolvated and collapsed above. This characteristic has been carefully studied, [3,4,5,6,7] and implemented in the development of artificial chaperones that capture and stabilize target proteins above LCST and

release proteins at temperatures below their LCST..[8,9] Stimuli other than temperature have been used to induce changes in the physical properties of p(NIPAm) NPs including pH,[10,11] ionic strength,[12,13] electrical potential,[14] and light.[15] The variety of stimuli capable of inducing a response in p(NIPAm) is why these hydrogels are worth investigating for application driven materials research.

In medicinal science, p(NIPAm) NPs have been evaluated for a variety of biomedical applications ranging from drug delivery,[16] tissue engineering,[17] and abiotic antidotes.[18,19] Alignate-polyacrylamide NP hydrogels were developed with high stiffness and toughness as an abiotic replacement for cartilage.[20] Hoshino *et al.* have demonstrated that co-NIPAm, *N*-(tert-butyl)acrylamide (TBAm), and acrylic acid (Aac) NPs can recognize and neutralize melittin, the active component in bee venom, *in vivo.*[21] Although both of these systems required additional functional monomers besides NIPAm, these studies highlight p(NIPAm) is a useful starting material for the development of biocompatible abiotic NPs.

Many p(NIPAm) NPs are co-polymerized with a cross-linking agent. Although cross-linking can result from non-covalent interactions, a number of biocompatible NPs are chemically cross-linked usually with *N,N'*-methylenebisacrylamide (MBis). While it is known that increasing the amount of MBis results in a reduced change in hydrodynamic diameter of p(NIPAm) NP hydrogels as they pass through the LCST,[22] very little is known about how alternative aliphatic cross-linkers alter the LCST and swelling behavior of p(NIPAm) NPs. Furthermore, the role cross-linking plays in NP-biomacromolecule interactions has not been fully studied. The current hypothesis regarding the binding of p(NIPAm) based NPs to biomacromolecules, such as proteins and peptides, suggests that minimal cross-linking density is preferred over highly cross-linked NPs in order to increase chain flexibility and favor a multi-point NP-biomacromolecule interaction.[19,23,24] It was previously

shown that the association and disassociation constant for NPs containing α-D-mannose groups that bind to the protein Con A, showed minimal cross-linking dependent binding.[24] However, this observation did not directly address how cross-linking alters a NP-biomacromolecule interaction under physiologically relevant conditions, and may not hold true across all NP systems.

 Investigating various cross-linkers at different incorporation ratios in a NP may elucidate fundamental aspects of how p(NIPAm) NPs function as abiotic affinity agents. Furthermore, the increase in effective local concentration of functional monomers brought upon by an increase in NP density as a result of increased cross-linking may result in greater binding affinities to a target analyte. In order to test this hypothesis, I used the well-studied melittin binding co-polymer system as my reference,[25] and compared neutralization efficiencies of NPs with different feed ratios of cross-linker using a hemolytic red blood cell assay.
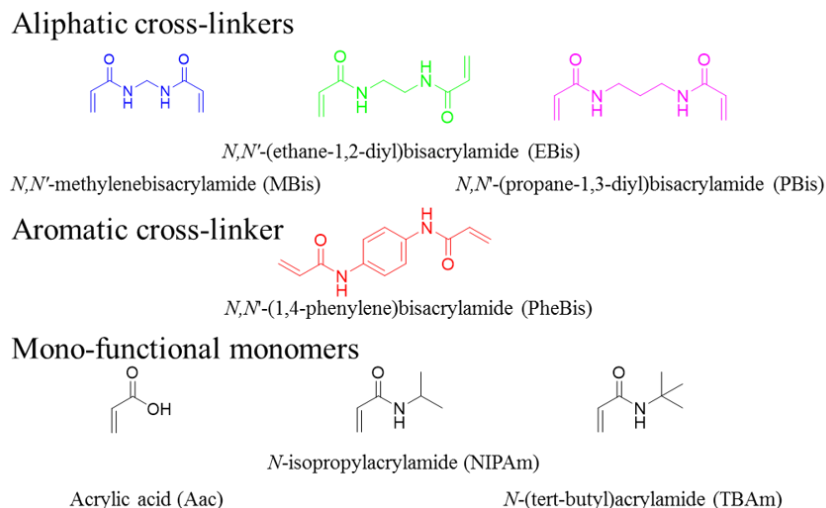
Figure 2.1. Cross-linkers and mono-functional monomers used for synthesizing NPs. NIPAm, TBAm and Aac were used in all the NPs while only one type of cross-linker was used for each NP with a feed ratio ranging from 0-25 mol%. Aac and TBAm were used to facilitate complementary non-covalent interaction of the NP to melittin.

C. Experimental

Preparation of p(NIPAm)-based NPs. A library of NPs was synthesized via an aqueous pseudo-precipitation polymerization using various ratios of monomers depicted in Figure 2.1. Information regarding room temperature polymerizations can be found in the supporting information. NPs containing 10% Aac, and 10% TBAm, X% cross-linker, and 80-X% NIPAm were synthesized at 60 ºC at either 32.5 or 65 mM total monomer concentration. Radical initiation occurred through thermal decomposition of ammonium persulfate (APS). The reaction was terminated after 3 h and purified by dialysis against deionized water, which was changed twice a day for 4 days. All of the NPs were synthesized in the presence of sodium dodecyl sulfate (0.6 mg/mL) to stabilize early oligomers and reduce particle size to a more therapeutically relevant diameter.[26] For NPs synthesized with PheBis, the cross-linker was not fully soluble initially but it was observed to dissolve as the polymerization proceeded. Yields were determined by mass recovery of a lyophilized sample of the purified NP solution. Details regarding NP compositions and synthetic conditions (Table 2.S1),and characterization (Table 2.S2-3; Figures 2.S1-S6) can be found in the supporting information.

Hemolytic Assay.[18] Bovine red blood cells (RBCs; Lampire Biological Laboratories, Pipersville, PA) were washed with phosphate buffered saline (PBS; 35 mM phosphate buffer/0.15 M NaCl, pH 7.3), collected by centrifugation (10 min, 3000 rpm), and resuspended in PBS. Washing was repeated until the supernatant was clear and colorless. In a microcentrifuge tube, melittin (1.8 µM final concentration) was preincubated with NPs (5-10 µg/mL) for 30 minutes at 37.5 ºC. Next a 6% RBC suspension was prepared in PBS and 100 µL of the suspension was mixed with the preincubated NP-melittin solution and incubated at 37.5 ºC for an additional 30 minutes. Samples were then centrifuged at 6000 rpm for 10 min, and the release of hemoglobin was quantified by

measuring the absorbance of the supernatant at 415 nm (A_{sample}). Controls for 0% and 100% neutralization consisted of RBC incubation with 1.8 µM melittin without NPs ($A_{melittin}$), and a RBC suspension without melittin and NPs ($A_{nomelittin}$). All NP samples were run in triplicate. Due to differences in final RBC concentrations, *Neutralization values are only comparable within the same assay.* However, *trends observed in neutralization are comparable between assays.* %Neutralization was calculated using the following equation:

$$(A_{sample} - A_{nomelittin}) / (A_{melittin} - A_{nomelittin}) \text{ x } 100 = \%\text{Neutralization}$$

D. Results and discussion

From previously published work, it was suggested that increasing cross-linking density results in reduced chain mobility and perhaps a reduced efficiency of neutralization of melittin.[19,23,24] However, this hypothesis has not been tested using *in vitro* assays. According to Hoshino *et al.,* NPs containing 40% TBAm, and 40% Aac showed the greatest ability to neutralize melittin via the red blood cell assay.[18] Using this composition as a starting point, I synthesized NPs and systematically increased MBis at the expense of NIPAm. No observable difference in binding was observed. Rather, it appears that NPs without any MBis neutralized melittin as efficiently as those containing the chemical cross-linker (Figure 2.S7). Given the significant electrostatic and hydrophobic complementarity to melittin, it is possible that cross-linking effects are unobservable for NPs with this level of affinity.

I decided to reduce the intrinsic affinity of the NP toward melittin to observe a change in neutralization with respect to cross-linking. To achieve this, p(NIPAm) NPs containing 10% TBAm and 10% Aac with varying amounts of cross-linker were synthesized. Furthermore, by changing the polymerization conditions to 3 h and 60 ºC, highly monodisperse NPs were synthesized with cross-linking densities as high as 20 mol% (Table 2.S2).

31

NPs cross-linked with MBis showed a direct correlation between neutralization of melittin and the degree of cross-linking, that is an increase in cross-linking incorporation resulted in greater neutralization efficiency (Figure 2.2a-b). Moreover, this trend seems to extend to NPs containing up to 15% MBis. Polymerizations with higher quantities of MBis at 65 mM total monomer concentration formed bulk gels and were not analyzed. In order to assess NPs with greater incorporations of cross-linker, the total concentration of monomers for the polymerization was reduced to 32.5 mM, and NPs containing 17% and 20% MBis were synthesized. Upon testing the difference in neutralization for NPs synthesized at 32.5 mM, it appears that twice the amount of cross-linker is required to achieve the same %neutralization as NPs synthesized at 65 mM (Figure 2.S8). Hence, it appears that the optimal amount of MBis is near the 15 mol% limit for NP synthesis at 65 mM total monomer concentration.
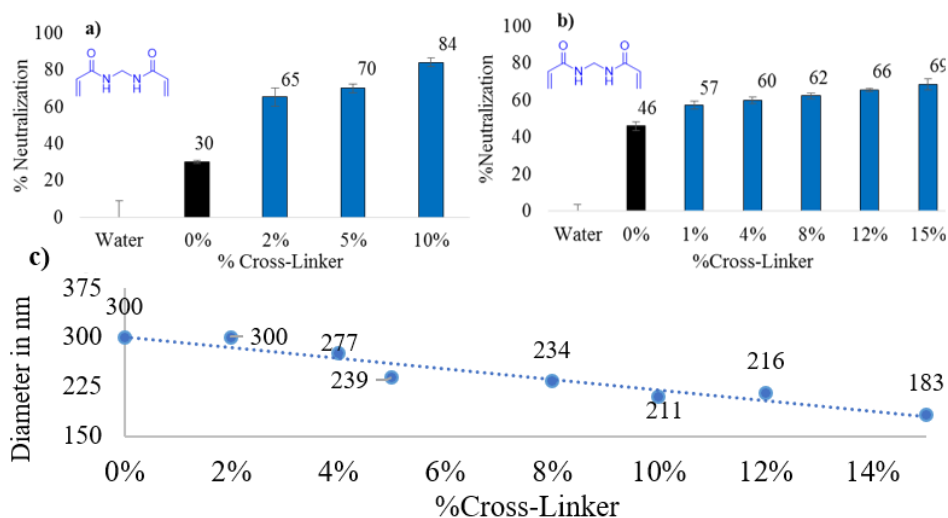
Figure 2.2. (a) RBC assay results using 10% Aac, 10% TBAm, X% MBis, and 80-X% NIPAm NPs. (b) A second RBC assay showing the reproducibility of the trend and increase in neutralization past 10% Mbis. (c) The change in hydrodynamic diameter with respect to cross-linking density under physiological conditions (PBS, 37.5 °C) for 10% Aac, 10% TBAm, X% Mbis, and 80-X% NIPAm NPs.

To establish if the trend observed in the RBC hemolytic assay is correlated with the size of the NP, the hydrodynamic diameter of each NP was measured in PBS at 37.5 °C. It appears that the size of the NP decreases linearly with increasing %MBis (Figure 2.2c). Hence, the hydrodynamic diameter is inversely correlated with the neutralization of melittin on a w/w basis. Assuming the total molecular weight of the NPs is of the same magnitude, then the density of the NP increases as a result of higher incorporation of MBis. An increase in the density and decrease in hydrodynamic volume of the NP would subsequently increase the effective concentration of functional monomers on the surface of the NP. This would reduce the entropic penalty of forming the multipoint interaction necessary for melittin neutralization. However, molecular weight data is needed to confirm this hypothesis.
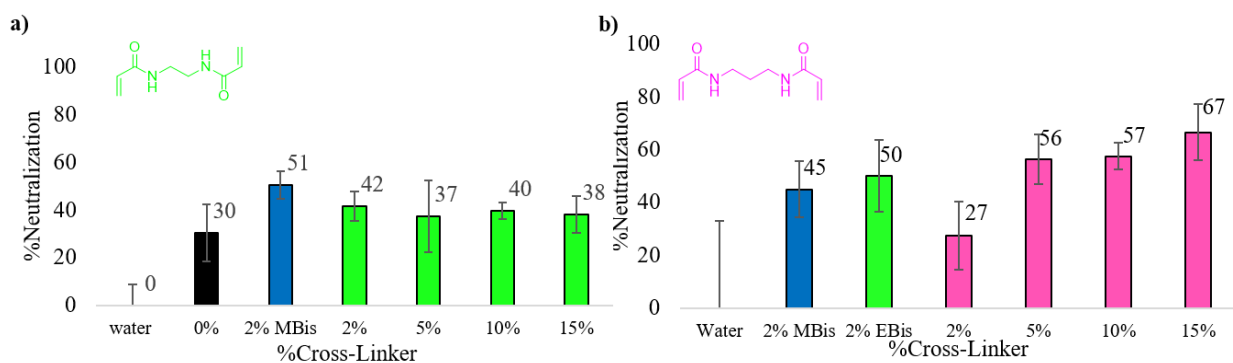
Figure 2.3. RBC assay results for NPs with various incorporation ratios of aliphatic cross-linkers. a) Assay probing the difference in %neutralization of melittin with increasing mol% EBis. b) The same study looking at PBis. All NPs assayed were synthesized with 10% Aac, 10% TBAm, X% cross-linker, and 80-X% NIPAm.

After finding a correlation between neutralization of melittin and cross-linking with MBis, I became interested in analyzing how changing the length of the aliphatic bridge in MBis would impact melittin neutralization. I synthesized NPs, as previously described, using 2-15% EBis and PBis. NPs cross-linked with PBis produced the same trend in neutralization as a function of cross-linking (Figure 2.3b), i.e., an increase in cross-linking results in greater neutralization efficiency.

However, the correlation between neutralization of melittin and cross-linking was not observed

for NPs cross-linked with EBis. Rather, all EBis NPs neutralized melittin the same (Figure 2.3a).
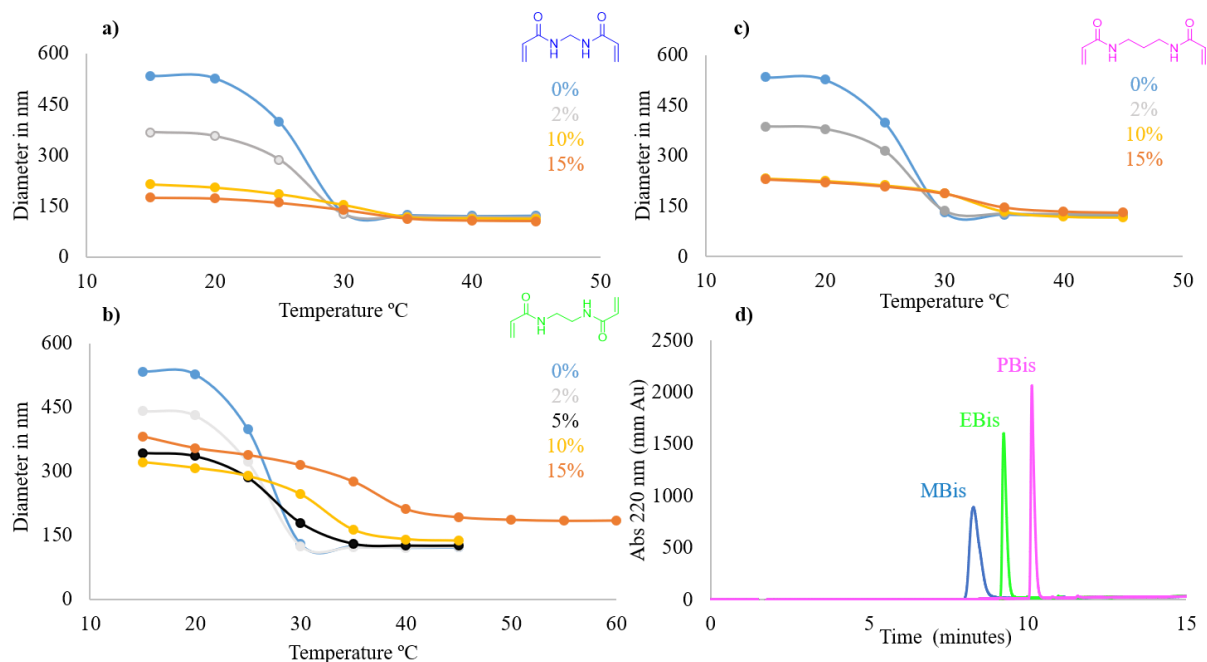
Figure 2.4. Characterization of NPs with aliphatic cross-linkers by DLS in H2O for 10% Aac, 10% TBAm, X% cross-linker and 80-X% NIPAm. a) MBis cross-linked NPs b) EBis and c) PBis. The curves generated serve as a visual guide between data points. d) Relative hydrophobicity of the aliphatic cross-linker monomers measured using reverse phase HPLC.

In order to understand the difference in neutralization trends and morphological differences

between cross-linking systems, LCST graphs were generated for each class of NP (Figure 2.4a-c).

In general, the degree of NP swelling as one passes through the LCST decreased when the amount

of cross-linker increased. However, NPs synthesized with high percentages of EBis were larger

both below and above LCST relative to MBis and PBis NPs (Figure 2.4a-c). Moreover, the 15%

EBis NP had a much larger hydrodynamic diameter than the 15% MBis and 15% PBis NPs in PBS

at 37.5 °C, the conditions used for the RBC assay (Table 2.S3). Initially it was hypothesized that

highly cross-linked EBis NPs favored a more highly hydrated core compared to MBis and PBis

cross-linked NPs due to the increased conformational flexibility compared to MBis, and reduced hydrophobicity compared to PBis. This would result in a NP with a greater hydrodynamic diameter at higher cross-linking incorporations. However, the 15% EBis NP does not reach the same final size at higher temperatures compared to the 15% MBis and 15% PBis NPs, which suggests that EBis does not result in a more hydrophilic core. Furthermore, the relative hydrophobicity of the aliphatic cross-linkers was compared using reverse-phase HPLC.[27] The results followed the trend in elution that matched the lengthening of the aliphatic bridge (Figure 2.4d), which suggests that EBis is not significantly more hydrophilic than MBis or PBis. A better explanation for the behavior observed in highly cross-linked EBis NPs may be a difference in reactivity between EBis and the other aliphatic cross-linkers. Reducing the reactivity of the cross-linker would localize its distribution toward the periphery of the NP and favor the formation of NPs with higher molecular weights. However, this has not been experimentally verified.

Discovering that highly cross-linked MBis NPs were the most efficient at neutralizing melittin led to the hypothesis that greater neutralization may be achieved if a more rigid cross-linker were used that is capable of forming additional non-covalent cross-links. Hence, I synthesized NPs containing the aromatic cross-linker, PheBis. Having an aromatic and hydrophobic cross-linker would disfavor a swollen core, and would potentially form non-covalent cross-links through π-π stacking interactions within the NP. Congruent with the hypothesis, PheBis NPs, with a targeted cross-linking density of 2%, outperformed MBis cross-linked NPs with the same targeted cross-linking density and highly cross-linked MBis NPs (Figure 2.5a). Compared to NPs cross-linked with aliphatic bridges, NPs with PheBis had a reduced hydrodynamic diameter at 2% cross-linking density under physiological conditions (Table 2.S3), and had a significantly lower LCST than the NPs synthesized with aliphatic cross-linkers (Figure 2.5b).
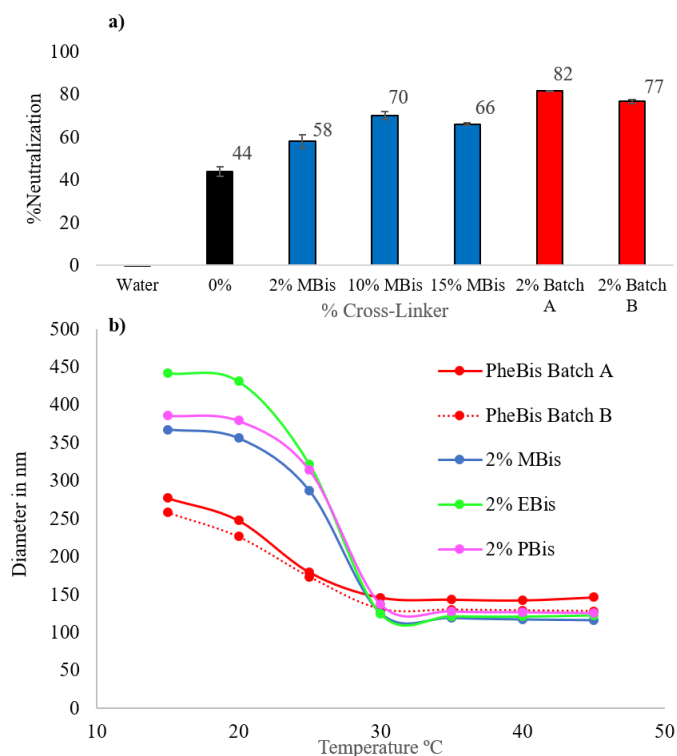
Figure 2.5. a) RBC assay results for NPs synthesized wth PheBis (red) as compared to NP synthesized with no cross-linker (black) and various amounts of Mbis (blue) b) LCST thermographs generated by DLS in H₂O for NPs synthesized with 2 mol% cross-linker. All NPs shown were synthesized with 10% Aac, 10% TBAm, X% cross-linker, and 80-X% NIPAm.

There was some concern about the incorporation of PheBis since the polymerization was not homogenous to begin with. However, LCST measurements and neutralization data for two separate PheBis NPs are consistent and the product is very monodisperse (Table 2.S2). Furthermore, broadening in the ^{1}H NMR spectra (Figure 2.S6), differences in hydrodynamic diameter compared to the 0% cross-linked NP (Table 2.S2) and absorbencies at 270-280 nm in the UV-Vis spectra (Figure 2.S9) are all indicative of PheBis incorporation.

E. Conclusion

Previous work suggests that lightly cross-linked NPs are preferred over highly cross-linked NPs when designing polymeric affinity agents. Using the initial 40% Aac, 40% TBAm system, no observable difference in neutralization was observed when changing the quantity of MBis cross-linker from 0-10 mol%. However, when the concentration of functional monomers was reduced to 10% Aac, and 10% TBAm, and polymerizations were run at 60 ℃, it became clear that increasing the concentration of MBis or PBis at the expense of NIPAm during the polymerization resulted in NPs capable of neutralizing melittin more efficiently.

EBis NPs did not follow this trend in neutralization. Rather, on a w/w basis, EBis containing NPs neutralized melittin the same regardless of cross-linking density. The LCST data suggest that highly cross-linked EBis NPs form fundamentally different NPs with larger hydrodynamic diameters above LCST compared to MBis and PBis NPs with the same cross-linking density. It is possible that the reactivity of the EBis cross-linker is lower compared to MBis and PBis resulting in NPs with greater molecular weights. However, this has not been experimentally verified. Although NPs cross-linked with EBis did not produce an increase in neutralization of melittin, this cross-linker has potential use in other hydrogel systems that require an elevated LCST since high level incorporation of EBis elevate the LCST.

Finally, using the hydrophobic and aromatic cross-linker PheBis, NPs had significantly greater neutralization efficiencies compared to NPs synthesized with comparable amounts of aliphatic cross-linkers. These results suggest that cross-linkers capable of other non-covalent interactions, such as π-π stacking, produce NPs that neutralize melittin more efficiently. A possible rational for this phenomenon is that core density reduces the hydrodynamic volume of the NP, which ultimately increases the surface area. Subsequently, the effective concentration of

functional monomers on the surface of the NP increases, which ultimately reduces the entropic penalty of forming the multi-point interaction necessary for melittin neutralization. However, molecular weight data is needed to verify this hypothesis.

This study is by no means exhaustive. Other cross-linkers with higher orders of functionality (tris or tetrakis acrylamide monomers) may produce NP hydrogels with greater densities and affinities to melittin. Also, other aromatic cross-linkers may perform better than PheBis NPs and are worth investigating. Most importantly, the results generated in this cross-linking study are useful for the development of other NP systems capable of binding new biomacromolecular targets. Undoubtedly, this work will be useful in manufacturing abiotic affinity hydrogels for cheaper alternatives to current protein purification techniques and antibody therapies.[28]

F. Supplemental Information

<u>Experimental:</u>

Materials: The following materials were obtained from commercial soures: *N*-isopropylacrylamide (NIPAm), ammonium persulfate (APS), *N,N,N',N'*-tetramethylethylenediamine, 1,4-phenylenediamine, and acryloyl chloride were obtained from SIGMA-ALDRICH Inc.; sodium dodecyl sulfate (SDS) was obtained from Aldrich Chemical Company, Inc.; *N,N'*-methylenebisacrylamide (Bis) was from Fluka; *N-tert*-butylacrylamide (TBAm), 1,2-diaminoethane, and 1,3-diaminopropane was from ACRŌS ORGANICS. All other solvents and chemicals were obtained from Fisher Scientific Inc. or VWR International LLC. NIPAm was recrystallized from hexanes, and 1,4-phenylenediamine was sublimed before use. Water used in polymerization and characterization was purified using a Barnstead Nanopure Diamond^{TM} system. UV-Vis absorption spectra were measured using a Thermo Scientific 2000c Nanodrop. Nanoparticle size and polydispersity was determined using a Malvern ZEN3600 dynamic light scattering (DLS) instrument with a disposable sizing cuvette. Lyophylization of polymer samples was determined using a Labconco Freezone 4.5. ^{1}H NMR spectra were acquired on a Bruker DRX500 spectrometer with a TCI (three channel inverse) cryoprobe. All measurements were run at 298 K and were analyzed using the MestReNova (version: 6.0.2-5475) program.

N,N'-(ethane-1,2-diyl)bisacrylamide
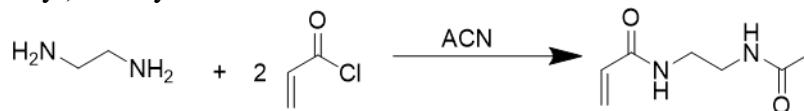
1,2-diaminoethane (15.0 mmol, 1 mL) was mixed with acetonitrile (20 mL). This mixture was added dropwise to a solution of acryloyl chloride (14.8 mmol, 1.2 mL) in acetonitrile (34 mL) at around 0 °C while stirring, and allowed to warm to room temperature, and kept at room temperature for 3 h. Insoluble salts were removed by filtration and the salts were rinsed with 20 mL of 60 °C acetonitrile.   The filtrate was then concentrated to 20 mL *in vacuo* and the product was recrystallized from acetonitrile in a -20 °C freezer overnight and white platelike crystals were collected by filtration (0.548 g, 44%): ^{1}H NMR (500 MHz, CDCl$_3$): δ 3.56 (m, 4H, (CH$_2$)$_2$), 5.66 (dd, *J*= 10.5, 1.5 Hz, 2H, (=CH$_2$)$_2$), 6.13 (dd, *J*= 17.0, 10.5 Hz, 2H, (=CH$_2$)$_2$), 6.27 (dd, *J*= 17.0, 1.5 Hz, 2H, (=CH)$_2$), 6.63 (s, 2H, (NH)$_2$); ESMS *m / z* calcd for C$_8$H$_{12}$N$_2$O$_2$Na (M + Na)$^+$ 191.08, found 191.04; mp = 140 °C (Lit.[29] mp = 138-140 °C).
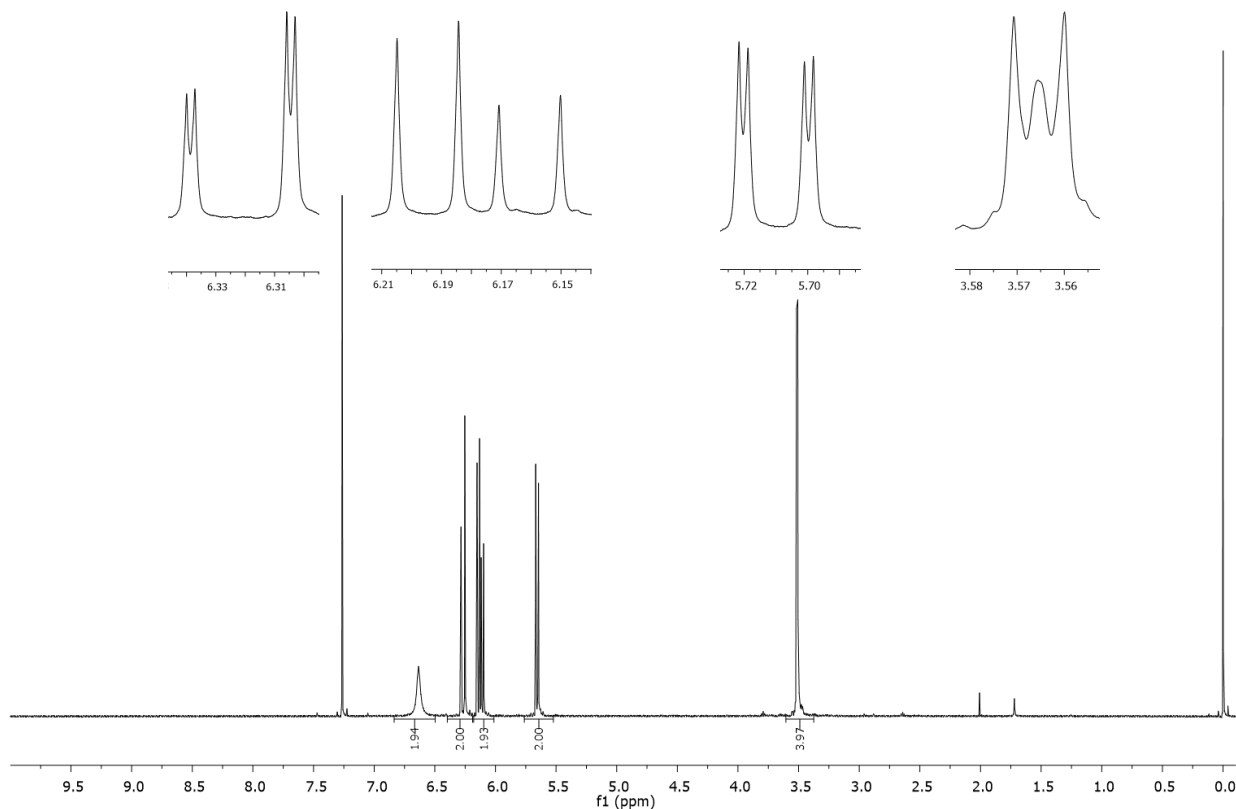
N, N'-(propane-1,3-diyl)bisacrylamide
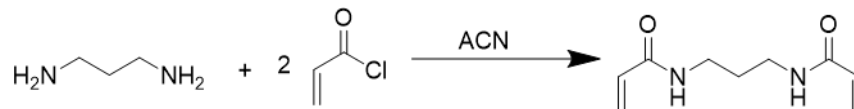
Similar to the procedure for *N,N'*-(ethane-1,2-diyl)bisacrylamide, 1,3-diaminopropane (11.9 mmol, 1 mL) was mixed with acetonitrile (20 mL). This mixture was added dropwise to a solution of acryloyl chloride (14.8 mmol, 1.2 mL) in acetonitrile (34 mL) at around 0 °C, while stirring, and was allowed to warm to room temperature and kept at room temperature for 3 h. Insoluble salts were removed by filtration and the salts were rinsed with 20 mL of 60 °C acetonitrile. The filtrate was then concentrated to 20 mL *in vacuo* and the product was recrystallized from acetonitrile in a -20 °C freezer overnight and white platelike crystals were collected by filtration (0.304 g, 23%): ^{1}H NMR (500 MHz, CDCl$_3$): δ 1.76 (app tt, *J*= 6.0, 2.0 Hz, 2H, CH$_2$), 3.44 (app q, *J*= 6.0), 5.71 (dd, *J*= 10.0, 1.5 Hz, 2H, (=CH$_2$)$_2$), 6.20 (dd, *J*= 17.0, 10.0 Hz, 2H, (=CH$_2$)$_2$), 6.34 (dd, *J*= 17.0, 1.5 Hz, 2H, (=CH)$_2$), 6.57 (s, 2H, (NH)$_2$). ESMS *m / z* calcd for C$_9$H$_{14}$N$_2$O$_2$Na (M + Na)$^+$ 205.1, found 205.06; mp = 115 °C (Lit. 114-116 °C).

N,N'-(1,4-phenylene)bisacylamide

1,4-phenylenediamine (5.6 mmol, 605.6 mg) was mixed with acetone (25 mL), and cooled to 0 ℃ in an ice bath. Acryloyl chloride (11 mmol, 898.0 µL) was mixed with acetone (15 mL), and added dropwise to the solution of 1,4-phenylenediamine, while stirring, and allowed to warm to room temperature and kept at room temperature overnight. The solution was then washed with saturated NaHCO$_3$, filtered and the solid was washed with 100 mL of cold H$_2$O. The crude product was recrystallized from EtOH/MeOH, to afford white crystals that were collected by filtration (1.1890 g, 87%): ^{1}H NMR (500 MHz, DMSO): δ 5.76 (dd, *J*= 10.0, 2.5 Hz, 2H, (=CH$_2$)$_2$), 6.26 (dd, *J*= 17.0, 2.0 Hz, 2H, (=CH$_2$)$_2$), 6.42 (dd, *J*= 17.0, 10.0, 2H, (=CH)$_2$), 7.64 (s, 4H, (Phe-H)$_4$), 10.14 (s, 2H, (NH)$_2$); ESMS *m / z* calcd for C$_{12}$H$_{12}$N$_2$O$_2$Na (M + Na)$^+$ 239.08, found 239.04; mp > 275 ℃ (Lit. 243 ℃).
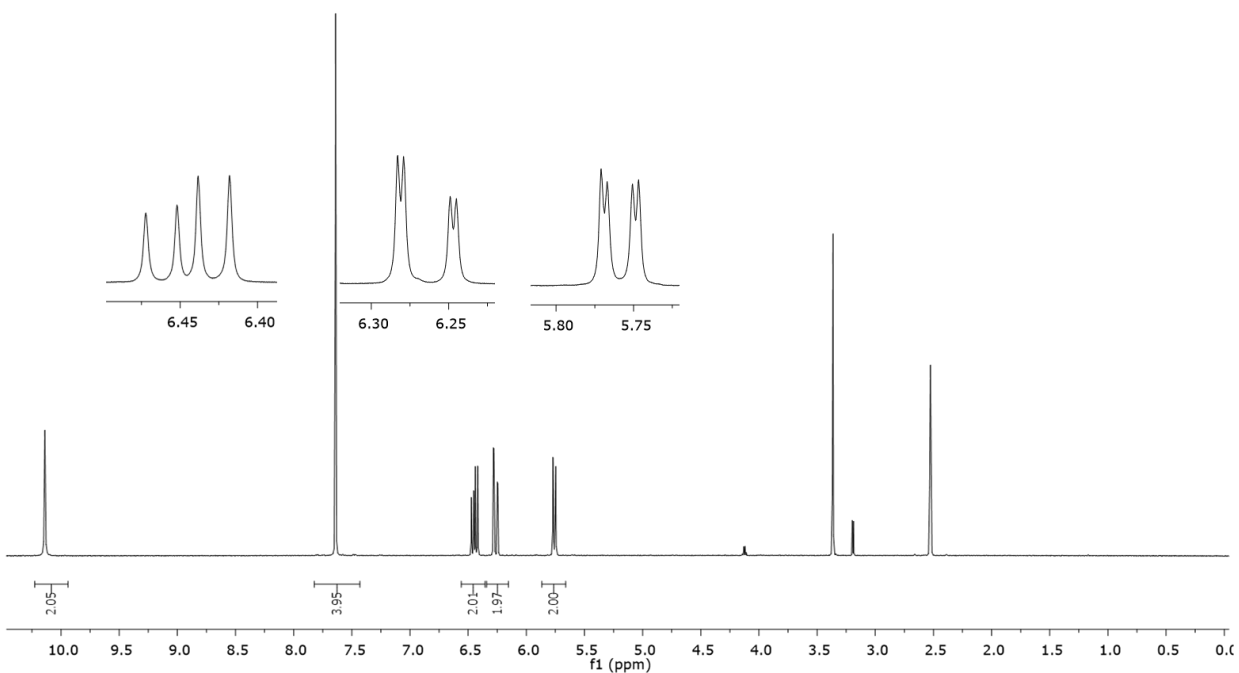
Room Temperature Polymerization

NIPAm (20-(X) mol%), Aac (40 mol%), TBAm (40 mol%), MBis (X mol%), and SDS (30 mg, 1 µmol) were dissolved in water (50 mL) to a total monomer concentration of 6.5 mM. The resulting solution was degassed with nitrogen for 30 minutes while stirring. Ammonium persulfate (30 mg dissolved in 1 mL H_2O) and *N,N,N',N'*-tetramethylethylenediamine (15 µL) was added to the degassed solution, and kept under a nitrogen atmosphere at 25ºC for 17 h. The polymerization was quenched by exposing the reaction to air, and the reaction mixture was transferred to a 12,000-14,000 MWCO membrane and dialyzed against an excess of deionized water (changed twice a day) for 4 days.

60 ºC Polymerization

NIPAm (80-(X) mol%), Aac (10 mol%), TBAm (10 mol%), cross-linker (X mol%), and SDS (30 mg, 1 µmol) were dissolved in water (50 mL) to a final monomer concentration of either 32.5 mM or 65 mM. The resulting solution was degassed with nitrogen for 30 minutes while stirring. Ammonium persulfate (30 mg dissolved in 1 mL H_2O) was added to the degassed solution, and the reaction mixture was heated to 60 ºC under nitrogen for 3 h. The polymerization was quenched by exposing the reaction mixture to air, and the reaction mixture was transferred to a 12,000-14,000 MWCO membrane and dialyzed against an excess of deionized water (changed twice a day) for 4 days.

Characterization of Nanoparticles

Dynamic light scattering (DLS) was used to characterize the size and dispersity of the NPs. All NPs were measured in nanopure water at 25 ºC. Selected NPs were measured at various temperatures in water and phosphate buffer saline (PBS; 35 mM phosphate buffer/0.15 M NaCl, pH 7.3) at 37.5 ºC. All samples were allowed to equilibrate at the designated temperature for 200

seconds prior to each measurement and were measured at a scattering angle of 173°. Concentrations and yields were determined by lyophilizing a known volume of the purified NP solution and weighing the obtained dry polymer samples. Around 15 mg of the lyophilized NP was then dissolved in CD_3OD and a ^1H NMR was taken to qualitatively show the change in NIPAm relative to TBAm as cross-linking density increased.

Hemolytic Red Blood Cell Assay

Bovine red blood cells (RBCs; Lampire Biological Laboratories, Pipersville, PA) were washed with PBS, collected by centrifugation (10 min, 3000 rpm), and resuspended in PBS. Washing was repeated until the supernatant was sufficiently clear. In a microcentrifuge tube, melittin (1.8 µM final concentration) was preincubated with NPs (5-10 µg/mL) for 30 minutes at 37.5 ºC. A 6% RBC suspension was prepared in PBS and 100 µL of the suspension was mixed with the preincubated NP-melittin solution and incubated at 37.5 ºC for an additional 30 minutes. Samples were then centrifuged at 6000 rpm for 10 minutes, and the release of hemoglobin was quantified by measuring the absorbance of the supernatant at 415 nm (A_{sample}). Controls for 0% and 100% neutralization consisted of RBC incubation with 1.8 µM melittin without NPs ($A_{melittin}$), and a RBC suspension without melittin and NPs ($A_{nomelittin}$). All NPs samples were run in triplicate. For NPs containing 40% Aac and 40% TBAm, 5 µg/mL NP concentrations were used, and for NPs containing 10% Aac and 40% TBAm, 10 µg/mL NP concentrations were used. Due to uncontrollable differences in final RBC concentrations, **Neutralization values are only comparable within the same assay.** However, **trends observed in neutralization are comparable between assays.** %Neutralization was calculated using

$(A_{sample} - A_{nomelittin}) / (A_{melittin} - A_{nomelittin})$ x 100 = %Neutralization

Hydrophobicity of Monomers

Hydrophobicity of the aliphatic cross-linkers (MBis, EBis, PBis) was compared using a Hewlet Packard series 1100 HPLC (0% to 100% ACN/H_2O in 27 minutes, λ=220 nm) with an Agilent eclipse C18 column (5 μm, 4.6 × 100 mm) with a flow rate of 1.2 mL /minute.

Table 2.S1. Summary of polymerization conditions, and feed of monomers (mol%)

NP	Conc. mM	T(°C) polym.	Aac (mol%)	TBAm (mol%)	NIPAm (mol%)	MBis (mol%)	EBis (mol%)	PBis (mol%)	PheBis (mol%)	% Yield[a] (mass)
1	6.5	25	40	40	20	0	—	—	—	61
2	6.5	25	40	40	19	1	—	—	—	35
3	6.5	25	40	40	18.5	1.5	—	—	—	40
4	6.5	25	40	40	18	2	—	—	—	36
5	6.5	25	40	40	17.5	2.5	—	—	—	42
6	6.5	25	40	40	17	3	—	—	—	53
7	6.5	25	40	40	16.5	3.5	—	—	—	43
8	6.5	25	40	40	16	4	—	—	—	44
9	6.5	25	40	40	15	5	—	—	—	54
10	6.5	25	40	40	14	6	—	—	—	65
11	6.5	25	40	40	12	8	—	—	—	89
12	6.5	25	40	40	10	10	—	—	—	58
13	65	60	10	10	80	0	—	—	—	40
14	65	60	10	10	79	1	—	—	—	83
15	65	60	10	10	78	2	—	—	—	37
16	65	60	10	10	76	4	—	—	—	81
17	65	60	10	10	75	5	—	—	—	58
18	65	60	10	10	72	8	—	—	—	87
19	65	60	10	10	70	10	—	—	—	41
20	65	60	10	10	68	12	—	—	—	87
21	65	60	10	10	65	15	—	—	—	95
22	65	60	10	10	60	20	—	—	—	—
23	65	60	10	10	55	25	—	—	—	—
24	32.5	60	10	10	78	2	—	—	—	77
25	32.5	60	10	10	70	10	—	—	—	81
26	32.5	60	10	10	63	17	—	—	—	99
27	32.5	60	10	10	60	20	—	—	—	90
28	65	60	10	10	78	—	2	—	—	77
29	65	60	10	10	75	—	5	—	—	70
30	65	60	10	10	70	—	10	—	—	68
31	65	60	10	10	65	—	15	—	—	73
32	65	60	10	10	78	—	—	2	—	89
33	65	60	10	10	75	—	—	5	—	88
34	65	60	10	10	70	—	—	10	—	84
35	65	60	10	10	65	—	—	15	—	83
36	65	60	10	10	78	—	—	0	2	40
37	65	60	10	10	78	—	—	0	2	69

[a]Yields were determined by mass recovery of lyophilized samples for each NP.
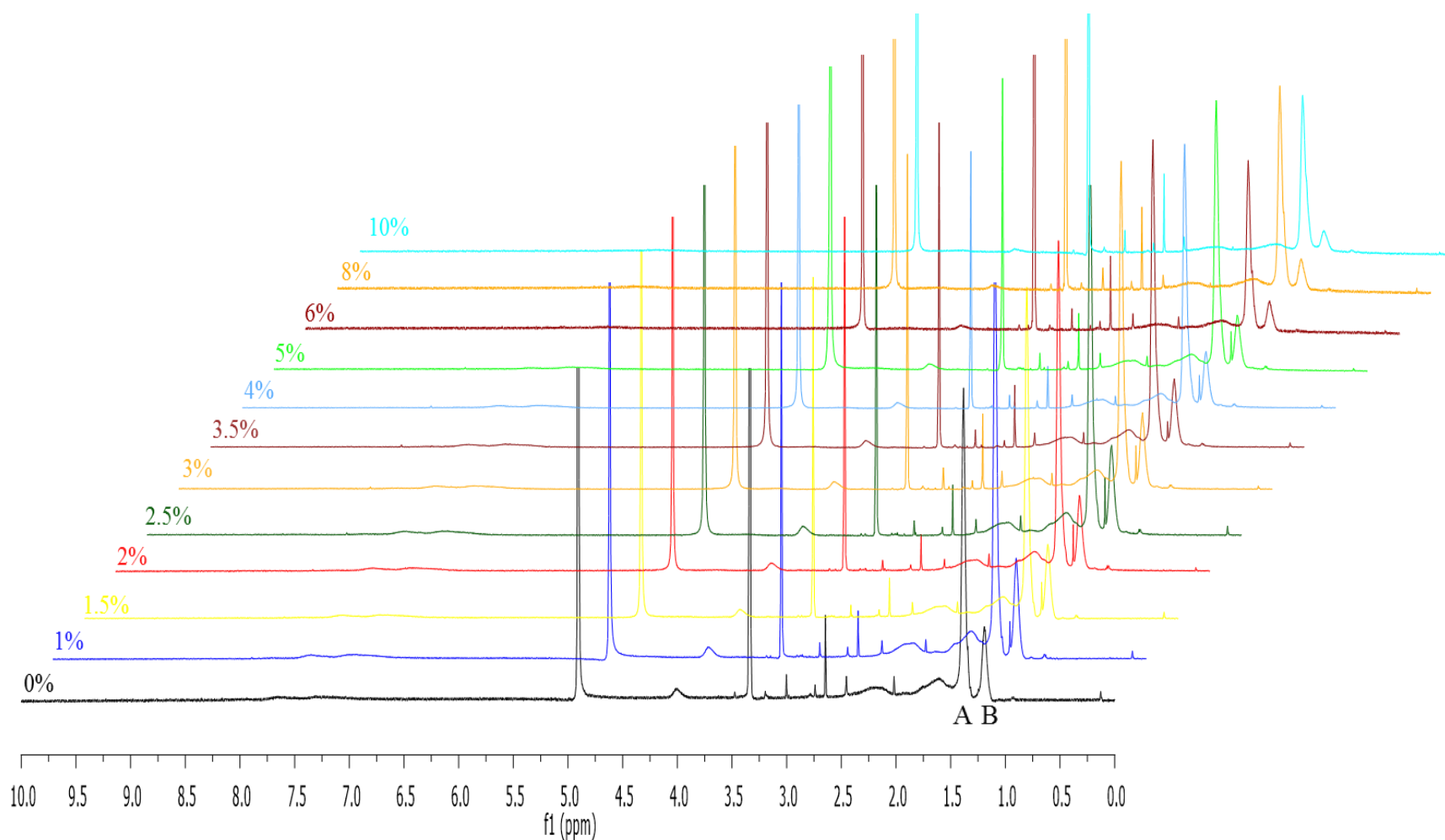
Figure 2.S1. ^{1}H NMR spectra of the 40% Aac, 40% TBAm NPs cross-linked with various feed ratios of MBis synthesized at 25 °C (NP 1-12) measured in CD$_3$OD. Peak A represents the *tert*-butyl methyl protons from TBAm, and peak B represents the methyl protons of NIPAm. The percentage listed at the left of each spectra represents the mol% feed of MBis used in each polymerization. The ratio of the NIPAm to TBAm methyl protons decreases as more MBis monomer is added at the expense of the NIPAm monomer.
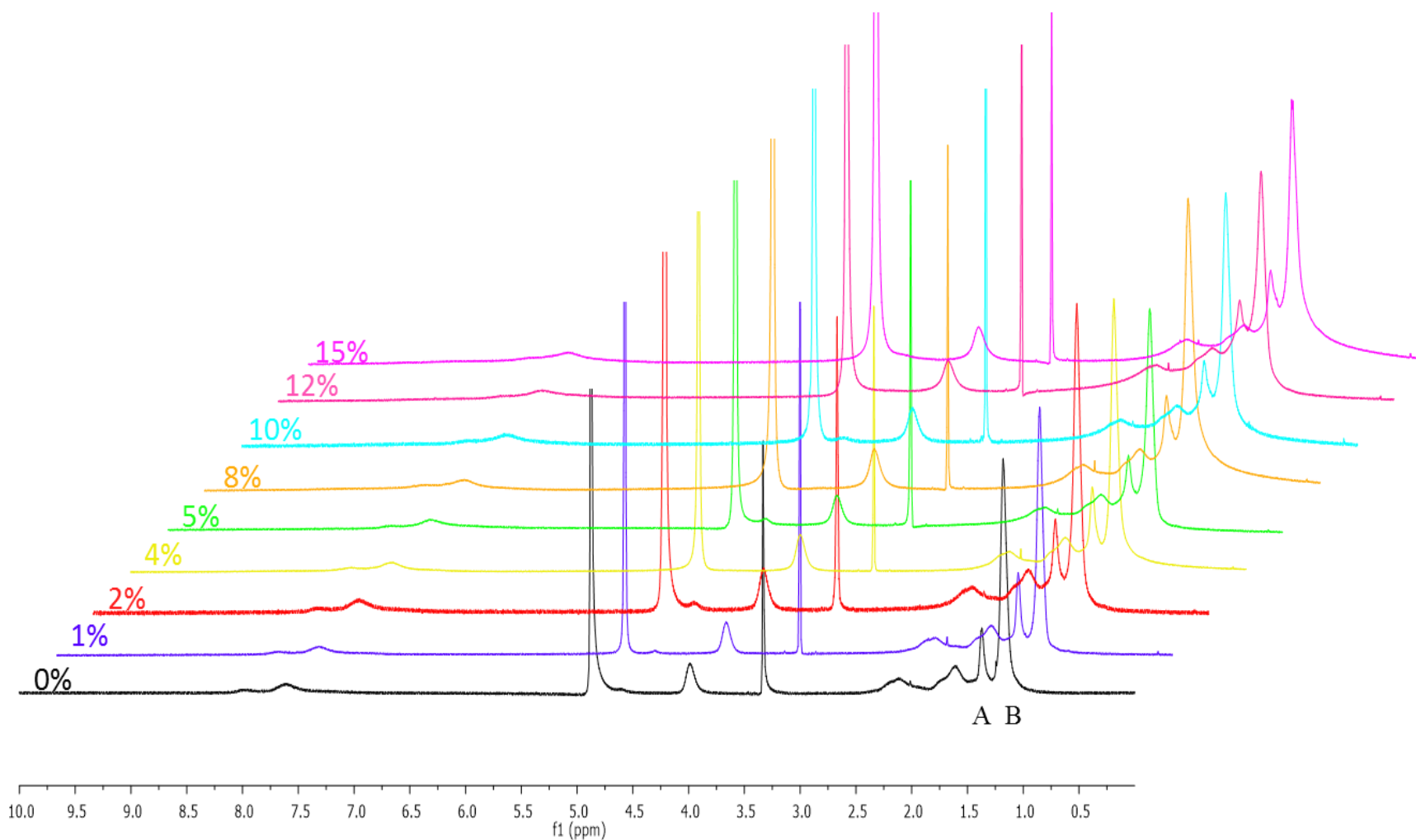
Figure 2.S2. ^{1}H NMR spectra of the 10% Aac, 10% TBAm NPs cross-linked with various feed ratios of MBis synthesized at 60 °C with a total monomer concentration of 65 mM (NP 13-21) measured in CD$_3$OD. Peak A represents the *tert*-butyl methyl protons from TBAm, and peak B represents the methyl protons of NIPAm. The percentage listed at the left of each spectra represents the mol% feed of MBis used in each polymerization. The ratio of the NIPAm to TBAm protons appears to decrease as more MBis monomer is added at the expense of the NIPAm monomer. However, this observation is obstructed as peak broadening increases with higher feed ratios of MBis.
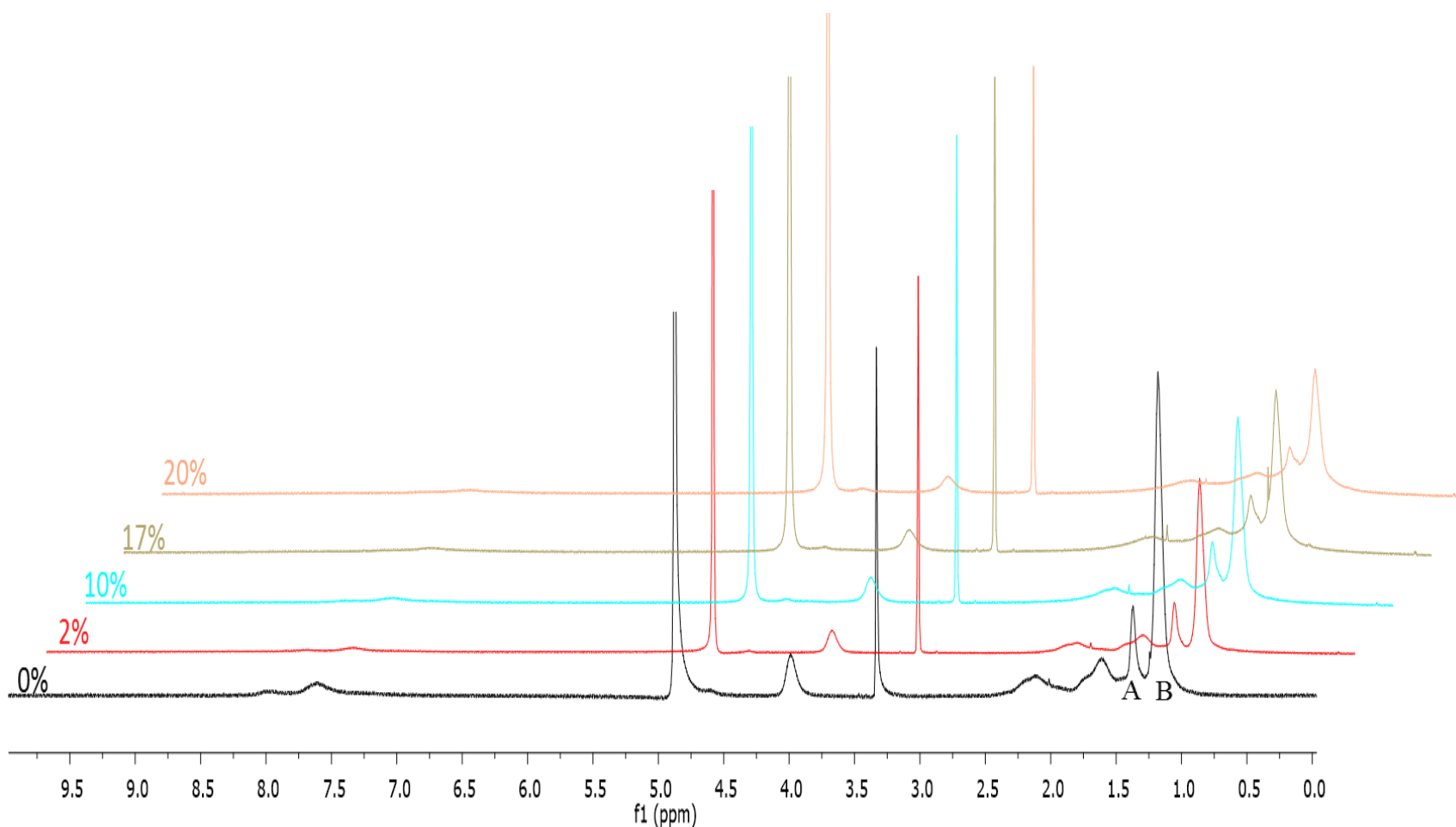
Figure 2.S3. ^{1}H NMR spectra of the 10% Aac, 10% TBAm NPs cross-linked with MBis synthesized at 60 °C with a total monomer concentration of 32.5 mM with the 0% cross-linker NP (65 mM monomer concentration) shown as a reference (NP 13, 24-27) measured in CD$_3$OD. Peak A represents the *tert*-butyl methyl protons from TBAm, and peak B represents the methyl protons of NIPAm. The percentage listed at the left of each spectra represents the mol% feed of MBis used in each polymerization. The ratio of the NIPAm to TBAm methyl protons appears to decrease as more MBis monomer is added at the expense of the NIPAm monomer. However, this observation is obstructed as peak broadening increases with higher feed ratios of MBis.
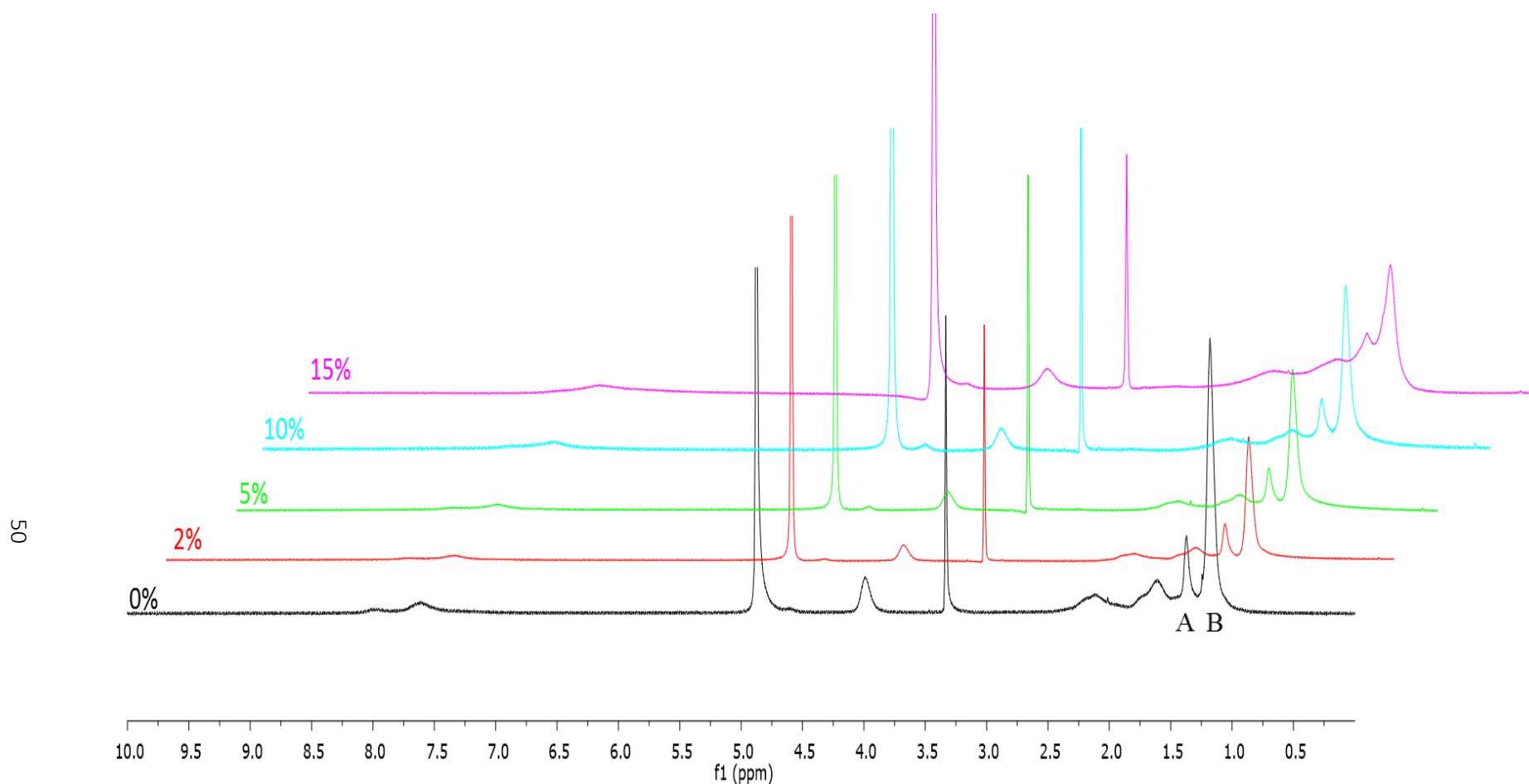
Figure 2.S4. ^{1}H NMR spectra of the 10% Aac, 10% TBAm NPs cross-linked with EBis synthesized at 60 °C with a total monomer concentration of 65 mM with the 0% cross-linker NP (65 mM monomer concentration) shown as a reference (NP 13, 28-31) measured in CD$_3$OD. Peak A represents the *tert*-butyl methyl protons from TBAm, and peak B represents the methyl protons of NIPAm. The percentage listed at the left of each spectra represents the mol% feed of EBis used in each polymerization. The ratio of the NIPAm to TBAm methyl protons appears to decrease as more EBis monomer is added at the expense of the NIPAm monomer. However, this observation is obstructed as peak broadening increases with higher feed ratios of EBis.
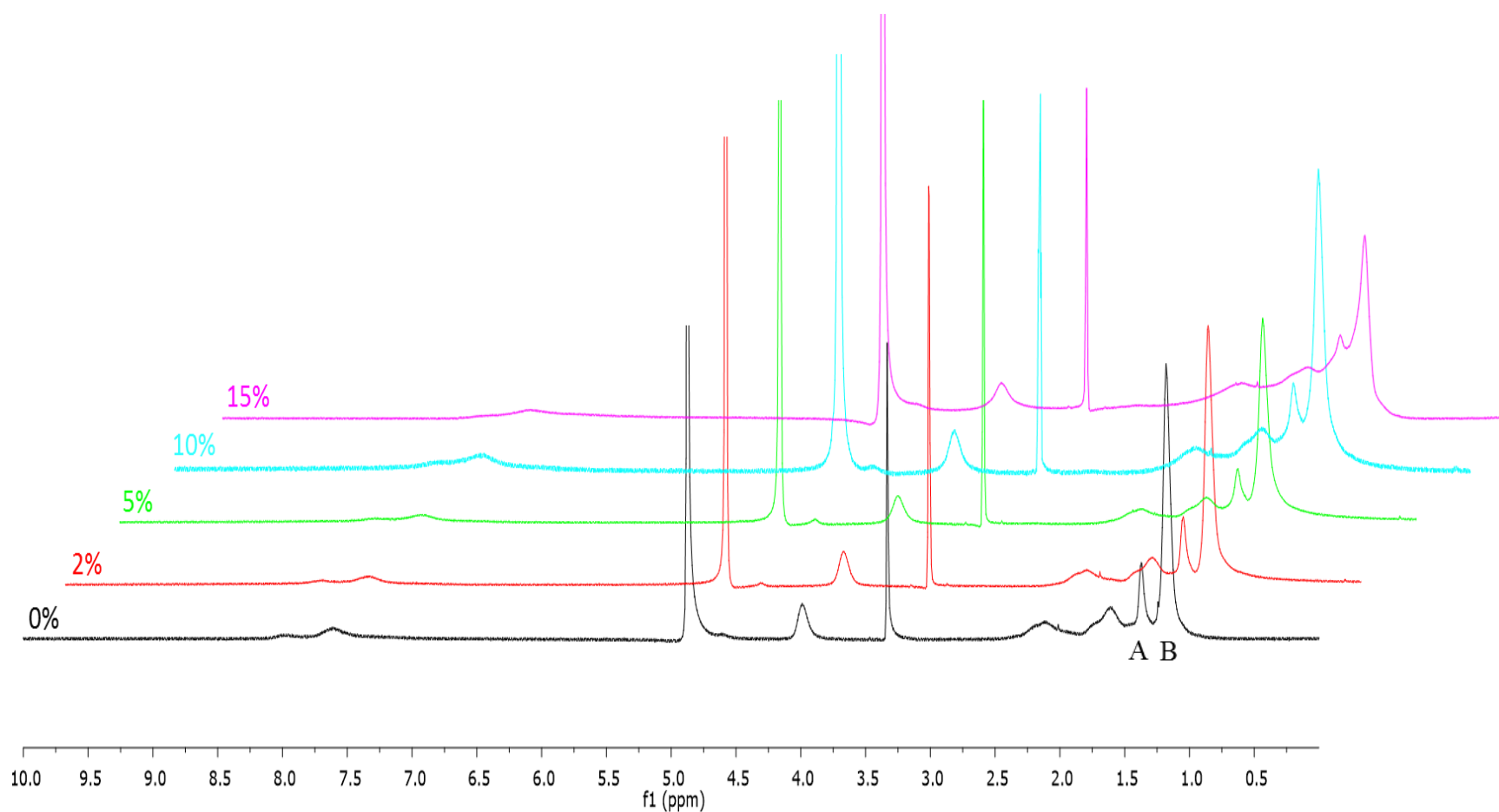
Figure 2.S5. ^{1}H NMR spectra of the 10% Aac, 10% TBAm NPs cross-linked with PBis synthesized at 60 ºC with a total monomer concentration of 65 mM with the 0% cross-linker NP (65 mM monomer concentration) shown as a reference (NP 13, 32-35) measured in CD$_3$OD. Peak A represents the *tert*-butyl methyl protons from TBAm, and peak B represents the methyl protons of NIPAm. The percentage listed at the left of each spectra represents the mol% feed of PBis used in each polymerization. The ratio of the NIPAm to TBAm methyl protons appears to decrease as more PBis monomer is added at the expense of the NIPAm monomer. However, this observation is obstructed as peak broadening increases with higher feed ratios of PBis.
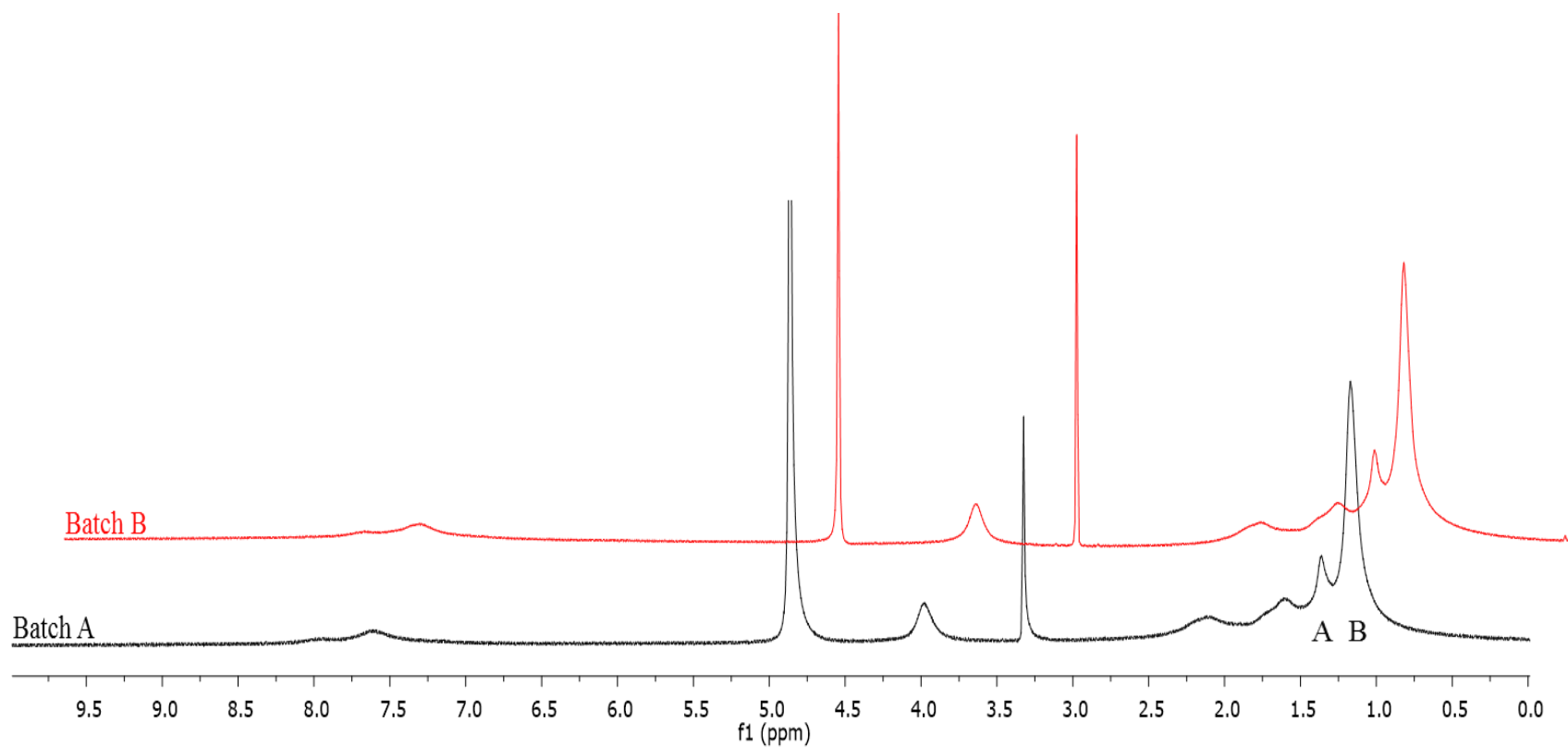
Figure 2.S6. ^{1}H NMR spectra of replicate 10% Aac, 10% TBAm, 78% NIPAm, 2% PheBis NPs (NP 36-37) synthesized at 60 ℃ with a total monomer concentration of 65 mM measured in CD$_3$OD. Homology between the two spectra suggests that PheBis NPs can be synthesized reproducibly. Qualitative analysis of the peak width of both these NPs suggests that chain mobility is comparable to highly cross-linked MBis NPs. Peak A represents the *tert*-butyl methyl protons from TBAm, and peak B represents the methyl protons of NIPAm.

Table 2.S2. Hydrodynamic Diameter of NPs in H_2O

NP	15 °C H₂O (d.nm)	PDI	20 °C H₂O (d.nm)	PDI	25 °C H₂O (d.nm)	PDI	30 °C H₂O (d.nm)	PDI	35 °C H₂O (d.nm)	PDI	40 °C H₂O (d.nm)	PDI	45 °C H₂O (d.nm)	PDI
1	—	—	—	—	PDQ	PDQ	—	—	—	—	—	—	—	—
2	—	—	—	—	58	0.17	—	—	—	—	—	—	—	—
3	—	—	—	—	68	0.24	—	—	—	—	—	—	—	—
4	—	—	—	—	55	0.26	—	—	—	—	—	—	—	—
5	—	—	—	—	60	0.28	—	—	—	—	—	—	—	—
6	—	—	—	—	49	0.22	—	—	—	—	—	—	—	—
7	—	—	—	—	45	0.36	—	—	—	—	—	—	—	—
8	—	—	—	—	PDQ	PDQ	—	—	—	—	—	—	—	—
9	—	—	—	—	PDQ	PDQ	—	—	—	—	—	—	—	—
10	—	—	—	—	PDQ	PDQ	—	—	—	—	—	—	—	—
11	—	—	—	—	PDQ	PDQ	—	—	—	—	—	—	—	—
12	—	—	—	—	PDQ	PDQ	—	—	—	—	—	—	—	—
13	534	0.22	527	0.21	399	0.10	131	0.10	125	0.05	122	0.05	123	0.02
14	—	—	—	—	265	0.08	—	—	—	—	—	—	—	—
15	368	0.05	356	0.07	287	0.05	126	0.08	120	0.05	118	0.03	117	0.06
16	—	—	—	—	235	0.06	—	—	—	—	—	—	—	—
17	—	—	—	—	222	0.04	—	—	—	—	—	—	—	—
18	—	—	—	—	191	<0.01	—	—	—	—	—	—	—	—
19	215	<0.01	205	0.07	186	0.06	153	0.04	117	0.06	114	0.05	112	0.03

Table 2.S2. continued

NP	15 ℃ H₂O (d.nm)	PDI	20 ℃ H₂O (d.nm)	PDI	25 ℃ H₂O (d.nm)	PDI	30 ℃ H₂O (d.nm)	PDI	35 ℃ H₂O (d.nm)	PDI	40 ℃ H₂O (d.nm)	PDI	45 ℃ H₂O (d.nm)	PDI
20	—	—	—	—	181	0.03	—	—	—	—	—	—	—	—
21	174	0.06	173	0.04	161	0.06	139	0.06	114	0.03	108	0.03	106	0.04
22	—	—	—	—	—	—	—	—	—	—	—	—	—	—
23	—	—	—	—	—	—	—	—	—	—	—	—	—	—
24	—	—	—	—	250	0.06	—	—	—	—	—	—	—	—
25	—	—	—	—	180	0.07	—	—	—	—	—	—	—	—
26	—	—	—	—	172	0.01	—	—	—	—	—	—	—	—
27	—	—	—	—	202	0.04	—	—	—	—	—	—	—	—
28	429	0.10	420	0.06	346	0.07	169	0.12	116	0.08	114	0.06	113	0.01
29	343	0.07	336	0.04	284	0.06	179	0.07	130	0.05	126	0.02	126	0.03
30	273	0.04	260	0.08	248	0.04	227	0.05	168	0.03	119	0.04	113	0.03
31	329	0.04	323	0.04	317	0.01	290	0.01	252	0.03	185	0.06	166	0.06
32	386	0.04	380	0.03	315	0.03	137	0.04	128	0.04	127	0.02	126	0.01
33	—	—	—	—	245	0.04	—	—	—	—	—	—	—	—
34	233	0.04	225	0.06	212	0.03	189	0.06	133	0.03	118	0.02	116	0.04
35	230	0.04	222	0.06	209	0.03	188	0.03	147	0.02	134	0.01	131	0.01
36	278	0.03	248	0.04	180	0.07	146	0.06	144	0.04	143	0.04	147	0.04
37	259	0.09	227	0.06	174	0.05	131	0.04	130	0.04	129	0.01	128	0.04

Size measurements that gave unreliable data as determined by the Malvern zetasizer instrument are labeled as PDQ (poor data quality), and their sizes were not reported. PDI is defined by the Malvern software as $(\sigma / dm)^2$ where σ = the standard deviation.

Table 2.S2. continued

NP	50 ºC H₂O (d.nm)	PDI	55 ºC H₂O (d.nm)	PDI	60 ºC H₂O (d.nm)	PDI
31	187	0.01	185	<0.01	186	0.02

Table 2.S3. Hydrodynamic Diameter of NPs in PBS at 37.5 ºC

NP	37.5 ºC PBS (d.nm)	PDI
13	300	0.02
15	300	0.02
16	277	0.04
17	239	0.02
18	234	0.06
19	211	0.03
20	216	<0.01
21	183	<0.01
28	306	0.05
29	255	<0.01
30	234	0.02
31	312	0.06
32	317	0.02
33	253	<0.01
34	220	0.01
35	227	0.01
36	271	0.02
37	252	0.03

A
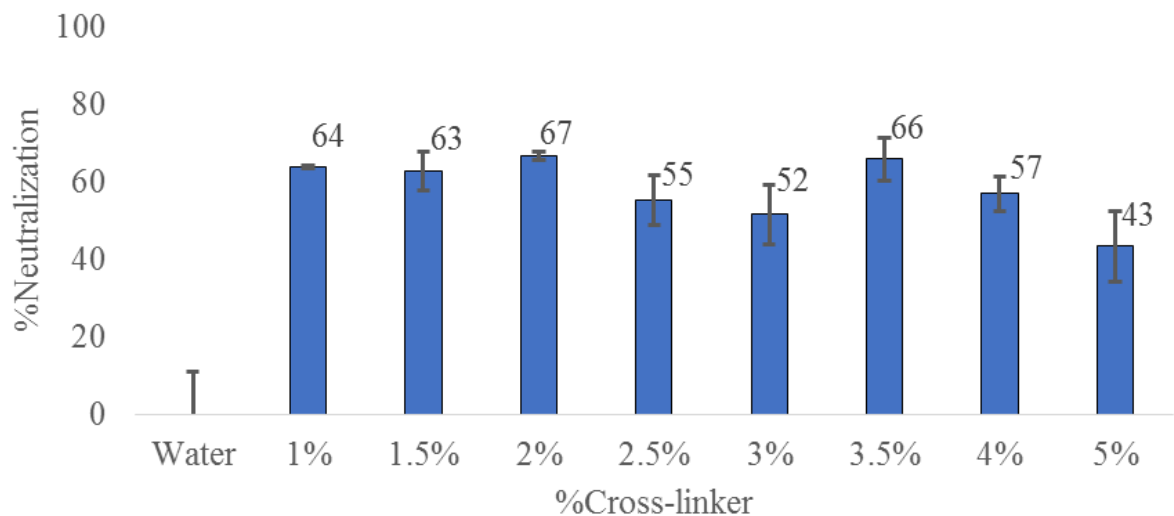
B
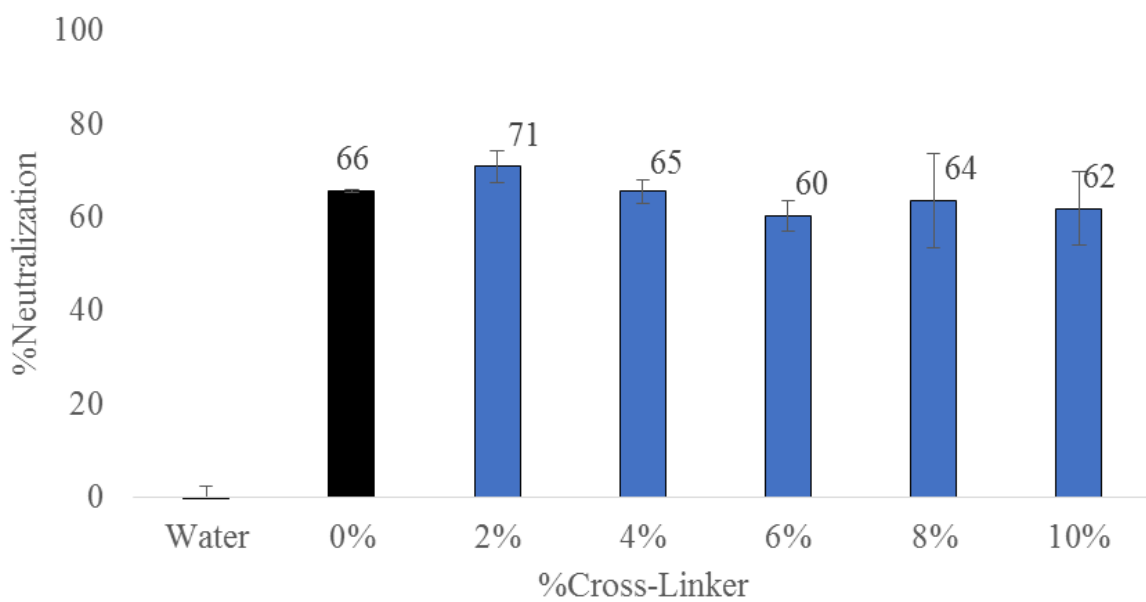
Figure 2.S7. %Neutralization for MBis cross-linked NPs (Blue) and NPs without any chemical cross-linker (black) synthesized at room temperature at 6.5 mM total monomer concentration. All NPs were assayed at 5 µg/mL.
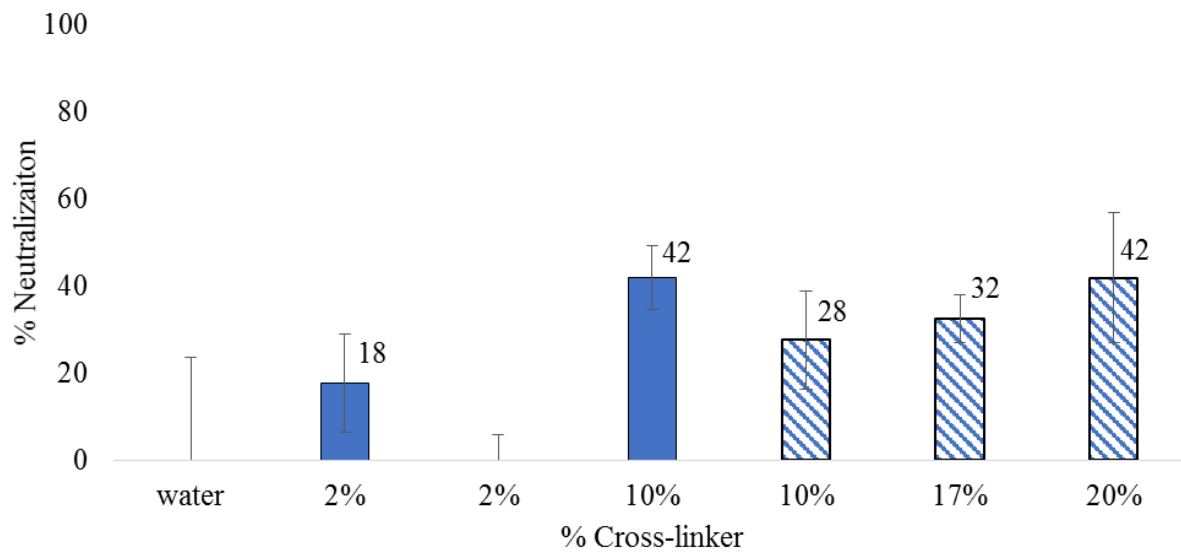
Figure 2.S8. Hemolytic RBC assay results for MBis cross-linked NPs synthesized at 60 ℃ at 65 mM monomer concentration (solid blue) and 32.5 mM total monomer concentration (striped blue). All NPs were tested at 10 µg/mL.
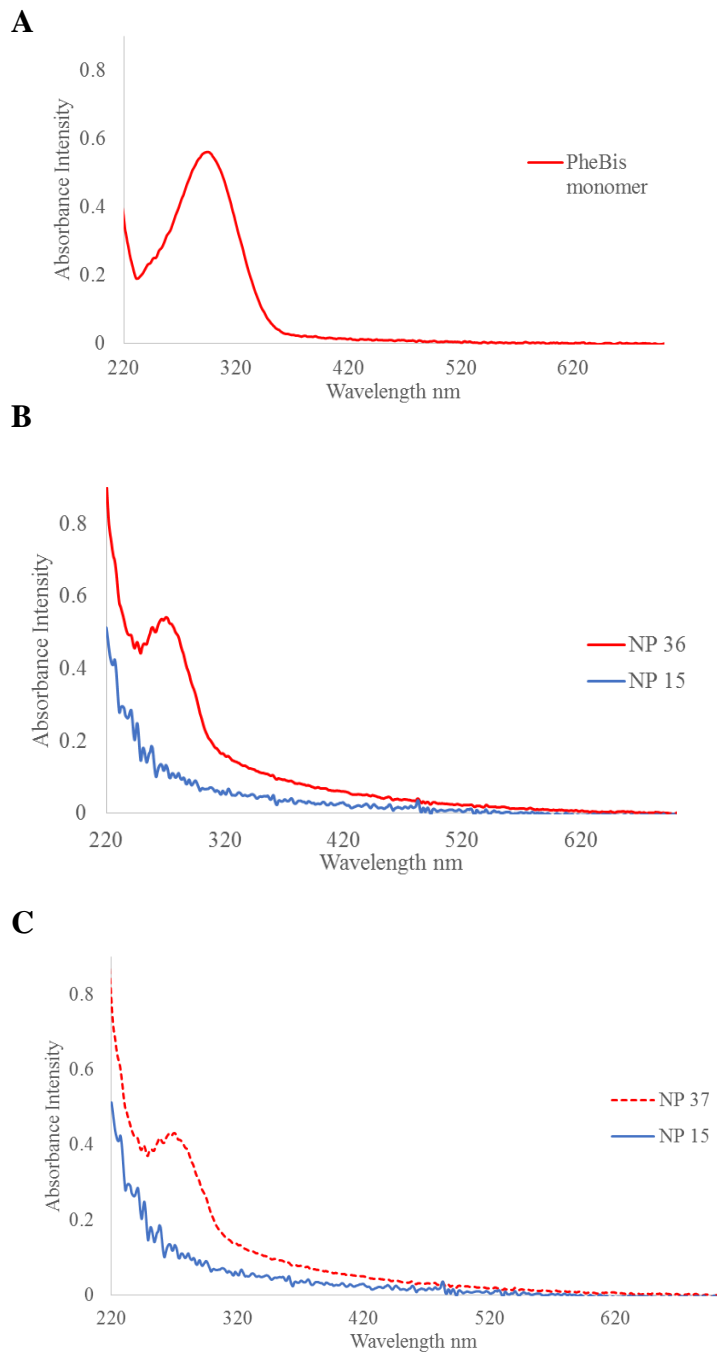
Figure 2.S9. UV-Vis absorbance spectra for the PheBis cross-linker (A), and two independent batches of PheBis cross-linked NPs (B, C; NP 36, 37) at a concentration of 43 µg/mL in H_2O. Similarities in the absorbance spectra between the two batches suggests that PheBis cross-linked NPs can be made reproducibly regardless of the partial solubility of the cross-linker in H_2O. The MBis cross-linked NP (15) is included in spectra B and C for comparison. The peak corresponding to the PheBis cross-linker is slightly blue-shifted in spectra B and C relative to spectra A due to the reduced conjugation from the reacted vinyl groups on the cross-linker.

G. References

     (1)   Karg, M.; Hellweg, T.: New "smart" poly(NIPAM) microgels and nanoparticle microgel hybrids: Properties and advances in characterisation. *Curr. Opin. Colloid. In.* **2009**, *14*, 438-450.

     (2)   Pelton, R. H.; Chibante, P.: Preparation of aqueous latices with *N*-isopropylacrylamide. *Colloid Surface* **1986**, *20*, 247-256.

     (3)   Tanaka, T.; Ishiwata, S. i.; Ishimoto, C.: Critical Behavior of Density Fluctuations in Gels. *Phys. Rev. Lett.* **1977**, *38*, 771-774.

     (4)   Shibayama, M.; Tanaka, T.; Han, C. C.: Small angle neutron scattering study on poly(*N*-isopropyl acrylamide) gels near their volume-phase transition temperature. *J. Chem. Phys.* **1992**, *97*, 6829-6841.

     (5)   Shibayama, M.; Tanaka, T.; Han, C. C.: Small-angle neutron scattering study on weakly charged temperature sensitive polymer gels. *J. Chem. Phys.* **1992**, *97*, 6842-6854.

     (6)   Shibayama, M.; Tanaka, T.; Han, C., C.: Small-angle neutron scattering study on poly(*N*-isopropyl acrylamide-co-acrylic acid) copolymer solutions. *J. Phys. IV France* **1993**, *03*, C8-25-C28-28.

     (7)   Wu, C.; Zhou, S.: Volume Phase Transition of Swollen Gels: Discontinuous or Continuous? *Macromolecules* **1997**, *30*, 574-576.

     (8)   Lu, D.; Liu, Z.; Zhang, M.; Wang, X.; Liu, Z.: Dextran-grafted-PNIPAAm as an artificial chaperone for protein refolding. *Biochem. Eng. J.* **2006**, *27*, 336-343.

     (9)   Yoshimatsu, K.; Lesel, B. K.; Yonamine, Y.; Beierle, J. M.; Hoshino, Y.; Shea, K. J.: Temperature-Responsive "Catch and Release" of Proteins by using Multifunctional Polymer-Based Nanoparticles. *Angew. Chem. Int. Edit.* **2012**, *51*, 2405-2408.

     (10)   Hoare, T.; Pelton, R.: Highly pH and Temperature Responsive Microgels Functionalized with Vinylacetic Acid. *Macromolecules* **2004**, *37*, 2544-2550.

     (11)   Kratz, K.; Hellweg, T.; Eimer, W.: Influence of charge density on the swelling of colloidal poly(*N*-isopropylacrylamide-co-acrylic acid) microgels *Colloid Surface A* **2000**, *170*, 137-149.

     (12)   Shibayama, M.; Ikkai, F.; Inamoto, S.; Nomura, S.; Han, C. C.: pH and salt concentration dependence of the microstructure of poly(*N*-isopropylacrylamide-co-acrylic acid) gels. *J. Chem. Phys.* **1996**, *105*, 4358-4366.

     (13)   Karg, M.; Pastoriza-Santos, I.; Rodriguez-González, B.; von Klitzing, R.; Wellert, S.; Hellweg, T.: Temperature, pH, and Ionic Strength Induced Changes of the Swelling Behavior of PNIPAM−Poly(allylacetic acid) Copolymer Microgels. *Langmuir* **2008**, *24*, 6300-6306.

     (14)   Fernández-Nieves, A.; Márquez, M.: Electrophoresis of ionic microgel particles: From charged hard spheres to polyelectrolyte-like behavior. *J. Chem. Phys.* **2005**, *122*, -.

     (15)   Atsushi Suzuki, T. T.: Phase transition in polymer gels induced by visible light. *Nature* **1990**, *346*, 345-347.

     (16)   Zhang, X.; Yang, P.; Dai, Y.; Ma, P. a.; Li, X.; Cheng, Z.; Hou, Z.; Kang, X.; Li, C.; Lin, J.: Multifunctional Up-Converting Nanocomposites with Smart Polymer Brushes Gated Mesopores for Cell Imaging and Thermo/pH Dual-Responsive Drug Controlled Release. *Adv. Funct. Mater.* **2013**, *23*, 4067-4078.

     (17)   Ohya, S. N., Yasuhide; Matsuda, Takehisa.: Thermoresponsive Artificial Extracellular Matrix for Tissue Engineering: Hyaluronic Acid Bioconjugated with Poly(*N*-isopropylacrylamide) Grafts. *Biomacromolecules* **2001**, *2*, 856-863.

(18)   Hoshino, Y.; Koide, H.; Furuya, K.; Haberaecker, W. W.; Lee, S.-H.; Kodama, T.; Kanazawa, H.; Oku, N.; Shea, K. J.: The rational design of a synthetic polymer nanoparticle that neutralizes a toxic peptide in vivo. *Proc. Natl. Acad. Sci. U.S.A.* **2012**, *109*, 33-38.

(19)   Weisman, A.; Chen, Y. A.; Hoshino, Y.; Zhang, H.; Shea, K.: Engineering Nanoparticle Antitoxins Utilizing Aromatic Interactions. *Biomacromolecules* **2014**, *15*, 3290-3295.

(20)   Li, J.; Illeperuma, W. R. K.; Suo, Z.; Vlassak, J. J. Hybrid Hydrogels with Extremely High Stiffness and Toughness. *ACS Macro Lett*. **2014**, *3*, 520-523.

(21)   Hoshino, Y.; Koide, H.; Urakami, T.; Kanazawa, H.; Kodama, T.; Oku, N.; Shea, K. J.: Recognition, Neutralization, and Clearance of Target Peptides in the Bloodstream of Living Mice by Molecularly Imprinted Polymer Nanoparticles: A Plastic Antibody. *J. Am. Chem. Soc.* **2010**, *132*, 6644-6645.

(22)   Berndt, I.; Pedersen, J. S.; Lindner, P.; Richtering, W.: Influence of Shell Thickness and Cross-Link Density on the Structure of Temperature-Sensitive Poly-*N*-Isopropylacrylamide−Poly-*N*-Isopropylmethacrylamide Core−Shell Microgels Investigated by Small-Angle Neutron Scattering. *Langmuir* **2005**, *22*, 459-468.

(23)   Hoshino, Y.; Nakamoto, M.; Miura, Y.: Control of Protein-Binding Kinetics on Synthetic Polymer Nanoparticles by Tuning Flexibility and Inducing Conformation Changes of Polymer Chains. *J. Am. Chem. Soc.* **2012**, *134*, 15209-15212.

(24)   Nakamoto, M.; Hoshino, Y.; Miura, Y.: Effect of Physical Properties of Nanogel Particles on the Kinetic Constants of Multipoint Protein Recognition Process. *Biomacromolecules* **2013**, *15*, 541-547.

(25)   Hoshino, Y.; Urakami, T.; Kodama, T.; Koide, H.; Oku, N.; Okahata, Y.; Shea, K. J.: Design of Synthetic Polymer Nanoparticles that Capture and Neutralize a Toxic Peptide. *Small* **2009**, *5*, 1562-1568.

(26)   Blackburn, W.; Lyon, L. A.: Size-controlled synthesis of monodisperse core/shell nanogels. *Colloid Polym. Sci.* **2008**, *286*, 563-569.

(27)   Krokhin, O. V.; Spicer, V.: Peptide retention standards and hydrophobicity indexes in reversed-phase high-performance liquid chromatography of peptides. *Anal. Chem.* **2009**, *81*, 9522-9530.

(28)   Hoshino, Y. L., Haejoo; Miura, Yoshiko.: Interaction between synthetic particles and biomacromolecules: fundamental study of nonspecific interaction and design of nanoparticles that recognize target molecules. *Polym. J.* **2014**, *46*, 537-545.

(29)   Shea, K. J.; Stoddard, G. J.; Shavelle, D. M.; Wakui, F.; Choate, R. M.: Synthesis and characterization of highly crosslinked poly(acrylamides) and poly(methacrylamides). A new class of macroporous polyamides. *Macromolecules* **1990**, *23*, 4497-4507.

Chapter 3

Engineering the protein corona of a synthetic polymer nanoparticle for broad-spectrum sequestration and neutralization of venomous biomacromolecules

A. Abstract

Biochemical diversity of venom extracts often occurs within a small number of shared protein families. Developing a sequestrant capable of broad-spectrum neutralization across various protein isoforms within these protein families is a necessary step in creating broad-spectrum antivenom. Using *directed synthetic evolution* to optimize a nanoparticle (NP) formulation capable of sequestering and neutralizing venomous phospholipase A_2 (PLA_2), we demonstrate that broad-spectrum neutralization and sequestration of venomous biomacromolecules is possible via a single optimized NP formulation. Furthermore, this optimized NP showed selectivity for venomous PLA_2 over abundant serum proteins, was not cytotoxic, and showed substantially long dissociation rates from PLA_2. These findings suggest that it may show efficacy as an in vivo venom sequestrant and may serve as a generalized lipid-mediated toxin sequestrant.

B. Introduction

Snake envenomation is recognized by the World Health Organization (WHO) as a neglected tropical disease.[1] Annually, 4.5 million people suffer from snakebites, 2.7 million suffer serious morbid injuries, and over 100,000 die as a result of snake envenomation.[2,3] The majority of the deaths occur in rural regions in South and Southeast Asia where individuals do not have immediate access to health care facilities capable of treating afflicted individuals.[4] In India alone, an estimated

35,000-50,000 people die annually from snake envenomation and 97% of these mortalities occur in rural regions.[5]

Current methods of treating snake envenomation rely on the acquisition and administration of polyclonal antibodies from surrogate animals.[6] Unfortunately, in many areas, this approach has not been effective due to variations in venom composition that exist between different species and even populations within the same species.[7,8] The interspecific and intraspecific variability of snake venom has led many experts in the field to abandon the idea of creating a broad-spectrum antidote for snake venom.[8] Moreover, the high cost of antivenom production has resulted in the discontinuation of African snake antivenom and coral snake antivenom from the world's leading suppliers.[9,10] This is a major concern in Africa considering this region is home to many of the world's most venomous snake populations. Hence, there is a high global demand for an inexpensive and effective alternative to current antivenom therapeutics.

While there is a great deal of variability across snake venoms, there is also a rather striking level of homology.[11] Venomous protein toxins can often be partitioned into a small number of protein families that are found abundantly in the venoms of numerous animals. For example, the protein family phospholipase A_2 (PLA_2) is found in many snake venoms, honey bee venoms, and scorpion venoms. Despite the fact that these families of protein toxins occur across multiple species, securing an effective antivenom is complicated by the diversity of protein isoforms found within each protein family. For example, over 300 different isoforms of PLA_2 have been sequenced.[12] PLA_2, like many protein families found in venom, contains a large number of highly conserved disulfide bonds.[11] This structural conservation and robust scaffold allows for a high degree of variation of exposed amino acid residues allosteric to the active site leading to diverse pharmacological profiles across the PLA_2 protein family. This diversity on the primary sequence

level is likely the reason why immunoglobulin based antivenoms are highly specific to particular venom compositions and often show poor cross-reactivity.[8] Consequently, a challenge for any broad-spectrum antivenom is to develop an affinity reagent that recognizes features and similarities that are shared across venomous protein families but are unique with respect to abundant serum proteins to allow for selective sequestration.

Herein, we describe a novel approach to this problem. We have been developing strategies for the synthesis of abiotic protein/peptide affinity reagents. Non-toxic hydrogel copolymer nanoparticles (NPs) have been engineered with affinity and selectivity to peptide toxins, enzymes, signaling proteins and other large biomacromolecules (fibrinogen, IgG) through a *directed synthetic evolution* process.[13] These synthetic polymer NPs are analogous to biological protein affinity reagents (antibodies, aptamers, etc.). Examples include selective capture and programed release of lysozyme from complex protein mixtures (egg white),[14] a NP with specificity for the Fc domain of IgG,[15] in vitro inhibition of PSMα3, an amphiphilic defensive peptide secreted by methicillin-resistant Staphylococcus aureus that disrupts cellular membranes, in the presence of serum proteins,[16] and sequestration/neutralization of the peptide toxin melittin from the blood stream of a living mouse.[17] More recently a polymer NP was developed with engineered affinity for a vascular endothelial growth factor ($VEGF_{165}$). The NP inhibits binding of the signaling protein to its receptor VEGFR-2, preventing receptor phosphorylation and downstream $VEGF_{165}$-dependent endothelial cell migration.[18]

These findings and the success of our in vivo synthetic toxin neutralization studies prompted the search for a synthetic NP composition capable of sequestering and neutralizing PLA_2 toxins from various venom extracts. Our NP selection process differs from that of the immune system. NP-protein affinity arises broadly from similarities that are characteristic of specific classes of toxins.

PLA$_2$ interacts with lipid membranes and lipoprotein particles.[19] These features may be shared not only across isoforms but even different families of proteins. Hence, it is likely that during the process of formulating and optimizing a NP capable of neutralizing venomous PLA$_2$, the NP will also be able to sequester similar venomous proteins and peptides. Indeed, an ingenious use of biological membranes has been employed as a "toxin sponge" for toxins with membrane affinity.[20] However, since PLA$_2$, a membrane hydrolyzing enzyme, is a significant component of most snake venoms, this approach would not be successful. Our synthetic polymer NPs, which lack phospholipids, would not be vulnerable to PLA$_2$-catalyzed degradation.

C. Directed synthetic evolution strategy

Venomous PLA$_2$ enzymes are generally characterized by their low molecular weight (13-16 kDa), Ca^{2+}-dependency, and a conserved active site histidine/aspartic acid dyad.[21] Unlike mammalian PLA$_2$, which are relatively non-toxic and pharmacologically benign, venomous PLA$_2$ are capable of producing a variety of pharmacological effects, making them one of the most toxic components of snake, honey-bee, and scorpion venom.[22-24] In the presence of phosphatidylcholine, PLA$_2$ catalyzes the production of lysophosphatidylcholine, which is known to induce hemolysis.[25] This property allows for the activity of enzymatically active PLA$_2$ isoforms to be monitored indirectly through hemolytic assays.[26]

Using this assay, a first-generation library (Table 3.S1) of functionally diverse NPs were analyzed for their ability to inhibit PLA$_2$ induced erythrocyte lysis. It was discovered that NP 1_5, consisting of 20% acrylic acid, 40% *N*-phenylacrylamide, 38% *N*-isopropylacrylamide, and 2% *N,N'*-methylenebisacrylamide (Figure 3.1C), showed a decrease in erythrocyte lysis when tested against *Bungarus caeruleus* (Indian Krait) venom (Figure 3.1A). Furthermore, it appears that NP 1_5 does not prevent hemolysis by scavenging the lysophosphoatidylcholine (Figure 3.1B).

Rather, it is likely inhibiting the production of lysophosphatidylcholine by directly interacting with PLA$_2$.
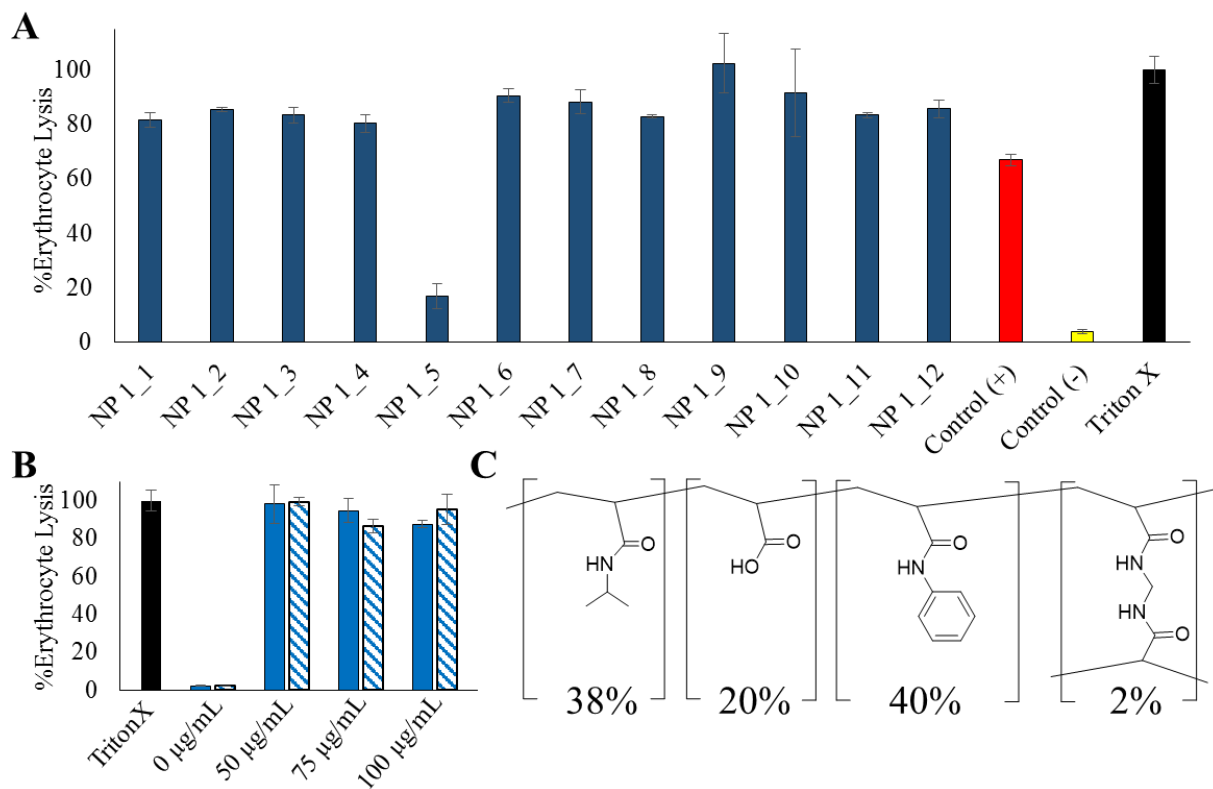
Figure 3.1. First round of NP optimization (A) Erythrocyte lysis assay results for first generation library of NPs (500 µg/mL) incubated with Indian Krait venom (1 µg/mL) and phosphatidylcholine (100 µg/mL). Control (+, red) represents no NPs, Control (-,yellow) represents no venom or NPs, and all data was normalized to Triton X (black). (B) Erythrocyte lysis assay results for NP 1_5 (500 µg/mL) incubated with lysophosphatidylcholine (solid blue) versus lysophosphatidylcholine incubated without NPs (striped blue) at various concentrations of lysophosphatidylcholine. (C) Monomer feed ratio for NP 1_5.

Using NP 1_5 as our lead formulation, a second generation library of NPs were synthesized with systematically varied feed ratios of the four monomers (Table 3.S3). The optimization conditions used to *evolve* the lead formulation from the first generation were made more rigorous by using honey-bee venom instead of snake venom. Honey-bee venom contains two hemolytic principle components: PLA$_2$ and melittin. Melittin is a ~3 kDa hemolytic pore forming peptide that comprises 50% of the dry mass of honey-bee venom.[27] The activity of melittin works

65

synergistically with that of PLA$_2$ found in honey-bee venom by releasing phospholipids from lysed cellular membranes allowing for lipid shuttling to occur between melittin and PLA$_2$.[28] Thus, monitoring the inhibition of honey-bee venom induced hemolysis through an erythrocyte lysis assay allows for congruent analysis of anti-PLA$_2$ activity and anti-melittin activity. Furthermore, this relatively simplified venom system can be used to test whether or not a single NP composition can inhibit multiple venomous biomacromolecules simultaneously.
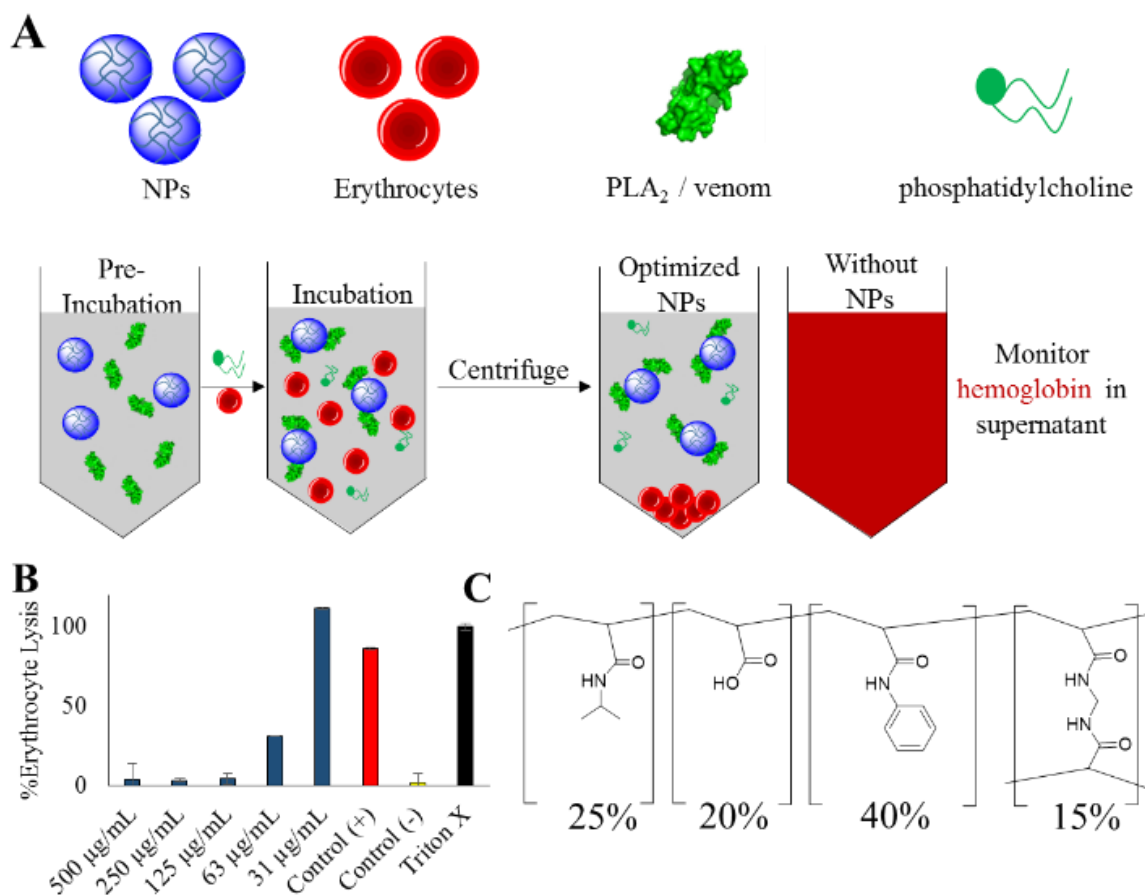
Figure 3.2. Second round of NP optimization (A) PLA$_2$ activity assay used to analyze inhibition of enzymatic hydrolysis of phosphatidylcholine to lysophosphatidylcholine (hemolytic). (B) Erythrocyte lysis results using 10 µg/mL of whole honey-bee venom (~15% PLA$_2$) and various concentrations of NP 2_12 (blue). Control (+, red) represents no NPs, Control (-,yellow) represents no venom or NPs, and all data was normalized to Triton X (black). (C) Feed ratio of monomers used to synthesize NP 2_12.

Using a concentration of 10 µg/mL of whole honey-bee venom, the second generation library of NPs were analyzed for their inhibitive properties (Figures 3.S8-18). Moreover, the experimental procedure was made more stringent by increasing the final incubation from 15 min to 1 h. Under these conditions, the inhibition of erythrocyte lysis when testing for anti-PLA$_2$ activity by NP 1_5 was overwhelmed. However, it was observed that the amount of cross-linker incorporated into the monomer feed ratio was directly correlated with the inhibition of erythrocyte lysis (Figure 3.S13). The NP 2_12, synthesized with the greatest feed ratio of cross-linker (Figure 3.2C), was able to inhibit PLA$_2$ induced erythrocyte lysis at concentrations as low as 63 µg/mL (Figure 3.2B), and melittin induced erythrocyte lysis at concentrations lower than 0.3 mg/mL (Figure 3.S16). While the reasons for this trend in cross-linking are not obvious, it is clear that cross-linking significantly impacts the neutralization of venomous PLA$_2$. More importantly, these results suggest that dissimilar biomacromolecules can be neutralized by a single NP formulation, which is a necessary milestone in our pursuit of a broad-spectrum toxin sequestrant.

While control experiments were performed on both generations of NPs to ensure that the NPs were not responsible for any observed erythrocyte lysis, the lead NP (NP 2_12) was also subjected to an MTT cell viability test using human immortalized myelogenous leukemia K562 cells. Control experiments were run to establish background absorption at 490 nm in PBS in the presence or absence of NP 2_12 when treated with the MTT dye. However, no cytotoxicity was observed even at NP concentrations as high as 500 µg/mL (Figure 3.S20).

D. Protein corona analysis

Following an envenomation, venom proteins are rapidly diluted in the blood stream of the afflicted individual. Thus, selectivity for the targeted venom proteins over abundant serum proteins is required. This challenge must be addressed directly when developing a polymer sequestrant.
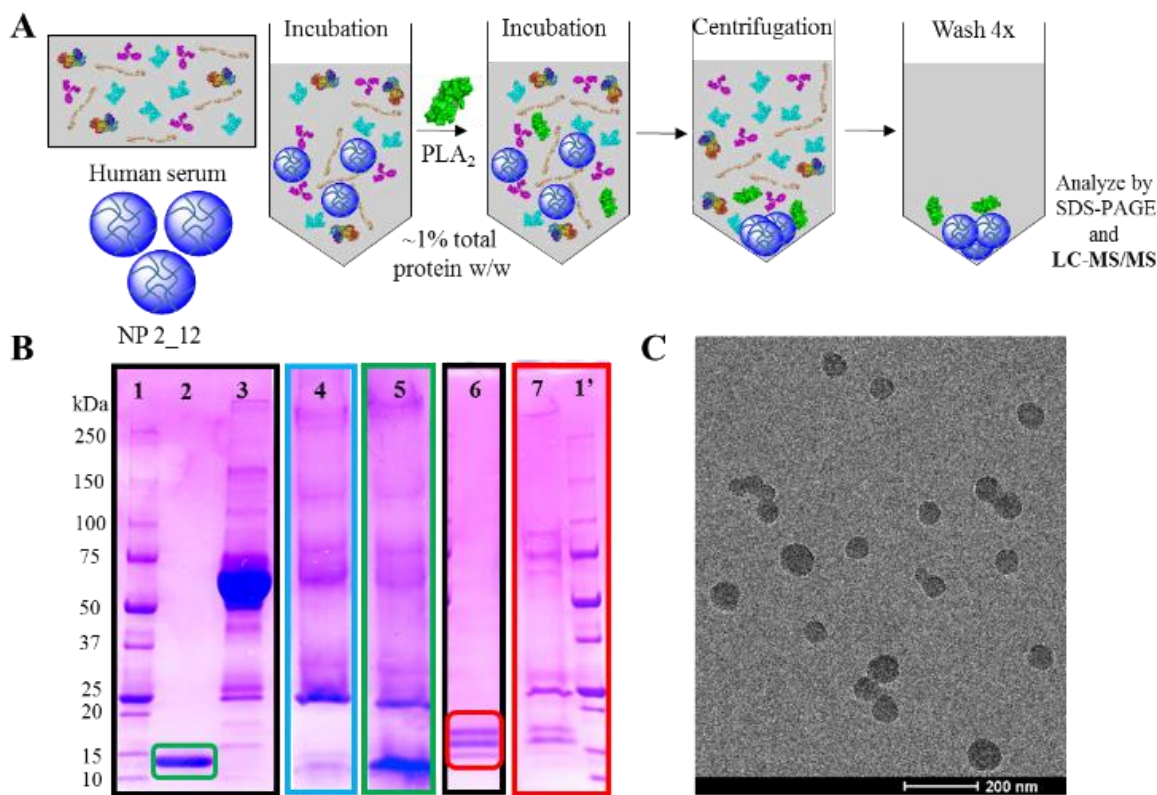
Figure 3.3. Selectivity experiments and TEM characterization of NP 2_12 (A) Strategy for analyzing selectivity for targeted venom proteins over human serum proteins. Serum was diluted to a final concentration of 25%, PLA$_2$ was diluted to a final concentration of 250 µg/mL, and NP 2_12 was diluted to a final concentration of 1 mg/mL. (B) PLA$_2$ selectivity experiments visualized by SDS-PAGE. (1/1') molecular weight ladder. (2) Purified PLA$_2$ from *Naja mossambica* venom. (3) Serum control. (4) NP 2_12 incubated in serum only. (5) NP 2_12 incubated in serum and PLA$_2$ from *Naja mossambica* venom. (6) Purified PLA$_2$ from honey-bee venom. (7) NP 2_12 incubated in ovine plasma and PLA2 from honey-bee venom. (C) Unstained TEM image of NP 2_12. Scale bar = 200 nm. Full gel images available in the supplemental information (Figures 3.S17-19).

Exposing NPs to complex biological mixtures results in the rapid adsorption of biomacromolecules onto NPs.[29,30] This rapid adsorption event results in a new and more therapeutically relevant chemical identity termed the *protein corona*, which can be further divided into two domains: a hard corona and a soft corona.[31] The two protein corona domains can be differentiated by the differences in kinetic dissociation rates (k_{off}). The hard corona describes biomacromolecules that slowly dissociate from the NP and the soft corona describes a layer of proteins that rapidly

dissociate from the NP or NP•hard corona complex. The composition of the hard and soft corona results from the cumulative contribution of a number of physicochemical parameters including size, shape, and the synthetic identity of NP.[32,33]

Monitoring the entire protein corona composition has been met with considerable challenges due to the rapidly exchanging soft-corona. However, established methods have been developed for analyzing the composition of the thermodynamic hard-corona via SDS-PAGE and LC-MS/MS (Figure 3.3A).[32] For purposes of venom protein sequestration, it is necessary that venom proteins adsorb within the thermodynamic and slowly-exchanging hard-corona.

Using concentrated human serum and purified fractions of PLA$_2$ from *Naja mossambica* venom (~1% w/w total protein), the hard protein corona of NP 2_12 was analyzed. In the absence of any PLA$_2$, it appears that the majority of the serum proteins have minimal affinity to NP 2_12 (Figure 3.3B4). However, upon introducing PLA$_2$ after a 5 min pre-incubation in serum, a significant amount of PLA$_2$ appears in the NP protein corona (Figure 3.3B5). This experiment demonstrates that serum proteins can be displaced by high-affinity venomous PLA$_2$ in the hard corona of the NP, which is a requirement for in vivo venom sequestration/neutralization. This experiment was conducted a second time using bee venom PLA$_2$, which also showed selective association to the NP over ovine plasma proteins (Figure 3.3B7). These findings demonstrate that a single synthetically optimized NP formulation (NP 2_12) can sequester a variety of PLA$_2$ isoforms and may function as a broad-spectrum venomous-PLA$_2$ sequestrant.
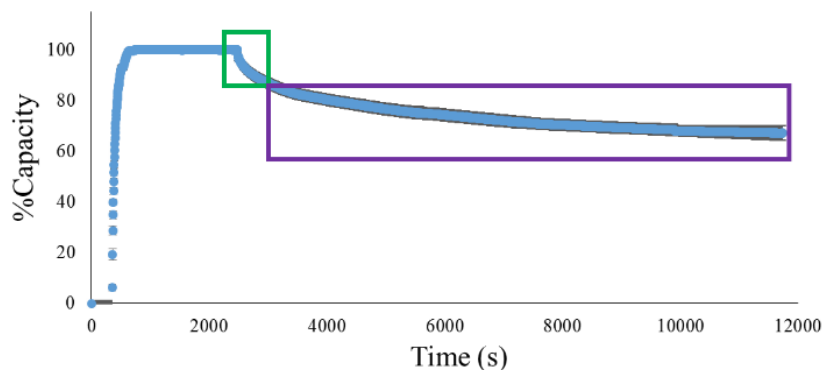
Figure 3.4. Kinetic analysis of the dissociation of bee venom $PLA_2 \cdot NP$ 2_12 using NP 2_12 immobilized surface plasmon resonance (SPR) under flow conditions.

In order to understand the selectivity for PLA_2 over other serum proteins, the bands observable by SDS-PAGE were digested and analyzed by mass spectrometry (Table 3.S5). Of the nine proteins found in the hard-corona, three were apolipoproteins (Apo-A1, Apo-E, and Apo-B100). In, particular Apo-A1 appears to be the major serum protein bound to NP 2_12. These proteins associate with lipoprotein particles and are important for trafficking lipids throughout the blood-stream.[34] This corona profile suggests that the NP is mimicking a natural substrate of PLA_2 (lipoprotein particles composed of glycerophospholipids) and explains why this NP composition is capable of sequestering PLA_2 with sufficient selectivity over abundant serum proteins. This also explains why NP 2_12 is capable of neutralizing the pore-forming toxin melittin from bee-venom and may act as a broad-spectrum sequestrant for lipid-mediated toxins.

Building on this discovery, we studied the dissociation kinetics for bee venom $PLA_2 \cdot NP$ 2_12. From previous studies aimed at understanding hydrogel-biomacromolecule interactions, it was found that the interaction of NIPAm-based NPs with charged biomacromolecules is dominated by entropically driven processes which can be related to the expulsion of water from the NP hydrogel upon binding.[35] In the present system, a surface plasmon resonance (SPR)

analysis revealed that following a rapid k_{on}, k_{off} was characterized by rapid desorption of a small (<20%) fraction of absorbed protein (perhaps from the soft corona) followed by a much slower desorption of the remaining (>80%) protein. Under the flow conditions of the SPR experiment, a significant fraction of the bound protein (~80%, largely PLA_2), remains tightly bound. The time needed to release the majority of bound PLA_2 from the NP is likely longer than the time needed to clear the $PLA_2 \bullet NP$ 2_12 complex in vivo (Figure 3.4). This kinetic data lends credibility to the notion that broad-spectrum sequestration of lipid-mediated toxins may be accomplished via a single optimized NP formulation.

E. Supplemental Information

Materials:

The following materials were obtained from commercial sources: *N*-isopropylacrylamide (NIPAm), ammonium persulfate (APS), 1,4-phenylenediamine, *N*-phenylacrylamide, acryloyl chloride*,* L-phenylalanine, *Naja sputatrix* venom, *Bungarus caeruleus* venom, and *Crotalus atrox* venom, *Apis mellifera* (Honey-bee) Phosphatidylcholine, Phospholipase A$_2$ from Honey-bee venom, Phospholipase A$_2$ from *Naja mossambica* venom, ovine plasma, human serum, and lysophosphatidylcholine were obtained from SIGMA-ALDRICH Inc.; sodium dodecyl sulfate (SDS) was obtained from Aldrich Chemical Company, Inc.; *N,N'*-methylenebisacrylamide (MBis) was from Fluka; *N*-tert-butylacrylamide (TBAm) was from ACRŌS ORGANICS. All other solvents and chemicals were obtained from Fisher Scientific Inc. or VWR International LLC. NIPAm was recrystallized from hexanes, and 1,4-phenylenediamine was sublimed before use. Water used in polymerization and characterization was purified using a Barnstead Nanopure Diamond^{TM} system. 12-14 kDa MWCO cellulose membranes were purchased from Spectrum Laboratories. Precast SDS-PAGE gels (4-15% Mini-Protean), Coomassie Brilliant Blue R-250 and molecular weight ladder (Precision plus protein standards) were purchased from Bio-rad Laboratories. Bovine Red Blood cells, Ovine plasma and human serum were purchased from Lampire Biological Laboratories.

Instrumentation:

 UV-Vis absorption spectra were measured using a Thermo Scientific 2000c Nanodrop or a SpectraMax Plus 384 Microplate Reader. Nanoparticle size and polydispersity was determined using a Malvern ZEN3600 dynamic light scattering (DLS) instrument with a disposable sizing cuvette. Lyophilization of polymer samples was performed using a Labconco Freezone 4.5. ^{1}H

NMR spectra were acquired on a Bruker DRX500 spectrometer with a TCI (three channel inverse) cryoprobe. All measurements were run at 298 K and were analyzed using the MestReNova (version: 6.0.2-5475) program. TEM Images were obtained on a FEI Tecnai G2 TF20 high resolution TEM operated at an accelerating voltage of 200 kV.

General Procedures:

Nanoparticle Synthesis

Nanoparticles were synthesized following a previously reported procedure.[16] Monomers corresponding to the designated feed ratio, and SDS (30 mg, 1 µmol) were dissolved in water (50 mL) to a final monomer concentration of 65 mM. 5 mL of acetone was used to dissolve the aromatic monomers before adding to the bulk aqueous solution. The resulting solution was degassed with nitrogen for 30 min while stirring. Ammonium persulfate (30 mg dissolved in 1 mL H_2O) was added to the degassed solution, and the reaction mixture was heated to 60 ℃ under nitrogen for 3 h. The polymerization was quenched by exposing the reaction mixture to air, and the reaction mixture was transferred to a 12,000-14,000 MWCO membrane and dialyzed against an excess of deionized water (changed twice a day) for 4 d.

Characterization of Nanoparticles

Dynamic light scattering (DLS) was used to characterize the size and dispersity of the NPs. All NPs were measured in nanopure water at 25 ℃. Selected NPs were measured at various temperatures in water and 50 mM Tris buffer (150 mM NaCl, 10 mM $CaCl_2$, pH = 7.50), at 37 ℃. All samples were allowed to equilibrate at the designated temperature for 200 seconds prior to each measurement and were measured at a scattering angle of 173°. Concentrations and yields were determined by lyophilizing a known volume of the purified NP suspension and weighing the obtained dry polymer samples.

Generation 1 NPs.

Bungarus caeruleus venom hemolytic assay

Bovine red blood cells (RBCs; Lampire Biological Laboratories, Pipersville, PA) were washed with 50 mM Tris buffer (with 150 mM NaCl, 10 mM $CaCl_2$, pH = 7.50), collected by centrifugation (10 min, 3000 rpm), and resuspended in Tris buffer. Washing was repeated until the supernatant was sufficiently clear after which A 10% RBC suspension was prepared in tris buffer. In a 96-well plate *Bungarus caeruleus* venom (1 µg/mL final concentration) was preincubated with NPs (0, 0.1, and 0.5 mg/mL final concentration) for 15 minutes at 37 ℃. After 15 min, phosphatidylcholine (100 µg/mL final concentration) followed by RBCs (5% final concentration) were mixed with the preincubated NP-venom suspension and incubated at 37 ℃ for an additional 15 min. Samples were then centrifuged at 4000 rpm for 10 min, and the release of hemoglobin was quantified by measuring the absorbance of the supernatant at 415 nm (A_{sample}). RBCs incubated with the detergent triton-X (1%) were used to normalize the absorbance values. All Samples were run in triplicate.

$(A_{sample} - A_{tris\ bufer}) / (A_{triton-X} - A_{tris\ buffer})$ x 100 = %Erythrocyte lysis

Lysophosphatidylcholine assay

Bovine red blood cells were washed with tris buffer (with 150 mM NaCl, 10 mM $CaCl_2$, pH = 7.50) and collected as previously described. In a microcentrifuge tube, lysophosphatidylcholine (0-100 µg/mL) was incubated with and without NP 1_5 (0.5 mg/mL) for 15 min at 37 ℃. After 15 min, RBCs (5% final concentration) were mixed with the preincubated NP-lysophosphatidylcholine suspensions or the lysophosphatidylecholine-only solutions and incubated at 37 ℃ for an additional 15 min. Samples were then centrifuged at 4000 rpm for 10 min, and the release of hemoglobin was quantified by measuring the absorbance of the supernatant

at 415 nm (A_{sample}). RBCs incubated with the detergent triton-X (1%) were used to normalize the absorbance values. All Samples were run in triplicate.

$(A_{sample} - A_{tris\ bufer}) / (A_{triton-X} - A_{tris\ buffer}) \times 100 = \%\text{Erythrocyte lysis}$

Generation 2 NPs.

Whole honey-bee venom hemolytic assay

PLA$_2$ and melittin inhibition: The hemolytic assay protocol was modified for the honey bee-venom to allow for more rigorous testing. Briefly, honey-bee venom (10 µg/mL) was incubated with the second-generation NPs (0.5 mg/mL, or as indicated) for 15 min (37 ℃) in tris buffer (with 150 mM NaCl, 10 mM CaCl$_2$, pH = 7.50). Next, phosphatidylcholine (100 µg/mL final concentration) followed by RBCs (5% final concentration) were mixed and incubated at 37 ℃ for 1 h. Results were normalized to the detergent control. All samples were run in triplicate and quantified as previously described.

Melittin inhibition: Honey-bee venom (10 µg/mL) was incubated with the second-generation NPs (0.5 mg/mL) for 15 min (37 ℃) in tris buffer (with 150 mM NaCl, 10 mM CaCl$_2$, pH = 7.50). Next, RBCs (5% final concentration) were mixed and incubated at 37 ℃ for 1 h. Results were normalized to the detergent control. All samples were run in triplicate and quantified as previously described.

PLA$_2$ selectivity in human serum

In a microcentrifuge tube, NP 2_12 (1 mg/mL final concentration) was incubated with human serum (25% final concentration) in phosphate buffer saline (Dulbecco's) for 5 min at 37 ℃. Next, phospholipase A$_2$ (250 µg/mL final concentration) was added to the NP 2_12/human serum mixture and incubated for an additional 45 min at 37 ℃. The suspension was then centrifuged at 10,000 RPM for 10 min, and the supernatant was replaced with fresh phosphate buffer saline four

consecutive times or until the supernatant was depleted of protein by SDS-PAGE (commassie blue stain). Next, 20 µL of SDS-PAGE sample preparation mixture was added to the NP pellet, mixed and heated to 95 ℃ for 10 minutes. Finally, the Mixture was centrifuged at 5,000 RPM and the bound proteins were analyzed by SDS-PAGE (100 V).

Tryptic Digest of Gel Entrapped Proteins

Excised gel bands where washed in a 100 µL of a 50:50 of 100mM NH_4HCO_3/CH_3CN for 10 min. The supernatant was removed and 30 µL of CH_3CN was added for 10 min. The wash step was repeated until the gels appeared colorless (3x). Finally, the gels were placed in a vacuum oven (45 ℃) to dry (5-10 min). Next, 10-20 µL of 10 mM DTT (DTT solution prepared using 50 mM NH_4HCO_3 buffer) and was incubated at 60 ℃ for 1 h. After cooling to RT, equal volume of 50 mM iodoacetic acid (prepared in 50 mM NH_4HCO_3) and incubated for 45 min at 45 ℃ in the dark. Next, the supernatant was discarded and 10-20 µL of 50 mM NH_4HCO_3 buffer to each excised gel band and incubate at RT for 10 min. The supernatant was removed and 50 µL of 100 mM NH_4HCO_3 was added for 5-10 min. The supernatant was removed and 30 µL of CH_3CN for added for 10 min. The NH_4HCO_3 and CH_3CN washes were then repeated twice, and finally the bands were dried for 5-10 minutes using a vacuum oven (45 ℃) for 5-10 min. Next, 50 µL of porcine trypsin (50 mM NH_4HCO_3, 20 ng/µL) was added to each dried gel band for 45 min at 4 ℃, and then incubated at 37 ℃ overnight. Following, 20 µL of deionized H_2O to each gel band for 5 min. The supernatant was removed and transferred to a new microcentrifuge tube. 30 µL of 50% CH_3CN/1% TFA was added to each microcentrifuge tube containing the gel band for 10 min. After which, the supernatant was removed and transferred to the previous supernatant-only microcentrifuge tubes. The 50% CH_3CN/1% TFA wash was repeated 3 times. Finally, the supernatant tube was dried using a vacuum oven, and re-suspended in 50% CH_3CN/1% TFA.

LCMS-MS Protocol

Following in-gel digestion with porcine trypsin, extracted peptides were separated on a BEH C18 nanotile column and analyzed by MSE on a SYNAPT G2 instrument with a triziac source (Waters). Data were analyzed using ProteinLynx Global Server software (PLGS 3.0) with the human proteome database in addition to the proteins found on www.uniprot.org from *Naja mossambica* venom. The LC gradient was linear 2% B to 95 % B in 40 minute and the column was re-equilibrated for the next run. The MSE was performed by keeping the collision voltage at 6 eV to generate an MS spectra and later ramped up between 15-45 eV to generate the MS/MS spectra. The PLGS will process the MS and MS/MS data to accommodate the multiple peaks that were generated from multiple precursor ion and assign the appropriate peptide fragment for each ion.

TEM Characterization

8 µL of NP 2_12 (1 mg/mL) was placed on a glow discharged TEM grid (Ultrathin Carbon Type-A, 400 mesh) and let stand for 1 min. The solution was removed by filter paper and the grid was left to air dry for 10 min. Next the grid was loaded into the instrument (FEI Tecnai G2 TF20 high resolution TEM operated at an accelerating voltage of 200 kV) for imaging.

Surface Plasmon Resonance (SPR)

The NP immobilized SPRI chips were created by the modified procedure for SPRI from previous work.[16] The Au coated SPRI chips were coated by thermally evaporated chromium (1 nm) as an adhesion layer and Au (45 nm) on SF10 glass slides (18 ×18 mm; Schott Glass). Before coating, those slides were cleaned by plasma cleaner (PDC-32G; Harrick Plasma) and then treated with Sigmacote.[36] The SPRI chips were rinsed with ethanol and nanopure water and dried by nitrogen before use. SPR measurements were carried out with SPR imager II (GWC Technologies,

Madison, WI) at room temperature. The SPRI chip was flushed with PBS buffer at pH 7.4. After obtaining flat baseline, NP 2_12 was immobilized on the chip by using 0.5 mg/mL and 1.0 mg/mL of the NP samples in PBS buffer. The NP immobilization was monitored with SPRI.   Next, bee-venom PLA$_2$ (20 µM) was introduced to the NP immobilized chip at RT. After saturation was reached, fresh PBS buffer was flowed over the PLA$_2$•NP immobilized SPRI chip. Data was normalized by fixing the maximum ΔR% at 100% capacity.

Nanoparticle toxicity test-MTT assay (cell viability assay)

K562 cells were counted with a countess automated cell counter, centrifuged at 1500 rpm, redispersed in PBS (phosphate buffered Saline solution from Sigma) and 200,000 cells per well were seeded in a 96 well plate. A mixture of PBS 5X (30 µL), X mL of NP (final concentration: 100, 200, 300, 400 and 500 µg/mL), 120-X µL of nanopure water was prepared. Two controls were also prepared, one with no NPs, and one with only cells in PBS. 150 µL was added to the pelleted cells, mixed again with a multichannel pipet, and incubated for 30 min at 37 °C in a humidified 5% CO$_2$ incubator. The cells were pelleted by centrifugation at 3000 rpm and the supernatant was removed and replaced with 100 µL of fresh media (RPMI 1640 Medium including 10% fetal bovine serum and 1% Pen Strep from Gibco). The MTT (3-(4,5-Dimethylthiazol-2-yl)-2,5-Diphenyltetrazolium Bromide from molecular probe, 10 µL, 12 mM solution in PBS) regent was added and the wells mixed with a multichannel pipet. The mixtures were then incubated at 37 °C in a humidified 5% CO$_2$ incubator for 4h, centrifuged at 3000 rpm, and all the media was replaced with DMSO (100 µL, Dimethylsulfoxide from ATCC). The solutions were incubated at 37 °C for 20 min, mixed and absorbance was read at 570 nm by Microplate reader (Bio-RAD).

Table 3.S1. Feed of Monomers used for each *first-generation* NP and %Yield

NP	NIPAm (mol%)	Bis (mol%)	Aac (mol%)	TBAm (mol%)	PAA (mol%)	APhe (mol%)	% Yield
1_1	98	2	-	-	-	-	76
1_2	78	2	20	-	-	-	47
1_3	58	2	-	40	-	-	93
1_4	38	2	20	40	-	-	86
1_5	38	2	20	-	40	-	63
1_6	78	2	10	10	-	-	37
1_7	78	2[a]	10	10	-	-	69
1_8	48	2	40	10	-	-	70
1_9	53	2	5	40	-	-	89
1_10	50	5	5	40	-	-	86
1_11	78	2	-	-	-	20	83
1_12	58	2	-	-	-	40	90

Abbreviations: *N*-isopropylacrylamide (NIPAm); *N,N'*-methylenebisacrylamide (Bis); acrylic acid (Aac); *N-tert*-butylacrylamide (TBAm); *N*-phenylacrylamide (PAA); *N*-acryloyl L-Phenylalanine (APhe)
[a]NP synthesized with 2% PheBis (Phenylene-bis acrylamide) cross-linker not MBis

Table 3.S2. NP size measured using dynamic light scattering for each *first-generation* NP

NP	d. nm 25 ºC H₂O	PDI[a]	d. nm 37 ºC Buffer	PDI
1_1	151	0.02	1132	0.23
1_2	297	0.02	PDQ[b]	PDQ
1_3	81	0.02	PDQ	PDQ
1_4	86	0.02	208	0.11
1_5	69	0.07	120	0.03
1_6	287	0.05	257	0.05
1_7	133	<0.01	231	0.04
1_8	271	0.07	PDQ	PDQ
1_9	86	0.04	133	0.08
1_10	95	0.06	109	0.05
1_11	89	0.06	230	0.05
1_12	92	0.04	275	0.01

[a]Poly dispersity index (PDI) represents (standard deviation/diameter)^2
[b]PDQ represents poor data quality determined by the Malvern software

Table 3.S3. Feed of Monomers used for each *second-generation* NP and %Yield

NP	NIPAm (mol%)	Bis (mol%)	Aac (mol%)	TBAm (mol%)	PAA (mol%)	APhe (mol%)	% Yield
2_1	73	2	20	-	5	-	76
2_2	68	2	20	-	10	-	47
2_3	58	2	20	-	20	-	93
2_4	48	2	20	-	30	-	86
2_5	53	2	5	-	40	-	63
2_6	48	2	10	-	40	-	37
2_7	38	2	20	-	40	-	69
2_8	28	2	30	-	40	-	70
2_9	40	0	20	-	40	-	89
2_10	35	5	20	-	40	-	86
2_11	30	10	20	-	40	-	83
2_12	25	15	20	-	40	-	90

Abbreviations: *N*-isopropylacrylamide (NIPAm); *N,N'*-methylenebisacrylamide (Bis); acrylic acid (Aac); *N-tert*-butylacrylamide (TBAm); *N*-phenylacrylamide (PAA); *N*-acryloyl L-Phenylalanine (APhe)

Table 3.S4. NP size measured using dynamic light scattering for each *second-generation* NP

NP	d. nm 25 ºC H_2O	PDI[a]	d. nm 37 ºC Buffer	PDI
2_1	278	0.04	324	0.04
2_2	167	0.035	233	0.025
2_3	137	0.05	217	0.005
2_4	120	0.027	175	0.086
2_5	96	0.071	106	0.002
2_6	103	0.084	130	0.042
2_7	102	0.15	158	0.066
2_8	97	0.068	148	0.016
2_9	90	0.055	123	0.047
2_10	97	0.108	128	0.047
2_11	96	0.091	130	0.021
2_12	106	0.08	130	0.021

[a]Poly dispersity index (PDI) represents (standard deviation/diameter)^2
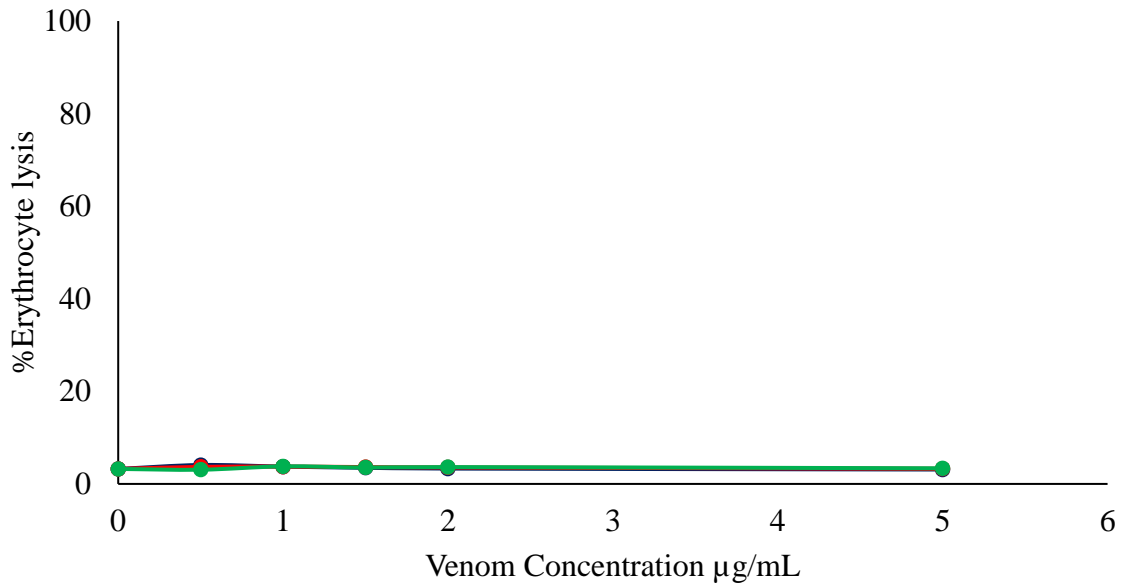
Figure 3.S1. %Erythrocyte lysis without the addition of phosphatidylcholine at various venom concentrations. *Bungarus caeruleus* (blue), *Naja sputatrix* (red), *Crotalus atrox* (green). The data is normalized against a triton-X (detergent) control.
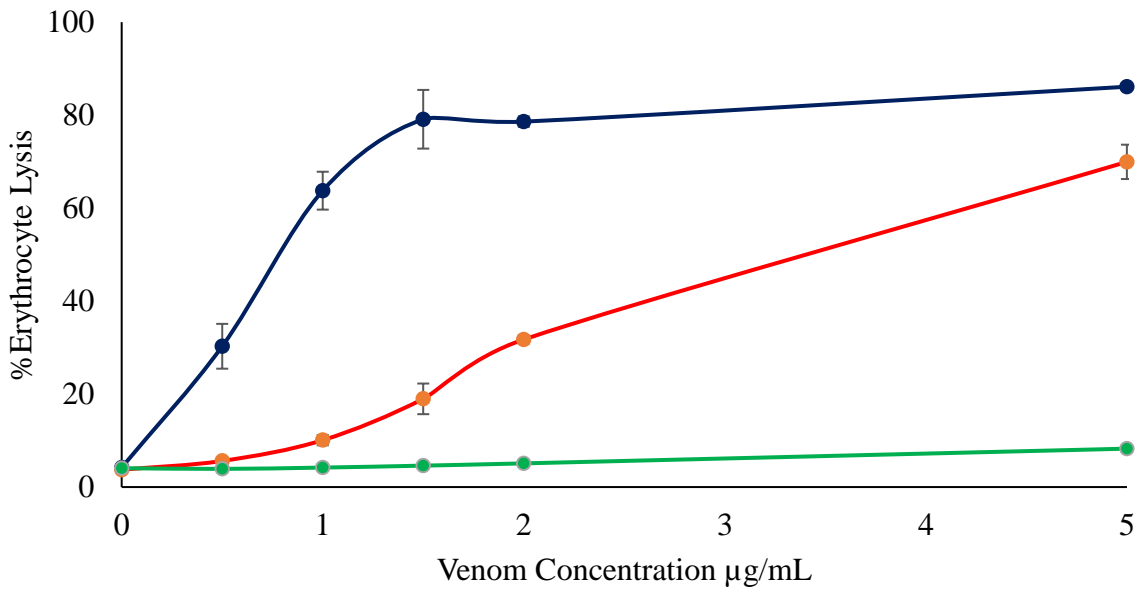
Figure 3.S2. %Erythrocyte lysis observed with the addition of 100 µg/mL phosphatidylcholine at various venom concentrations. *Bungarus caeruleus* (blue), *Naja sputatrix* (red), *Crotalus atrox* (green). The data is normalized against a triton-X (detergent) control.
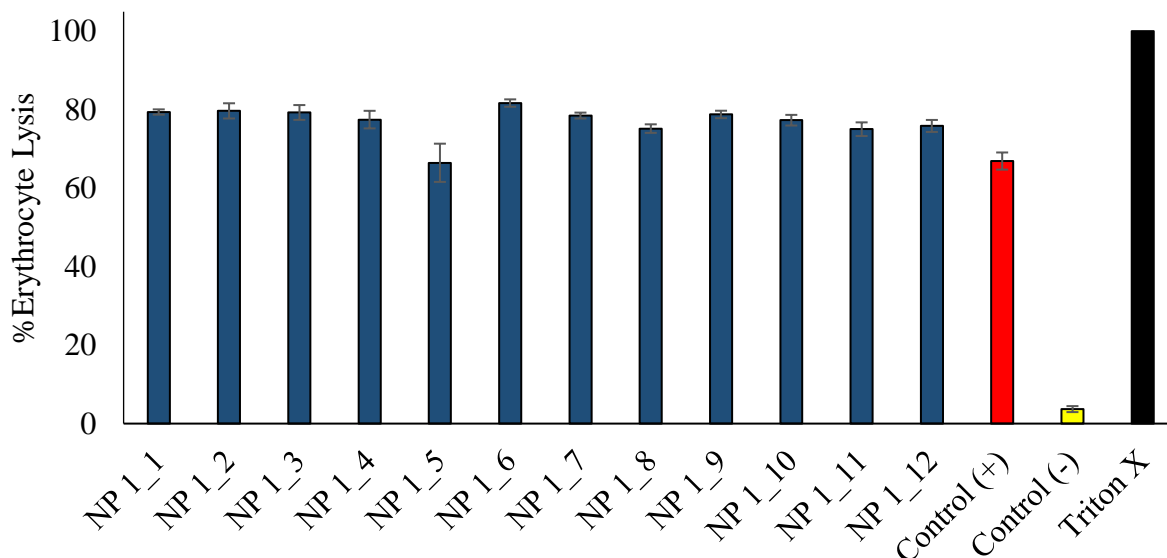
Figure 3.S3. %Erythrocyte lysis observed for NPs 1-12 (0.1 µg/mL) incubated with *Bungarus caeruleus* venom (1 µg/mL) and phosphatidylcholine (100 µg/mL). Control (+, red) represents Venom incubated without NPs, Control (-, yellow) represents samples without venom or NPs, and Control (Triton X, black) represents RBCs incubated with the detergent triton-X. The data is normalized against the triton-X (detergent) control.
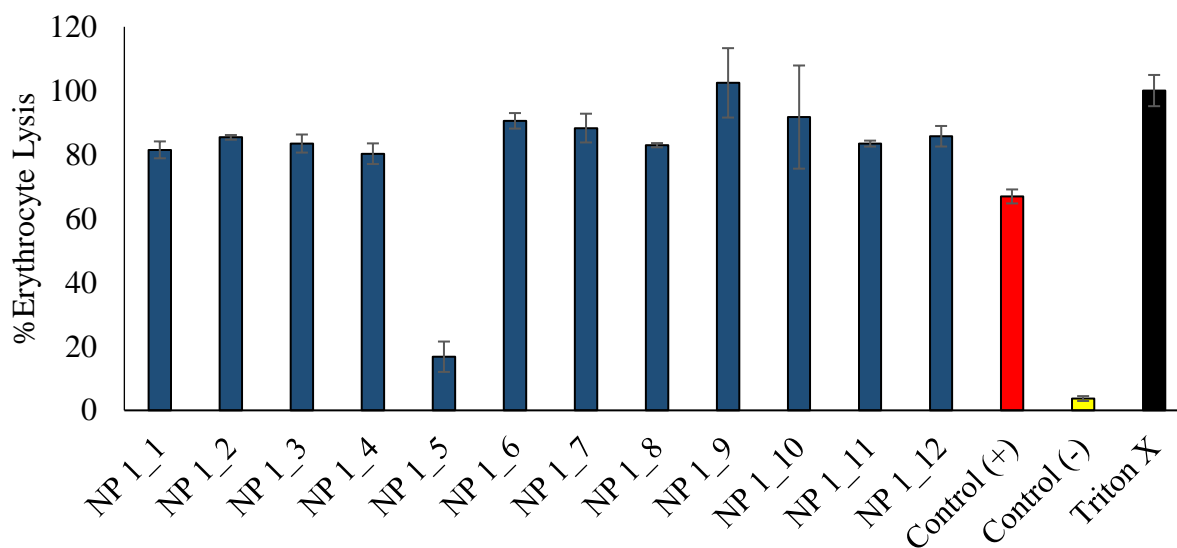
Figure 3.S4. %Erythrocyte lysis observed for NPs (0.5 µg/mL) incubated with *Bungarus caeruleus* venom (1 µg/mL) and phosphatidylcholine (100 µg/mL). Control (+, red) represents Venom incubated without NPs, Control (-, yellow) represents samples without venom or NPs, and Control (TX, black) represents RBCs incubated with the detergent triton-X. The data is normalized against the triton-X (detergent) control.
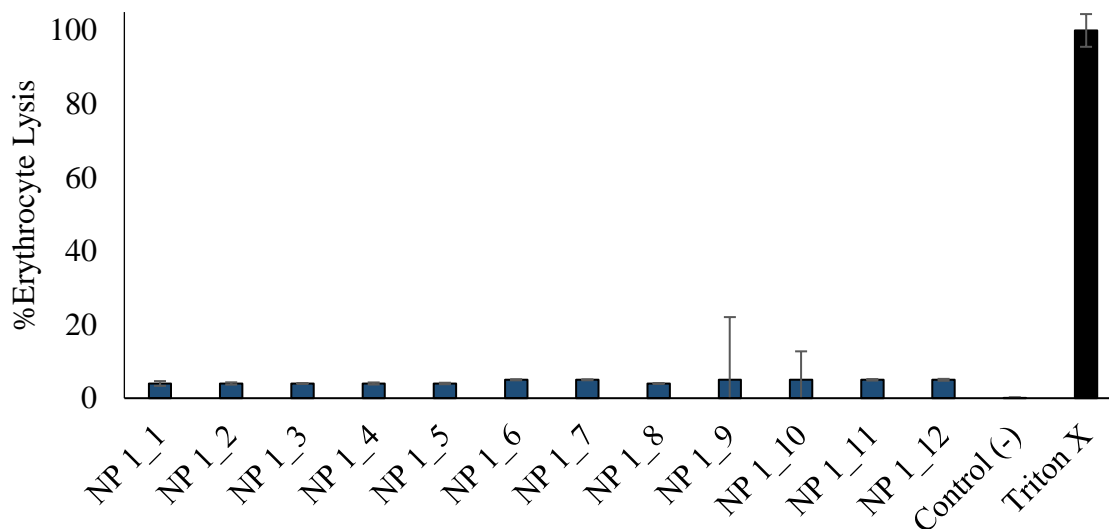
Figure 3.S5. %Erythrocyte lysis observed for NPs (0.5 µg/mL) incubated with phosphatidylcholine (100 µg/mL). Control (-) represents samples without NPs, and Control (TX, black) represents RBCs incubated with the detergent triton-X. The data is normalized against the triton-X (detergent) control.
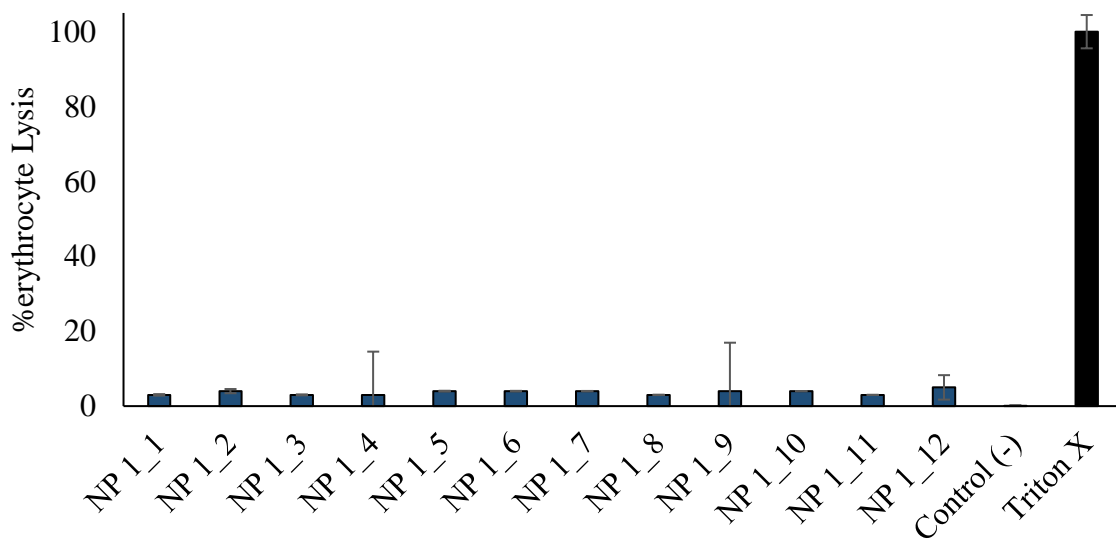
Figure 3.S6. %Erythrocyte lysis observed for NPs (0.5 µg/mL) incubated without phosphatidylcholine (100 µg/mL). Control (-) represents samples without NPs, and Control (TX, black) represents RBCs incubated with the detergent triton-X. The data is normalized against a triton-X (detergent) control.
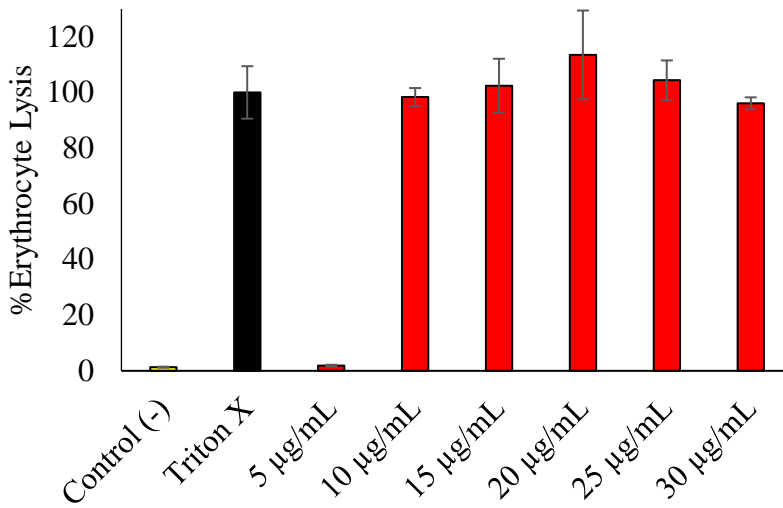
Figure 3.S7. Hemolysis of RBCs without the addition of phosphatidylcholine. Analyzing the onset of melittin hemolytic activity.
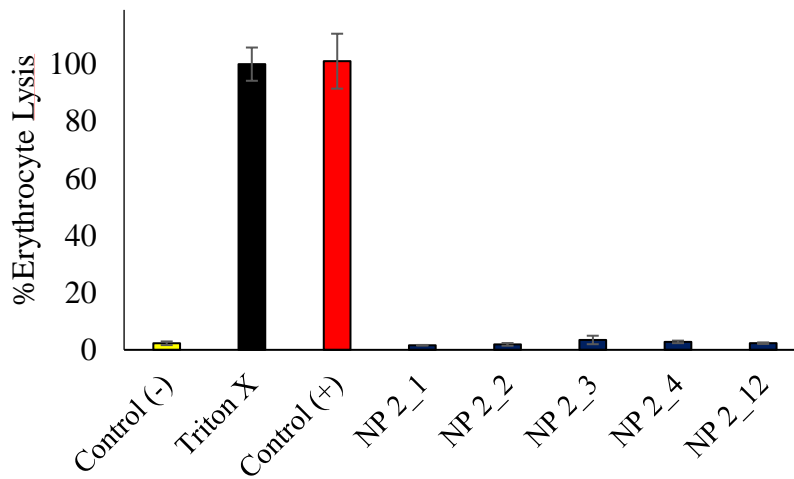
Figure 3.S8. Activity assay **without phosphatidylcholine** using 10 µg/mL of whole Bee venom and a final concentration of 0.5 mg/mL NP.
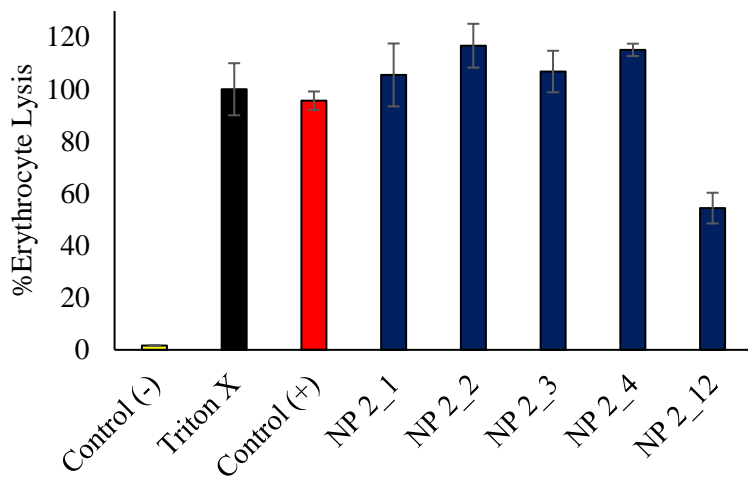
Figure 3.S9. Activity assay **with phosphatidylcholine** using 10 µg/mL of whole Bee venom and a final concentration of 0.5 mg/mL NP.
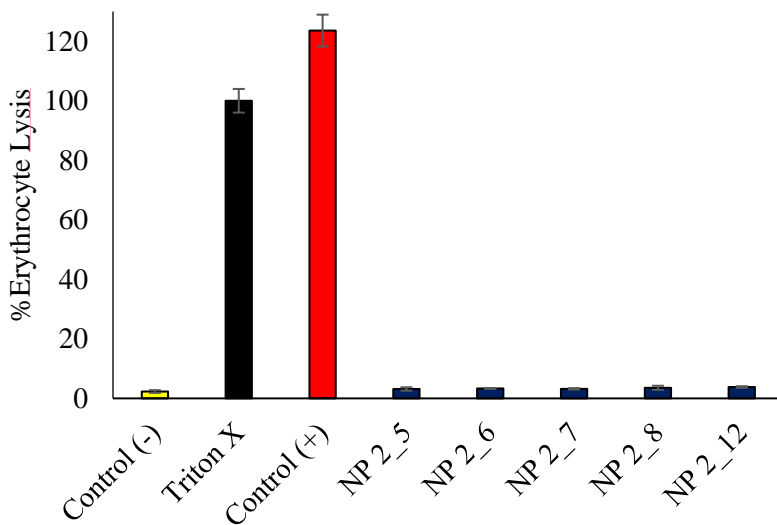
Figure 3.S10. Activity assay **without phosphatidylcholine** using 10 µg/mL of whole Bee venom and a final concentration of 0.5 mg/mL NP.
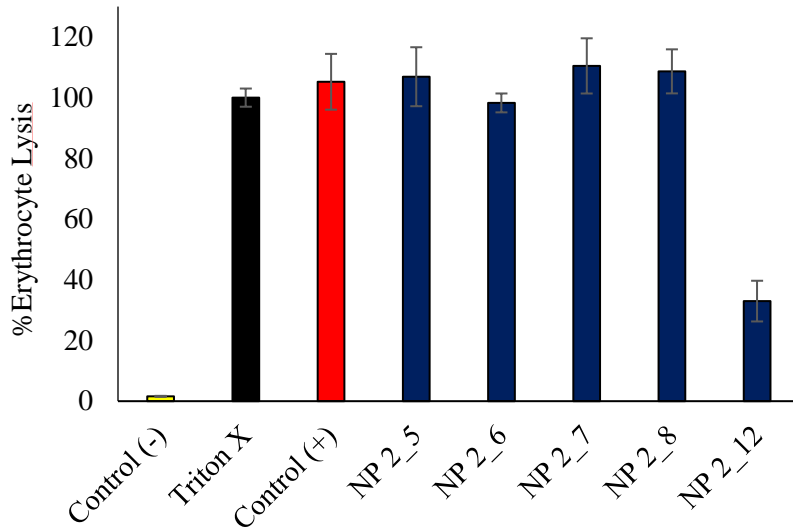
Figure 3.S11. Activity assay **with phosphatidylcholine** using 10 µg/mL of whole Bee venom and a final concentration of 0.5 mg/mL NP.
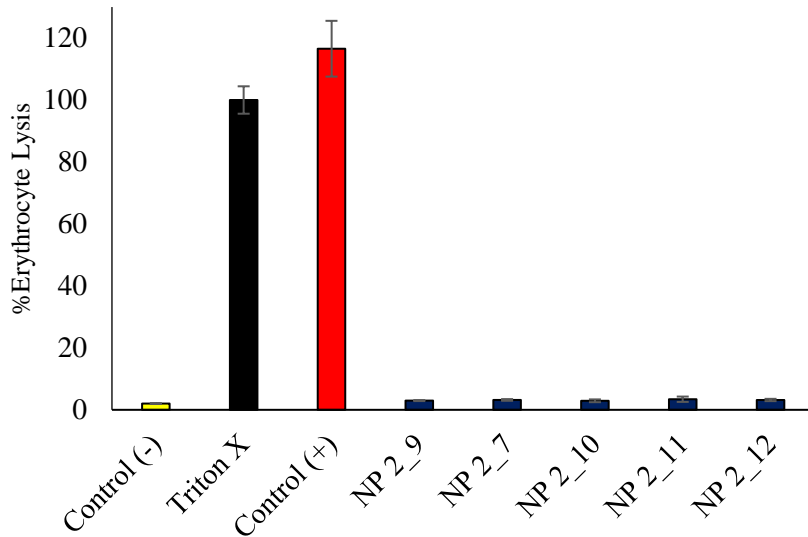
Figure 3.S12. Activity assay **without phosphatidylcholine** using 10 µg/mL of whole Bee venom and a final concentration of 0.5 mg/mL NP.
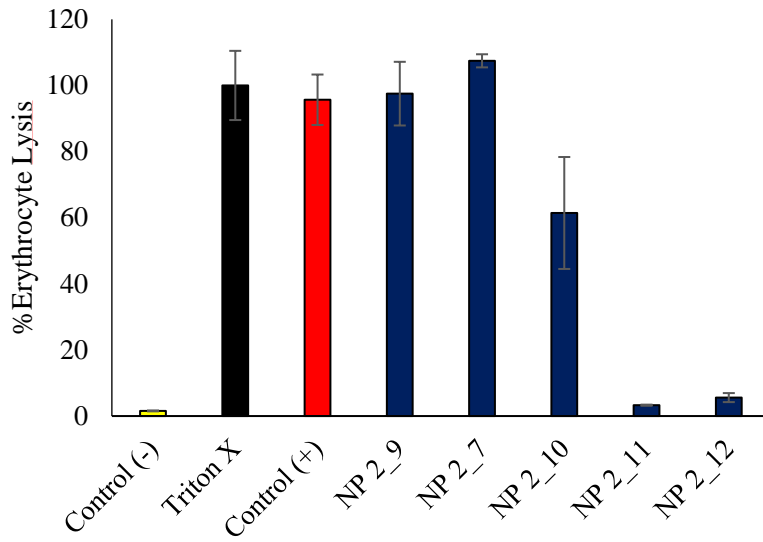
Figure 3.S13. Activity assay **with phosphatidylcholine** using 10 µg/mL of whole Bee venom and a final concentration of 0.5 mg/mL NP.
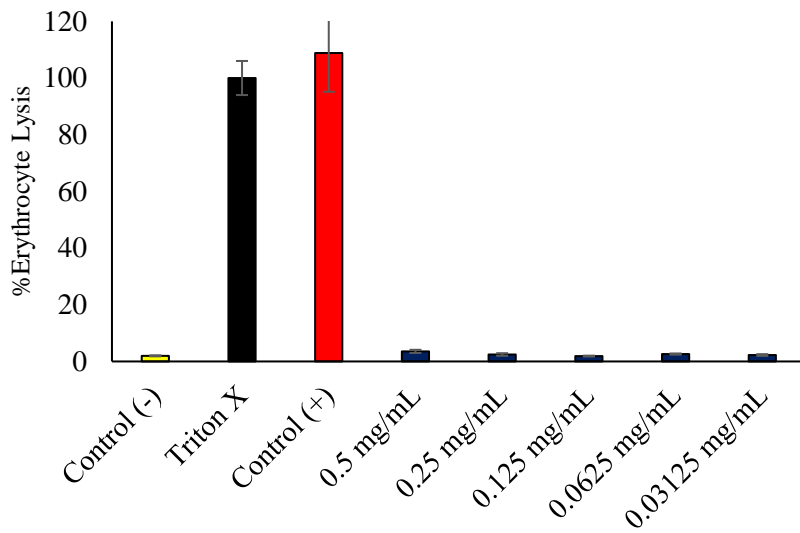
Figure 3.S14. Activity assay **without phosphatidylcholine** using 10 µg/mL of whole Bee venom and varying concentrations of NP2_11.
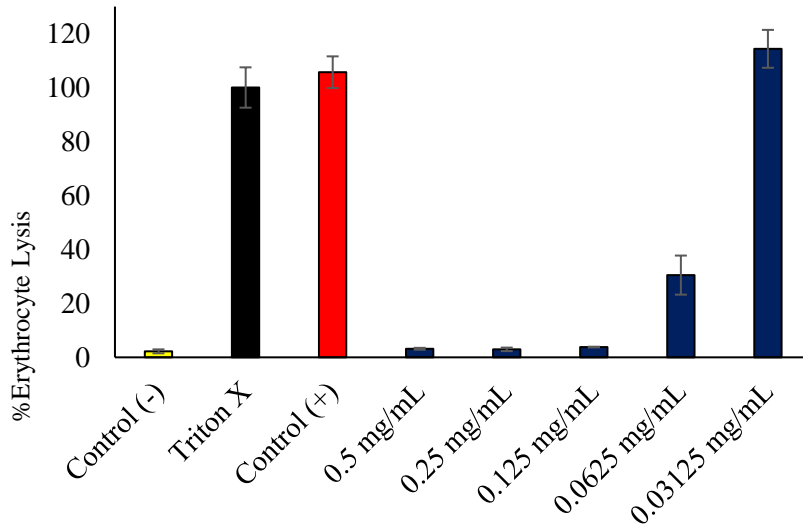
Figure 3.S15. Activity assay **with phosphatidylcholine** using 10 µg/mL of whole Bee venom and varying concentrations of NP2_11
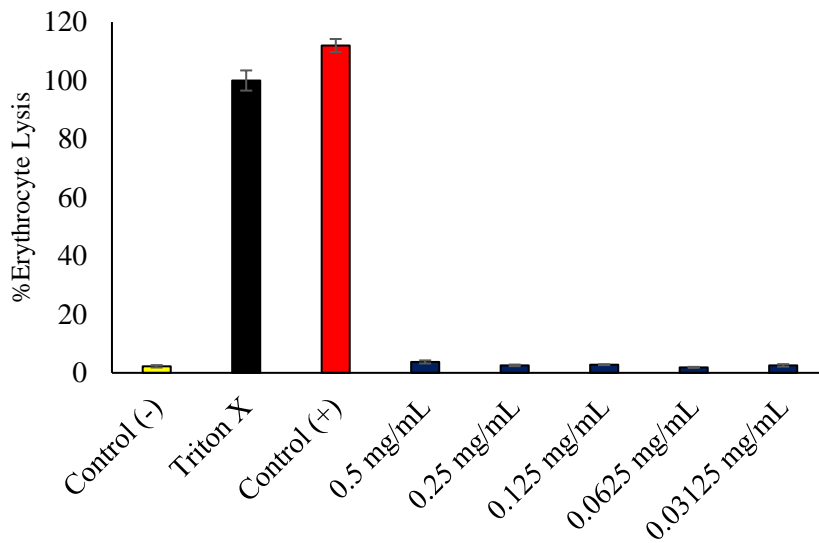
Figure 3.S16. Activity assay **without phosphatidylcholine** using 10 µg/mL of whole Bee venom and varying concentrations of NP2_12
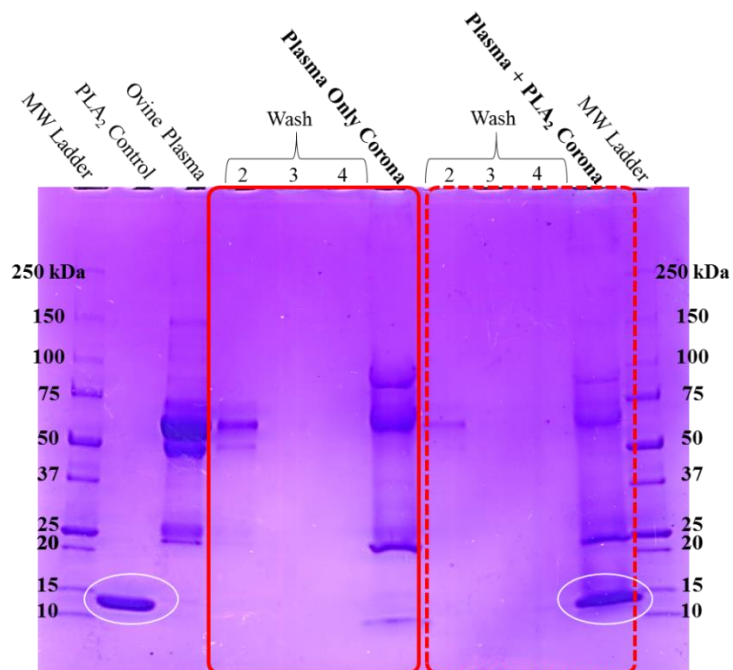
Figure 3.S17. Selectivity for PLA$_2$ from *Naja mossambica* venom (~1% w/w total protein) in ovine plasma (25%) using NP 2_12.
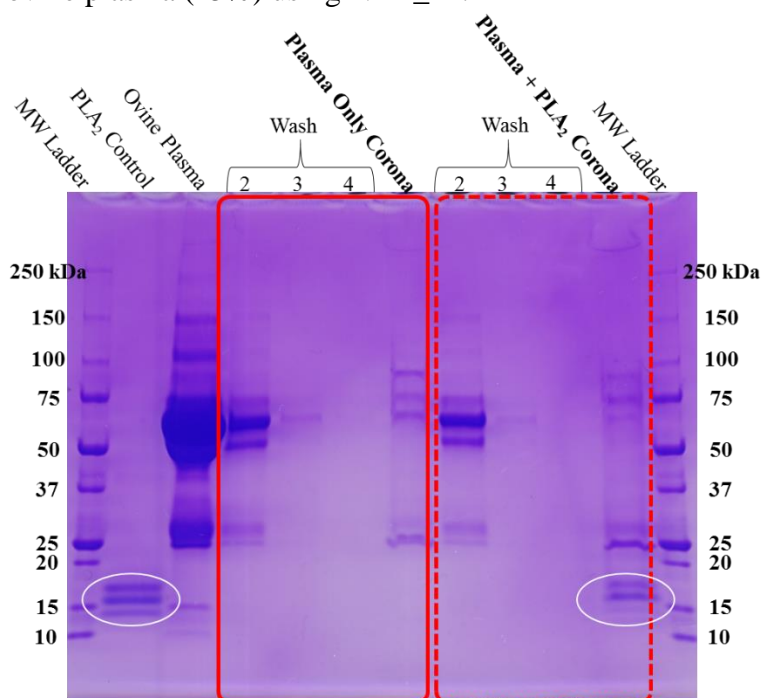
Figure 3.S18. Selectivity for PLA$_2$ from *Apis meliffera* venom (~1% w/w total protein) in ovine plasma (25%) using NP 2_12.
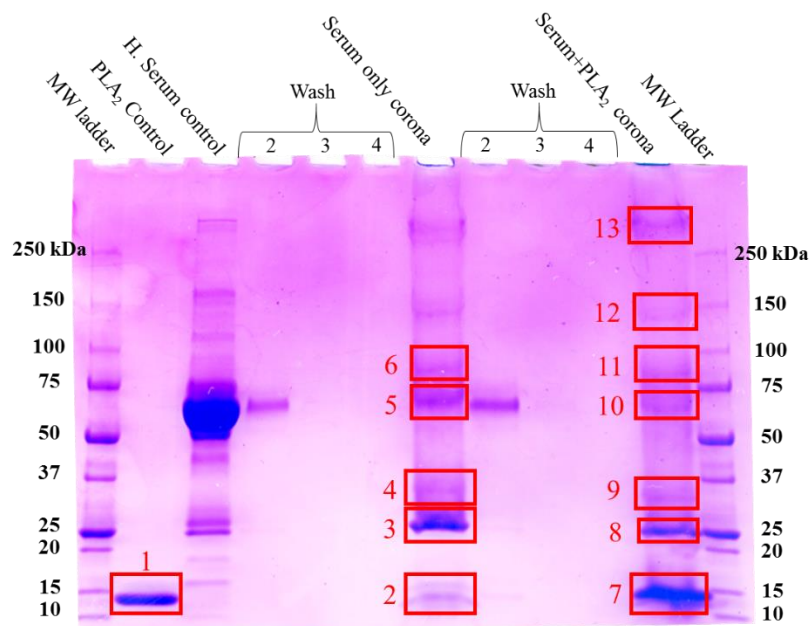
Figure 3.S19. Selectivity for PLA$_2$ from *Naja mossambica* venom (~1% w/w total protein) in human serum (25%) using NP 2_12. The labelled bands were excised and subjected to proteomic analysis. (see Table 3.S5)

Table 3.S5. LC-MS/MS results from digestion of the SDS-PAGE gel depicted in figure 3.S19.

Band	Accession	Entry	Description	mW (Da)	pI (pH)	PLGS Score[a]	Peptides	Theoretical Peptides	Coverage (%)
1	PA2A1_NAJMO	P00602	Naja mossambica Acidic phospholipase A2	13209	6.271	1302.784	5	8	22.0339
2	F8W696	tr	Human Apolipoprotein A-I	27891	5.7305	1494.101	3	25	13.8776
2	APOA1_HUMAN	P02647	Human Apolipoprotein A-I	30758	5.4316	1494.101	3	32	12.7341
3	APOA1_HUMAN	P02647	Human Apolipoprotein A-I	30758	5.4316	15630.63	26	32	56.9288
3	F8W696	tr	Human Apolipoprotein A-I	27891	5.7305	10804.39	19	25	49.7959
3	A0A087WZW8	tr	Human Ig kappa chain C region	12988	7.0781	763.4428	2	8	26.8908
3	A0A087X1V9	tr	Human Ig kappa chain C region	26079	7.0752	763.4428	2	12	13.3891
3	IGKC_HUMAN	P01834	Human Ig kappa chain C region	11601	5.5005	763.4428	2	7	30.1887
3	A0A075B6H6	tr	Human Ig kappa chain C region	11712	5.5005	763.4428	2	7	29.9065
3	A0A0U1RRF4	tr	Human Protein IGKV1-8	19954	8.6602	714.0437	1	9	9.8361
3	A0A087WWV8	tr	HUMAN Protein IGKV1-12	20055	8.1123	714.0437	1	9	9.7297
4	APOA1_HUMAN	P02647	Human Apolipoprotein A-I	30758	5.4316	5138.952	11	32	43.8202
4	F8W696	tr	Human Apolipoprotein A-I	27891	5.7305	3644.409	8	25	37.1429
4	APOE_HUMAN	P02649	Human Apolipoprotein E	36131	5.4829	4021.728	15	30	49.5268
4	H0Y7L5	tr	Human Apolipoprotein E (Fragment)	30618	8.2061	3622.581	9	27	35.6877
4	E9PEV4	tr	Human Apolipoprotein E (Fragment)	24631	5.5986	3304.42	8	21	37.5
4	E7ERP7	tr	Human Apolipoprotein E (Fragment)	24888	5.5986	3304.42	8	21	36.9863
5	ALBU_HUMAN	P02768	Human Serum albumin	69321	5.8608	3554.346	31	55	35.468

Band	Accession	Entry	Description	mW (Da)	pI (pH)	PLGS Score[a]	Peptides	Theoretical Peptides	Coverage (%)
5	A0A0C4DGB6	tr	Human Serum albumin	69181	5.9385	2904.132	21	53	32.2848
5	D6RHD5	tr	Human Serum albumin	52025	6.4307	2737.688	29	40	42.7015
5	H0YA55	tr	Human Serum albumin (Fragment)	51537	6.5552	2737.688	29	40	43.1718
5	B7WNR0	tr	Human Serum albumin	56175	6.8027	2737.688	29	43	39.6761
5	A0A087WWT3	tr	Human Serum albumin	45118	5.7026	2467.75	22	36	33.3333
5	C9JKR2	tr	Human Albumin, isoform CRA_k	47256	5.9238	2093.285	26	36	41.7266
5	H7C013	tr	Human Serum albumin (Fragment)	22844	5.8931	1461.061	5	22	21.3198
7	F8W696	tr	Human Apolipoprotein A-I	27891	5.7305	997.3894	5	25	17.9592
7	APOA1_HUMAN	P02647	Human Apolipoprotein A-I	30758	5.4316	997.3894	5	32	16.4794
7	PA2A1_NAJMO	P00602	Naja Mossambica Acidic phospholipase A2	13209	6.271	2770.474	6	8	22.0339
8	APOA1_HUMAN	P02647	Human Apolipoprotein A-I	30758	5.4316	14513.56	28	32	53.5581
8	F8W696	tr	Human Apolipoprotein A-I	27891	5.7305	9418.841	20	25	46.1224
8	A0A087WWV8	tr	Human Protein IGKV1-12	20055	8.1123	1535.01	2	9	18.3784
8	A0A087WZW8	tr	Human Ig kappa chain C region	12988	7.0781	1535.01	2	8	28.5714
8	A0A087X1V9	tr	Human Ig kappa chain C region	26079	7.0752	1535.01	2	12	14.2259
8	A0A0U1RRF4	tr	Human Protein IGKV1-8	19954	8.6602	1535.01	2	9	18.5792
8	IGKC_HUMAN	P01834	Human Ig kappa chain C region	11601	5.5005	1535.01	2	7	32.0755
8	A0A075B6H6	tr	Human Ig kappa chain C region (Fragment)	11712	5.5005	1535.01	2	7	31.7757
8	C1QC_HUMAN	P02747	Human Complement C1q subcomponent subunit C	25757	8.5444	565.0618	3	16	15.9184

Band	Accession	Entry	Description	mW (Da)	pI (pH)	PLGS Score[a]	Peptides	Theoretical Peptides	Coverage (%)
9	APOE_HUMAN	P02649	Human Apolipoprotein E	36131	5.4829	4803.459	13	30	49.5268
9	H0Y7L5	tr	Human Apolipoprotein E (Fragment)	30618	8.2061	4383.624	8	27	35.6877
9	E9PEV4	tr	Human Apolipoprotein E (Fragment)	24631	5.5986	4157.694	7	21	37.5
9	E7ERP7	tr	Human Apolipoprotein E (Fragment)	24888	5.5986	4157.694	7	21	36.9863
9	APOA1_HUMAN	P02647	Human Apolipoprotein A-I	30758	5.4316	584.0214	6	32	30.3371
9	F8W696	tr	Human Apolipoprotein A-I	27891	5.7305	500.5833	4	25	22.449
10	ALBU_HUMAN	P02768	Human Serum albumin	69321	5.8608	2066.65	21	55	34.1544
10	A0A087WWT3	tr	Human Serum albumin	45118	5.7026	1901.834	15	36	33.0808
10	C9JKR2	tr	Human Serum Albumin, isoform CRA_k	47256	5.9238	1518.171	16	36	35.9712
10	D6RHD5	tr	Human Serum albumin	52025	6.4307	1518.171	17	40	35.9477
10	H0YA55	tr	Human Serum albumin (Fragment)	51537	6.5552	1518.171	17	40	36.3436
10	B7WNR0	tr	Human Serum albumin	56175	6.8027	1518.171	17	43	33.4008
10	A0A0C4DGB6	tr	Human Serum albumin	69181	5.9385	1418.79	15	53	30.9603
10	H7C013	tr	Human Serum albumin (Fragment)	22844	5.8931	548.4787	5	22	29.4416
10	HRG_HUMAN	P04196	Human Histidine-rich glycoprotein	59540	7.0957	1564.894	9	33	18.4762
11	ANT3_HUMAN	P01008	Human Antithrombin-III	52568	6.3047	1058.862	11	37	30.6034
11	Q8TCE1	tr	Human Antithrombin-III	29073	8.9883	947.9147	4	20	26.2548
11	HRG_HUMAN	P04196	Human Histidine-rich glycoprotein	59540	7.0957	1055.375	6	33	14.0952
12	A8MUN2	tr	Human Apolipoprotein B-100	92560	7.1543	569.2287	12	78	25.2415

[a]A PLGS score cut off of 500 was used
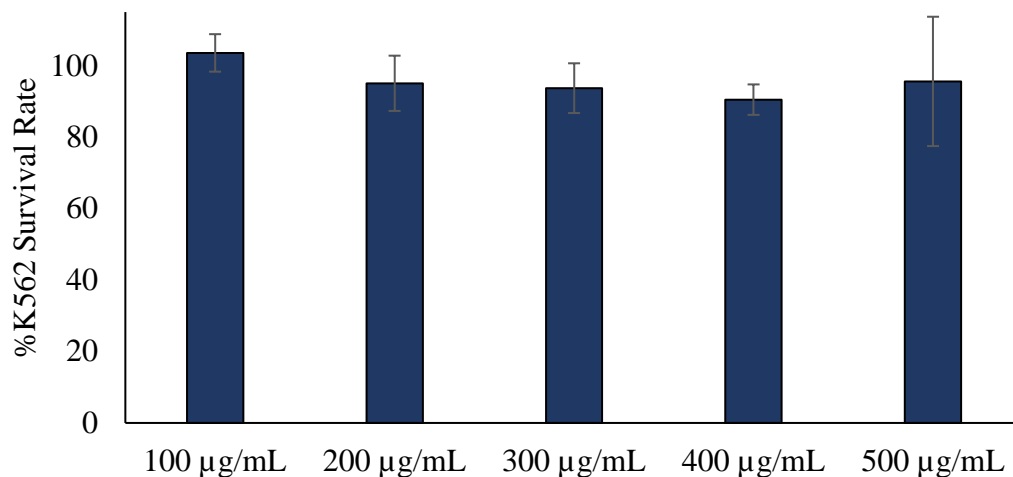
Figure 3.S20. MTT assay results examining K562 survival rate in the presence of NP 2_12 at various concentrations. The results were normalized to results incubated without NP 2_12. The survival rate is equal to the mean (+/-) the standard deviation ($n = 6$).

N,N'-(1,4-phenylene)bisacylamide (PheBis)
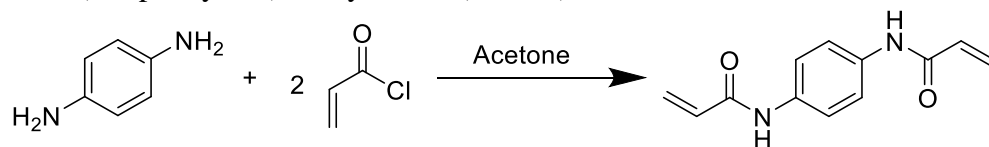
N,N'-(1,4-phenylene)bisacylamide was synthesized by the previously reported procedure with minor revisions.[37] 1,4-phenylenediamine (5.6 mmol, 605.6 mg) was mixed with acetone (25 mL), and cooled to 0 °C in an ice bath. Acryloyl chloride (11 mmol, 898.0 µL) was mixed with acetone (15 mL), and added dropwise to the solution of 1,4-phenylenediamine, while stirring, and allowed to warm to room temperature and kept at room temperature overnight. The solution was then washed with saturated $NaHCO_3$, filtered and the solid was washed with 100 mL of cold H_2O. The crude product was recrystallized from EtOH/MeOH, to afford white crystals that were collected by filtration (1.1890 g, 87%): ^1H NMR (500 MHz, DMSO): δ 10.14 (s, 2H, (NH)$_2$), 7.64 (s, 4H, (Phe-H)$_4$), 6.42 (dd, *J*= 17.0, 10.0, 2H, (=CH)$_2$), 6.26 (dd, *J*= 17.0, 2.0 Hz, 2H, (=CH$_2$)$_2$), 5.76 (dd, *J*= 10.0, 2.5 Hz, 2H, (=CH$_2$)$_2$; ESMS *m / z* calcd for $C_{12}H_{12}N_2O_2Na$ (M + Na)$^+$ 239.08, found 239.04; mp > 275 °C (Lit. 243 °C).
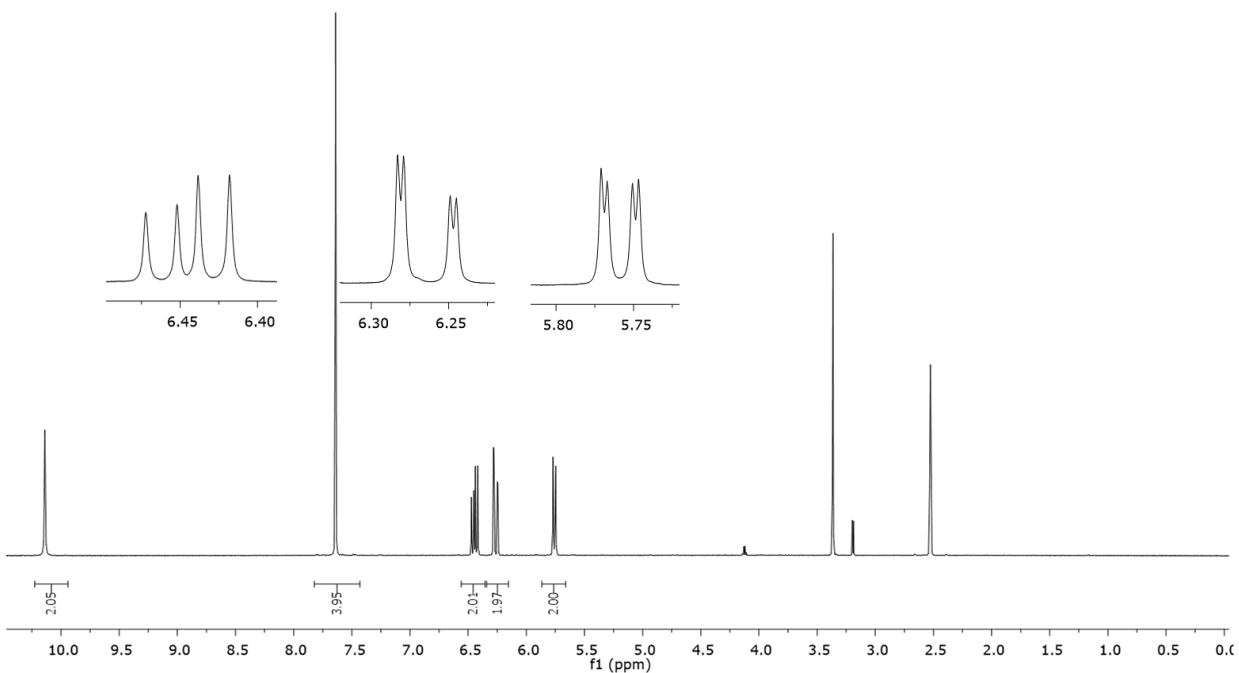
N-acryloyl L-Phenylalanine (APhe)
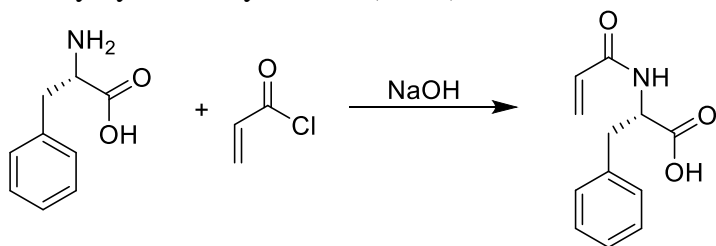
L-Phenylalanine (3.63 g, 0.020 mol) was dissolved in 20 mL of 2M sodium hydroxide aqueous solution. After the solution became transparent, acryloyl chloride (1.75 mL, 0.022) was added dropwise with vigorous stirring while the reaction mixture was kept below 0 ℃ by external ice-bath cooling. After the addition was completed, the stirring was continued for an additional 2 h at room temperature and a white powder precipitated. The mixture was acidified to pH 2 with concentrated hydrochloride acid. The obtained white product was recrystallized with water (2.74 g, 45.7% yield):: ^{1}H NMR (500 MHZ, CD$_3$OD): δ 7.24~7.16 (m, 5 H, C$_6$$H_5$), 6.27~6.13 (dd, J = 17.5 Hz, 10.5 Hz, 1 H, CH=CH$_2$), 6.21~6.13 (d, J = 17.5 Hz, 1 H, CH=CH_2 $_{trans}$), 5.62 (d, J = 10.5 Hz, 1 H, CH=CH_2 $_{cis}$), 4.75~4.71 (m, CHCH$_2$), 3.25~3.20 (m, 1 H, CH_2CH), 3.01~2.96 (m, 1 H, CH_2CH); ESMS m / z calcd for C$_{12}$H$_{13}$NNaO$_3$ [M + Na]$^+$ 242.2263, found 242.3; mp 122.5~124 ℃
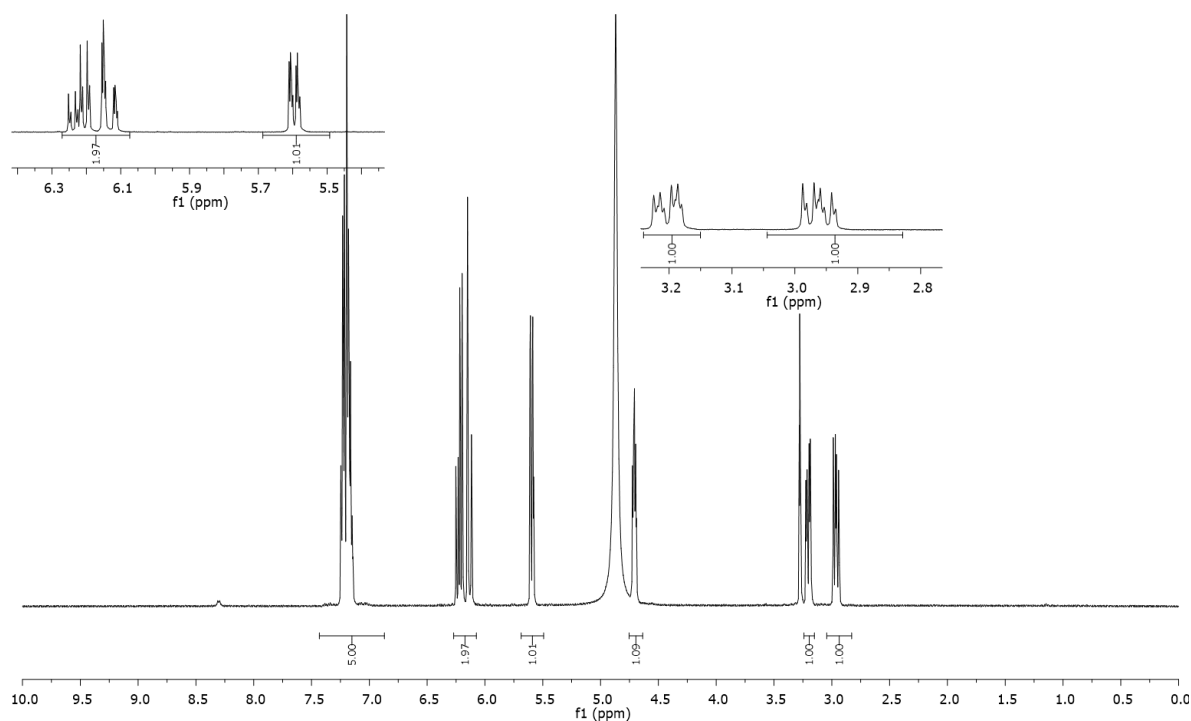
F. References

(1)   Williams, D.; Gutierrez, J. M.; Harrison, R.; Warrell, D. A.; White, J.; Winkel, K. D.; Gopalakrishnakone, P.; Worki, G. S. B. I.: The Global Snake Bite Initiative: an antidote for snake bite. *Lancet* **2010**, *375*, 89-91.

(2)   Gutierrez, J. M.; Williams, D.; Fan, H. W.; Warrell, D. A.: Snakebite envenoming from a global perspective: Towards an integrated approach. *Toxicon* **2010**, *56*, 1223-1235.

(3)   Kasturiratne, A.; Wickremasinghe, A. R.; de Silva, N.; Gunawardena, N. K.; Pathmeswaran, A.; Premaratna, R.; Savioli, L.; Lalloo, D. G.; de Silva, H. J.: The Global Burden of Snakebite: A Literature Analysis and Modelling Based on Regional Estimates of Envenoming and Deaths. *PLoS Med.* **2008**, *5*, 1591-1604.

(4)   Alirol, E.; Sharma, S. K.; Bawaskar, H. S.; Kuch, U.; Chappuis, F.: Snake Bite in South Asia: A Review. *PLoS Neglect. Trop. D.* **2010**, 4.

(5)   Mohapatra, B.; Warrell, D. A.; Suraweera, W.; Bhatia, P.; Dhingra, N.; Jotkar, R. M.; Rodriguez, P. S.; Mishra, K.; Whitaker, R.; Jha, P.; Collaborators, M. D. S.: Snakebite Mortality in India: A Nationally Representative Mortality Survey. *PLoS Neglect. Trop. D.* **2011**, *5*.

(6)   Angulo, Y.; Estrada, R.; Gutierrez, J. M.: Clinical and laboratory alterations in horses during immunization with snake venoms for the production of polyvalent (Crotalinae) antivenom. *Toxicon* **1997**, *35*, 81-90.

(7)   Fry, B. G.; Wickramaratna, J. C.; Jones, A.; Alewood, P. F.; Hodgson, W. C.: Species and regional variations in the effectiveness of antivenom against the in Vitro neurotoxicity of death adder (Acanthophis) venoms. *Toxicol. Appl. Pharm.* **2001**, *175*, 140-148.

(8)   Fry, B. G.; Winkel, K. D.; Wickramaratna, J. C.; Hodgson, W. C.; Wuster, W.: Effectiveness of snake antivenom: Species and regional venom variation and its clinical impact. *J. Toxicol-Toxin Rev.* **2003**, *22*, 23-34.

(9)   Hoffman, R. S.: Antidote shortages in the United States: impact and response. *Clin. Toxicol.* **2014**, *52*, 157-159.

(10)   Schiermeier, Q. Africa braced for snakebite crisis. *Nature* **2015**, *525*, 299.

(11)   Reeks, T. A.; Fry, B. G.; Alewood, P. F. Privileged frameworks from snake venom. *Cell. Mol. Life Sci.* **2015**, *72*, 1939-1958.

(12)   Fry, B. G.: From genome to "venome": Molecular origin and evolution of the snake venom proteome inferred from phylogenetic analysis of toxin sequences and related body proteins. *Genome Res.* **2005**, *15*, 403-420.

(13)   O'Brien, J.; Shea, K. J.: Tuning the Protein Corona of Hydrogel Nanoparticles: The Synthesis of Abiotic Protein and Peptide Affinity Reagents. *Acc. Chem. Res.* **2016**, *49*, 1200-1210.

(14)   Yoshimatsu, K.; Lesel, B. K.; Yonamine, Y.; Beierle, J. M.; Hoshino, Y.; Shea, K. J.: Temperature-Responsive "Catch and Release" of Proteins by using Multifunctional Polymer-Based Nanoparticles. *Angew. Chem. Int. Edit.* **2012**, *51*, 2405-2408.

(15)   Lee, S. H.; Hoshino, Y.; Randall, A.; Zeng, Z. Y.; Baldi, P.; Doong, R. A.; Shea, K. J.: Engineered Synthetic Polymer Nanoparticles as IgG Affinity Ligands. *J. Am. Chem. Soc.* **2012**, *134*, 15765-15772.

(16)   Weisman, A.; Chen, Y. A.; Hoshino, Y.; Zhang, H. T.; Shea, K.: Engineering Nanoparticle Antitoxins Utilizing Aromatic Interactions. *Biomacromolecules* **2014**, *15*, 3290-3295.

(17)   Hoshino, Y.; Koide, H.; Furuya, K.; Haberaecker, W. W.; Lee, S. H.; Kodama, T.; Kanazawa, H.; Oku, N.; Shea, K. J.: The rational design of a synthetic polymer nanoparticle that neutralizes a toxic peptide in vivo. *P. Natl. Acad. Sci. U.S.A.* **2012**, *109*, 33-38.

(18)   Koide, H.; Yoshimatsu, K.; Hoshino, Y.; Lee, S. H.; Okajima, A.; Ariizumi, S.; Narita, Y.; Yonamine, Y.; Weisman, A. C.; Nishimura, Y.; Oku, N.; Miura, Y.; Shea, K.J.: A polymer nanoparticle with engineered affinity for a vascular endothelial growth factor (VEGF$_{165}$) *Nat. Chem.* **2017**, *9*, 715-722.

(19)   Gazi, I.; Tsimihodimos, V.; Filippatos, T.; Lourida, E.; Elisaf, M.; Tselepis, A.: Lipoprotein-associated phospholipase A$_2$ activity (Lp-PLA$_2$) as a predictor of small-dense LDL particles. *J. Hypertens.* **2006**, *24*, S395-S396.

(20)   Hu, C. M. J.; Fang, R. H.; Copp, J.; Luk, B. T.; Zhang, L. F.: A biomimetic nanosponge that absorbs pore-forming toxins. *Nat. Nanotechnol.* **2013**, *8*, 336-340.

(21)   Scott, D. L.; White, S. P.; Otwinowski, Z.; Yuan, W.; Gelb, M. H.; Sigler, P. B.: Interfacial Catalysis - the Mechanism of Phospholipase-A$_2$. *Science* **1990**, *250*, 1541-1546.

(22)   Fry, B. G.; Roelants, K.; Champagne, D. E.; Scheib, H.; Tyndall, J. D. A.; King, G. F.; Nevalainen, T. J.; Norman, J. A.; Lewis, R. J.; Norton, R. S.; Renjifo, C.; de la Vega, R. C. R.: The Toxicogenomic Multiverse: Convergent Recruitment of Proteins Into Animal Venoms. *Annu. Rev. Genom. Hum. G.* 2009, 10, 483-511.

(23)   Kini, R. M.: Excitement ahead: structure, function and mechanism of snake venom phospholipase A(2) enzymes. *Toxicon* **2003**, *42*, 827-840.

(24)   Kini, R. M.; Evans, H. J.: A Model to Explain the Pharmacological Effects of Snake-Venom Phospholipases-A2. *Toxicon* **1989**, *27*, 613-635.

(25)   Bierbaum, T. J.; Bouma, S. R.; Huestis, W. H.: Mechanism of Erythrocyte Lysis by Lysophosphatidylcholine. *Biochim. Biophys. Acta* **1979**, *555*, 102-110.

(26)   Alabdulla, I. H.; Sidki, A. M.; Landon, J.: An Indirect Hemolytic Assay for Assessing Antivenoms. *Toxicon* **1991**, *29*, 1043-1046.

(27)   Zhou, J. H.; Zhao, J.; Zhang, S. X.; Shen, J. Z.; Qi, Y. T.; Xue, X. F.; Li, Y.; Wu, L. M.; Zhang, J. Z.; Chen, F.; Chen, L. Z.: Quantification of melittin and apamin in bee venom lyophilized powder from Apis mellifera by liquid chromatography-diode array detector-tandem mass spectrometry. *Anal. Biochem.* **2010**, *404*, 171-178.

(28)   Cajal, Y.; Jain, M. K.: Synergism between mellitin and phospholipase A(2) from bee venom: Apparent activation by intervesicle exchange of phospholipids. *Biochemistry-Us* **1997**, *36*, 3882-3893.

(29)   Monopoli, M. P.; Aberg, C.; Salvati, A.; Dawson, K. A.: Biomolecular coronas provide the biological identity of nanosized materials. *Nat. Nanotechnol.* **2012**, *7*, 779-786.

(30)   Walkey, C. D.; Chan, W. C. W.: Understanding and controlling the interaction of nanomaterials with proteins in a physiological environment. *Chem. Soc. Rev.* **2012**, *41*, 2780-2799.

(31)   Fleischer, C. C.; Payne, C. K.: Nanoparticle-Cell Interactions: Molecular Structure of the Protein Corona and Cellular Outcomes. *Acc. Chem. Res.* **2014**, *47*, 2651-2659.

(32)   Lundqvist, M.; Stigler, J.; Elia, G.; Lynch, I.; Cedervall, T.; Dawson, K. A.: Nanoparticle size and surface properties determine the protein corona with possible implications for biological impacts. *P. Natl. Acad. Sci. U.S.A.* **2008**, *105*, 14265-14270.

(33)   Nel, A. E.; Madler, L.; Velegol, D.; Xia, T.; Hoek, E. M. V.; Somasundaran, P.; Klaessig, F.; Castranova, V.; Thompson, M.: Understanding biophysicochemical interactions at the nano-bio interface. *Nat. Mater.* **2009**, *8*, 543-557.

(34)   Saito, H.; Lund-Katz, S.; Phillips, M. C.: Contributions of domain structure and lipid interaction to the functionality of exchangeable human apolipoproteins. *Prog. Lipid Res.* **2004**, *43*, 350-380.

(35)   Zeng, Z. Y.; Patel, J.; Lee, S. H.; McCallum, M.; Tyagi, A.; Yan, M. D.; Shea, K. J.: Synthetic Polymer Nanoparticle-Polysaccharide interactions: A Systematic Study. *J. Am. Chem. Soc.* **2012**, *134*, 2681-2690.

(36)   Manuel, G.; Lupták, A.; Corn, R. M.: A Microwell–Printing Fabrication Strategy for the On-Chip Templated Biosynthesis of Protein Microarrays for Surface Plasmon Resonance Imaging. *J. Phys. Chem. C* **2016**, *120*, 20984-20990.

(37)   Al-Fulaij, O. A.; Elassar, A.-Z. A.; El-Dissouky, A.: Synthesis, characterization, and ligating behavior of poly[N,N-p-phenylene bisacryl (methacryl)amide]. *J. Appl. Polym. Sci.* **2006**, *101*, 2412-2422.

Chapter 4

Engineered nanoparticles bind elapid snake venom toxins and inhibit venom-induced dermonecrosis

A. Abstract

Envenomings by snakebites constitute a serious and challenging global health issue. The mainstay in the therapy of snakebite envenomings is the parenteral administration of animal-derived antivenoms. Significantly, antivenoms are only partially effective in the control of local tissue damage. A novel approach to mitigate the progression of local tissue damage that could complement the antivenom therapy of envenomings is proposed. We describe an abiotic hydrogel nanoparticle engineered to bind to and modulate the activity of a diverse array of PLA_2 and 3FTX isoforms found in Elapidae snake venoms. These two families of protein toxins share features that are associated with their common (membrane) targets, allowing for nanoparticle sequestration by a mechanism that differs from immunological (epitope) selection. The nanoparticles are non-toxic in mice and inhibit dose-dependently the dermonecrotic activity of *Naja nigricollis* venom.

B. Introduction

Envenomings by snakebites constitute a serious and challenging global health issue, which affects approximately 2.5 million people and causes more than 100,000 deaths annually. This situation is particularly acute in impoverished rural settings of sub-Saharan Africa, Asia and Latin America.[1-4] In addition, an estimated number of 400,000 people suffering snakebite envenomings end up with permanent physical and psychological sequelae which greatly affect their quality of life and generates a wave of social suffering in their families and communities.[4,5] Owing to its worldwide impact, the World Health Organization (WHO) recently included snakebite

envenoming as a category A disease in its list of Neglected Tropical Diseases.[4] The mainstay in the therapy of snakebite envenomings is the parenteral administration of animal-derived antivenoms, constituted by IgG or IgG fragments purified from the plasma of large animals immunized with venoms.[6,7] When prepared by using appropriate mixtures of venoms for immunization and following Good Manufacturing Practices (GMPs), antivenoms are safe and effective drugs which, if administered timely, can control the main pathophysiological manifestations of envenomings, especially those associated with systemic effects.[6,7]

However, there are several issues related to antivenom therapy that compromise their effectiveness. These include, but are not limited to, the fact that antivenoms must be administered in a timely manner in health facilities by trained health staff, thus limiting their use in rural settings in countries where public health services and health personnel are scarce.[8] Effective treatment is further complicated by the fact that antivenoms are specific for venoms used in immunization and those of closely related snake species.[7] Significantly, antivenoms are only partially effective in the control of local tissue damage characteristic of most viperid and some elapid snakebite envenomings, mostly owing to the rapid development of these effects and the often-delayed administration of antivenoms.[9,10] These delays can lead to permanent tissue damage and sequelae of various sorts.[11-14] There is a need therefore to develop novel therapeutic interventions, which could be administered in the field immediately following envenoming to arrest or mitigate the progression of local tissue damage and would hence complement the antivenom therapy of envenomings. Solutions to this problem must grapple with the biological complexity of snake venom as well as the social and economic challenges associated with the production, distribution, storage and timely administration of the therapy. An ideal fast response therapy should be

administered safely and effectively in a rural setting and be capable of inhibiting venom from diverse venomous species.

From a molecular standpoint, antivenom functions through a concerted neutralization process involving the interaction between polyclonal antibodies and their toxin-targets. Owing to the specificity of antibodies, the complexity of venoms requires an equally complex antibody mixture capable of selectively interacting with and neutralizing relevant venom proteins. As a consequence, toxins which are not recognized by antibodies are not neutralized. To maintain bioactivity with increasingly diverse chemical composition, venomous animals have hijacked along evolution privileged protein scaffolds with high densities of conserved disulfide cross-links capable of withstanding diversification of amino-acid compositions on the surface.[15] A process of accelerated evolution of snake venom toxins has resulted in the generation of great variation in surface residues which confer a wide spectrum of toxic activities within a limited number of molecular scaffolds.[16,17] This has an obvious impact in the ability of antibodies to recognize variable epitopes in toxins. This balance between diversity and homology is clearly manifest in snakes from the Elapidae family where most toxins consist of either the phospholipase A_2 (PLA$_2$, ~14 kDa) or the three finger toxin (3FTX, ~8 kDa) scaffold.[4]

Both PLA$_2$ and 3FTX protein families have many hundreds of isoforms capable of producing a range of pathophysiological effects.[18] However, amidst this immunological and functional variability, many share similar functional features that are distinct from abundant endogenous human proteins (Figure 4.1). Both toxin families have members that bind to cellular membranes and either catalyze the hydrolysis of phospholipids and hence the degradation of membrane bilayers (PLA$_2$) or imbed themselves into membranes causing membrane disorganization and cytotoxicity (cytotoxic 3FTXs).[19,20] Other 3FTXs bind with high affinity to

receptors in muscle cells or neurons, thus exerting a neurotoxic effect.[21] PLA$_2$ isoforms, which range from acidic to basic, generally maintain a conserved catalytic domain, which entails a hydrophobic cavity capable of extruding glycerophospholipids from phospholipid bilayers or lipoprotein particles.[22,23] Similarly, 3FTXs are generally cationic at neutral pH, however they have varying degrees of hydrophobicity in the loop regions that dictate the ultimate target of the toxin.[24,25] These exposed loop regions from both protein families contain the greatest variability (Figure 4.1).

The chemical and structural diversity of PLA$_2$ and 3FTX toxins are sufficient to challenge development of a broad-spectrum antibody preparation. However, these two families of protein toxins share features that are associated with their common targets allowing for sequestration by a mechanism that differs from immunological selection. Herein, we describe an abiotic hydrogel nanoparticle that indiscriminately associates with and modulates the activity of a diverse array of PLA$_2$ and 3FTX isoforms.
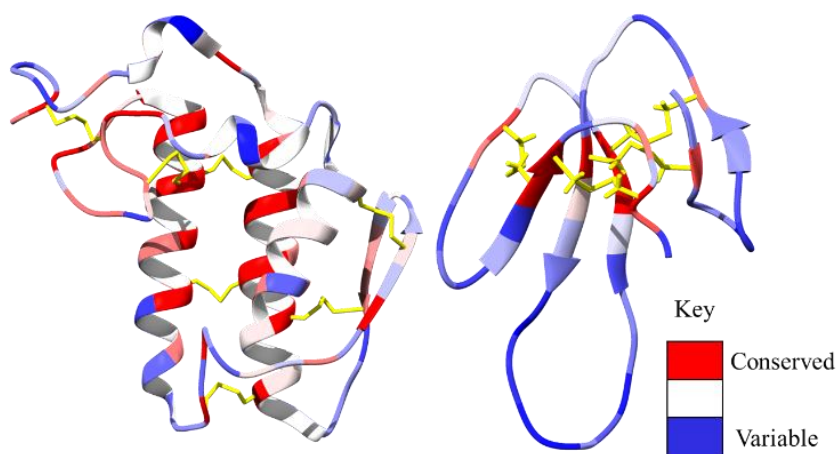
Figure 4.1. Regions of conserved (red) and variable (blue) amino acids from reviewed sequences on www.uniprot.org for PLA$_2$ (left, 27 sequences) and 3FTXs (right, 96 sequences) from the following elapid snake venoms: *Naja sputatrix*, *Naja mossambica*, *Bungarus caeruleus*, *Bungarus fasciatus*, *Naja haje*, *Naja melanoleuca*, *Naja nivea*, *Dendroaspis polylepsis*. The core structures depicted for PLA$_2$ and 3FTXs are from *Bungarus caeruleus* (PDB: 2OSN) and *Dendroaspis polylepsis* (PDB: 2MFA), respectively. Disulfide bonds are highlighted in yellow.

C. Abiotic approach to antivenom

Several natural and synthetic molecules have been explored as possible candidates for venom inhibitors.[26-28] Our approach differs from traditional strategies centered on immune-based neutralization or inhibition by small molecule inhibitors of variable chemical nature. We are developing abiotic synthetic polymer nanoparticle(s) (NPs) that have been engineered to sequester and neutralize several of the major toxic components of snake venoms.

Our first report described a synthetic polymer hydrogel NP that binds and inhibits the catalytic activity of PLA_2, one of the important families of protein toxins found in the venom of many species of snakes.[29]

When exposed to human serum alone, the NP associates with endogenous apolipoproteins, primarily apolipoprotein A-1, but upon addition of venom, the bound apolipoproteins are exchanged for venom PLA_2 proteins, suggesting that these materials could be used as a toxin sequestrant in a complex biological setting. This NP was shown to be non-toxic in vitro, as have similar NP hydrogels in vivo.[30-32] We now report an expanded study of the use of this abiotic toxin sequestrant. We have found that a single polymer NP is effective in capturing the two most important families of protein toxins common in Elapidae snakes: PLA_2 and 3FTX. In addition, the NP has also demonstrated in vitro and in vivo inhibition of toxic activities of *Naja nigricollis* venom, a medically relevant spitting cobra from sub-Saharan Africa which causes envenomings characterized by severe local tissue necrosis.[33] This finding offers promise that a broad-spectrum toxin sequestrant to mitigate local tissue damage may be accessible. The subcutaneous or intramuscular administration of these synthetic polymer NPs, shortly after the bite at the site of envenoming, have the potential to halt or reduce the extent of local tissue damage and prevent the systemic distribution of toxins post-envenoming.

D. Elapidae snake venom screening
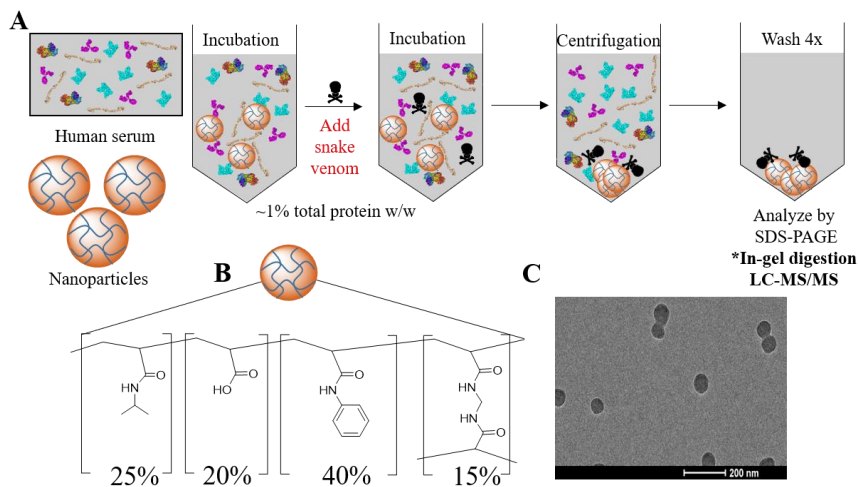
Figure 4.2. (A) Method used to analyze the binding of the synthetic NPs to various venoms. *A representative venom from a species of each genus tested was further analyzed by LC-MS/MS. (B) Composition of the synthetic NPs. (C) TEM image of the NPs (scale bar = 200 nm).

Our report begins with an evaluation of the affinity of the abiotic hydrogel NP against a variety of medically relevant elapid whole snake venoms. The monodisperse NP hydrogels (176 nm, 0.044 PDI by dynamic light scattering) (Figure 4.2C), synthesized via precipitation polymerization with a feed ratio of 20% acrylic acid, 40% *N*-phenylacrylamide, 25% *N*-isopropylacrylamide, and 15 % *N,N′*-methylenebis(acrylamide) (Figure 4.2B) was tested for toxin-selectivity in human serum by first subjecting the NP to concentrated human serum (25% (w/v), final concentration). Following a pre-incubation at 37 °C, a small quantity of whole venom (250 µg/mL, final concentration) was added to the NP-serum mixture and incubated. After centrifugation and multiple washing steps, the bound proteins that constitute the *hard* protein corona[34] of the NP were examined via SDS-PAGE (Fig. 4.2A). A representative venom extract from a species of each genus was further analyzed by LC-MS/MS to confirm that toxins found in the control experiments (Figure 4.3A) were also present in the NP-corona complex (Figure 4.3B) and to establish if the NP sequesters isoforms of both PLA_2 and 3FTXs families.

Compared to the serum-only control experiment (Figure 4.3 B1.0), which shows high quantities of apolipoprotein-A1, the venom-containing experiments (Figure 4.3 B2.1-2.8) show that very large quantities of low-molecular weight proteins (<15 kDa) are captured by the NP. Considering that venoms themselves are dominated by proteins with MWs below 15 kDa (Figure 4.3 A1.1-1.8), it is likely that the proteins of that MW in the NP binding experiments are the predominant ones in the venom. To verify this claim, the samples from experiments involving *Naja mossambica* (Figure 4.3 A1.1, B2.1), *Bungarus caeruleus* (Figure 4.3 A1.2, B2.2), and *Dendroaspis polylepsis* (Figure 4.3 A1.8, B2.8) venoms were analyzed by tandem mass spectrometry via an in-gel digestion with trypsin. The detected peptide fragments were analyzed using the uniprot database of known venom proteins for each species.[35] Although many of these venoms have been characterized and some of their toxins sequenced previously, the intraspecies variability of venoms does not guarantee that all toxin isoforms found in the database are present in appreciable amounts in our venom samples, and vice versa. Furthermore, many protein isoforms share high sequence identity which can render protein identification via trypsin digestion difficult. Nevertheless, proteomic analysis will at the very least establish whether the proteins in the venom control (Figure 4.3A) are found in the NP protein corona (Figure 4.3B).
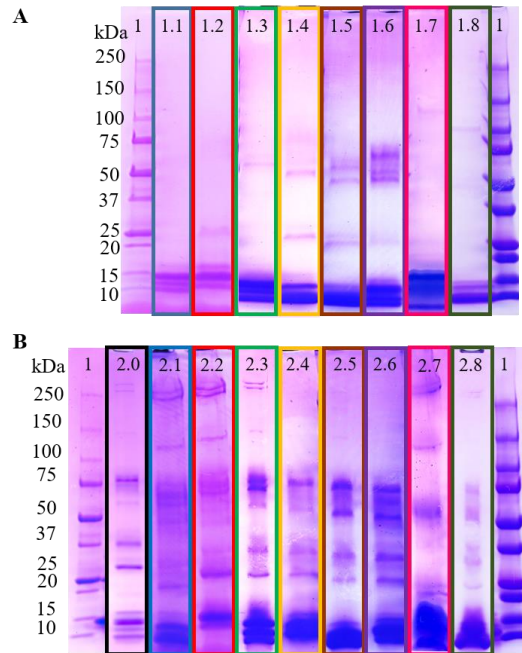
Figure 4.3. Nanoparticle binding to elapid snake venoms in concentrated human serum (A) Control experiments using the venom compositions of interest. (1) MW ladder. (1.1) Venom from *Naja mossambica*. (1.2) Venom from *Bungarus caeruleus*. (1.3) Venom from *Bungarus fasciatus*. (1.4) Venom from *Naja haje*. (1.5) Venom from *Naja nivea*. (1.6) Venom from *Naja melonoleuca*. (1.7) Venom from *Naja sputatrix*. (1.8) Venom from *Dendroaspis polylepis*. (B) NP selectivity results. (1) MW ladder. (2.0) Serum only control experiment. (2.1-2.8) NP selectivity results following the same venom-order described above. See Figures 4.S1-10 for full gel images.

Naja mossambica venom, which is largely composed of cytotoxins from the 3FTX family and PLA$_2$s, can induce extensive cutaneous necrosis in its victims.[33] While the number of 3FTXs and PLA$_2$ isoforms expressed in the venoms of this species likely varies ontogenetically and geographically, seven 3FTXs and three PLA$_2$ isoforms have been attributed to this snake venom via the Swiss-Prot database. Nine of the toxins were detected in the venom only control experiment (Fig. 4.3 A1.1) and eight of those toxins were found in the NP and serum containing experiment (Table 4.S1). The lack of neurotoxin 2 (3S13_NAJMO) in the NP hard-corona complex may be attributed to the overall low concentration of the neurotoxin in the venom. Regardless, this experiment verified that the NP sequestered nearly all the isoforms of the 3FTXs and PLA$_2$ toxins in *N.mossambica* venom in the presence of serum proteins.

A similar proteomic analysis was performed on the venom – serum uptake experiments from *Bungarus caeruleus*, the common krait from India. Envenoming by *B. caeruleus* results in severe neurotoxicity.[36] A major component of this venom is the PLA_2 heterodimeric neurotoxin β-bungarotoxin, which features a PLA_2 covalently attached to a Kunitz-type serine protease inhibitor.[37] LC-MS/MS analysis of the venom control (Fig. 4.3 A 1.2) revealed six proteins: Four monomeric PLA_2s and two PLA_2 toxins that are a component of β-bungarotoxin. LC-MS/MS analysis of the NP-*B. caeruleus* experiment (Fig. 4.3 B 2.2) revealed that all six proteins were present in the NP protein corona (Table 4.S2).

The third venom, *Dendroaspis polylepsis*, which is known for its fast-acting neurotoxic effect,[33] is well characterized and therefore a good candidate for proteomic assessment. Analysis of the venom control (Figure 4.3 A1.8) revealed eight unique 3FTXs and four different Kunitz-type serine protease inhibitors which in this venom correspond to dendrotoxins, a group of neurotoxins that block the voltage-sensitive potassium channels in neurons.[38] Seven of the eight 3FTXs were found in the NP protein corona (Fig. 4.3 B2.8), Moreover, three of the four dendrotoxins were also found in the NP corona along with an acetylcholinesterase (Table 4.S3). This underscores that NPs are able to bind not only 3FTXs and PLA_2s, but also dendrotoxins, which belong to a different structural family of neurotoxic venom proteins. This has evident therapeutic implications when dealing with mamba snake venoms.

Despite differences in toxin composition across different species, these venom-selectivity experiments support the hypothesis that the nanoparticles are able to bind to different structural determinants in different groups of toxins from elapid snake venom over abundant serum proteins. While the results indicate broad-sequestration of certain important venom toxins of elapid sakes by the NP, this does not necessarily translate to broad-neutralization of these toxins. To this point,

we focused on the neutralization of necrotizing toxins, whose neutralization by antivenoms is limited.[10] We identified venom from the African spitting cobra, *Naja nigricollis*, as an ideal candidate for this study since envenoming from this species is responsible for many cases in sub-Saharan Africa resultant in sequelae secondary to local cutaneous necrosis.[33,39]

E. Selectivity for *Naja nigricollis* venom
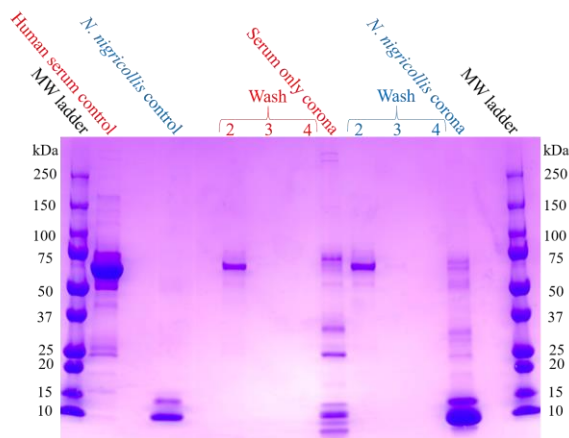
Figure 4.4. NP selectivity in human serum (red) and in human serum + *N. nigricollis* venom (blue).

The pathophysiology observed in envenomings caused by *N.nigricollis* results from a synergistic effect involving numerous PLA$_2$ and 3FTX isoforms.[10] 3FTXs, which comprise 73% of the venom of *N. nigricollis*,[40] are the major toxin family responsible for its toxicity.[10] We first evaluated the protein corona of the NP in the presence of human serum and *N. nigricollis* venom as described in the previous section.

Compared to the serum only control experiment, the addition of venom after an initial serum incubation resulted in a dominant protein band in the molecular weight range observed in the venom control (<15 kDa) (Figure 4.4). In the presence of serum alone, the NP favorably associates with proteins of varying molecular weights. However, there is a distinct change in the distribution and a new dominant molecular weight band (<15 kDa) in the venom-containing corona

experiment. Proteins that comprised the NP corona were identified via in gel digestion followed by proteomic identification. Unlike the previous proteomic studies, venom from *N. nigricollis* only has four toxins attributed to it in the UniProt database: one full-length PLA$_2$, two 30 amino acid fragments of PLA$_2$ and a 51amino acid peptidase inhibitor called nawaprin. We therefore extended the database to include toxin sequences from the closely related species *Naja pallida* which includes two 3FTXs (cytotoxin and neurotoxin). Analysis confirmed that all the toxins observed in the *N. nigricollis* venom control were also observed in the NP protein corona (Table 4.S4). These results were quite similar to the proteomics analysis of the related *N. mossambica* venom-selectivity study in the previous section and reinforce the concept that the NP is able to bind the most relevant toxin families in these snake venoms.

F. In vitro inhibition of *Naja nigricollis* venom

The toxin uptake studies with whole venom from the spitting cobra *N. nigricollis* and other elapid snakes in the presence of serum proteins were encouraging. However, sequestration does not necessarily translate to inhibition of toxicity. *N. nigricollis* induces cytotoxicity and produces substantial myonecrosis. To establish if the NP is capable of neutralizing myonecrosis in vitro, we designed a cell viability study of rat skeletal muscle cells (L6) in the presence of *N. nigricollis* venom and the NP.

The MTT assay was used to visualize metabolically active cells in the evaluation of the inhibition of venom induced cytotoxicity by the NP. Figure 4.S11 shows the cell viability of L6 cells incubated with *N. nigricollis* venom (1-30 µg/mL, n=4-5) in the presence and absence of 80 µg/mL NP. Results indicate that the NP is effective at neutralizing the toxicity from *Naja nigricollis* venom. A concentration of 7 µg/mL of *N. nigricollis* venom resulted in almost 100% cytotoxicity of L6 cells in the absence of the NP. This concentration was selected for further

experiments to study the dose-response curve of the NP (Figure 4.5). The results show a dose-dependent relationship between NP concentration and cell survival (Figure 4.5). The first concentration to have a significant effect on cell survival is 49.6 µg/mL which resulted in 50% cell survival (half maximal effective concentration, EC_{50}). In addition, a ratio of venom: NP (w/w) ranging from 1:5 to 1:7 resulted in near complete inhibition of cytotoxicity. This was substantially more potent than the reported ratio of South African antivenom (SAMIR) which required a ratio greater than 1:150 venom : antivenom (w/w) to completely inhibit *N. nigricollis* venom-induced cytotoxicity in L6 cells.[41]
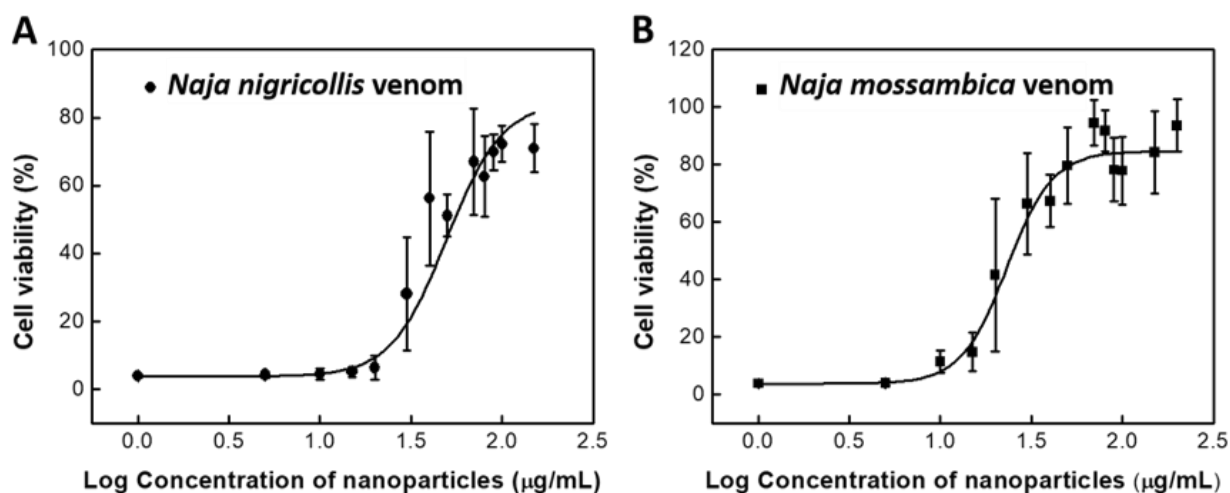
Figure 4.5. Dose-response curve of inhibition of cytotoxicity in L6 muscle cells by the NP against administration of 7 µg/mL of (A) *N. nigricollis* venom and (B) 7 µg/mL of *N. mossambica* measured 14 h after exposure to the cells (n=4-5).

We also evaluated the efficacy of the NP to inhibit cytotoxicity of *Naja mossambica* venom, another member of the Elapidae snake family to ensure that this result was not exceptional (Figure 4.5B). The calculated EC_{50} is 23.2 µg/mL and a ratio ranging from 1:6 to 1:7 venom : NP (w/w) brought about complete neutralization of *N. mossambica* venom toxicity in L6 cells. The NPs have a much higher capacity than the reported ratio of SAMIR which required a ratio greater than 1:500 venom: antivenom (w/w) to completely suppress cytotoxicity induced by this venom.[41]

G. In vivo studies with the venom of *Naja nigricollis*

Both selective uptake studies with whole venom and the in vitro results suggest the NP functions as a sequestrant for the major protein toxins of elapid snakes. We proceeded with an evaluation of the ability to mitigate in vivo the necrotic effects of venom of the African spitting cobra *N. nigricollis*. In contrast with envenomings by the majority of cobras (*Naja* sp), which are characterized by neurotoxic manifestations, those inflicted by *N. nigricollis* are characterized by a prominent cytotoxic effect, clinically manifested by blistering and local cutaneous necrosis, which often end up in permanent sequelae such as chronic ulceration, hypertrophic scars, keloid formation, blindness and, in some cases, malignant transformation.[11,33] Previous in vitro studies and our current observations demonstrated the ability of NPs to sequester and inhibit PLA_2s and cytotoxins of the 3FTX family from the venom of the spitting cobra *N. mossambica*,[29] and a closely related species, *N. nigricollis*. We next evaluated the ability of the NP to inhibit the necrotic activity of the venom of *N. nigricollis* in skin. To this end, a mouse experimental model developed in one of our laboratories[10] was used to assess the efficacy of NPs.

H. Assessment of toxicity of NPs

Before assessing the ability of NPs to inhibit venom in vivo, the potential toxicity of NPs was studied. Mice receiving 100 µL of NPs (5.5 mg/mL) by the intravenous route did not show any evidence of toxicity nor any change in their behavior, as compared to mice receiving PBS. All of them survived the 24 h observation period. Mice injected intramuscularly in the gastrocnemius with 50 µL of NPs did not show any problem for mobilization, and the plasma CK activity was not increased as compared to the plasma CK activity of mice injected with PBS (302 ± 352 U/L and 206 ± 120 U/L, respectively; $p > 0.05$) thus indicating lack of myotoxicity. Moreover, intradermal injection of NPs did not cause any macroscopic effect in the skin. Histological

assessment of tissue sections from liver, kidneys and heart (after intravenous injection), gastrocnemius muscle (after intramuscular injection), and skin (after intradermal injection) showed a normal microscopic appearance (Figure 4.6D; Figure 4.S12) which did not differ from that of tissue sections obtained from mice injected with PBS. Thus, under our experimental conditions, NPs did not induce toxicity in mice.

I. Inhibition of dermonecrosis

The NPs inhibited dose-dependently the dermonecrotic activity of *N. nigricollis* venom, as visually assessed by the reduction or abrogation of the necrotic area (Figure 4.6A; Figure 4.S13). The estimated IR_{50} was 1.1 (NP : venom, w:w). Histological assessment confirmed the inhibition of skin necrosis. Tissue from mice injected with venom incubated with PBS showed a characteristic necrotic pattern, similar to that described by Rivel *et al*.[10] These lesions are characterized by a central dark necrotic core and a peripheral whitish ring. Necrosis is characterized by loss of epidermis and of skin appendages, together with the accumulation of a hyaline fibrinoid material, together with an abundant inflammatory infiltrate with predominance of polymorphonuclear leucocytes (Figure 4.6B). In contrast, skin samples from mice receiving venom and NPs showed preservation of the epidermis and of the dermal structure and skin appendages, i.e. inhibition of necrosis. However, the epidermis had an increased number of epithelial cell layers and there was an inflammatory infiltrate in the dermis (Figure 4.6C), both of which reveal an ongoing inflammatory process in the absence of necrosis. Tissue from mice injected with NPs alone showed a histomorphology indistinguishable from that of mice receiving PBS alone (Figure 4.6D).
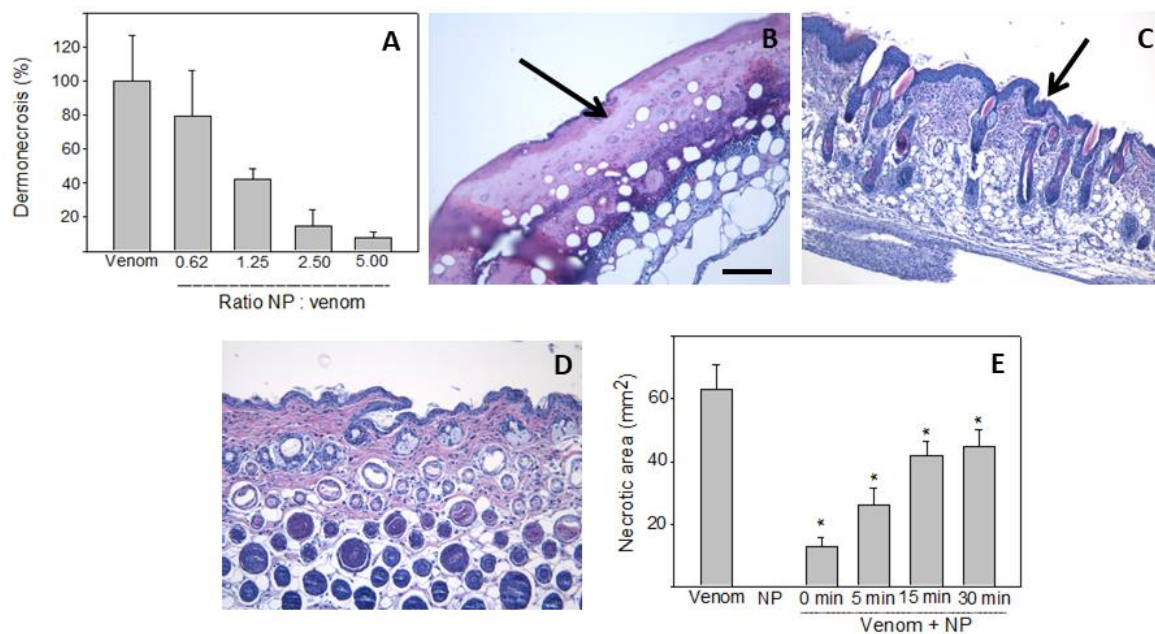
Figure 4.6. Inhibition of dermonecrotic activity of *N. nigricollis* venom by NPs. (A) A fixed amount of venom was incubated with variable amounts of NPs to attain several NP : venom (w : w) ratios. Controls included venom incubated with saline solution instead of NPs. Upon incubation, aliquots of the mixtures, containing 100 µg venom, were injected intradermally, in the ventral abdominal region, into groups of five mice. Seventy-two hours after injection, mice were sacrificed and the areas of necrotic lesions in the inner side of the skin were measured. Necrosis was expressed as percentage, 100% corresponding to the necrotic area (60 mm^2) in mice receiving venom alone. NPs inhibited, dose-dependently, the dermonecrotizing activity of the venom. (B, C, D) Light micrographs of sections of the skin of mice 72 h after injection of 100 µg *N. nigricollis* venom incubated with saline solution (B), with NPs at a NP : venom (w : w) ratio of 5.0 (C), or after injection of NPs alone (D). In (B) there is ulceration, with loss of epidermis and the formation of a hyaline proteinaceous material (arrow); skin appendages are absent and there is a prominent inflammatory infiltrate. In (C) NPs inhibited the ulcerative effect, evidenced by the presence of epidermis (arrow) and skin appendages, whereas an inflammatory infiltrate is observed in the dermis. Skin injected with NPs alone (D) shows a normal histological pattern. Hematoxylin-eosin staining. Bar represents 100 µm. (E) Inhibition of dermonecrosis by *N. nigricollis* venom in experiments involving intradermal injection of 100 µg venom (in 50 µL) followed by the injection of 50 µL of NP suspension (5.5 mg/mL), in the same region of venom injection, at various time intervals. A significant reduction in the extent of dermonecrosis was observed in all mice treated with NPs, as compared to mice receiving venom alone (* $p < 0.05$), although the extent of inhibition decreased as the time lapse between envenoming and NP administration increased. NP alone did not induce skin damage.

114

When inhibition experiments were performed by first injecting the venom and then, at various time intervals, the NPs, dermonecrosis was significantly reduced in all cases, although inhibition diminished as time lapse between envenoming and treatment increased (Figure 4.6E).

J. Conclusion

These results establish that an abiotic synthetic polymer NP, engineered to bind to and modulate the activity of a diverse array of PLA_2 and 3FTX isoforms found in Elapidae snake venoms, inhibit dose-dependently the dermonecrotic activity of *N. nigricollis* venom, the most important clinical manifestation of envenomings by African spitting cobras. These two families of protein toxins share features that are associated with their ability to bind and disrupt cell membrane targets, thus allowing for NP sequestration that arises from a mechanism that differs from immunological (epitope) selection.

K. Supplemental information

Materials:

The following materials were obtained from commercial sources: *N*-isopropylacrylamide (NIPAm), ammonium persulfate (APS), *N*-phenylacrylamide, acrylic acid, sodium dodecyl sulfate (SDS) was obtained from Aldrich Chemical Company, Inc.; *N,N'*-methylenebisacrylamide (Bis) was from Fluka. All other solvents and chemicals were obtained from Fisher Scientific Inc. or VWR International LLC. NIPAm was recrystallized from hexanes before use. Water used in polymerization and characterization was purified using a Barnstead Nanopure Diamond™ system. 12-14 kDa MWCO cellulose membranes were purchased from Spectrum Laboratories. Precast SDS-PAGE gels (4-15% Mini-Protean), Coomassie Brilliant Blue R-250 and molecular weight ladder (Precision plus protein standards) were purchased from Bio-rad Laboratories. Human serum was purchased from Lampire Biological Laboratories. *Bungarus caeruleus* and *Naja sputatrix* venom was purchased from Sigma Aldrich. *Naja nigricollis* venom was purchased from Latoxan. *Naja mossambica, Bungarus fasciatus, Naja haje, Naja nivea, Naja melonoleuca* and *Dendroaspis polylepsis* venom was graciously donated from LUNA Innovations Inc. All other materials were purchased from commercial sources.

Instrumentation:

Nanoparticle size and polydispersity was determined using a Malvern ZEN3600 dynamic light scattering (DLS) instrument with a disposable sizing cuvette. Lyophilization of polymer samples was performed using a Labconco Freezone 4.5. TEM image was obtained on a FEI Tecnai G2 TF20 high resolution TEM operated with an accelerating voltage of 200 kV.

Nanoparticle Synthesis:

N-phenylacrylamide (191.33 mg), *N*-isopropylacrylamide (191.33 mg), acrylic acid (44.57 mg) *N, N'*-methylenebisacrylamide (75.15 mg) and sodium dodecylsulfate (30 mg, 1 µmol) were dissolved in a 10% acetone solution in water (50 mL) to a final monomer concentration of 65 mM. The resulting solution was degassed with nitrogen for 30 min while stirring. Ammonium persulfate (30 mg dissolved in 1 mL H2O) was added to the degassed solution, and the reaction mixture was heated to 60 ℃ under nitrogen for 3 h. The polymerization was quenched by exposing the reaction mixture to air, and the reaction mixture was transferred to a 12,000-14,000 MWCO membrane and dialyzed against an excess of deionized water (changed twice a day) for 4 d. 72% yield.

Nanoparticle Characterization:

Dynamic light scattering (DLS) was used to characterize the size and dispersity of the nanoparticle after dialysis. Nanoparticle measurements were performed at 37 °C in PBS (Dulbecco's) and allowed to equilibrate at the designated temperature for 200 seconds prior to each measurement and were measured at a scattering angle of 173°. Concentration and yield was determined by lyophilizing a known volume of the purified nanoparticle suspension and weighing the obtained dry polymer samples.

TEM Characterization

8 µL of nanoparticles (1 mg/mL) was injected on a glow discharged TEM grid (Ultrathin Carbon Type-A, 400 mesh) and let stand for 1 min. The solution was removed by filter paper and the grid was left to air dry for 10 min. Next the grid was loaded into the instrument (FEI Tecnai G2 TF20 high resolution TEM operated at an accelerating voltage of 200 kV) for imaging.

Venom Selectivity in Human Serum

In a microcentrifuge tube, the nanoparticle (1 mg/mL final concentration) was incubated with human serum (25% final concentration) in phosphate buffer saline (Dulbecco's) for 5 min at 37 °C. Next, venom (250 µg/mL final concentration) was added to the nanoparticle/human serum mixture and incubated for an additional 45 min at 37 °C. The suspension was then centrifuged at 10,000 RPM for 10 min, and the supernatant was replaced with fresh phosphate buffer saline four consecutive times or until the supernatant was depleted of protein by SDS-PAGE (commassie blue stain). Next, 20 µL of SDS-PAGE sample preparation mixture was added to the nanoparticle pellet, mixed and heated to 95 °C for 10 minutes. Finally, the Mixture was centrifuged at 5,000 RPM and the bound proteins were analyzed by SDS-PAGE (100 V).

In Gel Digest

The designated slices were cut to 1mm by 1 mm cubes and destained 3 times by first washing with 100 µL of 100 mM ammonium bicarbonate for 15 minutes, followed by addition of the same volume of acetonitrile (ACN) for 15 minutes. The supernatant was and samples were dried in a speedvac. Samples were then reduced by mixing with 200 µL of 100 mM ammonium bicarbonate-10 mM DTT and incubated at 56C for 30 minutes. The liquid was removed and 200 µL of 100 mM ammonium bicarbonate-55mM iodoacetamide was added to gel pieces and incubated at room temperature in the dark for 20 minutes. After the removal of the supernatant and one wash with 100 mM ammonium bicarbonate for 15 minutes, same volume of ACN was added to dehydrate the gel pieces. The solution was then removed and samples were dried in a speedvac. For digestion, enough solution of ice-cold trypsin (0.01 µg/µL) in 50 mM ammonium bicarbonate was added to cover the gel pieces and set on ice for 30 min. After complete rehydration, the excess trypsin solution was removed, replaced with fresh 50 mM ammonium bicarbonate, and left overnight at

37 °C. The peptides were extracted twice by the addition of 50 µL of 0.2% formic acid and 5 % ACN and vortex mixing at room temperature for 30 min. The supernatant was removed and saved. A total of 50 µL of 50% ACN-0.2% formic acid was added to the sample, which was vortexed again at room temperature for 30 min. The supernatant was removed and combined with the supernatant from the first extraction. The combined extractions are analyzed directly by liquid chromatography (LC) in combination with tandem mass spectroscopy (MS/MS) using electrospray ionization.

LC-MS/MS analysis:

LC-MS-MS: Trypsin-digested peptides were analyzed by ultra high-pressure liquid chromatography (UPLC) coupled with tandem mass spectroscopy (LC-MS/MS) using nano-spray ionization. The nanospray ionization experiments were performed using a Orbitrap fusion Lumos hybrid mass spectrometer (ABSCIEX) interfaced with nano-scale reversed-phase UPLC (Thermo Dionex UltiMate™ 3000 RSLC nano System) using a 25 cm, 75-micron ID glass capillary packed with 1.7-µm C18 (130) BEHTM beads (Waters corporation). Peptides were eluted from the C18 column into the mass spectrometer using a linear gradient (5–80%) of ACN (Acetonitrile) at a flow rate of 375 µL/min for 1h. The buffers used to create the ACN gradient were: Buffer A (98% H_2O, 2% ACN, 0.1% formic acid) and Buffer B (100% ACN, 0.1% formic acid). Mass spectrometer parameters are as follows; an MS1 survey scan using the orbitrap detector (mass range (m/z): 400-1500 (using quadrupole isolation), 120000 resolution setting, spray voltage of 2200 V, Ion transfer tube temperature of 275 °C, AGC target of 400000, and maximum injection time of 50 ms) was followed by data dependent scans (top speed for most intense ions, with charge state set to only include +2-5 ions, and 5 second exclusion time, while selecting ions with minimal intensities of 50000 at in which the collision event was carried out in the high energy collision cell

(HCD Collision Energy of 30%), and the fragment masses where analyzed in the ion trap mass analyzer (With ion trap scan rate of turbo, first mass m/z was 100, AGC Target 5000 and maximum injection time of 35ms). Data analysis was carried out using the Byonic™ (Protein Metrics Inc.).

In vitro *Naja nigricollis* and *Naja mossambica* venom inhibition

The rat skeletal muscle myoblast cell line, L6, was offered by the collaborator, Luna. L6 cells were grown in 150 cm^2 flasks in culture DMEM media supplemented with 10%FBS and 1% penicillin, incubated at 37 °C with 5% CO_2. Cells were lifted using the trypsin and centrifuged at 800 rpm for 5 min to obtain the pellet. The cell pellet was suspended in culture DMEM media supplemented with 2% FBS and 1% penicillin and seeded into 96 well-well cell culture plates (about 1,5000 cells /per well counted by cell counter). Plates were incubated at 37 °C with 5% CO_2. Media changed from the wells every second day until cell differentiation was (appearance of long striated cells, observed by eye using light microscope) was observed.

Cell proliferation assay

Concentration dependence of *Naja nigricollis* venom

Media were removed from the wells and wells were washed once with pre-warmed PBS. *Naja nigricollis* venom stock solution was diluted to 1 to 30 µg/mL in DMEM media and added into the wells. After 5min, 80 µg/mL nanoparticle was added into the wells. Culture media controls (cell and media with no venom) and the control without the addition of the nanoparticles were also run in parallel. The plate was incubated at 37 °C with 5% CO_2 for 14h. After 14h, the cell culture plate was removed from the incubator and washed with pre-warmed PBS three times. 50 mL Fresh DMEM media and the MTT (3-(4,5-Dimethylthiazol-2-yl)-2,5-Diphenyltetrazolium Bromide from molecular probe, 10 mL, 12 mM solution in PBS) reagent was added and the wells mixed with a multichannel pipette. The mixtures were then incubated at 37 °C in a humidified 5% CO_2

120

incubator for 3h and all the media was replaced with DMSO (100 µL, Dimethylsulfoxide). The solutions were incubated at 37 °C for 20 min, mixed and absorbance was read at 570 nm by Microplate reader (Bio-RAD).

Concentration dependence of the nanoparticles

7µg/mL venom was added into the wells and various concentrations of the nanoparticle from 1 to 150 µg/mL were added to the wells 5 min later. Culture media controls (cell and media with no venom) and the control without the addition of the nanoparticles were also run in parallel. MTT assay was used to evaluate the cell viability at 570 nm.

Calculation of the nanoparticle efficacy

Half maximal effective concentration (EC50) refers to the concentration of the nanoparticle which induces a response halfway between the baseline and the maximum after a certain exposure time. The equation was shown below.

$$Y = (Bottom) + \frac{(Top) - (Bottom)}{1 + (\frac{X}{EC50})^{-(Hill\ coefficient)}}$$

Where Y is the cell viability, Bottom is 0 (the lowest cell viability), Top is 100 (the highest cell viability) and the Hill coefficient gives the largest absolute value of the slope of curve. Origin 8 is used to fit a following sigmoidal function and calculate EC 50.

In vivo protocols

Materials and methods:

The venom of *N. nigricollis* was purchased from Latoxan and was obtained from adult specimens of this species collected in Cameroon. Venom was stored at -20 °C and was dissolved just before each experiment.

Animal experiments

Mice of the CD-1 strain of 18-20 g body weight were used throughout the study. All animals received food and water *ad libitum* and were submitted to a daily light : dark cycle of 12 h each. The protocols used in animal experiments were approved by the Institutional Committee for the Care and Use of Laboratory Animals (CICUA) of the University of Costa Rica (CICUA 82-8).

Assessment of toxicity of nanoparticles

A group of five mice received 100 µL of a nanoparticle suspension (5.5 mg/mL) by the intravenous (i.v.) route in the caudal vein. A control group of mice received 100 µL of 0.12 M NaCl, 0.04 M phosphate, pH 7.2 solution (PBS) under otherwise identical conditions. Mice were closely observed for signs of acute toxicity and changes in behavior during 4 h, and then left for 24 h to assess lethality. At this time, mice were sacrificed by CO_2 inhalation and tissue samples from heart, liver and kidney were collected and immediately placed in fixative (3.8 % formalin). After routine processing and embedding in paraffin, 4 µm sections were obtained and stained with hematoxylin-eosin for histological observation. Another group of mice received 100 µL of the nanoparticle suspension (5.5 mg/mL) intramuscularly in the right gastrocnemius muscle. Control mice received the same volume of PBS. Three hours after injection, a blood sample was collected from the tail, and the creatine kinase (CK) activity of plasma was quantified, by using a commercial kit (CK LIQUI-UV, Stanbio Lab., Texas, USA), as an index of myonecrosis (Gutiérrez et al., 1980). At 24 h after injection mice were sacrificed by CO_2 inhalation and a sample of the injected gastrocnemius muscle was obtained and processed for histological evaluation as described above. Another group of mice received 100 µL of a nanoparticle suspension (5.5 mg/mL) by the intradermal route of injection in the ventral abdominal region. Seventy-two hour after injection, animals were sacrificed

as described, a sample of injected skin was obtained and placed in 3.8 % formalin solution, and processed for histological evaluation as described above.

Inhibition of dermonecrotic activity

Mixtures containing a fixed dose of venom and variable amounts of NPs, both dissolved in PBS, were prepared as to have NP : venom ratios (w : w) of 5, 2.5, 1.25 and 0.62. Controls included venom incubated with PBS only and NPs incubated with PBS only. Mixtures were incubated at 37 °C for 30 min. Then, aliquots of 100 µL of the mixtures, containing 100 µg venom, were injected intradermally, in the abdominal ventral region, into groups of five mice. This venom dose was selected because it induces a necrotic lesion in the skin of approximately 60 mm^2 and had been previously used in the description of the skin necrosis induced by this venom (Rivel et al., 2016). Seventy-two hours after injection, mice were sacrificed by CO_2 inhalation, their skin was removed, and the area of necrosis in the inner side of the skin was measured. Inhibition was expressed as the Median Inhibitory Ratio (IR$_{50}$), corresponding to the NP : venom ratio at which the area of the necrotic lesion was reduced by 50% as compared to controls injected with venom alone. Skin tissue samples were then placed in fixative solution and processed for histological evaluation as described above.

In another set of experiments, groups of five mice received an intradermal injection of 100 µg venom, dissolved in 50 µL of PBS. Then, at various time intervals (0, 5, 15 and 30 min), 50 µL of NPs (5.5 mg/mL) were injected intradermally at the same site of venom injection. A control group of mice received venom and then PBS instead of NPs. After 72 h the necrotic area was assessed as described.

Statistical analysis

The significance of the differences between mean values of experimental groups was assessed by Analysis of Variance (ANOVA), followed by Tukey test for comparing pairs of means.

Figure 4.1 Conservation of 3FTX and PLA$_2$

Amino Acid sequences of PLA$_2$ and 3FTX isoforms from *Naja sputatrix*, *Naja mossambica*, *Bungarus caeruleus*, *Bungarus fasciatus*, *Naja haje*, *Naja melanoleuca*, *Naja nivea*, *Dendroaspis polylepsis* were downloaded from www.uniprot.org and exported as a single FASTA file (one each for PLA$_2$ and 3FTXs). These sequences were then aligned using the free software program clustal omega and the alignment files were exported as .clustal files. Next, the experimentally solved structures for PLA$_2$ from *Bungarus caeruleus* (PDB: 2OSN) and 3FTXs from *Dendroaspis polylepsis* (PDB: 2MFA), were opened in the free software program chimera (UCSF, 2017). The .clustal files were then imported into chimera and analyzed for amino acid conservation. Disulfide bonds were then highlighted in yellow.
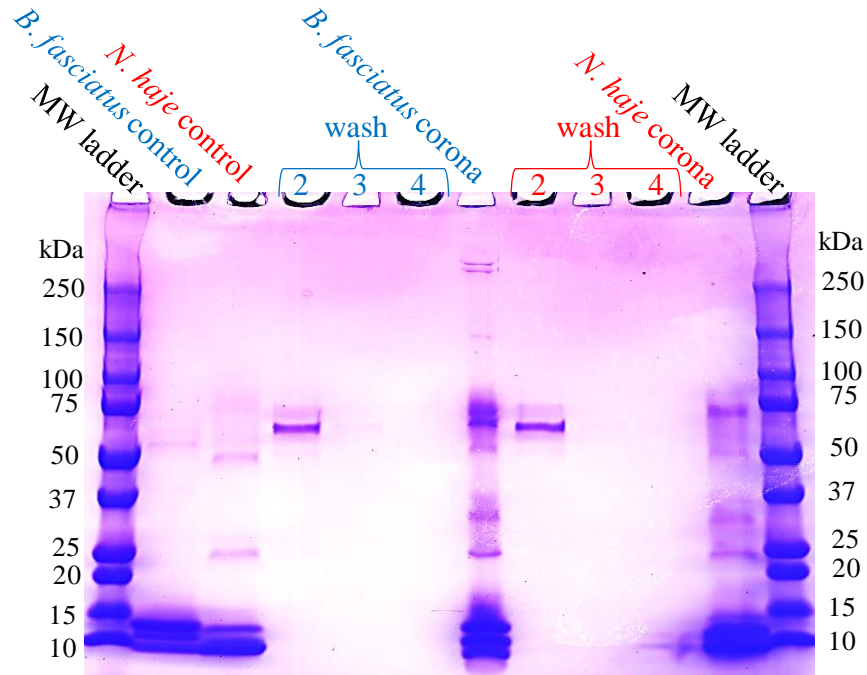
Figure 4.S1. NP selectivity experiment for *Bungarus fasciatus* venom (blue) and *Naja haje* venom (red) using 1% (w/w) venom in 25% human serum.
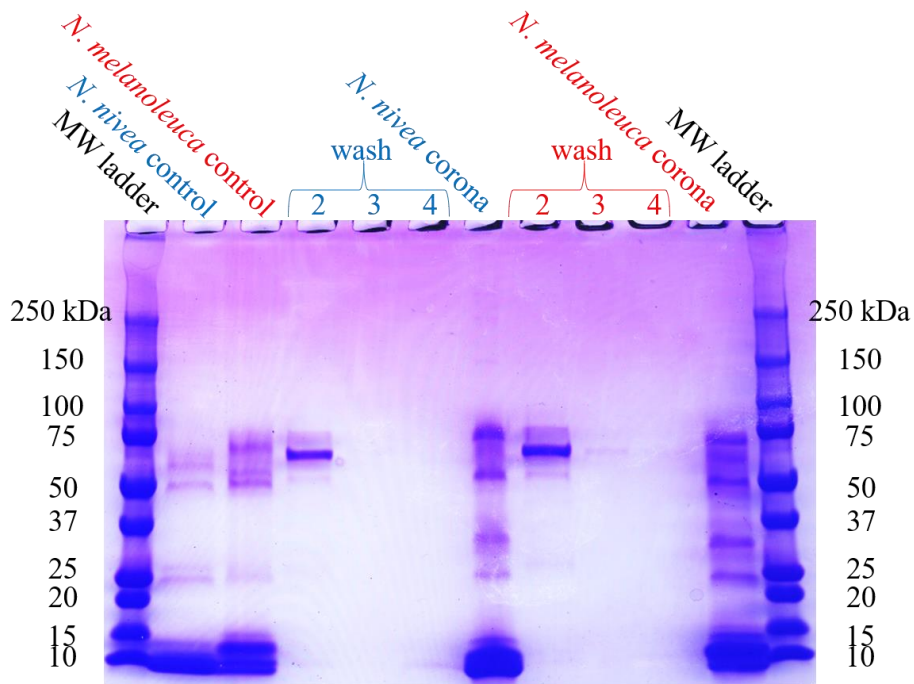
Figure 4.S2. NP selectivity experiment for *Naja nivea* venom (blue) and *Naja melanoleuca* venom (red) using 1% (w/w) venom in 25% human serum.
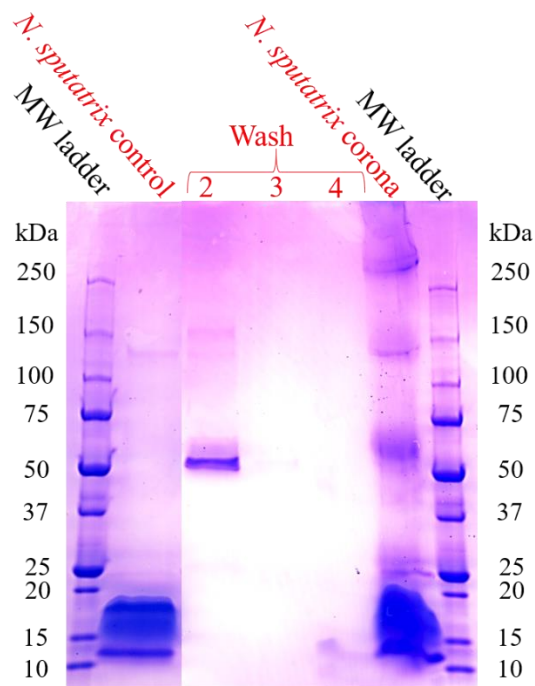
Figure 4.S3. NP selectivity experiment for *Naja sputatrix* venom (red) using 1% (w/w) venom in 25% human serum.
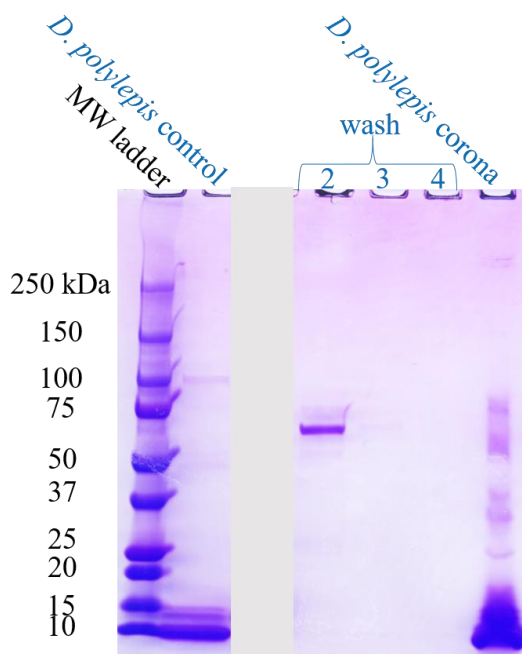
Figure 4.S4. NP selectivity experiment for *Dendroaspis polylepis* venom (blue) using 1% (w/w) venom in 25% human serum.
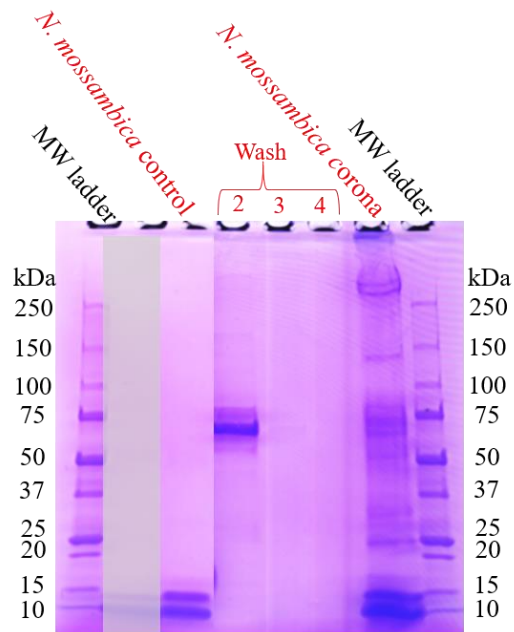
Figure 4.S5. NP selectivity experiment for *Naja mossambica* venom (red) using 1% (w/w) venom in 25% human serum.
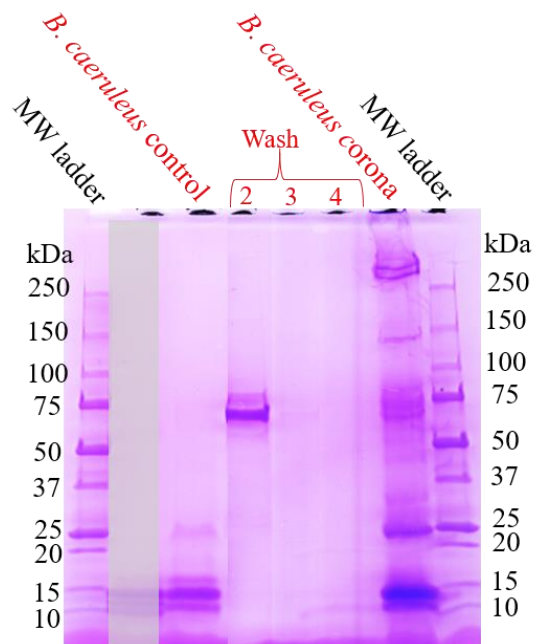
Figure 4.S6. NP selectivity experiment for *Bungarus caeruleus* venom (red) using 1% (w/w) venom in 25% human serum.
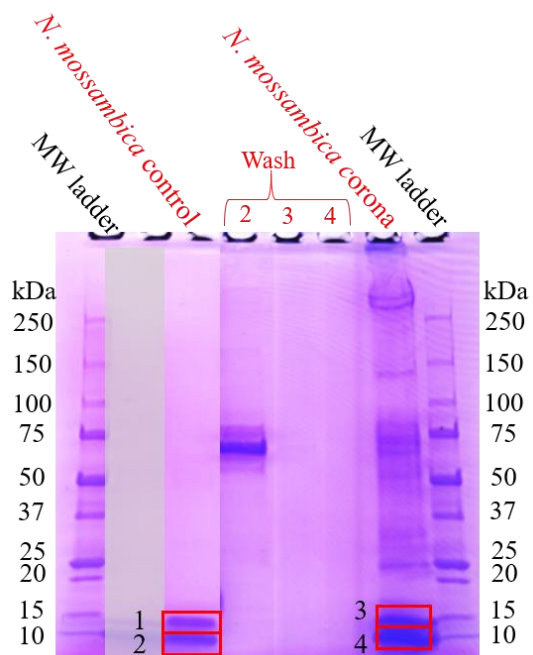
Figure 4.S7. Gel bands selected for trypsin digestion and LC-MS/MS proteomics analysis for *Naja mossambica* selectivity experiment.
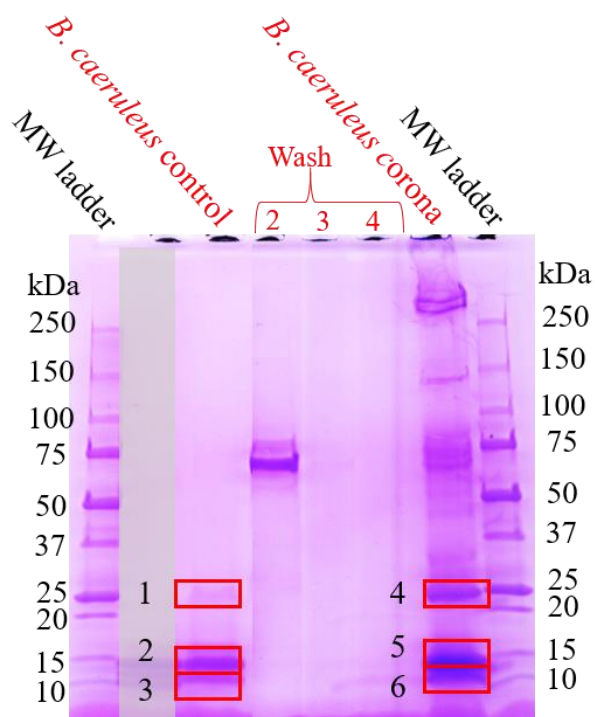
Figure 4.S8. Gel bands selected for trypsin digestion and LC-MS/MS proteomics analysis for *Bungarus caeruleus* selectivity experiment.
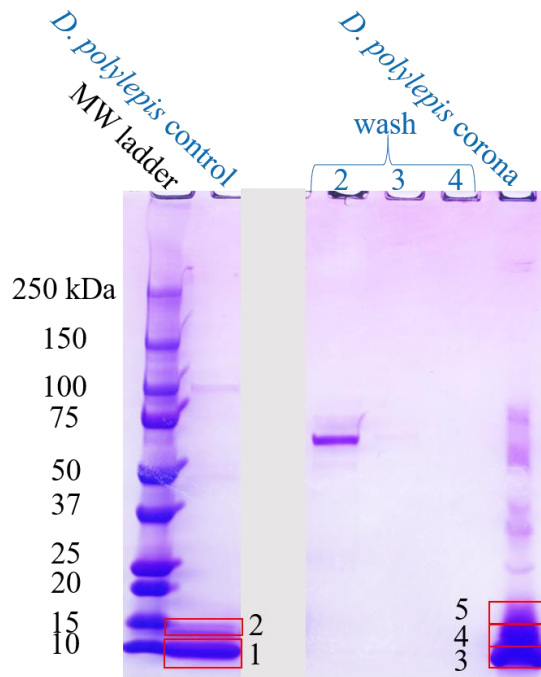
Figure 4.S9. Gel bands selected for trypsin digestion and LC-MS/MS proteomics analysis for *Dendroaspis polylepis* selectivity experiment.
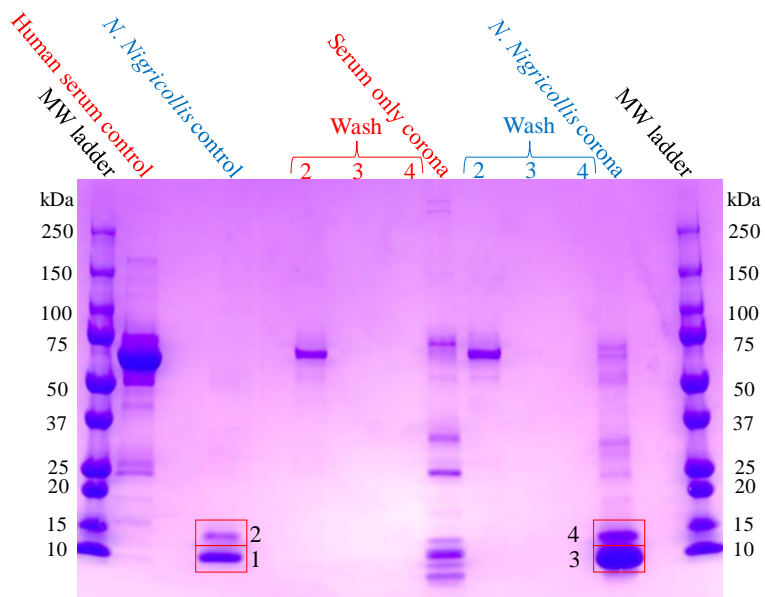
Figure 4.S10. Gel bands selected for trypsin digestion and LC-MS/MS proteomic analysis for *Naja nigricollis* selectivity experiment.
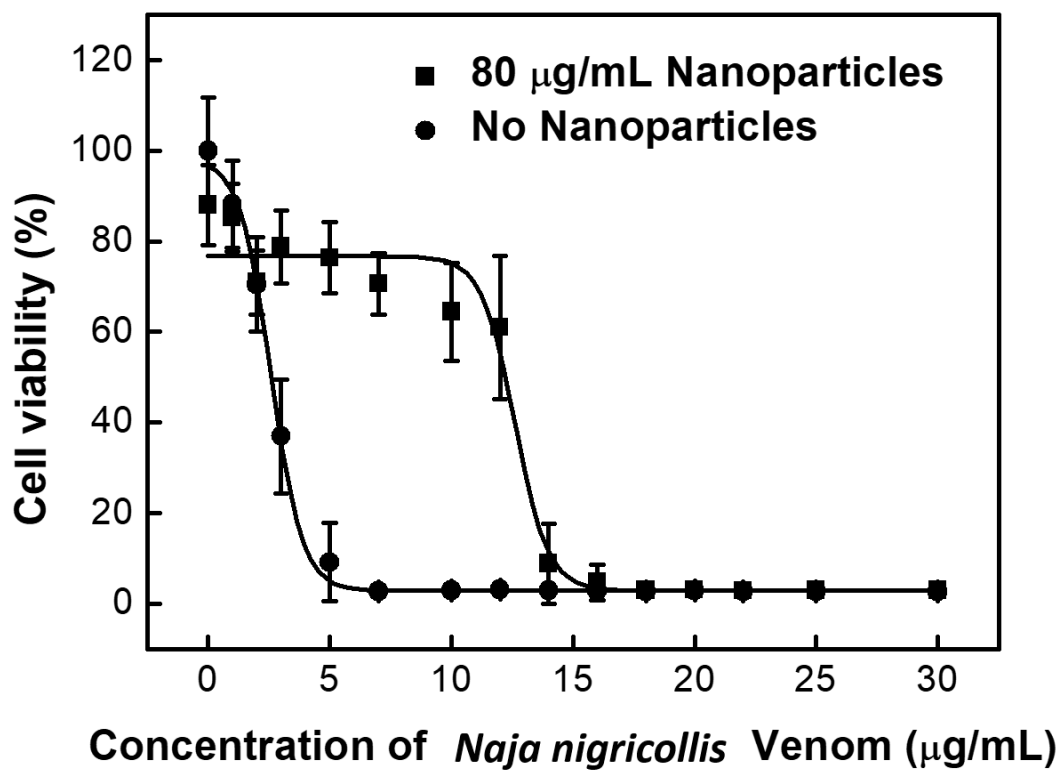
Figure 4.S11. The cell viability of L6 cells incubated with *Naja nigricollis* venom (1-30 µg/mL, n=4-5) in the presence (■) and absence (●) of 80 µg/mL nanoparticle, respectively.
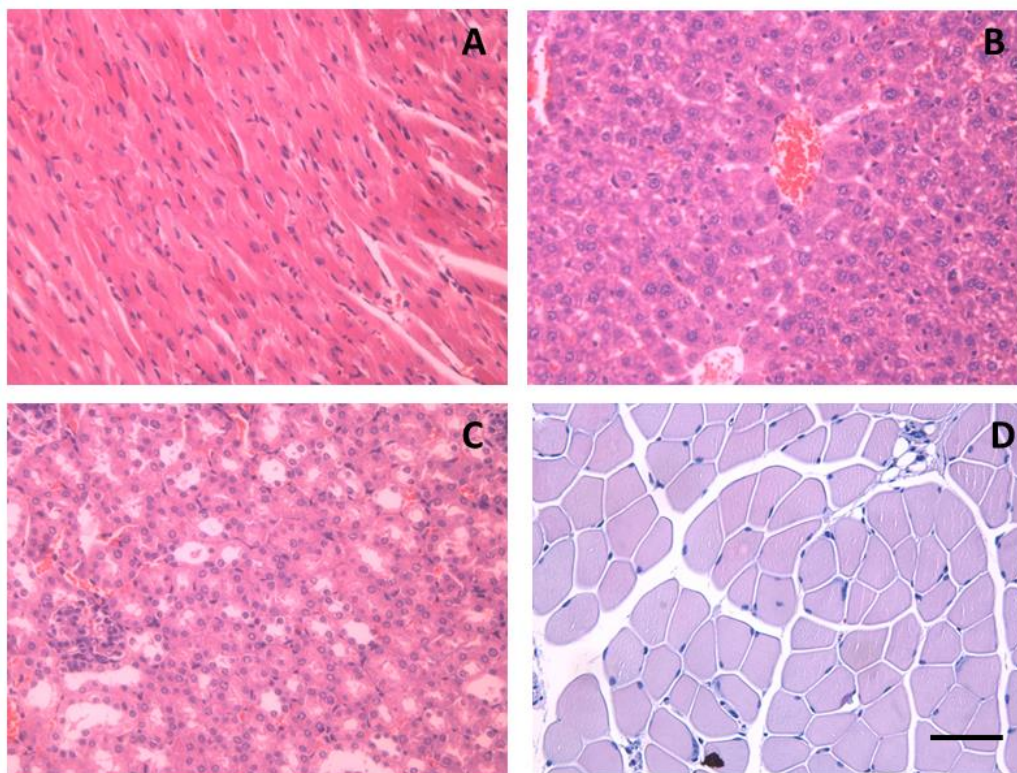
Figure 4.S12 Light micrographs of sections from heart (A), liver (B), kidney (C) and skeletal muscle (D) from mice injected with nanoparticles. Mice (18-20 g body weight) were injected with either 100 µL of nanoparticles in saline solution (5.5 mg/mL) by the intravenous (i.v.) route in the caudal vein, or intramuscularly (i.m.) in the right gastrocnemius. Mice injected i.v. were sacrificed at 24 h, and samples of heart, liver and kidneys were obtained. Mice injected i.m. were sacrificed at 24 h, and a sample of the injected gastrocnemius muscle was obtained. Tissues were fixed in 3.7% formalin solution and processed routinely for embedding in paraffin. No histopathological alterations are observed in any of the tissues. Hematoxylin-eosin staining. Bar represents 100 µm.
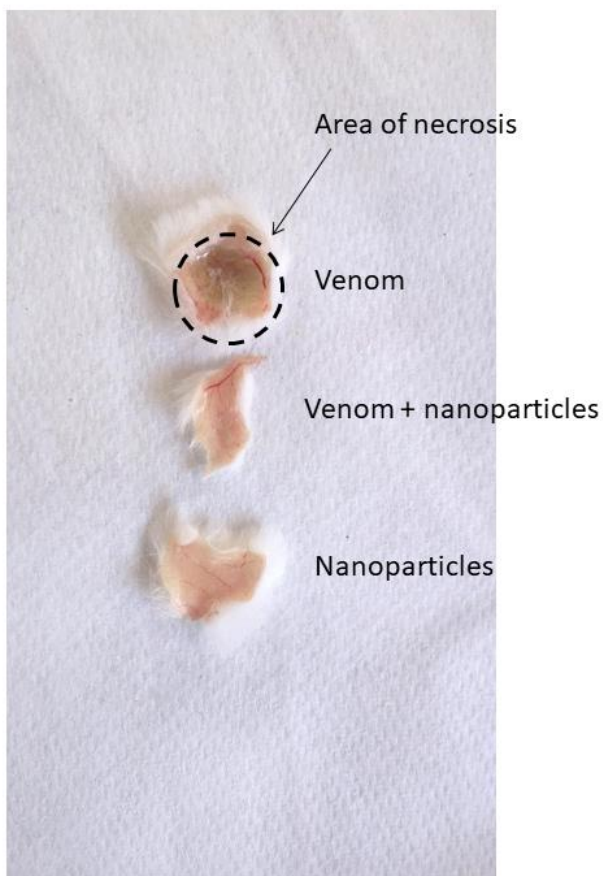
Figure 4.S13 Macroscopic assessment of the inhibition of dermonecrotic activity of *N. nigricollis* venom by NPs. Venom and NPs were mixed at a NP : venom ratio of 5.0 (w/w) and incubated for 30 min at room temperature. Controls included venom incubated with saline solution (venom) and NPs incubated with saline solution (nanoparticles). Then, aliquots of each mixture were injected intradermally in the ventral abdominal region of mice (18-20 g body weight). After 72 h, animals were sacrificed, their skin removed and the inner side of the skin observed for the presence of necrosis. A dark area of necrosis is observed only in the skin of mice receiving venom incubated with saline solution. Dermonecrosis was totally abrogated by the NPs, whereas NPs incubated with saline did not induce any effect.

Table 4.S1. Identification of toxins in *Naja mossambica* venom experiment using digested SDS-PAGE gel bands depicted in Figure 4.S7.

Protein name	Entry name	AA	C_1 %Cov	Peptides	C_2 %Cov	Peptides	NP_3 %Cov	Peptides	NP_4 %Cov	Peptides
Cytotoxin 1	3SA1_NAJMO	60	30	3	83.33	90	63.33	25	83.33	104
Cytotoxin 2	3SA2_NAJMO	60	30	3	70	76	50	24	90	97
Cytotoxin 3	3SA3_NAJMO	60	--	--	53.33	32	--	--	71.67	63
Cytotoxin 4	3SA4_NAJMO	60	--	--	78.33	38	25	2	68.33	50
Cytotoxin 5	3SA5_NAJMO	60	26.67	2	53.33	22	26.67	8	55	26
Acidic PLA2 CM-I	PA2A1_NAJMO	118	90.68	80	22.88	4	88.98	83	--	--
Basic PLA2 CM-II	PA2B2_NAJMO	118	92.37	114	32.2	7	90.68	115	61.02	12
Basic PLA2 CM-III	PA2B3_NAJMO	118	96.61	133	22.88	5	93.22	180	70.34	17
Short neurotoxin 1	3S13_NAJMO	62	45.16	11	--	--	--	--	--	--
Short neurotoxin 3	3S11_NAJMO	62	--	--	--	--	--	--	--	--
CRiSP	CRVP_NAJMO	30	--	--	--	--	--	--	--	--
SVMP	VM3M1_NAJMO	609	--	--	--	--	2.135	1	--	--

AA (amino acid length of venom protein), Peptides (total number of observed peptides), %Cov (%Coverage of sequence)

Table 4.S2. Identification of toxins found in *Bungarus caeruleus* experiment using digested SDS-PAGE gel bands depicted in Figure 4.S8.

Protein name	Entry name	AA	C_1 %Cov	#PTs	C_2 %Cov	#PTs	C_3 %Cov	#PTs	NP_4 %Cov	#PTs	NP_5 %Cov	#PTs	NP_6 %Cov	#PTs
α-δ-BTX-4	3L2A_BUNCE	76	--	--	--	--	--	--	--	--	--	--	--	--
Acidic PLA2 1	PA2A1_BUNCE	137	5.839	2	31.39	15	10.95	3	5.84	3	32.85	14	10.95	5
Basic PLA2 2	PA2B5_BUNCE	137	--	--	64.23	41	26.28	4	30.66	6	--	--	42.34	23
Basic PLA2 3	PA2B3_BUNCE	137	--	--	43.07	17	--	--	--	--	32.85	14	--	--
Basic KPLA2	PA2B_BUNCE	145	--	--	37.24	27	--	--	--	--	28.97	28	--	--
Beta-BuTX A1 Chain	PA2B1_BUNCE	147	15.65	2	64.63	55	19.05	3	54.42	8	71.43	82	55.1	17
Beta-BuTX A2 Chain	PA2B2_BUNCE	147	26.53	4	61.9	50	26.5	3	44.22	7	62.77	44	54.42	10

AA (amino acid length of venom protein), #PTs (number of peptides), %Cov (%Coverage of sequence)

Table 4.S3. Identification of toxins found in *D. polylepsis* experiment using digested SDS-PAGE gel bands depicted in Figure 4.S9.

Protein name	Entry Name	AA	C_1 %Cov	#PTs	C_2 %Cov	#PTs	NP_3 %Cov	#PTs	NP_4 %Cov	#PTs	NP_5 %Cov	#PTs
Kunitz-type serine protease inhibitor	VKTHB_DENPO	57	40.35	2	--	--	--	--	--	--	--	--
	VKTE_DENPO	59	55.93	5	--	--	55.93	4	55.93	6	55.93	4
	VKTHK_DENPO	79	35.44	7	--	--	--	--	32.91	6	35.44	7
	VKTH1_DENPO	60	85	15	63.3	6	78.33	11	85	14	71.67	11
Alpha-elapitoxin-Dpp2a	3L21_DENPO	72	--	--	--	--	--	--	--	--	--	--
Alpha-elapitoxin-Dpp2b	3L23_DENPO	72	--	--	--	--	--	--	--	--	--	--
Alpha-elapitoxin-Dpp2c	3L22_DENPO	72	--	--	--	--	--	--	--	--	--	--
Alpha-elapitoxin-Dpp2d	3L24_DENPO	72	90.28	13	59.7	7	66.67	7	90.28	12	90.28	9
Adrenergic toxin rho-elapitoxin-Dp1a	3SIMB_DENPO	65	41.54	3	38.5	2	--	--	--	--	29.23	1
Adrenergic toxin rho-elapitoxin-Dp1b	3SI3_DENPO	65	**	**	**	**	--	--	--	--	**	**
Short neurotoxin 1	3S11_DENPO	60	38.33	3	--	--	--	--	--	--	36.67	2
Calciseptin	3SLS_DENPO	60	61.67	4	--	--	--	--	43.33	2	43.33	2
Toxin FS-2	3SL2_DENPO	60	--	--	--	--	--	--	**	**	**	**
Acetylcholinesterase toxin C	3SEC_DENPO	61	55.74	3	62.3	4	--	--	62.29	4	62.29	4
Muscarinic toxin alpha	3SIMA_DENPO	66	78.79	6	50	2	--	--	--	--	--	--
Mambalgin-1	3SX1_DENPO	78	49.12	3	49.1	3	--	--	49.12	3	49.12	3
Mambalgin-2	3SX2_DENPO	57	**	**	**	**	--	--	**	**	**	**
Toxin MIT1	MIT1_DENPO	81	66.67	7	55.6	4	--	--	59.26	5	55.55	4

AA (amino acids in venom protein), #PTs (number of unique peptides), %Cov (%Coverage of sequence)

**Unable to distinguish between the venom protein listed above

Table 4.S4. Identification of toxins found in *N. nigricollis* experiment using digested SDS-PAGE gel bands depicted in Figure 4.S10.

Protein name	Entry Name	AA	C_1 %Cov	#PTs	C_2 %Cov	#PTs	NP_3 %Cov	#PTs	NP_4 %Cov	#PTs
PLA2 Basic	PA2B4_NAJNG	118	--	--	72.03	14	--	--	94.07	19
PLA2 CM-I [fragment]	PA2B1_NAJNG	30	--	--	--	--	--	--	--	--
PLA2 CM-II [fragment]	PA2B2_NAJNG	30	--	--	--	--	--	--	--	--
Nawaprin	WAPN_NAJNG	51	--	--	--	--	--	--	--	--
Cytotoxin 1	3SA1_NAJPA	60	58.33	8	43.33	3	43.33	5	43.33	3
Short neurotoxin 1	3S11_NAJPA	61	--	--	--	--	--	--	--	--

AA (amino acid length of venom protein), #PTs (number of unique peptides), %Cov (%Coverage of sequence)

L. References

(1)   Chippaux, J. P.: Snake-bites: appraisal of the global situation. *Bull. World Health Organ.* **1998**, *76*, 515-524.

(2)   Harrison, R. A.; Hargreaves, A.; Wagstaff, S. C.; Faragher, B.; Lalloo, D. G.: Snake envenoming: a disease of poverty. *PLoS Negl. Trop. Dis.* **2009**, *3*, e569.

(3)   Williams, D.; Gutierrez, J. M.; Harrison, R.; Warrell, D. A.; White, J.; Winkel, K. D.; Gopalakrishnakone, P.; Worki, G. S. B. I.: The Global Snake Bite Initiative: an antidote for snake bite. *Lancet* **2010**, *375*, 89-91.

(4)   Gutierrez, J. M.; Calvete, J. J.; Habib, A. G.; Harrison, R. A.; Williams, D. J.; Warrell, D. A.: Snakebite envenoming. *Nat. Rev. Dis. Primers* **2017**, *3*, 17063.

(5)   Williams, S. S.; Wijesinghe, C. A.; Jayamanne, S. F.; Buckley, N. A.; Dawson, A. H.; Lalloo, D. G.; de Silva, H. J.: Delayed Psychological Morbidity Associated with Snakebite Envenoming. *PloS Neglect. Trop. D.* **2011**, *5*.

(6)   Warrell, D. A.: Snake bite. *Lancet* **2010**, *375*, 77-88.

(7)   Gutierrez, J. M.; Leon, G.; Lomonte, B.; Angulo, Y.: Antivenoms for snakebite envenomings. *Inflamm. Allergy Drug Targets* **2011**, *10*, 369-380.

(8)   Gutierrez, J. M.: Improving antivenom availability and accessibility: science, technology, and beyond. *Toxicon* **2012**, *60*, 676-687.

(9)   Gutierrez, J. M.; Leon, G.; Rojas, G.; Lomonte, B.; Rucavado, A.; Chaves, F.: Neutralization of local tissue damage induced by Bothrops asper (terciopelo) snake venom. *Toxicon* **1998**, *36*, 1529-1538.

(10)   Rivel, M.; Solano, D.; Herrera, M.; Vargas, M.; Villalta, M.; Segura, A.; Arias, A. S.; Leon, G.; Gutierrez, J. M.: Pathogenesis of dermonecrosis induced by venom of the spitting cobra, Naja nigricollis: An experimental study in mice. *Toxicon* **2016**, *119*, 171-179.

(11)   Warrell, D. A.; Ormerod, L. D.: Snake-Venom Ophthalmia and Blindness Caused by Spitting Cobra (Naja-Nigricollis) in Nigeria. *Am. J. Trop. Med. Hyg.* **1976**, *25*, 525-529.

(12)   Habib, A. G.; Kuznik, A.; Hamza, M.; Abdullahi, M. I.; Chedi, B. A.; Chippaux, J. P.; Warrell, D. A.: Snakebite is Under Appreciated: Appraisal of Burden from West Africa. *PLoS Negl. Trop. Dis.* **2015**, *9*, e0004088.

(13)   Jayawardana, S.; Gnanathasan, A.; Arambepola, C.; Chang, T. Chronic Musculoskeletal Disabilities following Snake Envenoming in Sri Lanka: A Population-Based Study. *PLoS Negl. Trop. D.* **2016**, *10*, e0005103.

(14)   Sitprija, V.; Sitprija, S.: Renal effects and injury induced by animal toxins. *Toxicon* **2012**, *60*, 943-953.

(15)   Reeks, T. A.; Fry, B. G.; Alewood, P. F.: Privileged frameworks from snake venom. *Cell. Mol. Life Sci.* **2015**, *72*, 1939-1958.

(16)   Calvete, J. J. Venomics: integrative venom proteomics and beyond. *Biochem. J.* **2017**, *474*, 611-634.

(17)   Ohno, M.; Menez, R.; Ogawa, T.; Danse, J. M.; Shimohigashi, Y.; Fromen, C.; Ducancel, F.; Zinn-Justin, S.; Le Du, M. H.; Boulain, J. C.; Tamiya, T.; Menez, A.: Molecular evolution of snake toxins: is the functional diversity of snake toxins associated with a mechanism of accelerated evolution? *Prog. Nucleic Acid Res. Mol. Biol.* **1998**, *59*, 307-364.

(18)   Fry, B. G.: From genome to "venome": molecular origin and evolution of the snake venom proteome inferred from phylogenetic analysis of toxin sequences and related body proteins. *Genome Res.* **2005**, *15*, 403-420.

(19)   Montecucco, C.; Gutierrez, J. M.; Lomonte, B.: Cellular pathology induced by snake venom phospholipase A_2 myotoxins and neurotoxins: common aspects of their mechanisms of action. *Cell. Mol. Life Sci.* **2008**, *65*, 2897-2912.

(20)   Dubovskii, P. V.; Utkin, Y. N.: Cobra cytotoxins: structural organization and antibacterial activity. *Acta Naturae* **2014**, *6*, 11-18.

(21)   Barber, C. M.; Isbister, G. K.; Hodgson, W. C. Alpha neurotoxins. *Toxicon* **2013**, *66*, 47-58.

(22)   Scott, D. L.; White, S. P.; Otwinowski, Z.; Yuan, W.; Gelb, M. H.; Sigler, P. B.: Interfacial catalysis: the mechanism of phospholipase A_2. *Science* **1990**, *250*, 1541-1546.

(23)   Gazi, I.; Lourida, E. S.; Filippatos, T.; Tsimihodimos, V.; Elisaf, M.; Tselepis, A. D.: Lipoprotein-associated phospholipase A_2 activity is a marker of small, dense LDL particles in human plasma. *Clin. Chem.* **2005**, *51*, 2264-2273.

(24)   Konshina, A. G.; Dubovskii, P. V.; Efremov, R. G.: Structure and dynamics of cardiotoxins. *Curr. Protein Pept. Sc.* **2012**, *13*, 570-584.

(25)   Tsetlin, V.: Snake venom alpha-neurotoxins and other 'three-finger' proteins. *Eur. J. Biochem.* **1999**, *264*, 281-286.

(26)   Soares, A. M.; Ticli, F. K.; Marcussi, S.; Lourenco, M. V.; Januario, A. H.; Sampaio, S. V.; Giglio, J. R.; Lomonte, B.; Pereira, P. S.: Medicinal plants with inhibitory properties against snake venoms. *Curr. Med. Chem.* **2005**, *12*, 2625-2641.

(27)   Perales, J.; Neves-Ferreira, A. G.; Valente, R. H.; Domont, G. B.: Natural inhibitors of snake venom hemorrhagic metalloproteinases. *Toxicon* **2005**, *45*, 1013-1020.

(28)   Laustsen, A. H.; Engmark, M.; Milbo, C.; Johannesen, J.; Lomonte, B.; Gutierrez, J. M.; Lohse, B.: From Fangs to Pharmacology: The Future of Snakebite Envenoming Therapy. *Curr. Pharm. Des.* **2016**, *22*, 5270-5293.

(29)   O'Brien, J.; Lee, S. H.; Onogi, S.; Shea, K. J.: Engineering the Protein Corona of a Synthetic Polymer Nanoparticle for Broad-Spectrum Sequestration and Neutralization of Venomous Biomacromolecules. *J. Am. Chem. Soc.* **2016**, *138*, 16604-16607.

(30)   Hoshino, Y.; Koide, H.; Furuya, K.; Haberaecker, W. W., 3rd; Lee, S. H.; Kodama, T.; Kanazawa, H.; Oku, N.; Shea, K. J.: The rational design of a synthetic polymer nanoparticle that neutralizes a toxic peptide in vivo. *Proc. Natl. Acad. Sci. U. S. A.* **2012**, *109*, 33-38.

(31)   Hoshino, Y.; Koide, H.; Urakami, T.; Kanazawa, H.; Kodama, T.; Oku, N.; Shea, K. J.: Recognition, neutralization, and clearance of target peptides in the bloodstream of living mice by molecularly imprinted polymer nanoparticles: a plastic antibody. *J. Am. Chem. Soc.* **2010**, *132*, 6644-6645.

(32)   Koide, H.; Yoshimatsu, K.; Hoshino, Y.; Lee, S. H.; Okajima, A.; Ariizumi, S.; Narita, Y.; Yonamine, Y.; Weisman, A. C.; Nishimura, Y.; Oku, N.; Miura, Y.; Shea, K. J.: A polymer nanoparticle with engineered affinity for a vascular endothelial growth factor ($VEGF_{165}$). *Nat. Chem.* **2017**, *9*, 715-722.

(33)   Warrell, D. A.: Clinical toxicology of snakebite in Africa and the Middle East/Arabian peninsula. In: Meier, J., White, J. (Eds.), *Handbook of Clinical Toxicology of Animal Venoms and Poisons*; CRC Press: Boca Raton, **1995**.

(34)   Lundqvist, M.; Stigler, J.; Elia, G.; Lynch, I.; Cedervall, T.; Dawson, K. A.: Nanoparticle size and surface properties determine the protein corona with possible implications for biological impacts. *P. Natl. Acad. Sci. U. S. A.* **2008**, *105*, 14265-14270.

(35)   Chen, C.; Huang, H.; Wu, C. H.: Protein Bioinformatics Databases and Resources. *Methods Mol. Biol.* **2017**, *1558*, 3-39.

(36)   Silva, A.; Maduwage, K.; Sedgwick, M.; Pilapitiya, S.; Weerawansa, P.; Dahanayaka, N. J.; Buckley, N. A.; Johnston, C.; Siribaddana, S.; Isbister, G. K.: Neuromuscular Effects of Common Krait (Bungarus caeruleus) Envenoming in Sri Lanka. *PLoS Negl. Trop. D.* **2016**, *10*, e0004368.

(37)   Kwong, P. D.; McDonald, N. Q.; Sigler, P. B.; Hendrickson, W. A.: Structure of beta 2-bungarotoxin: potassium channel binding by Kunitz modules and targeted phospholipase action. *Structure* **1995**, *3*, 1109-1119.

(38)   Laustsen, A. H.; Lomonte, B.; Lohse, B.; Fernandez, J.; Gutierrez, J. M.: Unveiling the nature of black mamba (Dendroaspis polylepis) venom through venomics and antivenom immunoprofiling: Identification of key toxin targets for antivenom development. *J. Proteomics* **2015**, *119*, 126-142.

(39)   Warrell, D. A.; Greenwood, B. M.; Davidson, N. M.; Ormerod, L. D.; Prentice, C. R. M.: Necrosis, Hemorrhage and Complement Depletion Following Bites by Spitting Cobra (Naja-Nigricollis). *Q. J. Med*. **1976**, *45*, 1-22.

(40)   Petras, D.; Sanz, L.; Segura, A.; Herrera, M.; Villalta, M.; Solano, D.; Vargas, M.; Leon, G.; Warrell, D. A.; Theakston, R. D.; Harrison, R. A.; Durfa, N.; Nasidi, A.; Gutierrez, J. M.; Calvete, J. J.: Snake venomics of African spitting cobras: toxin composition and assessment of congeneric cross-reactivity of the pan-African EchiTAb-Plus-ICP antivenom by antivenomics and neutralization approaches. *J. Proteome Res.* **2011**, *10*, 1266-1280.

(41)   Kalam, Y.; Isbister, G. K.; Mirtschin, P.; Hodgson, W. C.; Konstantakopoulos, N.: Validation of a cell-based assay to differentiate between the cytotoxic effects of elapid snake venoms. *J. Pharmacol. Toxicol. Met.* **2011**, *63*, 137-142.

Chapter 5

Analyzing the difference in affinity for various toxin isoforms to an optimized nanoparticle toxin sequestrant

A. Abstract

Imparting selectivity for certain biomacromolecules over others is perhaps the most challenging aspect of developing nanoparticles (NPs) with affinity and specificity. This is particularly difficult for therapeutic applications where one works in complex biological mixtures such as human serum. While NPs administered intravenously will initially be coated with highly mobile proteins such as albumin and globulins due to the Vroman effect, it is necessary that these proteins exchange for target biomacromolecules in order to elicit a desired biological response or sequester a target protein. Hoshino *et al.* and Koide *et al.* have demonstrated that such an exchange is possible by sequestering melittin and the signaling protein VEGF in vivo using optimized NP formulations.[1,2] The focus of this chapter is on the analysis of how the NP formulation optimized in chapter 3 with selectivity for venomous biomacromolecules from snake venom in concentrated human serum does not display the same calculated dissociation constant (K_d) one would expect to observe using a quartz crystal microbalance (QCM).

B. Background
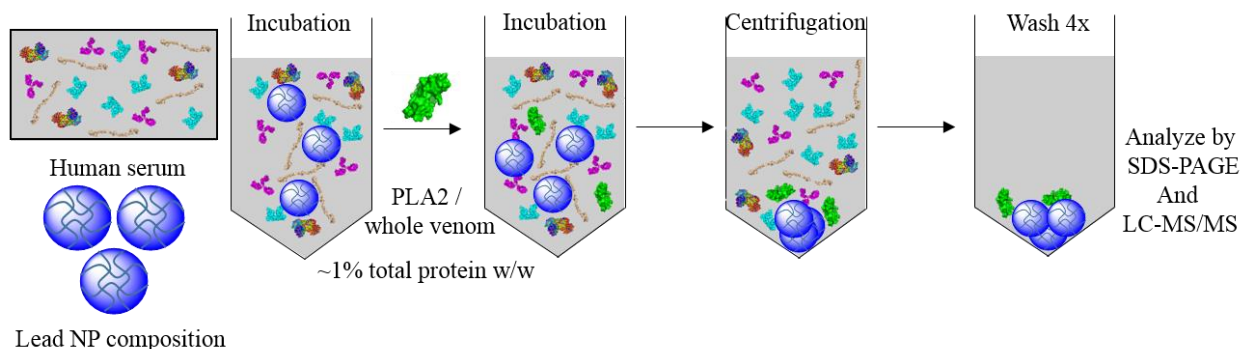
Figure 5.1. Strategy for analyzing selectivity for targeted venom proteins over human serum proteins. Serum was diluted to a final concentration of 25%, PLA_2/whole venom was diluted to a final concentration of 250 µg/mL, and NPs were diluted to a final concentration of 1 mg/mL.

Although there is a great deal of variability across snake venoms, there is also a rather striking level of similarity.[3] Often, the most potent venoms, such as *Bungarus* (Krait) or *Naja* (Cobra) venom, contain only two or three major protein families. In Elapidae snakes, which include the Krait and Cobra genera, the majority of the proteins can be subdivided into two protein families: Phospholipase A_2 (PLA_2) and three-finger toxins (3FTX).[4] Despite the fact that these families of protein toxins occur across multiple species, securing an effective antivenom is complicated by the diversity of protein isoforms found within each protein family. For example, both PLA_2 and 3FTXs have well over 300 different isoforms that have been sequenced and likely many more that have yet to be characterized.[5] This diversity on the primary sequence level is likely the reason why immunoglobulin based antivenoms are highly specific to particular venom compositions and often show poor cross-reactivity. Consequently, a challenge for any broad-spectrum antivenom for elapidae snakes is to develop an affinity reagent that recognizes structural features and similarities shared by venomous PLA_2 and 3FTX isoforms that are also unique with

respect to abundant serum proteins. In chapters 3 and 4, I demonstrated that that a NP synthesized with a feed ratio of 25% *N*-isopropylacrylamide, 20% acrylic acid, 40% *N*-phenylacrylamide and 15% *N, N'*-methylenebisacrylamide is capable of selectively sequestering nearly all members of the PLA$_2$ and 3FTX toxin families in the presence of concentrated human serum (Figure 5.1-5.2)
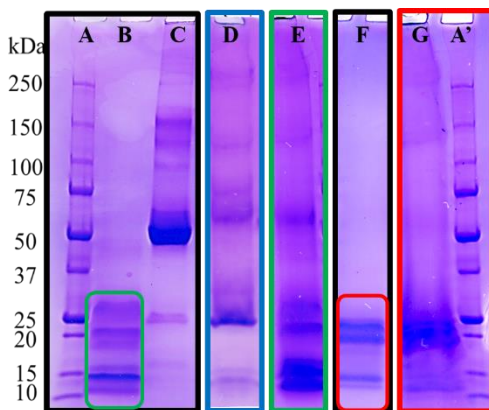
Figure 5.2. Example of Whole venom selectivity experiments using the protocol outlined in Figure 5.1 visualized by SDS-PAGE. (A/A') molecular weight ladder. (B) *Bungarus caeruleus* whole venom. (C) Serum control. (D) Lead NP incubated in serum only. (E) Lead NP incubated in serum and *Bungarus caeruleus* whole venom. (F) *Naja mossambica* whole venom. (G) Lead NP incubated in serum and *Naja mossambica* whole venom. For more information including proteomic verification of toxin selectivity see Chapter 4.

Compared to antibodies, synthetic hydrogel NPs bind proteins with a much more complex stoichiometry. This in turn will result in a distribution of binding affinities and requires critical analysis of equilibrium binding constants unique to their biological (antibody) counterparts. This point is perhaps best visualized in Figure 5.3. Here, the venom-binding NP is immobilized on the gold Surface Plasmon Resonance (SPR) chip then PLA$_2$ was introduced until saturation was achieved (100% capacity). The NP•biomacromolecule dissociation was monitored by flowing fresh PBS for an extended period of time (~7 h). Interestingly, complete dissociation was not observed over the time period in which we monitored.
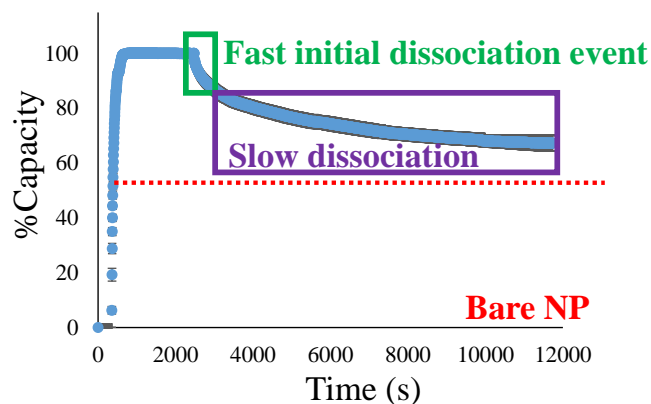
Figure 5.3. Kinetic dissociation of bee venom PLA_2 from the optimized venom protein NP sequestrant.

This lack of complete dissociation has raised a number of questions regarding soft materials interacting with biomacromolecules under physiological conditions. Recently evidence has emerged suggesting that polyethylene glycol (PEG), which is often used to increase circulation time for nanocarriers in vivo, achieves this characteristic largely due to its adsorption of apolipoprotein J (clusterin).[6] Considering the average plasma concentration of clusterin is roughly 50 µg/mL, it is likely that PEG first interacts with many other proteins before clusterin. However, upon binding clusterin, it becomes kinetically unfavorable to disassociate, and therefore does not occur under relevant time scales. A similar phenomenon was observed by Molinaro *et al.* upon developing a biomimetic proteolipid vesicle to increase the bioavailability of liposomal nano carriers. The goal of their work was to mimic the plasmalemma of leukocytes by using purified membrane-bound proteins from leukocytes during the liposome synthesis process. After subjecting these nano carriers in serum, dissociation of the leukocyte proteins was not observed.[7] These findings provide a framework to probe this complex kinetic adsorption/desorption phenomena.

One possible explanation for why complete dissociation from these NPs is kinetically very slow, is that the nature of these hydrogels produces a significantly greater desolvation effect compared to typical protein-protein interactions. Binding of a biomacromolecule to a hydrogel results in rapid internal and external structural rearrangement. The interior of hydrogels by definition is significantly more hydrated compared to proteins. This is evident when analyzing biomacromolecule-hydrogel interactions by isothermal titration calorimetry (ITC), which suggests binding is often dominated by entropy. This entropy is likely a result of the expulsion of water from the hydrogel. Although NP-protein and protein-protein interactions are electrostatic interactions which produces a displacement of mobile ions upon binding, the quantity of mobile ions able to dissociate is increased in the NP-protein interaction due to the internal solvation of NP hydrogels. In one study, this was shown to be the case by comparing DLS and ITC data, which showed that the NP does indeed initially collapse upon binding lysozyme.[8] Considering the stoichiometry of the NP•biomacromolecule complex at 100% capacity is upwards of 1:10, the degree of rearrangement and expulsion of water likely decreases significantly once capacity reaches 80%. Therefore, bound biomacromolecules dissociate rapidly when the energy needed to re-solvate the hydrogel is low. However, the majority of the bound proteins have a larger thermodynamic barrier for re-solvation to fully dissociate from the NP. This dynamic aspect of NP•biomacromolecule binding suggests that kinetic data and therefore affinity must be treated differently than typical protein-protein interactions or protein-ligand interactions. Thus, quantifying affinity and specificity requires the use of different experimental techniques aimed at monitoring the exchange of bound biomacromolecules and the degree of observed cooperativity or anti-cooperativity upon saturating a NP with a particular biomacromolecule. This is especially

important considering an entropy driven de-solvation may occur independent of *functional* selectivity.[9]

C. NP-immobilized quartz crystal microbalance study

The experimental technique used to examine selectivity (Figure 5.1) only provides a qualitative assessment of affinity. Thus, to attain a better understanding of binding strength, the NP was immobilized on a gold coated quartz crystal microbalance (QCM) sensor via simple adsorption and select 3FTX and PLA$_2$ isoforms (Figure 5.4) were introduced in systematically increasing concentrations to determine the equilibrium dissociation constant (K$_d$). The resulting plots were then fitted with the Langmuir equation using the program Origin to provide a comparative affinity constant for the toxin isoforms to the NP. All of the toxin isoforms used in this study with the exception of β-bungarotoxin from *Bungarus multicinctus* were shown to selectively associate to the NP via the NP selectivity protocol and confirmed using LC-MS/MS proteomic analysis (see chapter 4). That being said, closely related β-bungarotoxin isoforms from *Bungarus caeruleus* venom were identified in the *Bungarus caeruleus* proteomic analysis.

Table 5.1. Summary of protein toxin properties and calculated Langmuir-derived affinity constants

Toxin	Cardiotoxin	Alpha neurotoxin	Monomeric PLA$_2$	Beta-Bungarotoxin
Species	*N. mossambica*	*N. nigricollis*	*N. mossambica*	*B. caeruleus*
AA[a]	60	62	118	120[b], 61[c]
MW	6.8 kDa	6.9 kDa	13.2 kDa	20.5 kDa
pI	8.6	7.52	6.3	6.63[b], 7.92[c]
average K$_d$	9.7×10^{-7} M	5.7×10^{-5} M	5.0×10^{-7} M	9.1×10^{-6} M
Stdev K$_d$	4.2×10^{-7} M	3.2×10^{-5} M	2.3×10^{-7} M	7.2×10^{-6} M
n	7	4	4	5
PDB ID	2ccx	3nds	--	1bun

[a] Number of amino acids
[b] PLA$_2$ subunit of β-bungarotoxin
[c] Kunitz-type serine protease inhibitor subunit of β-bungarotoxin
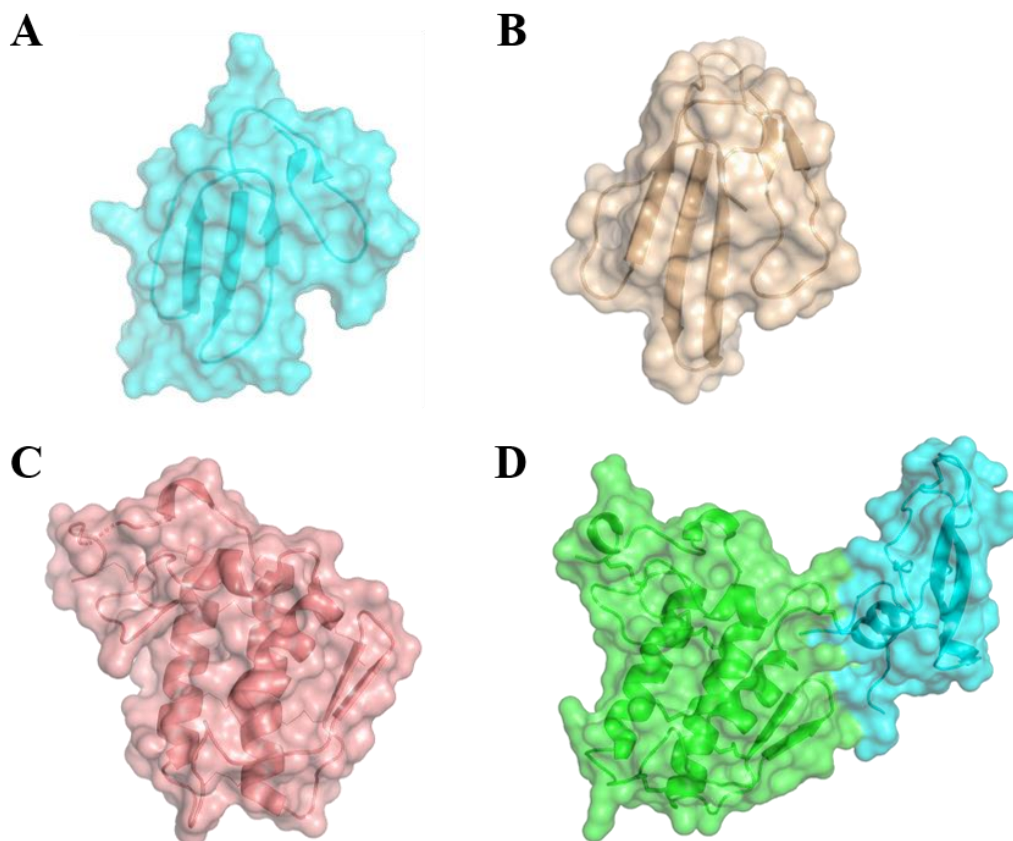
Figure 5.4 Crystal structures of select 3FTX and PLA$_2$ isoforms used in the NP immobilized QCM binding study. (A) Cardiotoxin, a 3FTX from *Naja mossambica* (B) α-neurotoxin, a 3FTX from *Naja nigricollis*. (C) Monomeric PLA$_2$ from *Bungarus caeruleus* venom *Note QCM study used a closely related monomeric PLA$_2$ from *Naja mossambica* which does not have a PDB crystal structure (D) Heterodimeric β-Bungarotoxin featuring a PLA$_2$ (green) covalently bound to a Kunitz-type serine protease inhibitor (blue) from *Bungarus multicinctus* venom

D. Cardiotoxin and α-neurotoxin QCM results

3FTXs are a class of structurally similar proteins that include neurotoxins, cardiotoxins and muscarinic toxins. They are characterized by three anti-parallel β-stranded loops (fingers) protruding from a hydrophobic core consisting of four conserved disulfide bonds. These highly cross-linked toxins are roughly 7 kDa and include the family of toxins known as cardiotoxins. Cardiotoxins are small necrotizing proteins found abundantly in the venom of spitting cobras. Compared to the other toxin isoforms used in this study, cardiotoxins are significantly more basic with an isoelectric point (pI) of 8.6. The complementary charge in addition to an abundance of

hydrophobic residues allowing for partial cell penetration of these proteins into cellular membranes[10] resulted in the lowest calculated average K_d (9.7×10^{-7} M) of the four toxins studied. Conversely, α-neurotoxin, a 3FTX found in the spitting cobra *Naja nigricollis* and *Naja pallida* had an average K_d of 5.7×10^{-5} M, two orders of magnitude higher than the cardiotoxin. The α-neurotoxin has a slightly lower pI of 7.52 thus reducing the degree of charge-charge complementarity between the acidic NP and the protein toxin. Furthermore, α-neurotoxin is known to impart toxicity via the arrest of nicotinic acetylcholine receptors[11] and therefore is less lipophilic compared to the cardiotoxin.

While there is a notable degree of variance in the observed change in frequency and in the shape of the binding isotherms within each set of experiments (Figures 5.S1-3), in general the cardiotoxin binding studies show a greater change in frequency (greater capacity) and a more pronounced slope compared to the α-neurotoxin. This suggests a greater degree of uncooperatively and reduced capacity for α-neurotoxin compared to cardiotoxin.[12] One explanation for this observation could be that the increased lipophilicity of the cardiotoxin allows for a greater degree of NP penetration compared to α-neurotoxin. This would increase the total available area of interaction (capacity) and would influence how the binding of higher-order stoichiometric proteins from more concentrated protein injections (50-100% capacity) are influenced by the lower-order stoichiometric proteins from the initial low concentration protein injections (0-50% capacity), which in turn influences the degree of cooperativity (slope of the binding isotherm).

E. Monomeric PLA₂ and β-bungarotoxin QCM results

Snake venom phospholipase A_2 enzymes are classically divided into two groups: Group I (*elapidae, hydrophiidae*) and group II *(viperade, crotalidae)*. The major structural distinction between the two groupings is their disulfide pattern and an extended 6-7 amino acid C-terminus

for group II PLA_2. Both groups have seven disulfide bonds and molecular weights between 13-15 kDa. However, the distribution of pharmacological activities between the two groups is highly variable.[4] This is likely a result of the lack of identification of functional PLA_2 receptors for most PLA_2 isoforms. An exception to this are PLA_2 isoforms that are part of β-bungarotoxin. β-bungarotoxin is a covalently bound PLA_2 (A-chain)-serine protease inhibitor (B-chain) heterodimer that binds to potassium channels on the presynaptic membrane of peripheral nerves. The kunitz-type serine protease inhibitor acts as a targeting moiety to the potassium channel. Once bound, the PLA_2 subunit begins hydrolyzing the phospholipids of the membrane resulting in increased permeability and ultimately depolarization leading to paralysis.

A www.uniprot.org search for β-bungarotoxin reveals that there are at least 20 different PLA_2 (chain A) subunits and all of these are from the *Bungarus* genus of elapidae snakes (group I PLA_2). Compared to monomeric PLA_2, the A-chain in β-bungarotoxin has only six disulfide bonds (C_{11}-C_{80} is missing), and has an additional cysteine residue (C_{15}) that attaches to the B-chain.

In chapter 3, clear evidence was presented demonstrating that the venom-binding NP selectively interacts with the same monomeric PLA_2 isoform from *Naja mossambica* venom used in this QCM study. Analysis of the serum proteins that also interact with this NP suggested that the selectivity arises from the lipoprotein-particle mimicry, a natural substrate of endogenous PLA_2 that this synthetic NP exhibits.

The calculated average K_d of the monomeric PLA_2 was 5.0×10^{-7} M, which was only modestly higher and statistically indistinguishable from the calculated average K_d of β-bungarotoxin (9.1×10^{-6} M). However, the two differ significantly in terms of relative capacity and in cooperativity. Monomeric PLA_2 reached saturation at a change in frequency roughly 10-fold lower than β-bungarotoxin (Figure 5.S4-6). While difficult to interpret, this pronounced difference

in frequency change is significant and suggests that simply comparing the calculated K_d values leaves out important information regarding the two binding events.

One speculative explanation for this observation is that the mode of binding between the monomeric and heterodimeric PLA_2 toxins differs considerably. If the monomeric PLA_2 binds in a manner that does not de-solvate the NP as significantly as that of than β-bungarotoxin, perhaps the frequency change at saturation would not be as pronounced. This hypothesis could be tested using isothermal titration calorimetry (ITC) to compare the relative endothermic signatures that are indicative to water expulsion from the interior of the NP. Unfortunately, because the QCM study is a surface based technique, it would be difficult to accurately compare these results with ITC derived data. This difference (surface versus solution based technique) would need to be taken into careful consideration when comparing the two data sets.

F. Conclusion

In summary, the binding affinity of four unique toxin isoforms to the venom-sequestering NP is highly variable. Although this NP is capable of selectively sequestering these toxins over serum proteins, the variance in calculated K_d values, the observed capacity and slope of the generated isotherm suggests that there is a great deal of variance in how the NP interacts with these toxins. To better understand why the observed selectivity for these toxins does not correlate well with the QCM binding study, additional quantitative experiments involving ITC must be performed. Additionally, it is worth investigating if high affinity serum proteins such as apolipoprotein A-1 aid certain toxin isoforms by increasing the affinity of the toxin to the NP. This complex set of experiments may be difficult to perform, but is necessary in order to fully understand the observed-broad spectrum selectivity this venom-binding NP appears to exhibit.

G. Supplemental information

<u>Materials</u>

PLA$_2$ from *Naja mossambica* venom and Cardiotoxins from *Naja mossambica* venom were purchased from Sigma Aldrich. β-bungarotoxin and from *Bungarus multicinctus* venom and α-neurotoxin from *Naja nigricollis* venom were purchased from Latoxan. All other reagents were purchased from commercial sources.

<u>Quartz crystal microbalance:</u>

QCM cells were washed with 1% SDS followed by nanopore water (10x, 500 µL) and dried using a gentle stream of air. The gold electrodes were then cleaned by pipetting 1 µL of 4 M peroxide, followed by 3 µL of concentrated sulfuric acid and after 10 min, the cells were washed with nanopore water (10x, 500 µL) and repeated two more times. Next, 500 µL of PBS was added to the cells and the cells were loaded into an Affinity Q4 QCM instrument (Initium Co. Ltd., Tokyo, Japan) and allowed to equilibrate. Next NP was immobilized onto the clean gold surface by pipetting a solution of NPs into the QCM cell at r.t. until the surface was saturated. The cells were then washed with PBS (500 µL, 3x) and then filled with fresh PBS and allowed to equilibrate in the instrument. Next, solutions of protein toxin isoforms (1 mg/mL PBS) were pipetted into the QCM cell at systematically increasing volumes pipetted after equilibration. The data was then plotted in Origin 6 and fitted with the Langmuir equation.
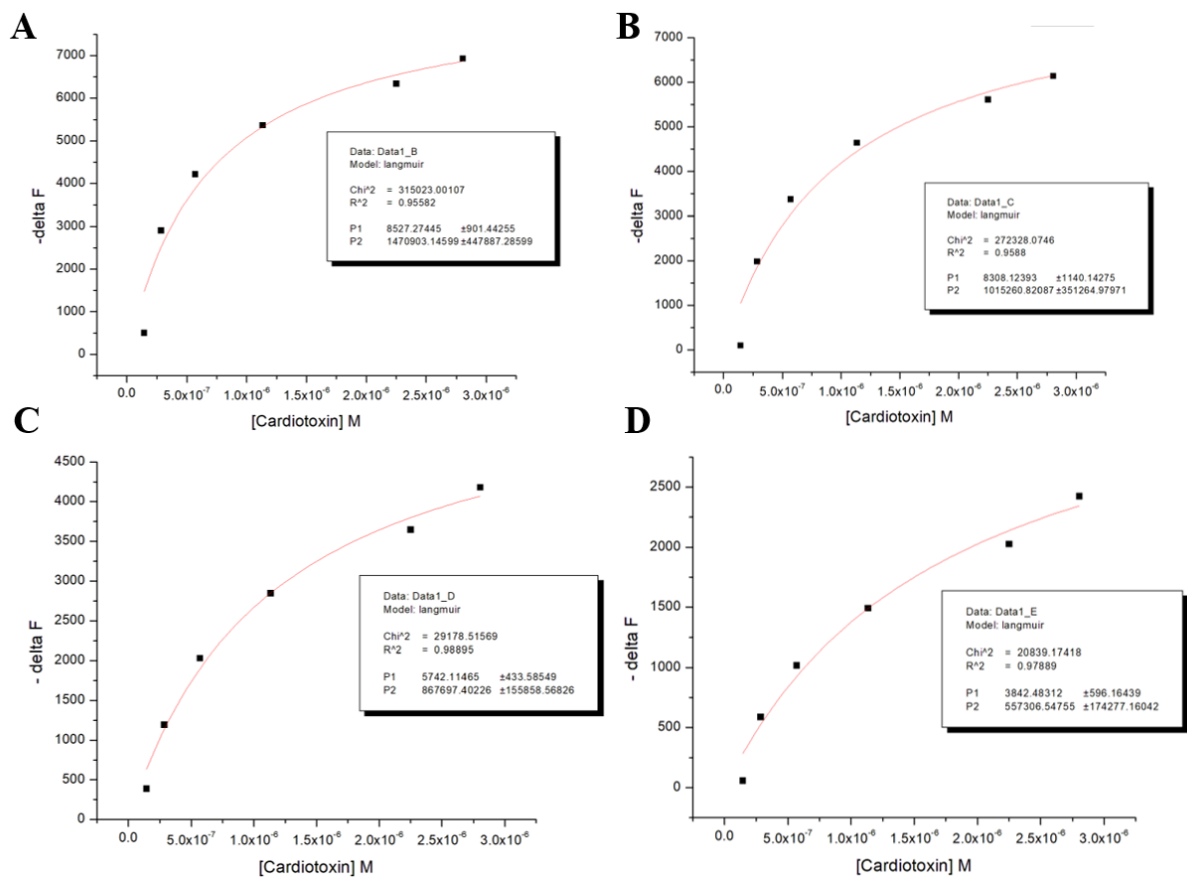
Figure 5.S1. QCM derived binding plots fitted with the Langmuir function for cardiotoxins from *Naja mossambica* (1 of 2).
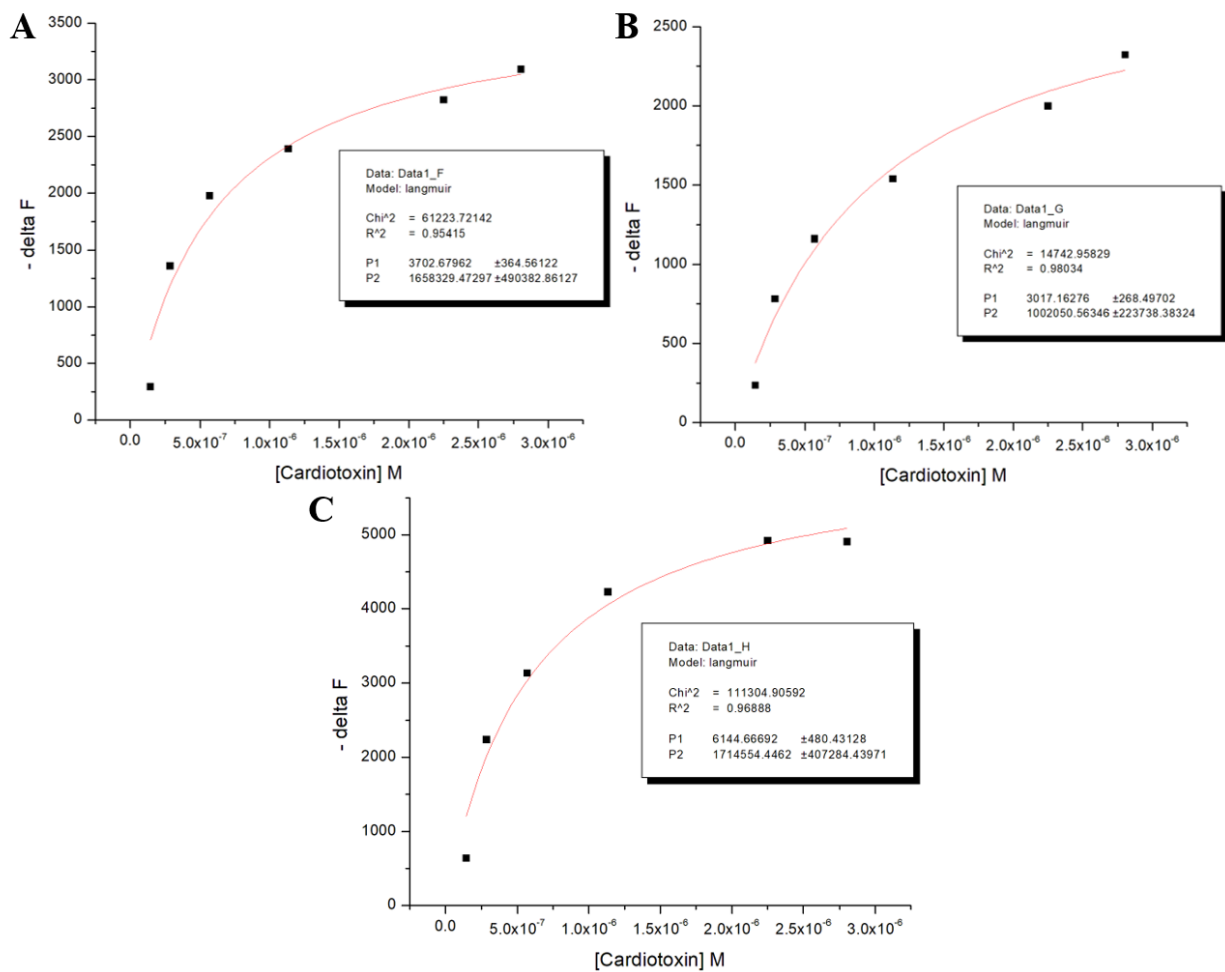
Figure 5.S2. QCM derived binding plots fitted with the Langmuir function for cardiotoxins from *Naja mossambica* (2 of 2).
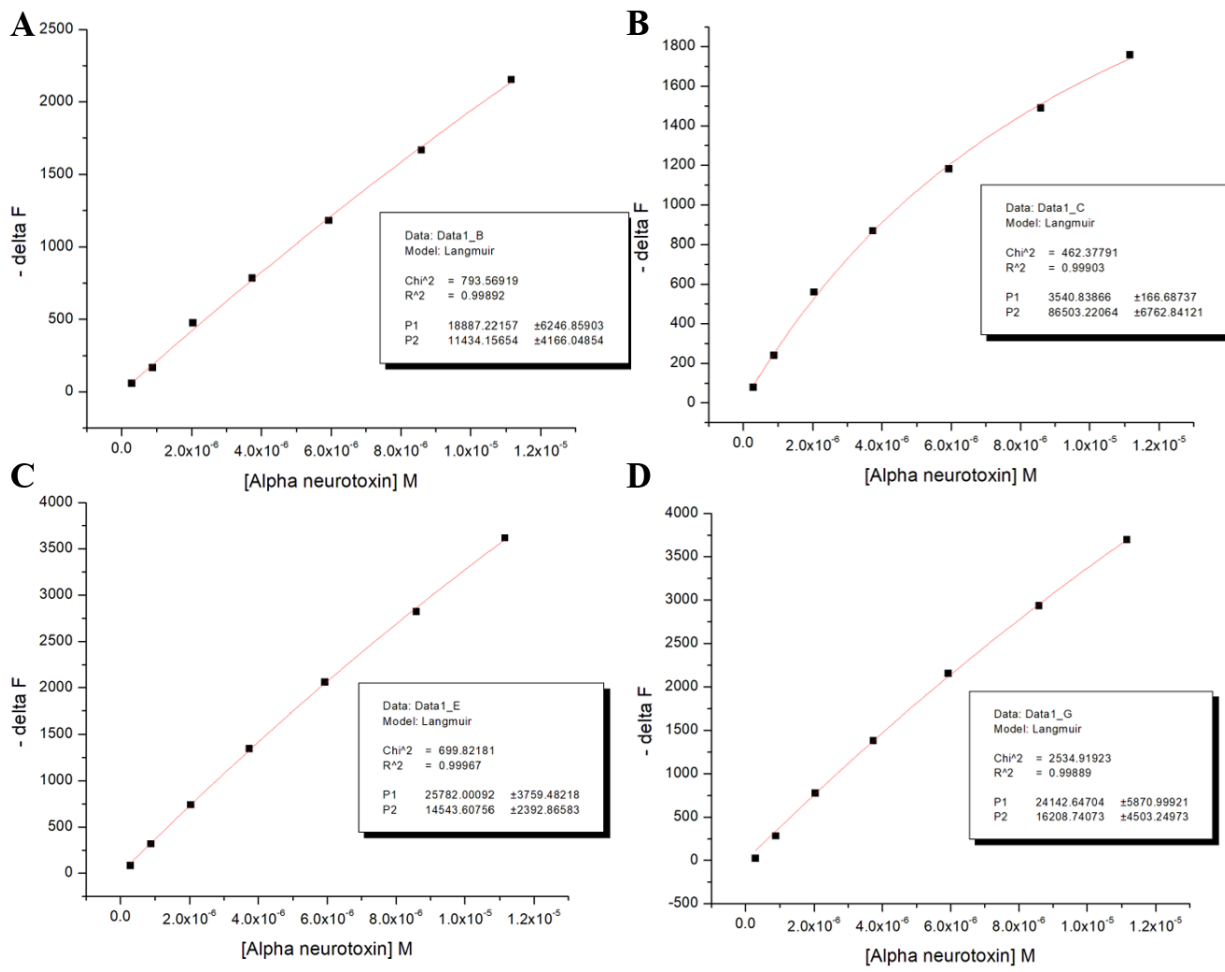
Figure 5.S3. QCM derived binding plots fitted with the Langmuir function for α-neurotoxin from *Naja nigricollis* venom.
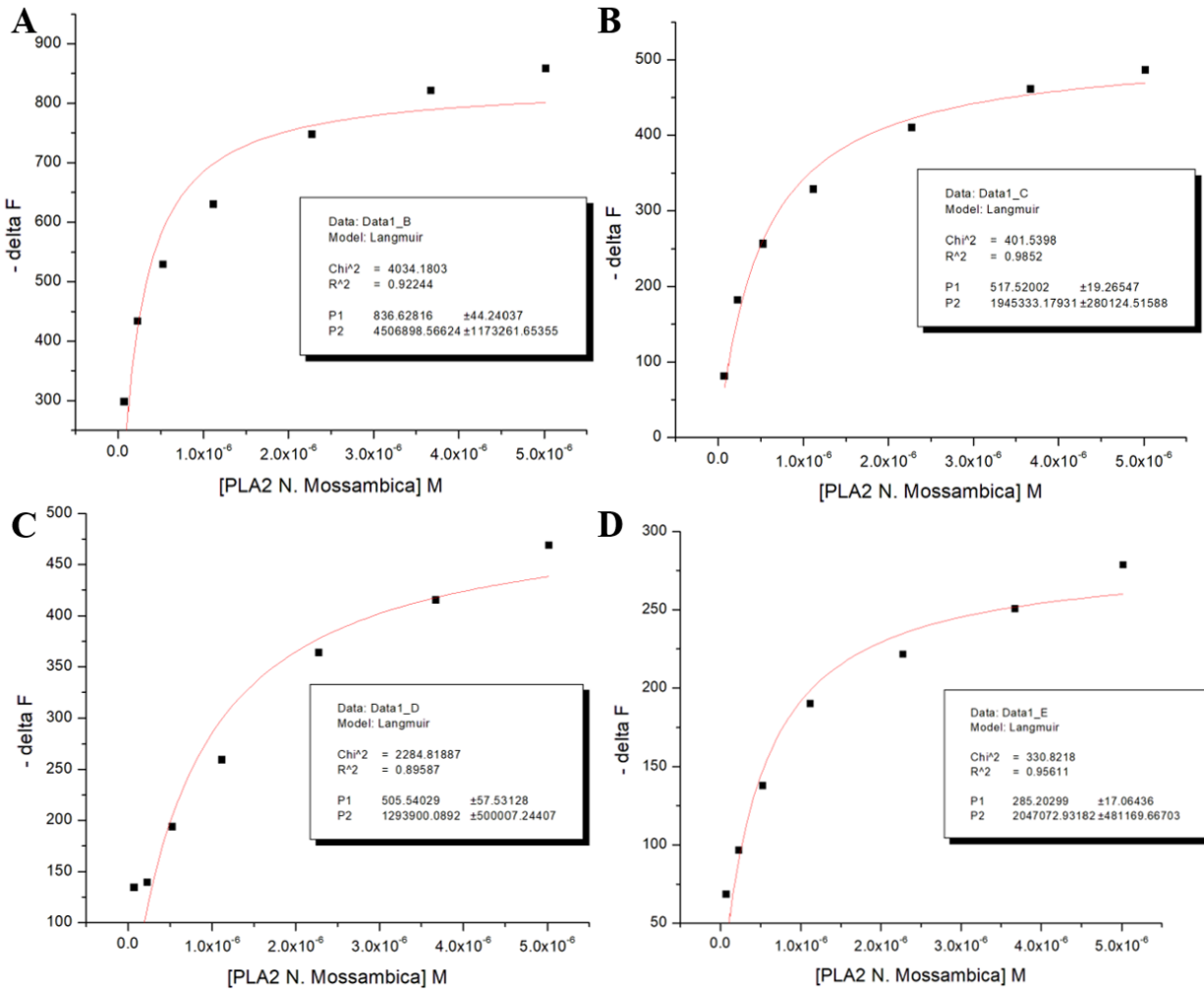
Figure 5.S4 QCM derived binding plots fitted with the Langmuir function for monomeric PLA_2 from *Naja mossambica* venom.
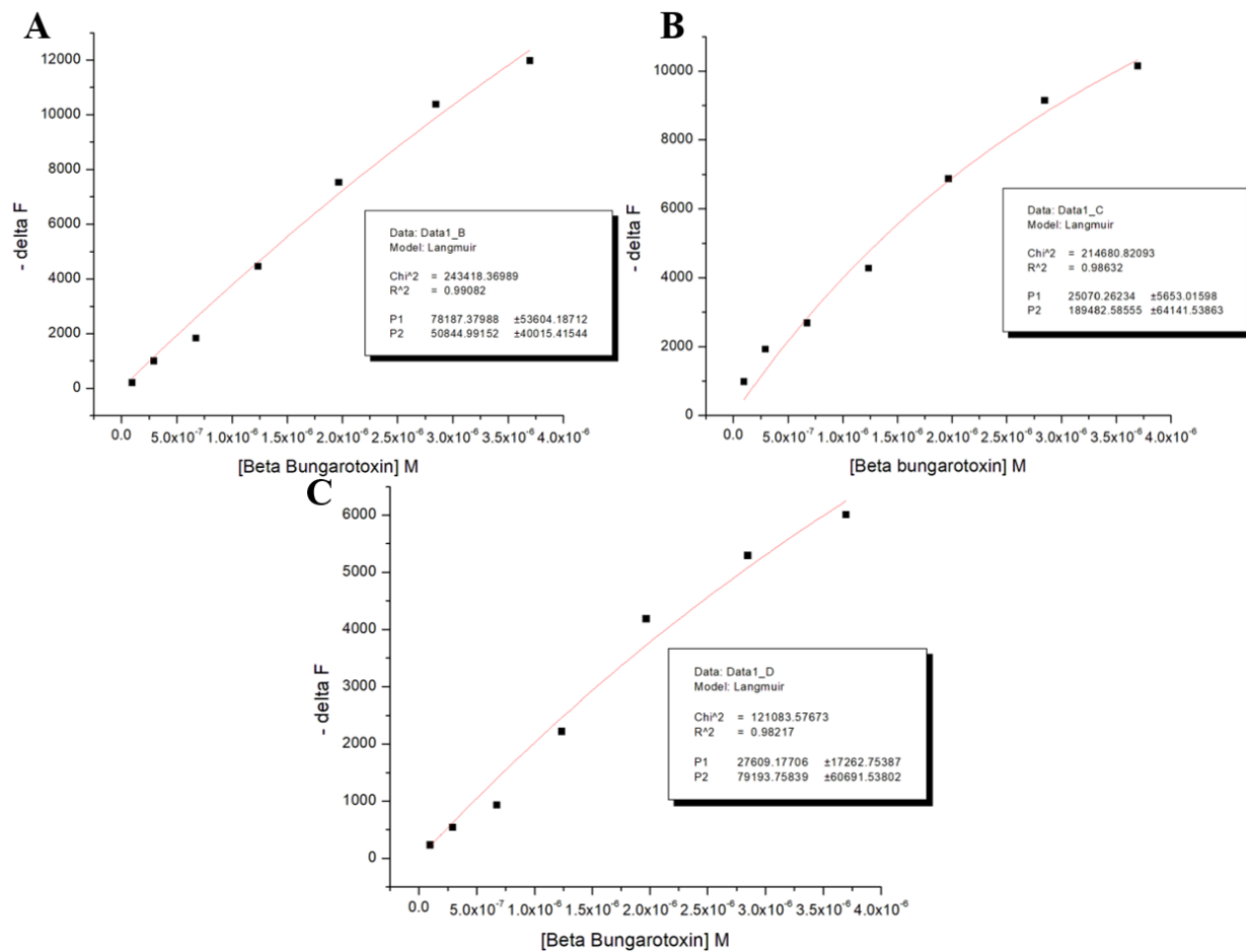
Figure 5.S5 QCM derived binding plots fitted with the Langmuir function for heterodimeric β-bungarotoxin from *Bungarus multicinctus* venom (1/2).
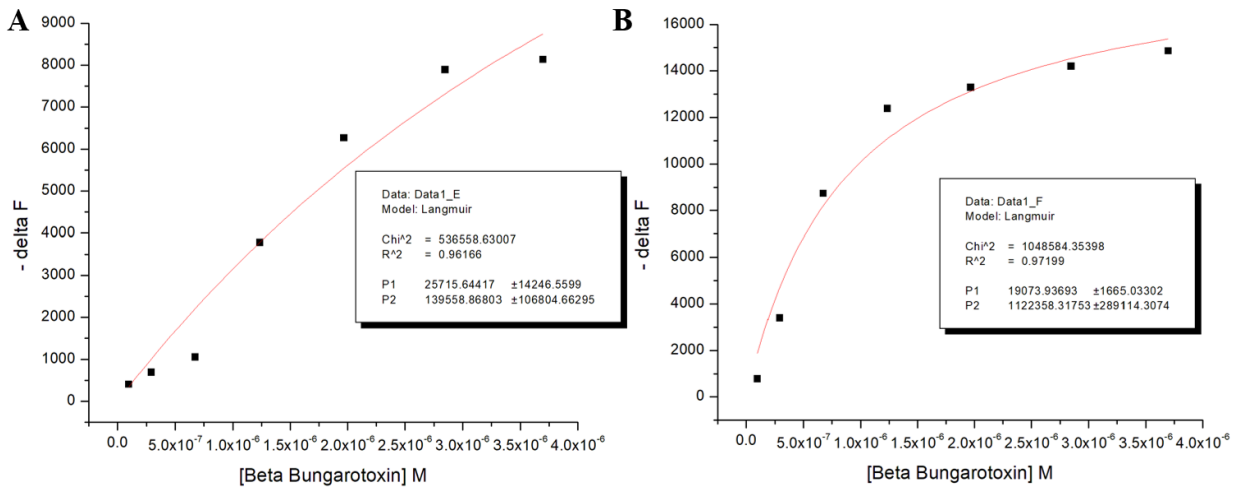
Figure 5.S6 QCM derived binding plots fitted with the Langmuir function for heterodimeric β-bungarotoxin from *Bungarus multicinctus* venom (2/2).

H. References

(1)   Koide, H.; Yoshimatsu, K.; Hoshino, Y.; Lee, S.-H.; Okajima, A.; Ariizumi, S.; Narita, Y.; Yonamine, Y.; Weisman, A. C.; Nishimura, Y.; Oku1, N.; Miura, Y.; Shea. K. J.: Synthetic Polymer Protein Affinity Reagents. A Polymer Nanoparticle with Engineered Affinity for a Vascular Endothelial Growth Factor (VEGF165). *Nat. Chem.* **2017**, *9*, 715-722.

(2)   Hoshino, Y.; Koide, H.; Furuya, K.; Haberaecker, W. W.; Lee, S. H.; Kodama, T.; Kanazawa, H.; Oku, N.; Shea, K. J.: The rational design of a synthetic polymer nanoparticle that neutralizes a toxic peptide in vivo. *P. Natl. Acad. Sci. U. S. A.* **2012**, *109*, 33-38.

(3)   Reeks, T. A.; Fry, B. G.; Alewood, P. F.: Privileged frameworks from snake venom. *Cell. Mol. Life Sci.* **2015**, *72*, 1939-1958.

(4)   Mackessy, S. P.: Handbook of venoms and toxins of reptiles; Taylor & Francis: Boca Raton, **2010**.

(5)   Fry, B. G.: From genome to "venome": Molecular origin and evolution of the snake venom proteome inferred from phylogenetic analysis of toxin sequences and related body proteins. *Genome Res.* **2005**, *15*, 403-420.

(6)   Schottler, S.; Becker, G.; Winzen, S.; Steinbach, T.; Mohr, K.; Landfester, K.; Mailander, V.; Wurm, F. R.: Protein adsorption is required for stealth effect of poly(ethylene glycol)- and poly(phosphoester)-coated nanocarriers. *Nat. Nanotechnol.* **2016**, *11*, 372-377.

(7)   Molinaro, R.; Corbo, C.; Martinez, J. O.; Taraballi, F.; Evangelopoulos, M.; Minardi, S.; Yazdi, I. K.; Zhao, P.; De Rosa, E.; Sherman, M. B.; De Vita, A.; Furman, N. E. T.; Wang, X.; Parodi, A.; Tasciotti, E.: Biomimetic proteolipid vesicles for targeting inflamed tissues. *Nat. Mater.* **2016**, *15*, 1037-1046.

(8)   Weisman, A.: Engineering the Nanoparticle-Protein Interface. **2016**. University of California, Irvine, PhD dissertation.

(9)   Zeng, Z.; Patel, J.; Lee, S. H.; McCallum, M.; Tyagi, A.; Yan, M.; Shea, K. J.: Synthetic polymer nanoparticle-polysaccharide interactions: a systematic study. *J. Am. Chem. Soc.* **2012**, *134*, 2681-2690.

(10)   Konshina, A. G.; Dubovskii, P. V.; Efremov, R. G.: Structure and dynamics of cardiotoxins. *Curr. Protein Pept. Sci.* **2012**, *13*, 570-584.

(11)   Servent, D.; Winckler-Dietrich, V.; Hu, H. Y.; Kessler, P.; Drevet, P.; Bertrand, D.; Menez, A.: Only snake curaremimetic toxins with a fifth disulfide bond have high affinity for the neuronal alpha7 nicotinic receptor. *J. Biol. Chem.* **1997**, *272*, 24279-24286.

(12)   Pino, P. D.; Pelaz, B.; Zhang, Q.; Maffre, P.; Nienhaus G. U.; Parak, W. J.: Protein corona formation around nanoparticles – from the past to the future. *Mater. Horiz.* **2014**, *1*, 301-313.

Chapter 6

Rapid evaluation of polymer –biomacromolecule interactions. A discovery platform for nanoparticle – biomacromolecule affinity pairs

A. Abstract

The development of nanomaterials for biological or biomedical applications requires an understanding of the formation and kinetic evolution of the protein corona. It is now understood that upon exposure to biological environments the physicochemical properties of nanoparticles can influence the composition of the protein corona. The protein corona in turn affects the biodistribution of the nanoparticles and their therapeutic and pathophysiological effects. It has also been established that by engineering the chemical composition of the nanoparticle, the protein corona can be "tuned" to achieve a highly specific protein-nanoparticle affinity pair. Given the diversity of synthetic materials, evaluation of nanoparticle-biomacromolecule interactions can be challenging. We report a rapid, and efficient high-throughput method for the evaluation of nanoparticle – biomacromolecule affinity. The method is suitable for rapidly screening materials that span a range of chemical compositions. The method is general and can lead to discovery of nanoparticle-protein affinity pairs as well as the influence of conditions that influence protein binding (temperature, pH, ionic strength).

B. Introduction

Protein-protein binding involves non-covalent contacts between amino acid side chains over an area often $> 1500 Å^2$.[1] The interactions can involve $> 20\text{-}25$ amino acid side chains from each protein. Since there are 20 canonical amino acids, the potential diversity of these interactions is enormous. Efforts to replace one of these proteins with an abiotic synthetic polymer or polymer nanoparticle (NP) can result in discovery of protein-NP affinity pairs, materials that can function

as abiotic protein affinity reagents.[2] The connection between the compositional (chemical) identity of a NP and the proteins that favorably associate with the NP is difficult to formulate on first principles. The complexity of the interaction prevents developing simple rules for predicting outcomes. Although some information regarding the biomacromolecule target is helpful to identify potential complementary functional monomers that could contribute to biomacromolecule affinity, current approaches are largely empirical.[3-5]

For example, small libraries of compositionally diverse NPs are screened individually for leads. NP composition is then systematically varied to optimize NP-protein affinity.[6] This process has been referred to as directed synthetic evolution,[2] and has resulted in the discovery of polymer NPs with antibody like affinity and selectivity for peptide and protein targets that function both in vitro and in vivo.[2,4,7] A disadvantage of this process is that it is time consuming and labor intensive. However, the potential for these abiotic materials to play a significant role as complements or alternatives to their biological counterparts motivates the development of more efficient methods for the discovery and screening of abiotic biological affinity materials. In this chapter, I describe a general method for evaluating polymer-biomacromolecule interactions using equilibrium dialysis.

C. Equilibrium dialysis

A bio-physicochemical property important for medicinal chemists is evaluation of off-target binding of a small molecule drug to plasma proteins to quantify the % free drug in the patients' blood-stream.[8] This type of assay, a protein binding assay, has been adapted for high-throughput automation by using a small volume 96 well equilibrium dialysis apparatus.[9] The basis of this technique is to integrate a semipermeable membrane into a 96 well format. The molecular weight cut off (MWCO) of the semipermeable membrane is lower than the MW of plasma proteins,

but significantly higher than the MW of the drug or small molecule being assayed. The plasma proteins are kept on one side of the membrane while the small molecule drug can readily permeate the membrane. Once the system reaches equilibrium, the concentration of the small molecule drug on the non-protein side of the membrane can be determined via HPLC-MS.[9] This data can then be used to calculate the % free drug and the effective concentration of active drug in the blood-stream.

D. Modified equilibrium dialysis
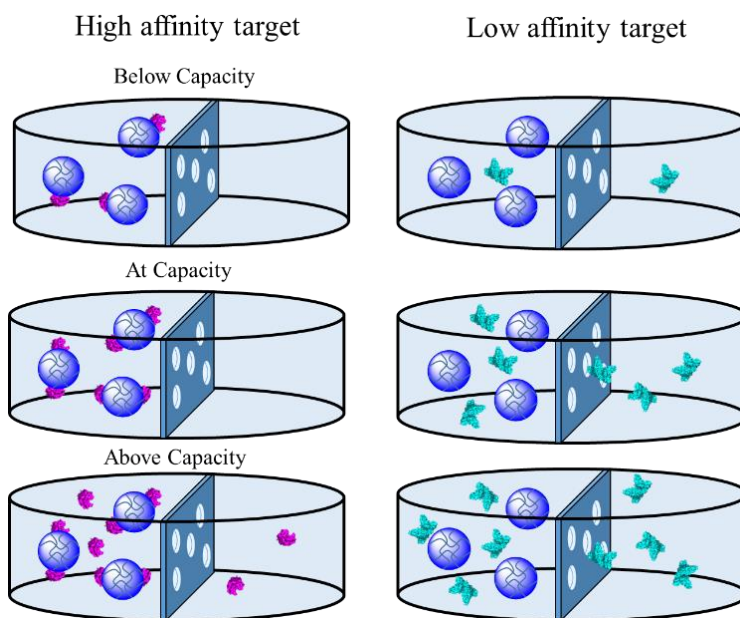
Figure 6.1. Graphical depiction of equilibrium protein concentrations at various stoichiometric ratios for a high affinity (left) and low affinity (right) target.

I have turned this traditional equilibrium dialysis method on its head. I adapted the high-throughput 96 well apparatus to analyze libraries of synthetic polymer NPs for their affinity to targeted biomacromolecules and to off-target biomacromolecules. The polymer NPs used in this study have molecular weights ranging from five to 75 million Da, much higher than typical proteins. Hence, I replaced the low MWCO membrane with a high MWCO membrane (1,000 kDa). This membrane allows diffusion of biomacromolecules (proteins) while retaining the high molecular weight polymer NPs (>10,000 kDa) on one side of the membrane (Figure 6.1). The

diffusion coefficient for a 30 kDa protein in water is estimated to be 10^{-6} (cm^2/s).[10] This value is sufficiently large to allow equilibrium to be achieved in the individual wells in a reasonable time. To ensure that equilibrium is reached for each protein analyzed, each set of experiments featured a NP-free control where instead of NPs, buffer is added to one side of the membrane and the protein is added to the other. At equilibrium, the concentration of protein is compared on both sides of the membrane to ensure that the protein concentrations were equal. Equilibrium was established for the protein lysozyme in ~12 h. To be on the conservative side I standardized the protocol to a 24 h equilibration period. In a second control I established confinement of the polymer NP. A fluorescein tagged NP, was added to one compartment of the well partitioned with the 1,000 kDa MWCO membrane. After 24 h the fluorescence of each compartment was measured. No fluorescence was detected in the "receiver" compartment.

In this system it is the protein that is quantified. Protein quantification can be achieved using any number of techniques.[11] In this study we used several methods including the Bradford assay. For the analysis of more complex systems including analysis of the NP corona,[12] I have found that SDS-PAGE is best to analyze the amount and type of bound protein to the NP.

The commercially available 1,000 kDa MWCO membrane is made of cellulose acetate. Our initial experiments were complicated by non-specific binding to the membrane, which hindered diffusion of proteins through the membrane which delayed the time to equilibrium. However, we have found that this issue can be circumvented by overnight soaking of the membrane in the buffer solution used in the experiment. Additionally, an external control featuring a protein solution that is equal to the theoretical equilibrium concentration can be used to verify the absence of non-specific binding.
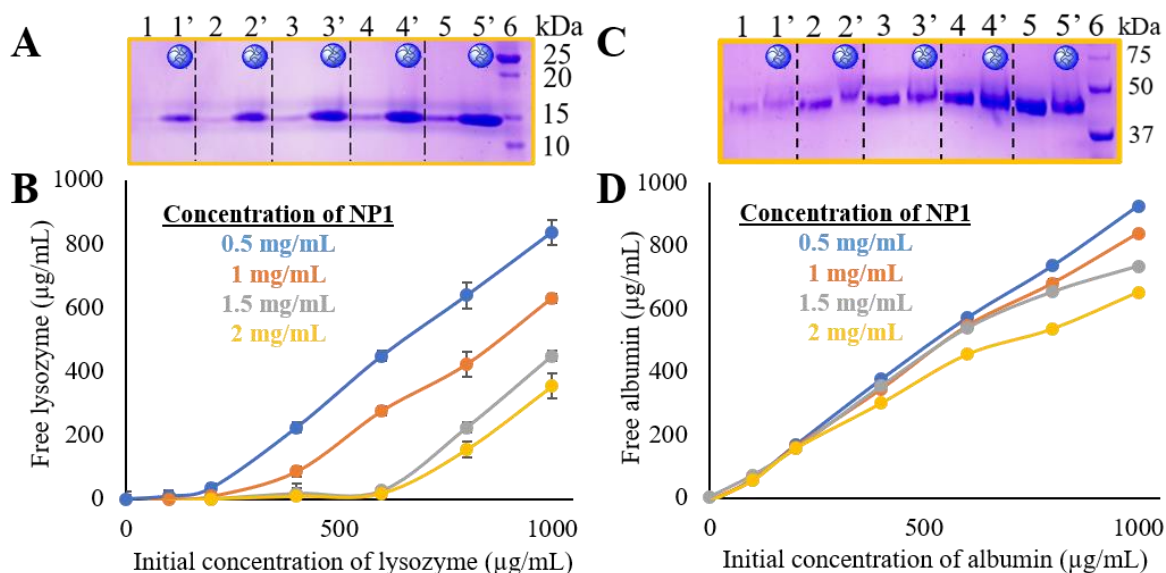
Figure 6.2. Equilibrium Dialysis results of the interaction of **NP1** and various concentrations of lysozyme or albumin. (**A**) Amount of lysozyme visualized by SDS-PAGE on the non-**NP1** containing half-well (1,2,3,4,5) or the **NP1** (2 mg/mL) containing half-well (1', 2', 3', 4', 5'). The initial concentrations of lysozyme were 200, 400, 600, 800 or 1000 µg/mL. (**B**) Equilibrium concentration of lysozyme determined from the non-**NP1** containing half-well via Bradford assay at various concentrations of **NP1**. (**C**) Amount of albumin visualized by SDS-PAGE on the non-**NP1** containing half-well (1,2,3,4,5) or the **NP1** (2 mg/mL) containing half-well (1', 2', 3', 4', 5'). (**D**) Equilibrium concentration of free albumin determined from the non-**NP1** containing half-well via Bradford assay at various concentrations of **NP1**. Free lysozyme and free albumin was quantified by doubling the concentration of lysozyme or albumin on the non-NP1 containing half-well.

After standardizing the protocol, I validated the utility of this technique by first testing a known NP-biomacromolecule affinity pair. **NP1**, a 2% crosslinked 100 nm hydrogel polymer NP comprised of 5% acrylic acid (Aac), 40% *N*-tertbutylacrylamide (TBAm) and 53% *N*-isopropylacrylamide (NIPAm) was previously shown to sequester lysozyme from chicken-hen egg white, a complex biological mixture containing roughly 54% ovalbumin and 3% lysozyme.[13] For these experiments both **NP1** (concentrations ranging from 0.5-2 mg/mL) and lysozyme or albumin (concentrations ranging from 100-1,000 µg/mL) were added to the "feed" side wells. The solutions were left to equilibrate for 24 h (Figure 6.2). Protein analysis (Bradford) was performed on the "receiver" well and the results are plotted in Figures 6.2B, 6.2D. In a separate analysis, the protein

concentration on the receiver side (whole #'s) and feed side containing the NPs, (prime #'s) was visualized via SDS-PAGE. Those results are shown in Figure 6.2A, 6.2C. The results from both analytical methods clearly confirm **NP1** affinity for lysozyme and parallel the reported differences in affinity of **NP1** to lysozyme and albumin.[13]
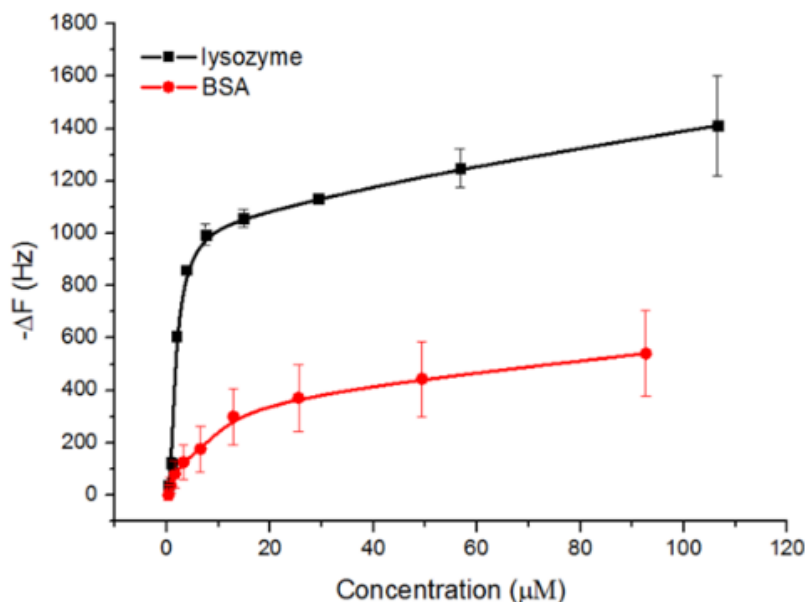
Figure 6.3. Binding isotherms of bovine serum albumin (red) and lysozyme (black) to a Quartz Crystal Microbalance (QCM) sensor coated with **NP1**.

The difference in protein affinity of **NP1** to albumin and lysozyme was independently corroborated by binding experiments using a quartz crystal microbalance (Figure 6.3). Fitting the binding isotherms with the Langmuir equation gave a disassociation constant (K_d) for albumin and lysozyme of 12.9 µM and 3.09 µM respectively. However, the most profound difference in the two isotherms was the difference in capacity. This difference is reflected in the equilibrium dialysis data. Rough estimates of the capacity of **NP1** for lysozyme using the equilibrium dialysis data is 0.6 mg lysozyme / 1 mg **NP1** (wt/wt). In contrast, the estimated capacity for albumin is <0.05 mg albumin / 1 mg **NP1**. At equilibrium, lysozyme was not detected in the receiving (non-**NP1**

containing) half-well until the initial lysozyme concentration exceeded 500 µg/mL. In contrast, albumin appeared in the receiver side at the lowest concentrations.
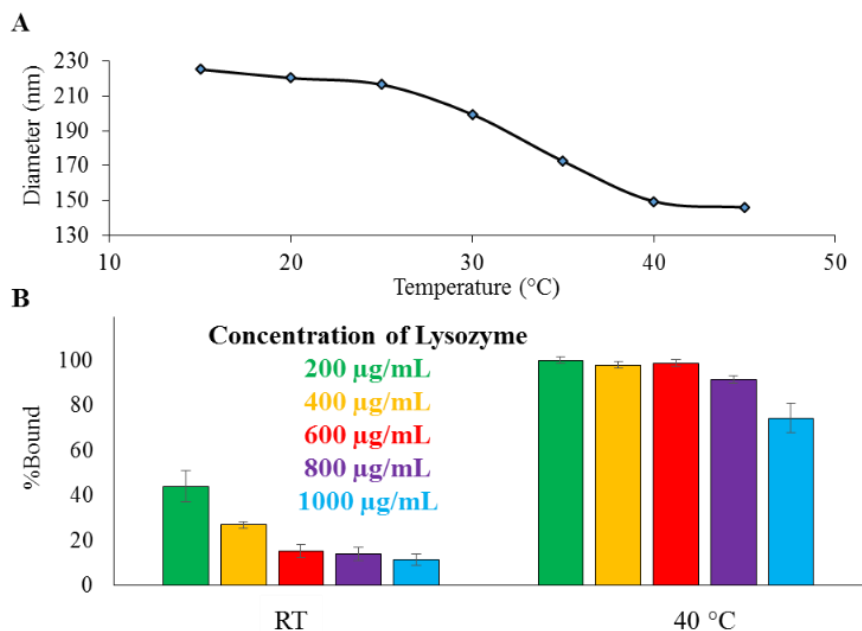
Figure 6.4. Equilibrium dialysis evaluation of the interaction of **NP2** (5% Aac, 20% TBAm, 73% NIPAm, 2% Bis) and lysozyme above (40°C) and below (22°C) the LCST of **NP2**. (**A**) **NP2** size as a function of temperature determined by dynamic light scattering (DLS) in PBS. (**B**) % Lysozyme bound to **NP2** using a Bradford assay. % Bound was calculated by doubling the concentration of lysozyme on the non-**NP2** containing half-well and subtracting that quantity from the initial concentration of lysozyme.

The NPs used in this study are derived from thermoresponsive polymers. Below their lower critical solution temperature (LCST) the polymers are solvent swollen but above their LCST, they are substantially de-solvated and collapsed. In many cases their biomacromolecule affinity is found to be sensitive to temperature.[2] For example, we have found that NP-biomacromolecule affinity is often greatest above the LCST. Since temperature is such an important parameter influencing biomacromolecule affinity, it is important to establish that the modified equilibrium dialysis apparatus can also be used to evaluate the temperature sensitivity of the NP-biomacromolecule interaction. The lysozyme – **NP2** system is one such case. **NP2** has affinity for lysozyme above its

LCST (40°C) but very low affinity below its LCST.[14] **NP2**, is comprised of the same functional monomers as **NP1,** but contains a lower percentage of TBAm. By reducing the amount of TBAm in the NP, the LCST of the NP shifts to a temperature above RT (Figure 6.4A). The binding of **NP2** for lysozyme was evaluated above and below its LCST in the modified equilibrium dialysis apparatus (Figure 6.4B). In the event, the affinity-temperature relationship is clearly reproduced. The results are presented as % lysozyme bound as a function of temperature at various lysozyme concentrations. The result establishes that the modified equilibrium dialysis apparatus can be conveniently used for screening the temperature dependence of biomacromolecule affinity.

Engineering a synthetic NP to simultaneously bind multiple biomacromolecules can create new applications for abiotic affinity reagents. For example, in the development of a synthetic NP for broad-spectrum venom sequestration and neutralization, it would be desirable for the NP to bind many toxin isoforms simultaneously. We've recently demonstrated this using an optimized NP composition featuring 40% *N*-phenylacrylamide, 20% AAc, 25% NIPAm, and 15% Bis (**NP3**).[4] This NP was shown to have high affinity and selectivity for phospholipase A_2 (PLA_2) toxins found abundantly in honey-bee venom and snake venom including the medically relevant spitting cobra *Naja mossambica*.[15] The swiss-prot database indicates that the venom from *N. mossambica* contains three different isoforms of PLA_2 (~14 kDa). Herein, we demonstrate that the equilibrium dialysis apparatus can rapidly identify selective sequestration of venomous isoforms in *N. mossambica* venom by SDS-PAGE analysis of both compartments of the equilibrium dialysis apparatus (Figure 6.5). In this experiment, *N. mossambica* venom at a concentration of either 1 mg/mL (Figure 6.5-5,6) or 0.5 mg/mL (Figure 6.5-7,8) was introduced on one side of the 1,000 kDa MWCO membrane and **NP3** at a concentration of either 0.5 mg/mL (Figure 6.5-5',7') or 1 mg/mL (Figure 6.5-6',8') was introduced on the opposite side of the membrane. After 24 h, the

contents on both sides of the membrane were removed and analyzed via SDS-PAGE. Qualitative analysis of the gel-band intensities of the diffusion control experiments (Figure 6.5-3,3',4,4') indicates that the various venom toxins can reach equilibrium after 24 h. Furthermore, the band intensities in the **NP3** containing experiments appear to correlate with both the quantity of venom and the quantity of **NP3** present in each well. In addition to providing further validation that equilibrium dialysis rapidly produces results that corroborate results from other established polymer-binding assays, the ability to analyze binding in complex media suggests unique competition studies between competing materials or competing proteins can be performed in a facile and high-throughput manner.
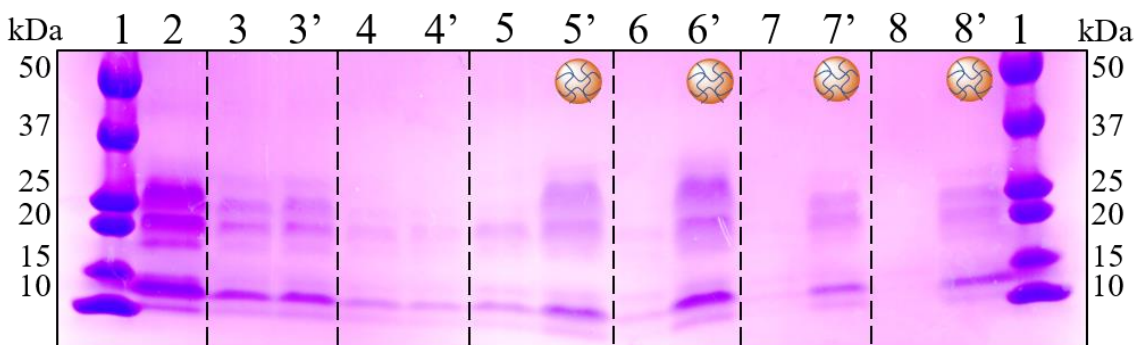
Figure 6.5. Equilibrium venom protein concentrations visualized by SDS-PAGE. Whole numbers (3,4,5…) represent the half-well containing venom at T_0. Prime numbers (3',4',5'…) represent the half-well containing either buffer or **NP3** as indicated. (**1**) MW ladder (**2**) *Naja mossambica* venom external control. (**3, 3'**) Internal equilibrium control using 1 mg/mL venom (**4, 4'**) Internal equilibrium control using 0.5 mg/mL venom (**5, 5'**) Equilibrium venom concentrations using 1 mg/mL venom and 0.5 mg/mL **NP3** (**6, 6'**) Equilibrium venom concentrations using 1 mg/mL venom and 1 mg/mL **NP3** (**7,7'**) Equilibrium venom concentrations using 0.5 mg/mL venom and 0.5 mg/mL **NP3**. (**8**) Equilibrium venom concentrations using 0.5 mg/mL venom and 1 mg/mL **NP3**.

In addition to temperature, we also examined how changes in pH can alter the binding of a NP to a target biomacromolecule. To this extent, we synthesized **NP4** with a feed ratio of 20% itaconic acid, 40% TBAm, 30% NIPAm, and 10% Bis cross-linker. The target in this case is an IgG (F(ab)$_2$ or FC) fragment. Compared to **NP3**, which showed no binding to either fragment at

pH 5.5 or pH 7.4 (Figure 5.S1), **NP4** binds F(ab)$_2$ at pH 5.5 but shows no affinity to F(ab)$_2$ at pH 7.4 and no affinity to FC at either pH. Using multi-angle laser light scattering (MALLS), we determined the Mn of **NP4** to be 6.42x10^7 Da. We then estimated the molar ratio of F(ab)$_2$ to **NP4** semi-quantitatively using ImageJ. Band intensities for the non-NP half wells in the pH 5.5 F(ab)$_2$ binding studies (Figure 6.S2B-5,6) were compared to the NP-free F(ab)$_2$ control (Figure 6.S2B-3,3') leading to an estimated stoichiometry of 200:1 (F(ab)$_2$:NP4).

E. Conclusion

The 96-well equilibrium dialysis apparatus is adaptable to fully automated robotics. Ultimately, This technique will be critical in the construction of a fully-automated system capable of synthesizing, purifying, and analyzing large diverse libraries of NPs. The interaction of biological macromolecules with synthetic materials is important to many fields of science. This technique does not require NPs. Any large object > 5,000 or 10,000 kDa can be used. This would include natural polymers, powders or pieces of plastic. Just as important is information about the absence of affinity for biological macromolecules. This screen provides that information as well. Finally, one can use this device to explore selectivity of a synthetic material for specific proteins in a complex biological milieu, for example serum. The equilibrium dialysis experiment coupled with SDS-PAGE can point rapidly to any selective adsorption of a protein from a complex mixture. I believe this technique will be of value to a broad spectrum of scientists working at the interface of biology and materials chemistry.

F. Supporting information

Materials:

The following materials were obtained from commercial sources: *N*-isopropylacrylamide (NIPAm), ammonium persulfate (APS), itaconic acid (Itac), acryloyl chloride, *Naja mossambica* venom, lysozyme, human serum albumin and fluorescein o-acrylate were obtained from SIGMA-ALDRICH Inc.; sodium dodecyl sulfate (SDS) was obtained from Aldrich Chemical Company, Inc.; *N,N'*-methylenebisacrylamide (MBis) was from Fluka; *N*-tertbutylacrylamide (TBAm) was from ACRŌS ORGANICS. IgG fragments were purchased from Jackson Immunoresearch Laboratories Incorporated. All other solvents and chemicals were obtained from Fisher Scientific Inc. or VWR International LLC. NIPAm was recrystallized from hexanes before use. Water used in polymerization and characterization was purified using a Barnstead Nanopure Diamond^{TM} system. 12-14 kDa MWCO cellulose membranes and 1,000 kDa MWCO cellulose ester membranes were purchased from Spectrum Laboratories. Precast SDS-PAGE gels (4-15% Mini-Protean), Coomassie Brilliant Blue R-250 and molecular weight ladder (Precision plus protein standards) were purchased from Bio-Rad Laboratories.

NP Synthesis:

Monomers corresponding to the designated feed ratio, and SDS (10 mg, 1 µmol) were dissolved in water (50 mL) to a final monomer concentration of 65 mM. The resulting solution was degassed with nitrogen for 30 min while stirring. Ammonium persulfate (30 mg dissolved in 1 mL H_2O) was added to the degassed solution, and the reaction mixture was heated to 60 °C under nitrogen for 3 h. The polymerization was quenched by exposing the reaction mixture to air, and the reaction mixture was transferred to a 12,000-14,000 MWCO membrane and dialyzed against an excess of deionized water (changed twice a day) for 4 d.

NP Characterization:

Dynamic light scattering (DLS) was used to characterize the size and dispersity of the NPs in PBS at room temperature. All samples were allowed to equilibrate for 200 seconds prior to each measurement and were measured at a scattering angle of 173°. Concentrations and yields were determined by lyophilizing a known volume of the purified NP solution and weighing the obtained dry polymer samples. All measurements were performed using a Malvern ZEN3600 dynamic light scattering (DLS) instrument with a disposable sizing cuvette

Quartz crystal microbalance:

The quartz-crystal microbalance (QCM) binding studies were performed following a known protocol.[5] Briefly, QCM cells were washed with 1% SDS followed by nanopore water (10x, 500 µL) and dried using a gentle stream of air. The gold electrodes were then cleaned by pipetting 1 µL of 4 M peroxide, followed by 3 µL of concentrated sulfuric acid and after 10 min, the cells were washed with nanopore water (10x, 500 µL) and repeated two more times. Next, 500 µL of PBS was added to the cells and the cells were loaded into an Affinity Q4 QCM instrument (Initium Co. Ltd., Tokyo, Japan) and allowed to equilibrate. Next NP1 was immobilized onto the clean gold surface by pipetting a solution of NP1 into the QCM cell at r.t. until the surface was saturated. The cells were then washed with PBS (500 µL, 3x) and then filled with fresh PBS and allowed to equilibrate in the instrument. Next, either a solution of lysozyme (1 mg/mL, PBS) or albumin (1 mg/mL, PBS) were pipetted into the QCM cell at systematically increasing volumes pipetted after equilibration. The data was then plotted in Origin 6 and fitted with the Langmuir equation.

Equilibrium dialysis general protocol:

1,000 kDa cellulose ester membranes were washed in buffer (PBS or 100 mM sodium phosphate buffer pH 5.5) overnight and then cut into single sheets to fit the equilibrium dialysis apparatus (2x12 cm). After placing the membrane over the half-well, the apparatus was assembled. Buffer or NPs at various concentrations were dispensed on one half well (100 µL) and the protein solution at various concentrations were dispensed into the other half-well on the other side of the membrane (100 µL). An adhesive cover, purchased from HTDialysis, was placed over the apparatus followed by tin-foil and left unagitated for 24 h at RT or 40 °C as indicated. After 24 h, 90 µL aliquots from each half well were transferred to a microcentrifuge tube. Next, the concentration of the NP-free half-wells were quantified either by Bradford or by SDS-PAGE stained with Coomassie-blue dye using both the NP-containing half well and the non-NP half-well.

Note: the Coomassie dye interacts strongly with the NP hydrogels which prevents protein equilibrium quantification of the NP-containing half-well via the Bradford assay.

NP diffusion control using fluorescein containing NP:

PBS (100 µL) was added to one half-well and the fluorescein containing NP (NP-F, 2 mg/mL), 100 µL was added to the other half well. Fluorescence was measured using an excitation wavelength of 450 nm. After 24 h, the fluorescence was measured on both sides of the membrane. No fluorescence was observed on the NP-free half-well.

Multi-Angle Laser Light Scattering:

Molecular weight was determined using a SEC-MALS (Malvern Viskotek GPC/SEC triple detection system) system. The system was run in PBS. The column (Viscotek A7000) was heated to 30°C and the system was calibrated to a polyethylene oxide standard. NP4 was prepared by dialyzing in PBS for 3h changing the PBS 1x each hour. The NP4 sample was diluted in PBS

(2.44 mg/mL) and injected onto the column. Injections of 100 µL were used with a flow rate of 1

mL/min. The MW was determined to be 1.49×10^8 and Mn was determined to be 6.42×10^7.

Table 6.S1. NP monomer feed ratios (mol%) yields and characterization data.

	Aac	TBAm	NIPAm	Bis	Phe	Itac	d. nm PBS	PDI[b]	% Yield
NP1	5	40	53	2	--	--	101	0.043	83
NP2	5	10	83	2	--	--	211	0.035	91
NP3	20	--	25	15	40	--	176	0.065	72
NP4	--	40	30	10	--	20	236	0.022	74
NP-F	10	10	77.9[a]	2	--	--	356	0.11	77

Monomer abbreviations: Acrylic acid (Aac), *N*-tertbutylacrylamide (TBAm), *N*-isopropylacrylamide (NIPAm), *N,N'*-methylenebisacrylamide (Bis), *N*-phenylacrylamide (Phe) and itaconic acid (Itac)
[a]NP synthesized with 1% fluorescein o-acrylate monomer
[b] Poly dispersity (PDI) represents (standard deviation/diameter)^2
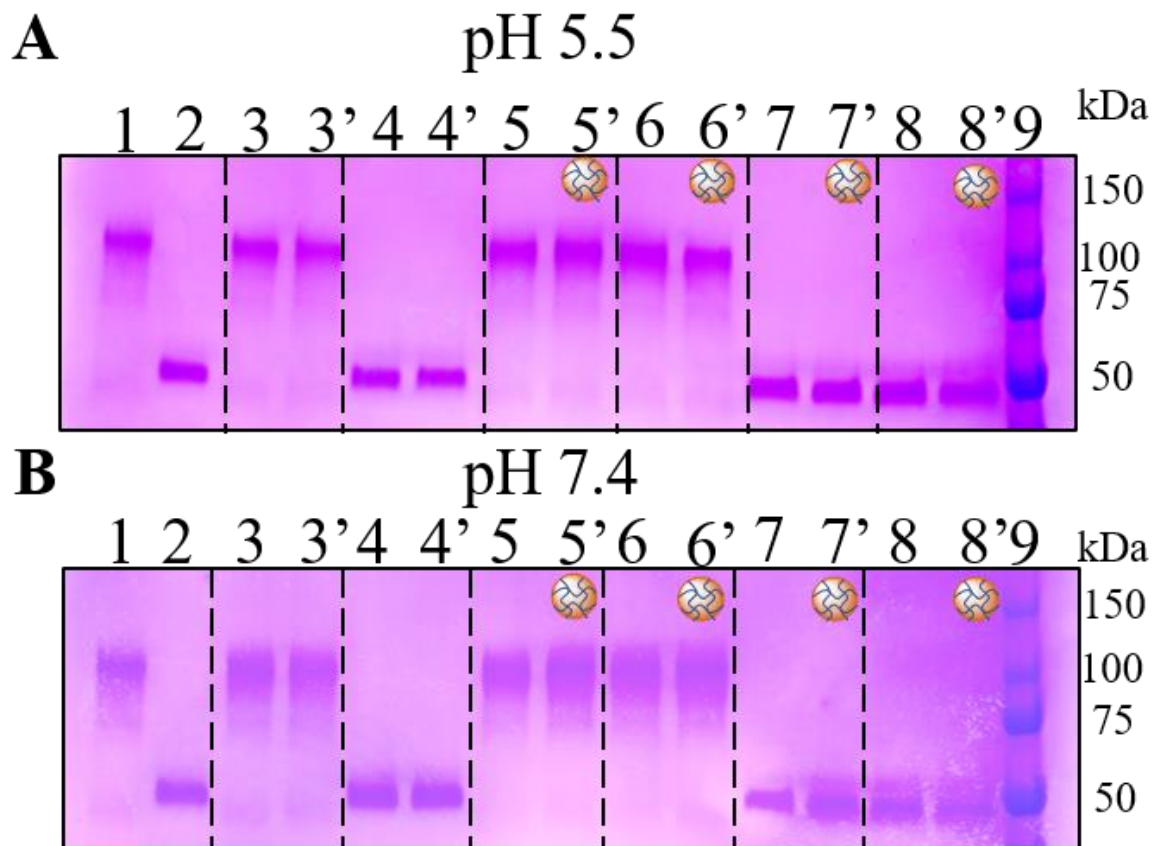
Figure 6.S1. pH dependent binding study using **NP3** and fragmented IgG (FC and F(ab)$_2$). Whole numbers (3,4,5,…) represent the half-well containing fragmented IgG at T$_0$. Prime numbers (3',4',5'…) represent the half-well containing buffer or **NP3** as indicated. Equilibrium concentrations of IgG fragments at pH (A) 5.5 and (B) pH 7.4 visualized via SDS-PAGE (**1**) F(ab)$_2$ external control. (**2**) FC external control. (**3, 3'**) Equilibrium F(ab)$_2$ internal control. (**4, 4'**) Equilibrium FC internal control. (**5,5'**) Equilibrium F(ab)$_2$ concentrations using 0.5 mg/mL NP4. (**6, 6'**) Equilibrium F(ab)$_2$ concentrations using 1 mg/mL **NP3**. (**7, 7'**) Equilibrium FC concentrations using 0.5 mg/mL NP4. (**8,8'**) Equilibrium FC concentrations using 1 mg/mL **NP3**. (**9**) MW ladder.
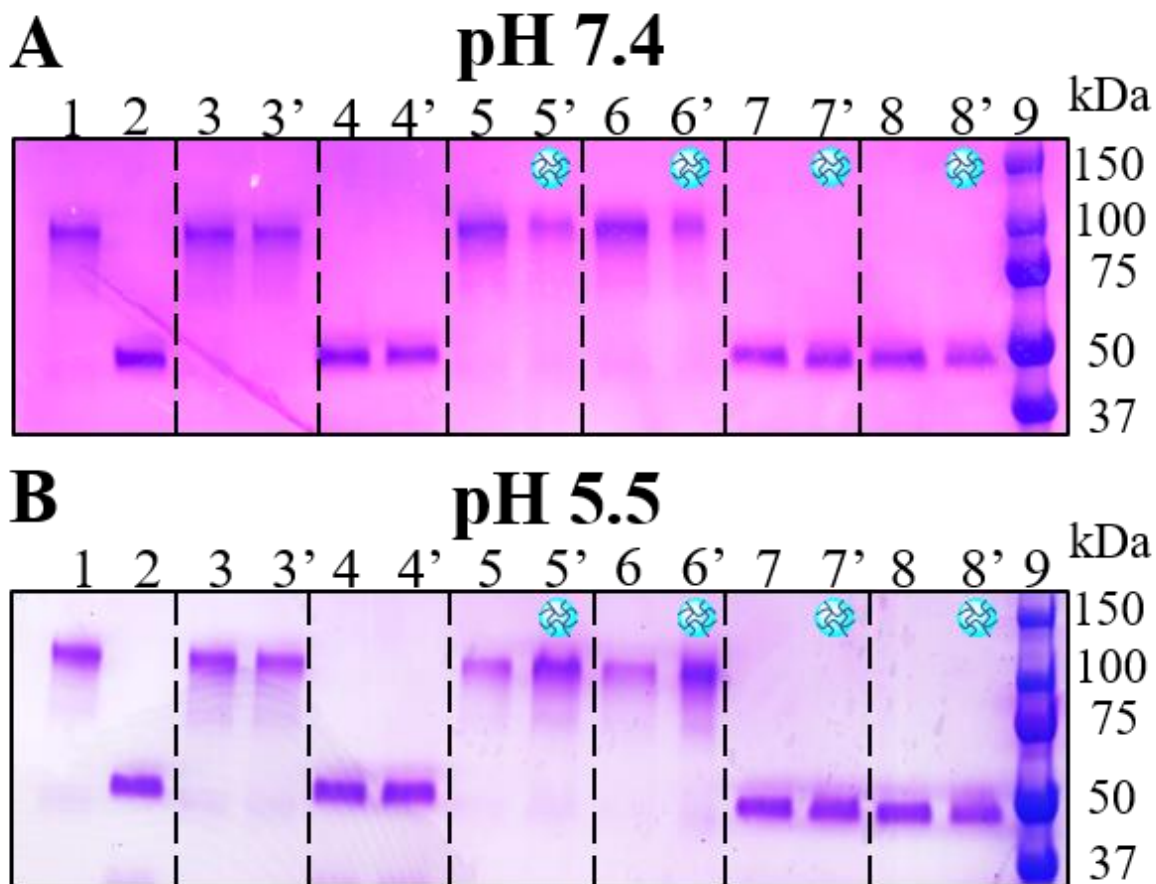
Figure 6.S2. pH dependent binding study using **NP4** and fragmented IgG (FC and F(ab)$_2$). Whole numbers (3,4,5,…) represent the half-well containing fragmented IgG at T$_0$. Prime numbers (3',4',5'…) represent the half-well containing buffer or **NP4** as indicated. Equilibrium concentrations of IgG fragments at pH (**A**) 7.4 and (**B**) pH 5.5 visualized via SDS-PAGE (**1**) F(ab)$_2$ external control. (**2**) FC external control. (**3, 3'**) Equilibrium F(ab)$_2$ internal control. (**4, 4'**) Equilibrium FC internal control. (**5,5'**) Equilibrium F(ab)$_2$ concentrations using 0.5 mg/mL **NP4**. (**6, 6'**) Equilibrium F(ab)$_2$ concentrations using 1 mg/mL NP4. (**7, 7'**) Equilibrium FC concentrations using 0.5 mg/mL NP4. (**8,8'**) Equilibrium FC concentrations using 1 mg/mL NP4. (**9**) MW ladder.

173

G. References

(1)   Jones, S.; Thornton, J. M.: Principles of protein-protein interactions. *Proc. Natl. Acad. Sci. U. S. A.* **1996**, *93*, 13-20.

(2)   O'Brien, J.; Shea, K. J.: Tuning the Protein Corona of Hydrogel Nanoparticles: The Synthesis of Abiotic Protein and Peptide Affinity Reagents. *Acc. Chem. Res.* **2016**, *49*, 1200-1210.

(3)   Hoshino, Y.; Koide, H.; Furuya, K.; Haberaecker, W. W., 3rd; Lee, S. H.; Kodama, T.; Kanazawa, H.; Oku, N.; Shea, K. J.: The rational design of a synthetic polymer nanoparticle that neutralizes a toxic peptide in vivo. *Proc. Natl. Acad. Sci. U. S. A.* **2012**, *109*, 33-38.

(4)   O'Brien, J.; Lee, S. H.; Onogi, S.; Shea, K. J.: Engineering the Protein Corona of a Synthetic Polymer Nanoparticle for Broad-Spectrum Sequestration and Neutralization of Venomous Biomacromolecules. *J. Am. Chem. Soc.* **2016**, *138*, 16604-16607.

(5)   Weisman, A.; Chen, Y. A.; Hoshino, Y.; Zhang, H.; Shea, K.: Engineering nanoparticle antitoxins utilizing aromatic interactions. *Biomacromolecules* **2014**, *15*, 3290-3295.

(6)   Yonamine, Y.; Yoshimatsu, K.; Lee, S. H.; Hoshino, Y.; Okahata, Y.; Shea, K. J.: Polymer nanoparticle-protein interface. Evaluation of the contribution of positively charged functional groups to protein affinity. *ACS Appl. Mater. Interfaces* **2013**, *5*, 374-379.

(7)   Koide, H.; Yoshimatsu, K.; Hoshino, Y.; Lee, S. H.; Okajima, A.; Ariizumi, S.; Narita, Y.; Yonamine, Y.; Weisman, A. C.; Nishimura, Y.; Oku, N.; Miura, Y.; Shea, K. J.: A polymer nanoparticle with engineered affinity for a vascular endothelial growth factor (VEGF165). *Nat. Chem.* **2017**, *9*, 715-722.

(8)   Kwong, T. C.: Free drug measurements: methodology and clinical significance. *Clin. Chim. Acta* **1985**, *151*, 193-216.

(9)   Banker, M. J.; Clark, T. H.; Williams, J. A.: Development and validation of a 96-well equilibrium dialysis apparatus for measuring plasma protein binding. *J. Pharm. Sci.* **2003**, *92*, 967-974.

(10)   Young, M. E.; Carroad, P. A.; Bell, R. L.: Estimation of Diffusion-Coefficients of Proteins. *Biotechnol. Bioeng.* **1980**, *22*, 947-955.

(11)   Noble, J. E.; Bailey, M. J.: Quantitation of protein. *Methods Enzymol.* **2009**, *463*, 73-95.

(12)   Cedervall, T.; Lynch, I.; Lindman, S.; Berggard, T.; Thulin, E.; Nilsson, H.; Dawson, K. A.; Linse, S.: Understanding the nanoparticle-protein corona using methods to quantify exchange rates and affinities of proteins for nanoparticles. *Proc. Natl. Acad. Sci. U. S. A.* **2007**, *104*, 2050-2055.

(13)   Yoshimatsu, K.; Lesel, B. K.; Yonamine, Y.; Beierle, J. M.; Hoshino, Y.; Shea, K. J.: Temperature-responsive "catch and release" of proteins by using multifunctional polymer-based nanoparticles. *Angew. Chem. Int. Ed.* **2012**, *51*, 2405-2408.

(14)   Beierle, J. M.; Yoshimatsu, K.; Chou, B.; Mathews, M. A.; Lesel, B. K.; Shea, K. J.: Polymer nanoparticle hydrogels with autonomous affinity switching for the protection of proteins from thermal stress. *Angew. Chem. Int. Ed.* **2014**, *53*, 9275-9279.

(15)   Petras, D.; Sanz, L.; Segura, A.; Herrera, M.; Villalta, M.; Solano, D.; Vargas, M.; Leon, G.; Warrell, D. A.; Theakston, R. D.; Harrison, R. A.; Durfa, N.; Nasidi, A.; Gutierrez, J. M.; Calvete, J. J.: Snake venomics of African spitting cobras: toxin composition and assessment of congeneric cross-reactivity of the pan-African EchiTAb-Plus-ICP antivenom by antivenomics and neutralization approaches. *J. Proteome Res.* **2011**, *10*, 1266-1280.